Probabilistic Finite Element Analysis of Structures using the Multiplicative Dimensional Reduction Method

by

Georgios Balomenos

A thesis
presented to the University of Waterloo
in fulfillment of the
thesis requirement for the degree of
Doctor of Philosophy
in
Civil Engineering

Waterloo, Ontario, Canada, 2015

©Georgios Balomenos 2015

AUTHOR'S DECLARATION

I hereby declare that I am the sole author of this thesis. This is a true copy of the thesis, including any required final revisions, as accepted by my examiners.

I understand that my thesis may be made electronically available to the public.

Abstract

It is widely accepted that uncertainty may be present for many engineering problems, such as in input variables (loading, material properties, etc.), in response variables (displacements, stresses, etc.) and in the relationships between them. Reliability analysis is capable of dealing with all these uncertainties providing the engineers with accurate predictions of the probability of a structure performing adequately during its lifetime.

In probabilistic finite element analysis (FEA), approximate methods such as Taylor series methods are used in order to compute the mean and the variance of the response, while the distribution of the response is usually approximated based on the Monte Carlo simulation (MCS) method. This study advances probabilistic FEA by combining it with the multiplicative form of dimensional reduction method (M-DRM). This combination allows fairly accurate estimations of both the statistical moments and the probability distribution of the response of interest. The response probability distribution is obtained using the fractional moments, which are calculated from M-DRM, together with the maximum entropy (MaxEnt) principle. In addition, the global variance-based sensitivity coefficients are also obtained as a by-product of the previous analysis. Therefore, no extra analytical work is required for sensitivity analysis.

The proposed approach is integrated with the OpenSees FEA software using Tcl programing and with the ABAQUS FEA software using Python programing. OpenSees is used to analyze structures under seismic loading, where both pushover analysis and dynamic analysis is performed. ABAQUS is used to analyze structures under static loading, where the concrete damage plasticity model is used for the modeling of concrete. Thus, the efficient applicability of the proposed method is illustrated and its numerical accuracy is examined, through several

examples of nonlinear FEA of structures. This research shows that the proposed method, which is based on a small number of finite element analyses, is robust, computational effective and easily applicable, providing a feasible alternative for finite element reliability and sensitivity analysis of practical and real life problems. The results of such work have significance in future studies for the estimation of the probability of the response exceeding a safety limit and for establishing safety factors related to acceptable probabilities of structural failures.

Acknowledgements

At this point, I would like to express my sincere gratitude to my supervisor Professor Mahesh D. Pandey for his encouragement, guidance and support from the beginning till the end of my Ph.D. research. His valuable advices, knowledge, prompt responses to my queries and extreme help were decisive for the accomplishment of this research.

I would like to thank my committee members, Professor Andrzei S. Nowak, Professor Maria Anna Polak, Professor Susan L. Tighe and Professor Sagar Naik for their time, valuable comments and constructive feedback that enhanced my work. Especially, I would like to thank Professor Maria Anna Polak for her discussions and advices in the area of reinforced concrete.

I wholeheartedly would like to express my gratitude to Professor Stavroula J. Pantazopoulou for inspiring me to continue my studies towards the doctorate level and for her encouragement and guidance to elaborate my Ph.D. in Canada.

I would like to extend my deepest sincere gratitude to Professor Jeffrey S. West for serving as his Teaching Assistant for several courses, which gave me a lot of confidence and knowledge on how to deliver effectively any course material, making me to feel more than lucky to have served as one of his TAs.

From the bottom of my heart, I would like to express my thanks and appreciation to Aikaterini Genikosmou for her patience, continuous support, encouragement, unremitting help and longtime discussions which gave me confidence and strength to reach my goals.

I thankfully acknowledge my Greek friends Georgios Drakopoulos and Anastasios Livogiannis for inspiring and persuading me that programing is actually fun and Dr. Nikolaos Papadopoulos for his valuable advices and longtime discussions.

Many thanks go to my colleagues and friends; Kevin Goorts, Dr. Xufang Zhang, Olivier Daigle, Shayan Sepiani, Wei Jiang, Paulina Arczewska, Martin Krall, María José Rodríguez Roblero, Joe Stoner, Jeremie Raimbault, Dainy Manzana, Joe Simonji, Chao Wu and other graduate students with whom the days in Waterloo where wonderful.

The consistent financial support in form of Research Assistantship by the Natural Science and Engineering Research Council (NSERC) of Canada and the University Network of Excellence in Nuclear Engineering (UNENE) is gratefully appreciated and acknowledged.

The financial support in form of Teaching Assistantship by the Department of Civil and Environmental Engineering, University of Waterloo, is also gratefully appreciated.

Last but not least, words are not enough to express my thankfulness and gratitude to my adorable parents Kalliopi and Panagiotis and my loving sister Vasiliki for their incessant support, encouragement and love throughout my life and for standing by me to all my choices.

Georgios Balomenos,

Waterloo, Fall 2015

To

My Family

Table of Contents

List of Figures

Chapter 2

Chapter 3

Chapter 4

Chapter 5

Chapter 6

List of Tables

Chapter 3

Chapter 4

Chapter 5

Chapter 6

Chapter 1

Introduction

1.1 Motivation

The finite element method (FEM) is widely used in the analysis and design of the structural systems. Since uncertainties can be unavoidable in a real world problem, reliability analysis is necessary to be applied for quantifying the structural safety. Therefore, an integration of reliability analysis with the finite element analysis (FEA) is becoming popular in engineering practice, which is often termed as probabilistic finite element analysis (PFEA) or finite element reliability analysis (FERA).

In the context of FERA, basic issues are: (1) to minimize the function evaluations, especially when the evaluation of the model takes a long time, such as in a nonlinear FEA of a large scale structure; (2) to estimate as accurate as possible the probability distribution of the structural response, especially in FEA where the response function is defined in an implicit form; (3) to connect a general FEA software with a reliability platform, especially when knowledge of advanced programing languages is required for this connection.

Regarding the first issue, the reliability analysis may require an enormous amount of FEA solutions. For instance, Monte Carlo simulation (MCS) has the major advantage that accurate solutions can be obtained for any problem, but the method can become computationally expensive especially when the evaluation of the deterministic FEA takes a long time. Although MCS is versatile, well understood and easy to implement, the computational cost, i.e., the

number of required FEA-runs, in many cases can be prohibitive resulting to MCS being a barrier to the practical application of FERA.

Regarding the second issue, most reliability methods can be applied to simple structural systems which contain a small number of random variables and the limit state functions are formulated analytically, i.e., in an explicit form. In the FEA the output response can be in an implicit relation with the input random variables. Thus, even if we are able to calculate the probability statistics of the response, i.e., mean, standard deviation, etc., we have little knowledge with respect to the probability distribution of the response.

Regarding the third issue and to the best of author's knowledge, at this time there is no commercial software available that includes in its interface both finite element and reliability. Instead, the following are required to apply FERA: (1) to link general purpose FEA software, e.g., ABAQUS, with an existing reliability platform, e.g., NESSUS or ISIGHT; (2) to link a general purpose FEA program, e.g., OpenSees, with our own subroutine written in a compatible programing language, e.g., Tcl. The first approach has the ease-of-use advantage, based on the Graphical User Interface (GUI) of the reliability platforms. Thus, reliability platforms are beneficial especially for new users. The disadvantage of the first approach is the fact that it requires purchasing separately these reliability platforms and also the analyst may rely on the platforms without understanding the theoretical principles. On the other hand, the advantage of the second approach is that the analyst is not using the reliability platform as a "black-box" and also has the flexibility to program more reliability algorithms, e.g., FORM, SORM, etc., than the provided ones. The disadvantage of the second approach is that knowledge and/or experience on advanced programing languages may be prohibited for applying FERA and the analyst should have access to the source code of the deterministic analysis code.

Thus, the main motivation behind this research is to develop a computationally efficient, robust and easy to implement method, which can overcome potential issues on probabilistic FEA of structures.

1.2 Objectives and Research Significance

The goal of this research investigation is to develop a general computational framework for reliability and sensitivity analysis of structures, which are modeled and analyzed using finite elements with the consideration of uncertainties in material properties, geometry, loads, etc. The specific objectives of this research are:

- To apply a multiplicative form of dimensional reduction method (M-DRM) for approximating the structural response in practical problems.
- To estimate the probability distribution of the structural response using the M-DRM in conjunction with the maximum entropy principle, where fractional moments are considered as constraints.
- To examine the efficiency and the predictive capability of the proposed method for nonlinear FEA of large scale structures and for global sensitivity analysis.
- To connect uncertainty analysis with deterministic FEA software using programing code.
- To make use of M-DRM for examining the response variance of structures subjected to repeated earthquakes together with other input uncertainties.
- To make use of M-DRM for examining the predictive capability of current design codes and analytical models for the punching shear of reinforced concrete flat slabs.
- To investigate the relationship between the prestressing loss and the concrete strain of nuclear concrete containment wall segments.

The proposed framework for probabilistic FEA can provide us with realistic predictions. Therefore, this can be used as a basis for the development of rational criteria for serviceability and strength requirements of structures. In general, such predictions can lead to practical recommendations for future experimental, computational and analytical research programs.

1.3 Outline of the Dissertation

Chapter 2 provides an extensive literature review in reliability analysis, finite element analysis and how these two can be coupled together leading to finite element reliability analysis. The chapter closes with the basic concepts of sensitivity analysis.

Chapter 3 presents the basic concepts and the mathematical equations of the M-DRM, for calculating the statistical moments and the distribution of the response, together with sensitivity analysis. The Gauss quadrature scheme, the concept of the Maximum Entropy (MaxEnt) principle and the computational cost of M-DRM, are also presented. The required steps for applying the proposed method are illustrated through a simple example, where the punching shear resistance of a flat slab is calculated, due to uncertain input variables.

Chapter 4 presents the applicability of M-DRM for nonlinear FERA of structures under seismic loads. Two widely applicable methods are used, i.e., pushover and dynamic analysis, in order to examine the accuracy and the computational cost of M-DRM. The MCS and the first order reliability method (FORM) are also applied, while their results are used for sake of comparison with the M-DRM. Tcl programing code is developed, in order to link the OpenSees FEA software with the applied reliability methods.

Chapter 5 presents the applicability of M-DRM for nonlinear probabilistic FEA of 3D structures. The examined problem is the punching shear prediction of reinforced concrete slab-column

connections. Two reinforced concrete flat slabs (with and without shear reinforcement) are analyzed with the commercial FEA software ABAQUS. Python programing code is developed, in order to: (1) link the ABAQUS with the applied reliability methods; (2) extract the values of interest after each FEA trial. The M-DRM results are also used for sensitivity analysis and valuable observations are reported. Probabilistic analysis results using current design provisions and a punching shear model are critically compared to the M-DRM results.

Chapter 6 presents the probabilistic FEA of four prestressed concrete wall segments, which correspond to a 1/4 scale portion of a prototype nuclear containment structure. The chapter examines the probability of the average prestressing loss in tendons affecting the average hoop and axial concrete strains, in order to quantify the prestressing loss based on measured concrete strains during periodic inspection procedures, i.e., leakage rate test and/or proof test. In addition, the chapter presents two basic techniques for modeling the prestressed concrete using FEA. The proposed M-DRM is not used here, since the computational cost is affordable for the MCS.

Chapter 7 summarizes the findings and presents the conclusions of this study, together with the future research recommendations.

Chapter 2

Literature Review

2.1 Reliability Analysis

Civil engineers have to analyse and design structures that have to perform adequately during their lifetime. However, material properties, structural dimensions, applied loads, etc., may not have exactly the same observed values, even under identical conditions. Since the performance of the constructed structures depends on these values, engineers have to deal with this uncertainty (Benjamin and Cornell, 1970). In general, uncertainty is classified in two types namely aleatory and epistemic (Ang and Tang, 2007). Aleatory refers to the uncertainty related to the randomness of the natural phenomena, such as the magnitude and the duration of an earthquake. Epistemic refers to the uncertainty related to the inaccuracies of science, due to lack of knowledge and/or data (Der Kiureghian and Ditlevsen, 2009). Thus, probabilistic analysis can be used for incorporating these uncertainties in the analysis, since it allows characterizing the deterministic quantities of interest as random variables (Ditlevsen and Madsen, 1996).

Probability denotes the likelihood of occurrence of a predefined event (Melchers, 1987). Thus, the probability of failure denotes the probability that a structure will not perform adequately at a specific time, while reliability is the complement of the probability of failure as (Madsen et al., 1986).

$$Reliability = 1 - p_f \tag{2.1}$$

where p_f is the probability of failure. In structural engineering, reliability methods are usually divided in four categories as (Madsen et al., 1986; Nowak and Collins, 2000)

- Level I methods, which use partial safety factors for load and resistance in order to assure that the reliability of the structure is sufficient.
- Level II methods, which use approximate methods, such as the first order reliability method (FORM), where the probability of failure is calculated based on a limit state function.
- Level III methods, which use simulations, such as the Monte Carlo simulation (MCS), or numerical integration in order to calculate the probability of failure using the probability density function (PDF) of each input random variable.
- Level IV methods, which also take into account the cost and the benefits associated with the construction, the maintenance, the repairs, etc., of the structure. These are usually applied for structures of major economic importance, such as nuclear power plants, highway bridges, etc.

In general, reliability analysis helps engineers to judge whether or not the structure has been designed adequately (Madsen et al., 1986). Level III methods can be considered as the most accurate methods for calculating the probability of failure. However, in finite element analysis (FEA) of large scale and/or complex structures, this simulation analysis can be challenged due to the high computational cost. Thus, it is important to develop a method, which will allow the full probabilistic analysis of structures within a feasible computational time.

2.1.1 Monte Carlo Simulation

The Monte Carlo simulation (MCS) method, first presented by Metropolis and Ulam (1949), is a numerical method which solves problems by simulating random variables. The method was named after the casino games of the Monte Carlo city located at Monaco by its main originators

John von Neumann and Stanislav Ulam (Choi et al., 2007). The method requires the generator of many random (pseudo) numbers (Kroese et al., 2011). Thus, it became widely applicable with the evolution of computers (Sobol′, 1994).

The MCS has three basic steps: (1) select the distribution type of each random variable; (2) generate random numbers based on the selected distribution; (3) conduct simulations based on the generated random numbers. For the reliability analysis of structures, the limit state function can be used as (Nowak and Collins, 2000)

$$g(\mathbf{x}) = y_c - h(\mathbf{x}) \begin{cases} > 0 \Rightarrow safe\ state \\ = 0 \Rightarrow limit\ state \\ < 0 \Rightarrow failure\ state \end{cases} \tag{2.2}$$

where $g(\mathbf{x})$ is the limit state function, y_c is a safety threshold, $h(\mathbf{x})$ is the simulation result and $\mathbf{x}$ denotes the input random variables, i.e., $\mathbf{x} = x_1, x_2, \dots, x_n$. The probability of failure is then calculated approximately as (Choi et al, 2007)

$$p_f \approx N/N_f \tag{2.3}$$

where N is the total number of MCS trials and N_f is the number of trials for which the limit state function indicates a structural failure, i.e., $g(\mathbf{x}) \leq 0$. The total required trials of MCS are approximated using the binomial distribution as (Ang and Tang, 2007)

$$N \approx 1/\left(\mathrm{COV}^2 \times p_f\right) \tag{2.4}$$

where COV is the desirable coefficient of variation of the output response and p_f is the probability of failure. For civil engineering structures the probability of failure is usually between 10^{-2} to 10^{-6} (Sudret and Der Kiureghian, 2002). For instance, considering a 10% COV and an estimated probability of failure equal to 10^{-2}, the number of MCS that are needed is 10^4 trials. Thus, MCS can become computationally expensive, since its efficiency depends on the total number of required simulations.

2.1.2 First Order Reliability Method

The first order reliability method (FORM) is an approximate method for estimating the reliability index β, which is the shortest distance between the limit state function and the origin of the standard normal space (Hasofer and Lind, 1974). Thus, the input random variables **x** are transformed as uncorrelated standard random variables as (Nowak and Collins, 2000)

$$z_i = \frac{x_i - \mu_{x_i}}{\sigma_{x_i}} \tag{2.5}$$

where μ_{x_i} is the mean value and σ_{x_i} is the standard deviation of the random variable x_i.

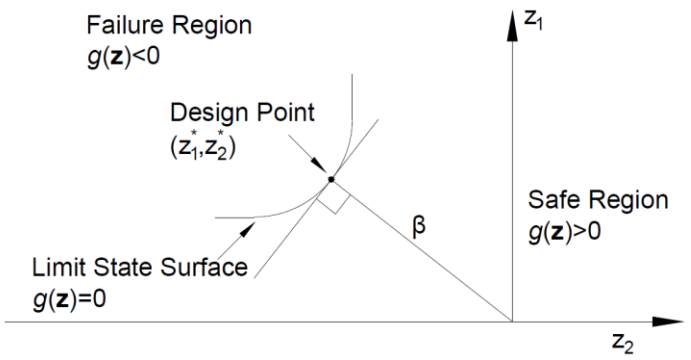

Fig. 2.1. Reliability index based on FORM.

FORM is considered as a constrained optimization problem as (Der Kiureghian and Ke, 1988)

$$\begin{cases} \textbf{Minimize}: \beta \\ \textbf{Subject to}: g(\mathbf{z}) = 0 \end{cases} \tag{2.6}$$

The above optimization can be computed using an iterative solution scheme, such as the HLRF method (Rackwitz and Fiessler, 1978), or using a numerical solution such as the solver command in Excel (Low and Tang, 1997). The probability of failure is then calculated based on the computed reliability index as (Sudret and Der Kiureghian, 2000)

$$p_f \approx \Phi(-\beta) = 1 - \Phi(\beta) \tag{2.7}$$

where Φ( ) is the standard normal cumulative distribution. Certain modifications have been proposed in literature (Liu and Der Kiureghian, 1991; Lee et al., 2002; Santosh et al., 2006) in order to improve the efficiency of the above optimization, while FORM may still not be accurate as it highly depends on the nonlinearity of the limit state function (Zhao and Ono, 1999; Sudret and Der Kiureghian, 2000; Koduru and Haukaas, 2010).

2.2 Finite Element Analysis

Partial differential equations are used to describe many engineering problems, while for arbitrary shapes these equations may not be solved by classical analytical methods (Fish and Belytschko, 2007). The finite element method (FEM) is the numerical approach which can solve approximately these partial differential equations, while the finite element analysis (FEA) is the computational technique which is used to obtain these approximate solutions (Hutton, 2004). Depending on the type of the problem, FEA can be used to analyze both structural (stress analysis, buckling, etc.) and non-structural problems (heat transfer, fluid flow, etc.) (Logan, 2007).

The term finite was coined by Clough (1960), although the starting paper of the engineering finite element method was published by Turner, Clough, Martin and Topp (Turner et al., 1956) and the FEM was initially developed to analyze structural mechanics problems (Zienkiewicz, 1995). However, it was recognized that it can be applied to any other engineering problem (Bathe, 1982). Nowadays, for structural problems the use of FEM is becoming more and more popular, since a simple personal computer can handle the analysis of an entire building (Rombach, 2011). The general steps of the FEM are (Liu and Quek, 2003): (1) to model the geometry; (2) to mesh the model (also called discretization); (3) to specify the properties of each

material; (4) to specify the boundary conditions, as well as the initial and loading conditions. Thus, the basic idea of FEA is to divide the structure into finite elements connected by nodes (Fig. 2.2) and then to obtain an approximate solution (Fish and Belytschko, 2007).

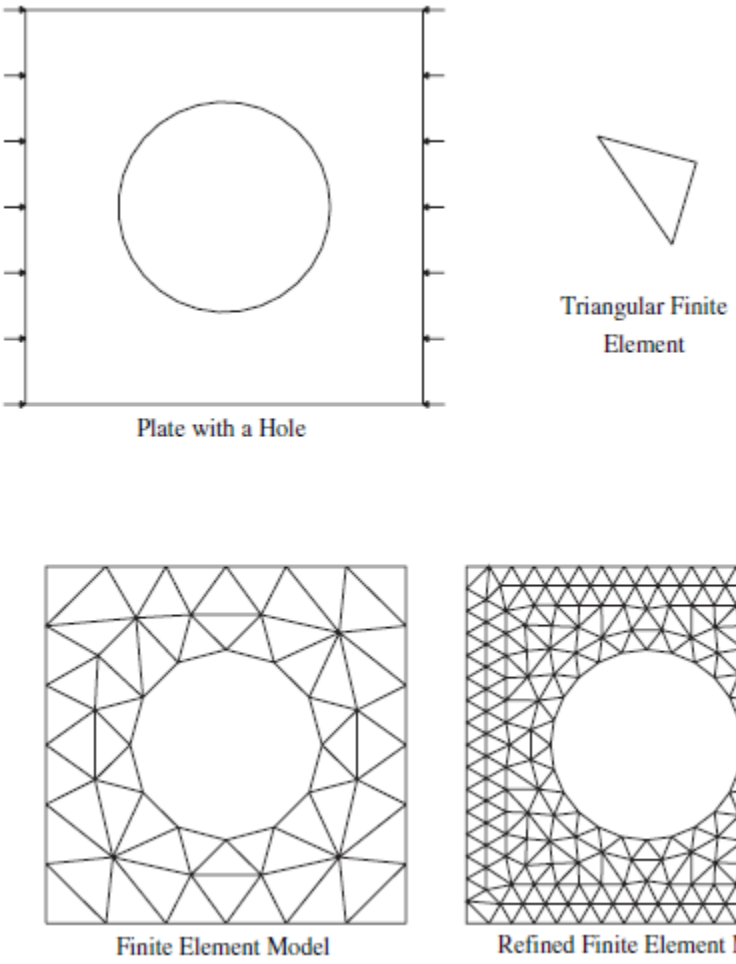

Fig. 2.2. Geometry, loads and finite element meshes (scanned from Fish and Belytschko, 2007).

This process of subdividing a complex system into their individual elements is a natural way that helps the researcher to understand its behavior (Zienkiewicz and Taylor, 2000). In addition, the progress in computer technology allows following this approach (Haldar and Mahadevan, 2000). Therefore, FEA has become a powerful tool that allows many engineering disciplines to design and analyze a wide array of practical problems. Although, this computational method permits the

accurate analysis of any large-scale engineering system, uncertainties are unavoidable when we deal with real world problems (Ang and Tang, 2007). Thus, there can be some degree of uncertainty, which has led the scientific community to recognize the importance of a stochastic approach to engineering problems (Stefanou, 2009).

2.3 Probabilistic Finite Element Analysis

The advances in computer technology make FEA applicable to complex problems (Haldar and Mahadevan, 2000). However, in order to predict the structural behaviour as realistically as possible, it should be taken into account the uncertainty in material properties, applied loads, dimensions, etc. (Stefanou, 2009). For that reason it is necessary to perform probabilistic finite element analysis (PFEA), which is often termed as finite element reliability analysis (FERA) (Haukaas and Der Kiureghian, 2004; 2006; 2007), when the probability of failure is also calculated, or stochastic finite element analysis (SFEA) (Haldar and Mahadevan, 2000; Sudret and Der Kiureghian, 2000; Stefanou, 2009), when the analysis involves random field probabilities.

At this time there is no commercial software available that has an interface including both FEA and uncertainty. Thus, in order to connect the deterministic FEA with reliability (Fig. 2.3), the first approach is to use a customized package with reliability capabilities, such as NESSUS (Thaker, et al. 2006), COSSAN (Schuëller and Pradlwarter, 2006; Patelli et al., 2012), ISIGHT (Akula, 2014) and DesignXplorer (Reh et al., 2006), which interact with the most commercial FEA software such as ABAQUS and ANSYS. More details regarding software packages, which interact with deterministic FEA software for structural reliability, can be found in a special issue of Structural Safety (Ellingwood, 2006).

Another approach is to use open source FEA software, e.g., OpenSees (McKenna et al., 2000), with reliability analysis capability (Der Kiureghian et al., 2006). A common difficulty with the second approach is that the user is required to have some experience in advanced programing languages, e.g., Tcl, in order to connect FEA with reliability analysis, since it can be a tedious task to write source code, especially for large scale and/or complex structures.

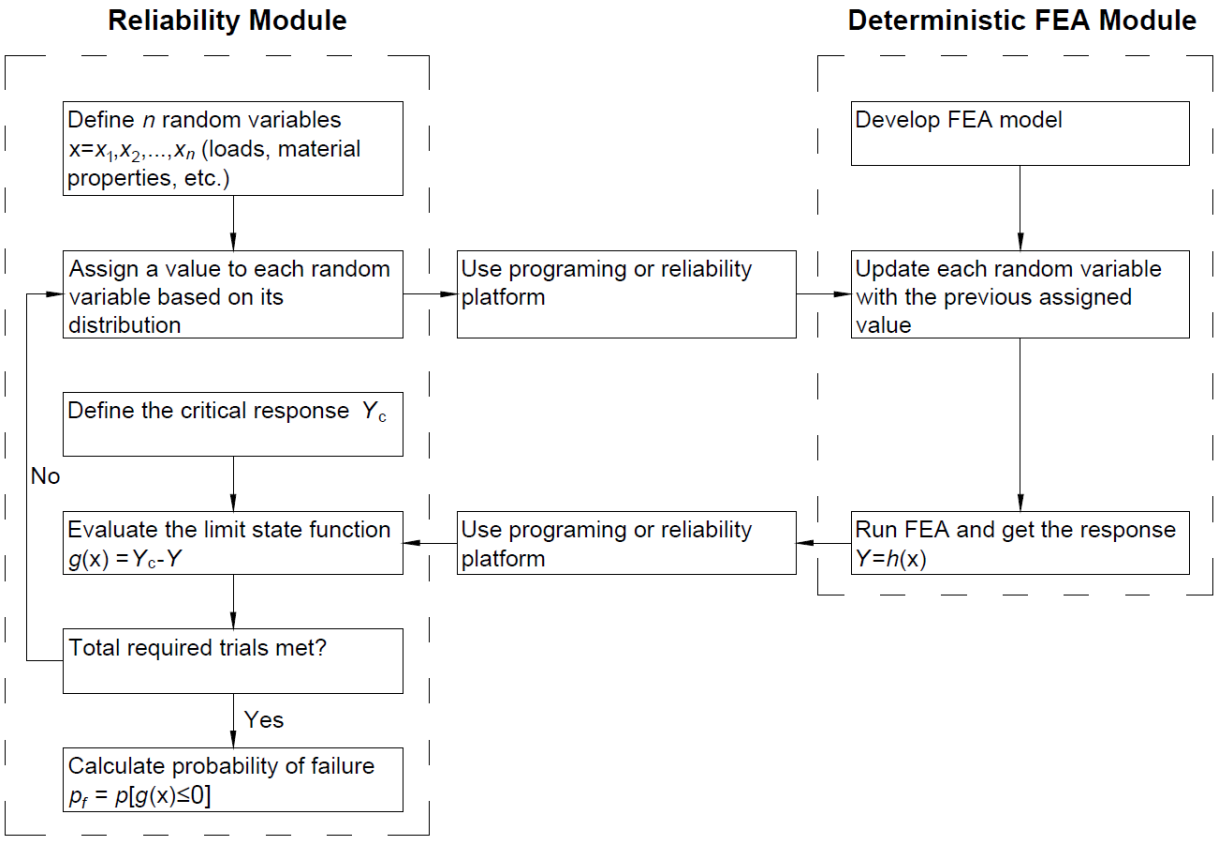

Fig. 2.3. Flowchart to connect reliability with finite element analysis.

After we establish the connection between FEA and uncertainty, we have to apply the reliability analysis. A widely known and easy to implement method for FERA is the MCS, where the deterministic FEA code is called repeatedly to simulate the structural response (Hurtado and Barbat, 1998). Then, MCS provides the statistical moments (mean and variance) primarily, as

well as the full distribution of the structural response of interest. Naturally, this approach is feasible only if the required time for each FEA run is fairly small (Papadrakakis and Kotsopoulos, 1999). In case of large scale and/or complex FEA models, approximate methods such as FORM have been used to replace MCS.

FORM evaluates the probability of failure based on a given performance function (Madsen et al. 1986). A potential drawback of FORM in FEA is that the performance function may not be available in an explicit form (Pellissetti and Schuëller, 2006). In general, FORM can be computationally efficient, though its accuracy highly depends on the degree of nonlinearity (Lopez et al., 2015) and for dynamic analysis problems is not generally feasible (Koduru and Haukaas, 2010).

2.4 Sensitivity Analysis

After applying the reliability analysis, sensitivity analysis is usually required as a diagnostic tool for the performance of the building (Saltelli et al., 2004). In other words, sensitivity analysis helps the researcher to understand which input random variable influences more and which less the output response (Castillo et al., 2008). Thus, the objective of sensitivity analysis is to quantify the variation of the output response with respect to the variation of each input random variable (Grierson, 1983). In addition, structural sensitivity analysis helps engineers to optimize the structural designs, so as structures to be economic, stable and reliable during their lifetime (Choi and Kim, 2005). Sensitivity analysis methods are usually categorized as Local and Global (Gacuci, 2003; Saltelli et al., 2008).

Local sensitivity analysis focuses on the output response uncertainty, while one input random variable varies at a time around a fixed value, i.e., nominal value (Sudret, 2008). The response

uncertainty can be measured based on numerous techniques such as finite-difference schemes, direct differentiation, etc., (Gacuci, 2003). For instance, one can use the partial derivative $\partial Y_i/\partial X_i$ of the model output function Y_i with respect to a particular random variable X_i, in order to measure the sensitivity of Y_i versus X_i. Using partial derivatives may be efficient in computational time, although it may not give accurate results when the model's degree of linearity is unknown (Saltelli et al., 2008).

Global sensitivity analysis focuses on the output response uncertainty, while input variables (considered singly or together with others) are varied simultaneously over their whole variation domain (Blatman and Sudret, 2010). Thus, it considers the entire variation domain of the input variables, contrary to Local which takes into account the variation locally, i.e., around a chosen point such as the nominal value (Gacuci, 2003). Therefore, it helps the analyst to determine all the critical parameters whose uncertainty affects most the output response (Homma and Saltelli, 1996). A state-of-the-art of Global sensitivity methods can be found in literature (Saltelli et al., 2000; 2008), which are classified as

- Regression-based methods, which estimate the relationship between two (or more) random variables (Ross, 2004), e.g., input and output, while the simplest relation between two variables is a straight line which is called linear regression (Ang and Tang, 2007). The correlation coefficient measures the degree of linearity between each input random variable and the output response, while higher the value of the coefficient of determination R^2 $(0 \leq R^2 \leq 1)$, higher the relationship (Montgomery and Runger, 2003). Thus, values of R^2 close to one indicate high influence of the input to the output. Although, with the advent of computers multiple regressions have become a quick and

easy to use tool (Morrison, 2009), in case of nonlinearity they fail to give adequate sensitivity measures (Saltelli and Sobol′, 1995).

- Variance-based methods also referred as “ANalysis Of VAriance” (ANOVA) techniques, which decompose the variance of the output to a summation variance of each input variable (Blatman and Sudret, 2010). A multi-dimensional integration describes the conditional variance of each input variable (Zhang and Pandey, 2014). Then, the correlation ratios are formulated (Sudret, 2008), which can be solved using simulation methods such as the Monte Carlo Simulation (Sobol′, 2001). The potential drawback here is the computational cost, because the ANOVA decomposition involves a series of high-dimensional integrations for each sensitivity coefficient (Zhang and Pandey, 2014). Therefore, the high dimensional model representation (HDMR) (Rabitz and Aliş, 1999) can be considered as a feasible alternative.

Chapter 3

Multiplicative Dimensional Reduction Method

3.1 Introduction

3.1.1 Background

The structural reliability analysis is conducted by modeling the structural response as a function of several input variables. For instance, when the capacity of a slab-column connection is evaluated, one output variable of interest is the punching shear strength. This can be evaluated as a function of input variables, such as the strength of concrete, the effective depth of slab, etc., which is denoted as

$$Y = h(\mathbf{x}) \tag{3.1}$$

where Y is a scalar response and $\mathbf{x}$ is a vector of input random variables, i.e., $\mathbf{x} = x_1, x_2, \dots, x_n$. Knowing the probability distribution of all variables $\mathbf{x}$, then the probability of a structural failure due to Y exceeding some critical value can be determined as (Nowak and Collins, 2000)

$$p_f = p(y_c - h(\mathbf{x}) \leq 0) \tag{3.2}$$

where p_f is the probability of failure and y_c is a critical threshold, where each response bigger than this threshold leads to structural failure. Note that the limit state function is defined as

$$g(\mathbf{x}) = y_c - h(\mathbf{x}) \tag{3.3}$$

For simplicity, the probability of failure can be further described by the following integral (Der Kiureghian, 2008)

$$p_f = \int_{\{g(\mathbf{x}) \leq 0\}} f_{\mathbf{x}}(\mathbf{x}) d\mathbf{x} \tag{3.4}$$

where $f_{\mathbf{x}}(\mathbf{x})$ is the joint probability density function (PDF) of the previous defined vector $\mathbf{x}$ and $\{g(\mathbf{x}) \leq 0\}$ represents the failure domain. According to Li and Zhang (2011), the above integral can be computed by using: (1) Direct integration, but the joint PDF is hardly available for real problems as it is defined implicitly and the dimension of the integral is usually large as it is equal to the number of uncertain parameters; (2) Simulations, such as Monte Carlo simulation (MCS), but this method usually requires considerably effort and computational time; (3) Approximate methods, such as fist- and second- order reliability methods (FORM and SORM), but they may give inaccurate solutions due to the nonlinearity of the limit state function.

The method of moment is another way for performing structural reliability (Li and Zhang, 2011), since it requires no iterations contrary to approximate methods and much less computational cost contrary to simulations. However, considering an L-point scheme to evaluate an n-dimensional integration results to L^n evaluations of the response Y, which may lead to an enormous computational cost. The point estimate method (Rosenblueth, 1975) and the Taylor series approximation can efficiently deal with this problem, while another recent approach is the high-dimensional model representation (HDMR) (Rabitz and Aliş, 1999; Li et al., 2001) or also called dimensional reduction method (DRM) (Rahman and Xu, 2004; Xu and Rahman, 2004). Using DRM a multivariate function is expressed as sum of lower order functions in an increasing hierarchy, thus can be called additive DRM (A-DRM). On the other hand, multiplicative DRM (M-DRM) expresses a multivariate function as product of lower order functions.

The idea of the multiplicative form of DRM, also called as factorized HDMR, was first presented by Tunga and Demiralp (2004; 2005). The analysis procedure requires two basic steps. First, A-DRM and M-DRM can be used to compute the integer moments, e.g., first and second integer

moment corresponds to the mean value and variance of the response, respectively. Then, using the Maximum Entropy (MaxEnt) principle (Jaynes, 1957) with fractional moment constraints (Inverardi and Tagliani, 2003), A-DRM and M-DRM can be used to compute the fractional moments which are used to estimate the distribution of response. Both A-DRM and M-DRM can perform the previous first step, while it has been shown that A-DRM is not practical for the computation of fractional moments (Zhang and Pandey, 2013). Thus, only M-DRM can be used, since it simplifies the computation of both integer and fractional moments of the response.

For both A-DRM and M-DRM, the response function $Y = h(\mathbf{x})$ is evaluated with respect to a reference fixed input point, known as the cut point, with coordinates c (Li et al., 2001)

$$c = (c_1, c_2, \dots, c_n) \tag{3.5}$$

where $c_1, c_2, \dots, c_n$ corresponds to the mean value of each random variables $x_1, x_2, \dots, x_n$.

Thus, an i^{th} cut function is obtained by fixing all the input random variables, except x_i, at their respective cut point coordinates, which are generally chosen as the mean values $(c_1, c_2, \dots, c_n)$ such that

$$h_i(x_i) = h(c_1, \dots, c_{i-1}, x_i, c_{i+1}, \dots, c_n) \tag{3.6}$$

Chowdhury et al. (2009a) used HDMR as a response surface approximation of a finite element method (FEM) code, where each cut function was discretely calculated at a finite number of points. Then each cut function was estimated at any other intermediate point by developing an interpolation scheme. Later, Rao et al. (2009; 2010) combined this approach with a FEM model of a large containment structure. Also, Chowdhury et al. (2009b) compared the response surface generation by HDMR and factorized HDMR. This chapter presents a new approach where M-DRM computes directly the fractional moments of the response and then these fractional moments are used to derive the distribution of the response without the need of simulations.

3.1.2 Objective

The objective of this chapter is to present a computationally efficient, robust and easy to implement method for finite element reliability and sensitivity analysis of structures, which can overcome potential issues, as they were introduced in the previous section. To achieve this objective, M-DRM is adopted as a compact surrogate of a finite element model of a structure. Thus, a new approach is presented in which fractional moments of the response are directly computed using M-DRM and the response distribution is derived without simulations, as discussed in the following sections. Monte Carlo simulation (MCS) has the major advantage that accurate solutions can be obtained for any problem, but when it comes to large scale or complex structures, where even the deterministic FEA takes too long, the proposed method can be proved efficient and the only suitable.

3.1.3 Organization

The organization of this chapter is as follows. Section 3.2, firstly presents the mathematic expression of M-DRM, which is used to approximate the response function. Then, section 3.2 illustrates how this expression is further adopted, in order to calculate the statistical moments and the probability distribution of the response. Section 3.2 also shows how many trials are required for the M-DRM implementation and how the M-DRM idea is further implemented for global sensitivity analysis. Section 3.3 presents the Gauss quadrature scheme, which is actually the first step that has to be performed before we apply the proposed M-DRM. Section 3.4 illustrates the implementation of M-DRM, through a simple example. For sake of comparison, MCS has been also performed in section 3.4. Finally, conclusions are summarized in Section 3.5.

3.2 Multiplicative Dimensional Reduction Method

3.2.1 Background

According to the additive DRM (A-DRM) method (Rabitz and Aliş, 1999; Li et al., 2001; Rahman and Xu, 2004; Chowdhury et al., 2009a), a scalar function is approximated in an additive form as

$$Y = h(\mathbf{x}) \approx \sum_{i=1}^{n} h_i(x_i) \ - (n-1)h_0 \tag{3.7}$$

or equivalently

$$Y = h(\mathbf{x}) \approx h_1(x_1) + h_2(x_2) + \cdots + h_n(x_n) \ - (n-1)h_0 \tag{3.8}$$

where $h_i(x_i)$ is an one-dimensional cut function as defined in Eq. (3.6) and h_0 defines the response when all random variables are fixed to their mean values, i.e.,

$$h_0 = h(c_1, c_2, \dots, c_n) = a\ constant \tag{3.9}$$

M-DRM follows the same approach with the A-DRM, but first the response function is transformed logarithmically, which derives the multiplicative approximation of the response function as

$$Y = h(\mathbf{x}) \approx h_0^{(1-n)} \times \prod_{i=1}^{n} h_i(x_i) \tag{3.10}$$

or equivalently

$$Y = h(\mathbf{x}) \approx h_0^{(1-n)} \times [h_1(x_1) \times h_2(x_2) \times \dots \times h_n(x_n)] \tag{3.11}$$

Thus, according to the M-DRM method a scalar function is approximated in a product form as shown in Eq. (3.10). The main benefit of the product form is the simplification of the computation of both integer and fractional moments of the response, as shown in the next section.

3.2.2 Evaluation of the Response Statistical Moments

Using M-DRM representation, a k^{th} statistical moment of the response function can be approximated as

$$E[Y^k] = E\left[\left(h(\mathbf{x})\right)^k\right] \approx E\left[\left(h_0^{(1-n)} \times \prod_{i=1}^{n} h_i(x_i)\right)^k\right] \tag{3.12}$$

or equivalently

$$E[Y^k] \approx \left(h_0^{(1-n)}\right)^k \times E\left[\left(h_1(x_1)\right)^k\right] \times E\left[\left(h_2(x_2)\right)^k\right] \times \ldots \times E\left[\left(h_2(x_2)\right)^k\right] \tag{3.13}$$

where the mathematical expectation operation is denoted as $E[\ ]$ and for $k = 1$, $E[Y^k] = E[Y]$ is the expected value of *Y*, i.e., the mean value of *Y*. Assuming that all input random variables are independent, Eq. (3.12) can be written as

$$E[Y^k] \approx h_0^{k(1-n)} \prod_{i=1}^{n} E\left[\left(h_i(x_i)\right)^k\right] \tag{3.14}$$

Then, we define the mean and mean square of an i^{th} cut function as ρ_i and θ_i , respectively, as

$$\rho_i = E[h_i(x_i)] \quad \text{and} \quad \theta_i = E[\left(h_i(x_i)\right)^2] \tag{3.15}$$

Using Eqs. (3.15) and (3.12), the mean (μ_Y) and the mean square (μ_{2Y}) of *Y* can be approximated as

$$\begin{aligned} \mu_Y = E[Y] &\approx h_0^{(1-n)} \times \prod_{i=1}^{n} \rho_i \\ \mu_{2Y} = E[Y^2] &\approx h_0^{(2-2n)} \times \prod_{i=1}^{n} \theta_i \end{aligned} \tag{3.16}$$

Then, the variance (V_Y) of the response can be obtained as

$$V_Y = \mu_{2Y} - (\mu_Y)^2 \approx (\mu_Y)^2 \times \left[\left(\prod_{i=1}^{n} \frac{\theta_i}{\rho_i^2}\right) - 1\right] \tag{3.17}$$

where the standard deviation (σ_Y) of the response function $Y = h(\boldsymbol{x})$ can be calculated as the square root of the variance. The evaluation of the mean or any other k^{th} product moment of response requires the calculation of a k^{th} moment of all the cut functions through one dimensional integration. The numerical integration can be significantly optimized using the Gauss quadrature formulas. For example, a k^{th} moment of an i^{th} cut function can be approximated as a weighted sum

$$E\left[\left(h_i(x_i)\right)^k\right] = \int_{X_i} [h(x_i)]^k f_i(x_i) dx_i \approx \sum_{j=1}^{L} w_j \left[h_i(x_j)\right]^k \tag{3.18}$$

where L is the number of the Gauss quadrature points, x_j and w_j are the coordinates and weights, respectively, of the Gauss quadrature points $(j = 1, \dots, L)$ and h_i $(i = 1,2, \dots, n)$ is the structural response when i^{th} cut function is set at j^{th} Gauss quadrature point. A set of commonly used Gauss quadrature points is given in a subsequent section.

3.2.3 Response Probability Distribution using Max Entropy Method

After obtaining the mean and variance of response, the problem that arises is the estimation of its probability distribution. Thus, we use the Maximum Entropy (MaxEnt) principle (Jaynes, 1957) with fractional moment constraints (Inverardi and Tagliani, 2003), i.e., $[Y^\alpha] = M_Y^\alpha$, where α is a fraction and not an integer. The MaxEnt principle states that by maximizing the Shannon (1949) entropy subjected to constraints supplied by the available information, e.g., moments of random variables, the most unbiased probability distribution of a random variable can be estimated.

The true entropy $(H[f])$ of the response variable Y is defined in terms of its probability density function $\left(f_Y(y)\right)$ as

$$H[f] = -\int_Y f_y(y) \ln[f_Y(y)]\, dy \tag{3.19}$$

The Lagrangian function associated with the MaxEnt problem is given as

$$\begin{aligned} \mathcal{L}[\lambda, \alpha; f_Y(y)] = &-\int_Y f_Y(y) \ln[f_Y(y)] dy - (\lambda_0 - 1)\left[\int_Y f_Y(y)\, dy - 1\right] \\ &- \sum_{i=1}^{m} \lambda_i \left[\int_Y y^{\alpha_i} f_Y(y) dy - M_Y^{\alpha_i}\right] \end{aligned} \tag{3.20}$$

where $\lambda = [\lambda_0, \lambda_1, \dots, \lambda_m]^T$ are the Lagrange multipliers and $\alpha = [\alpha_0, \alpha_1, \dots, \alpha_m]^T$ are the fractions associated with the fractional moments. For optimal solution, we apply the following key condition

$$\frac{\partial\, \mathcal{L}[\lambda, \alpha; f_Y(y)]}{\partial f_Y(y)} = 0 \tag{3.21}$$

This leads to the estimated PDF $\left(\hat{f}_Y(y)\right)$ of the true PDF $\left(f_Y(y)\right)$, which is defined as

$$\hat{f}_Y(y) = \exp\left(-\sum_{i=0}^{m} \lambda_i y^{\alpha_i}\right) \tag{3.22}$$

For $i = 0$, $\alpha_0 = 0$ and λ_0 is derived, based on the normalization condition that the integration of the PDF must be equal to one, as

$$\lambda_0 = ln\left[\int_Y \exp\left(-\sum_{i=1}^{m} \lambda_i y^{\alpha_i}\right) dy\right] \tag{3.23}$$

MaxEnt optimization procedure with integer moments constraints has been used (Ramírez and Carta, 2006), but the estimation error increases as the order of the integer moments increases (Pandey and Zhang, 2012). In order to overcome this, here we use fractional moments

constraints during the MaxEnt optimization, so as to obtain the estimated probability distribution. Furthermore, in contrast with integer moments, it has been shown that just a few fractional moments are extremely effective in summarizing the entire distribution (Pandey and Zhang, 2012; Zhang and Pandey, 2013). The fractional moment of a positive random variable Y is defined as (Inverardi and Tagliani, 2003)

$$E[Y^{\alpha}] = M_Y^{\alpha} = \int_Y y^{\alpha} f_Y(y)\, dy \tag{3.24}$$

where α is a real number. An interesting point is that M-DRM provides a convenient method for the estimation of a fractional moment using Eq. (3.14) as

$$M_Y^{\alpha} \approx \left(h_o{}^{(1-n)}\right)^{\alpha} \times E\left[\left(h_1(x_1)\right)^{\alpha}\right] \times E\left[\left(h_2(x_2)\right)^{\alpha}\right] \times \ldots \times E\left[\left(h_n(x_n)\right)^{\alpha}\right] \tag{3.25}$$

where h_0 represents the system response which is evaluated at the cut point and is calculated when all random variables are set equal to their mean values, n $(i = 1,2, \ldots, n)$ is the number of random variables and each expected value $E[\ ]$ is calculated similar to Eq. (3.18) as

$$E\left[\left(h_i(x_i)\right)^{\alpha}\right] \approx \sum_{j=1}^{L} w_j \left[h_i(x_j)\right]^{\alpha} \tag{3.26}$$

A novel aspect of the computational approach is that the fractions α_i $(i = 1,2, \ldots, m)$ do not need to be specified a priori, since they are calculated as a part of the entropy maximization procedure (Inverardi and Tagliani, 2003). In order to implement the idea of the MaxEnt optimization with fractional moments, an alternate formulation is used based on the minimization of the Kullback-Leibler (K−L) divergence, also called cross-entropy, between the true PDF $\left(f_Y(y)\right)$ and the estimated PDF $\left(\hat{f}_Y(y)\right)$ as (Kroese et al., 2011)

$$K\left[f, \hat{f} \right] = \int_Y f_Y(y) \ln\left[f_Y(y) \,/\, \hat{f}_Y(y)\right] dy$$
$$= \int_Y f_Y(y) \ln[f_Y(y)] dy - \int_Y f_Y(y) \ln\left[\hat{f}_Y(y)\right] dy \tag{3.27}$$

Substituting $H[f]$ from Eq. (3.19) and $\hat{f}_X(x)$ from Eq. (3.22) into Eq. (3.27) and taking into account Eq. (3.24), the K−L divergence is further written as

$$K\left[f, \hat{f} \right] = -H[f] + \lambda_0 + \sum_{i=1}^{m} \lambda_i M_Y^{\alpha_i} \tag{3.28}$$

The entropy ($H[f]$) of the true PDF is independent of λ and α. Thus, the K−L minimization implies the minimization of the following function

$$I(\lambda, \alpha) = K\left[f, \hat{f} \right] + H[f] = \lambda_0 + \sum_{i=1}^{m} \lambda_i M_Y^{\alpha_i} \tag{3.29}$$

Therefore, the MaxEnt parameters, i.e., the Lagrange multipliers (λ_i) and the fractional exponents (α_i), are obtained by applying the following optimization

$$\begin{cases} \textbf{Find}: \{\alpha_i\}_{i=1}^{m} \quad \{\lambda_i\}_{i=1}^{m} \\ \textbf{Minimize}: I(\lambda, \alpha) = \ln\left[\int_Y \exp\left(-\sum_{i=1}^{m} \lambda_i y^{\alpha_i}\right) dy\right] + \sum_{i=1}^{m} \lambda_i M_Y^{\alpha_i} \end{cases} \tag{3.30}$$

which is implemented in MATLAB using the simplex search method (Lagarias et al., 1998).

3.2.4 Computational Effort

M-DRM combined with the Gaussian quadrature results to a remarkable reduction of the number of evaluations of the response function. Suppose that the response is a function of n independent random variables and that an L-point Gauss quadrature is adopted for integration. All the moments of a cut function $h_i(x_i)$ can be calculated from L evaluations of the response. Thus, nL

response evaluations are required for all moments of all cut functions. An additional function evaluation is required to calculate h_0 (see Eq. (3.9)). Thus, an M-DRM based analysis requires only $(nL + 1)$ function evaluations to calculate all the moments, as well as the probability distribution of the response. For example, a problem with 40 random variables and a 7 point quadrature scheme will require 281 function evaluations.

In fact the numerical analysis is modular and it can be divided into two independent steps. In the first step, an input grid can be defined and all required function evaluations can be carried out using any suitable computer program. In the second step, these functions evaluations are used to calculate the moments and to estimate the probability distribution via the entropy maximization.

3.2.5 Global Sensitivity Analysis

3.2.5.1 Primary Sensitivity Coefficient

The influence of an input random variable x_i with respect to the output response Y, can be measured using the conditional variance $VAR\{E_{-i}[Y|x_i\,]\}$ as (Saltelli and Sobol′, 1995)

$$S_i = \frac{VAR\{E_{-i}[Y|x_i\,]\}}{VAR[Y]} = \frac{V_i\{E_{-i}[Y|x_i\,]\}}{V_Y} \qquad (\,0 \le S_i \le 1) \tag{3.31}$$

where S_i is the the primary sensitivity coefficient, i.e., the main effect of x_i on Y and E_{-i} denotes the expectation operation, i.e., the mean values, over all the variables except the random variable x_i.

The variance can be expressed as a difference between the mean square, $E[Y^2]$, and the square of the first product moment, $(E[Y])^2$, (Ang and Tang, 2007). Thus, S_i can be further described as

$$S_i = \frac{E_{-i}[Y^2|x_i] - \{E_{-i}[Y|x_i]\}^2}{V_Y} \tag{3.32}$$

where the conditional expectations $E_{-i}[Y^2|x_i]$ and $E_{-i}[Y|x_i]$ respectively denote the second $(k = 2)$ and the first $(k = 1)$ moment of response Y, while varying only x_i and holding other input variables fixed at the cut point c.

Using the M-DRM approximation, i.e., Eq. (3.12), the conditional expectations $E_{-i}[Y|x_i]$ is described as

$$\begin{aligned} E_{-i}[Y|x_i] &\approx E_{-i}\left[h_0^{(1-n)} \times \prod_{i=1}^{n} h_i(x_i)\right] \\ &= E\left[h_0^{(1-n)} \times h_i(x_i) \times \prod_{k=1,k\neq i}^{n} h_k(x_k)\right] \\ &= h_0^{(1-n)} \times E[h_i(x_i)] \times \prod_{k=1,k\neq i}^{n} E[h_k(x_k)] \end{aligned} \tag{3.33}$$

Using Eq. (3.15), the conditional expectation $E_{-i}[Y|x_i]$ can be further described as

$$E_{-i}[Y|x_i] \approx h_0^{(1-n)} \times E[h_i(x_i)] \times \prod_{k=1,k\neq 1}^{n} \rho_k \tag{3.34}$$

Using Eq. (3.15) and Eq. (3.34), the conditional expectation $E_{-i}[Y^2|x_i]$ can be described as

$$E_{-i}[Y^2|x_i] \approx h_0^{(2-2n)} \times E\left[\left(h_i(x_i)\right)^2\right] \times \left(\prod_{k=1,k\neq 1}^{n} \rho_k\right)^2 \tag{3.35}$$

or equivalently

$$E_{-i}[Y^2|x_i] \approx h_0^{(2-2n)} \times \theta_i \times \prod_{k=1,k\neq 1}^{n} \rho_k^2 \tag{3.36}$$

Using Eq. (3.15) and Eq. (3.34), the conditional expectation $\{E_{-i}[Y|x_i]\}^2$ can be described as

$$\{E_{-i}[Y|x_i]\}^2 \approx h_0^{(2-2n)} \times \{E[h_i(x_i)]\}^2 \times \left(\prod_{k=1,k\neq 1}^{n} \rho_k\right)^2 \tag{3.37}$$

or equivalently

$$\{E_{-i}[Y|x_i]\}^2 \approx h_0^{(2-2n)} \times \rho_i^2 \times \prod_{k=1,k\neq 1}^{n} \rho_k^2 \tag{3.38}$$

Recall that the product of the square of the first moment for all the cut functions i can be expanded as follows

$$\prod_{i=1}^{n} \rho_i^2 = \rho_i^2 \times \prod_{k=1,k\neq 1}^{n} \rho_k^2 \tag{3.39}$$

Substituting Eqs (3.17), (3.36), (3.38) into Eq. (3.32) and taking into account Eq. (3.39), the primary sensitivity coefficient S_i takes its final form as

$$S_i \approx \frac{(\theta_i/\rho_i^2) - 1}{(\prod_{i=1}^{n} \theta_i/\rho_i^2) - 1} \tag{3.40}$$

3.2.5.2 Total Sensitivity Coefficient

The total sensitivity coefficient takes into account the interactions between the input random variables, contrary to the primary sensitivity coefficient, and should be used when the aim is to identify the non-influential random variables in a model, rather than prioritizing the most influential ones (Saltelli et al., 2008). Homma and Saltelli (1996) first proposed the concept of the total sensitivity index, which focuses on how much the variance is reduced when all input random variables except x_i are fixed to their mean values. This variance reduction is defined as $V_{-i}[E_i(Y|x_{-i})]$, where here is defined a sub-vector x_{-i} of $(n-1)$ elements, which contains all the elements of x except x_{-i}. Thus, the remaining variance V_{Ti} of the model output Y after fixing x_i, is given as (Saltelli et al., 2008)

$$V_{Ti} = V_Y - V_{-i}[E_i(Y|x_{-i})] \tag{3.41}$$

Similar to Eq. (3.32) and considering the total variance identity $V_Y = V_{-i}[E_i(Y|x_{-i})\,] + E_{-i}[V_i(Y|x_{-i})\,]$, the total sensitivity coefficient S_{Ti} is defined as (Saltelli et al., 2008)

$$S_{Ti} = \frac{V_Y - V_{-i}[E_i(Y|x_{-i})\,]}{V_Y} = \frac{E_{-i}[V_i(Y|x_{-i})\,]}{V_Y} \tag{3.42}$$

In order to evaluate S_{Ti}, the conditional variance $V_i[Y|x_{-i}]$ has to be calculated first, similar to Eq. (3.32), recalling that the variance can be expressed as a difference between the second moment and the square of the first moment as (Ang and Tang, 2007)

$$V_i[Y|x_{-i}] = E_i[Y^2|x_{-i}] - \{E_i[Y|x_{-i}\,]\}^2 \tag{3.43}$$

Using the M-DRM approximation, i.e., Eq. (3.12), the conditional expectations $E_i[Y|x_{-i}]$ is expressed as

$$\begin{aligned} E_i[Y|x_{-i}] &\approx E\left[h_0^{(1-n)} \times \prod_{k=1,k\neq i}^{n} \left(h_k(x_k) \times h_i(x_i)\right)\right] \\ &= h_0^{(1-n)} \times E[h_i(x_i)] \times \prod_{k=1,k\neq 1}^{n} E[h_k(x_k)] \end{aligned} \tag{3.44}$$

Using Eq. (3.15) and Eq. (3.44), the conditional expectations $E_i[Y^2|x_{-i}]$ can be described as

$$E_i[Y^2|x_{-i}] \approx h_0^{(2-2n)} \times E\left[\left(h_i(x_i)\right)^2\right] \times \prod_{k=1,k\neq 1}^{n} E\left[\left(h_k(x_k)\right)^2\right] \tag{3.45}$$

or equivalently

$$E_i[Y^2|x_{-i}] \approx h_0^{(2-2n)} \times \theta_i \times \prod_{k=1,k\neq 1}^{n} \theta_k^2 \tag{3.46}$$

Using Eq. (3.15) and Eq. (3.44), the conditional expectations $\{E_i[Y|x_{-i}\,]\}^2$ can be described as

$$\{E_i[Y|x_{-i}\,]\}^2 \approx h_0^{(2-2n)} \times \{E[h_i(x_i)]\}^2 \times \prod_{k=1,k\neq 1}^{n} E\left[\left(h_k(x_k)\right)^2\right] \tag{3.47}$$

or equivalently

$$\{E_i[Y|x_{-i}\,]\}^2 \approx h_0^{(2-2n)} \times \rho_i^2 \times \prod_{k=1,k\neq 1}^{n} \theta_k^2 \tag{3.48}$$

Substituting Eqs (3.46), (3.48) into Eq. (3.43), conditional variance $V_i[Y|x_{-i}]$ is calculated as

$$V_i[Y|x_{-i}] \approx h_0^{(2-2n)} \times \left(\prod_{k=1,k\neq 1}^{n} \theta_k^2 \right) \times (\theta_i - \rho_i^2) \tag{3.49}$$

Subsequently, the expectation of the previous conditional variance, $E_{-i}[V_i(Y|x_{-i})\,]$, is obtained as

$$E_{-i}[V_i(Y|x_{-i})\,] \approx h_0^{(2-2n)} \times \left(\prod_{k=1,k\neq 1}^{n} \theta_k^2 \right) \times (\theta_i - \rho_i^2) \tag{3.50}$$

Recall that the product of the mean square for all the cut functions i can be expanded as follows

$$\prod_{i=1}^{n} \theta_i^2 = \theta_i^2 \times \prod_{k=1,k\neq 1}^{n} \theta_k^2 \tag{3.51}$$

Substituting Eqs (3.17), (3.50) into Eq. (3.42) and taking into account Eq. (3.51) the total sensitivity coefficient S_{Ti} takes its final form as

$$S_{Ti} \approx \frac{1 - (\rho_i^2/\theta_i)}{1 - (\prod_{i=1}^{n} \rho_i^2/\theta_i)} \tag{3.52}$$

By definition $S_{Ti} \geq S_i$, where $S_{Ti} = S_i$ when the random variable i does not have any interaction with any other input random variable. Thus, the difference $S_{Ti} - S_i$ measures how much the random variable i interacts with any other input random variable. $S_{Ti} = 0$ implies that the random variable i is non-influential, thus it does not affect the variance of the output and it can be fixed anywhere in its distribution. $\sum_i S_i = 1$ for additive models, $\sum_i S_i < 1$ for non-additive models and the difference $1 - \sum_i S_i$ indicates the presence of interactions within the model, i.e., $1 - \sum_i S_i = 0$ shows no presence of interactions, where $\sum_i S_i$ denotes the summation of all the S_i. Always $\sum_i S_{Ti} \geq 1$ where $\sum_i S_{Ti} = 1$ for a perfectly additive model (Saltelli et al., 2008).

3.3 Gauss Quadrature Scheme

The numerical integration of a function can be optimized by using the scheme of the Gauss quadrature. For instance, for the case of a Normal variable the Gauss-Hermite integration scheme can be used as shown in Table 3.1 (Zhang and Pandey, 2013).

For example, the Gauss-Hermite quadrature involves the approximation of an integral of the following form (Beyer, 1987; Kythe and Schäferkotterr, 2004; Zwillinger, 2011)

$$\int f(\mathbf{x})d\mathbf{x} = \int e^{-x^2} h(\mathbf{x})d\mathbf{x} \tag{3.53}$$

where according to Table 3.1 the Gauss-Hermite integral is approximated as

$$\int e^{-x^2} h(\mathbf{x})d\mathbf{x} \approx \sum_{j=1}^{L} w_j \, h(x_j) \tag{3.54}$$

where L is the number of evaluation points and w_j $(j = 1, \dots, L)$ are known as Gauss-Hermite Weights. Essentially, the function $h(x_j)$ is valuated based on a number of chosen evaluation points x_j and then the integral can be approximated as a weighted sum.

Gauss Points (z_j), also called abscissae, and Gauss Weights (w_j) of the five order rule $(L = 5)$ of Gauss-Legendre, Gauss-Hermite and Gauss-Laguerre quadratures, are summarized in Table 3.2. In case that more orders $(L > 5)$ of Gauss Points (z_j) and Gauss Weights (w_j) according to other orthogonal polynomials are needed, these can be found in literature (Davis and Rabinowitz, 1984; Beyer, 1987; Kythe and Schäferkotterr, 2004; Zwillinger, 2011).

For the case of the standard Normal random variable *Z*, the Gauss-Hermite points can be used, where its probability density function (PDF) is calculated as

$$f(z) = \frac{1}{\sqrt{2\pi}} \exp\left(-\frac{z^2}{2}\right) \tag{3.55}$$

So, a general Normal random variable X can be related to the standard Normal random variable Z with the following equation:

$$X = \mu + \sigma Z \tag{3.56}$$

where μ is the mean value and σ is the standard deviation of the Normal distribution. According to Eq. (3.56), the Gauss-Hermite point for X $\left(x_j\right)$ can be related to the Gauss-Hermite point for Z $\left(z_j\right)$ via the following transformation

$$x_j = \mu + \sigma z_j \tag{3.57}$$

where z_j are the Gauss points obtained from Table 3.2.

Furthermore, the Lognormal distribution is used when a random variable cannot take a negative value. Thus, if ln(X) follows the Normal distribution then X follows the Lognormal, where its PDF is calculated as (Ang and Tang, 2007)

$$f(x) = \frac{1}{x\,\zeta\,\sqrt{2\pi}}\,\exp\left(-\frac{[\ln(x) - \lambda]^2}{2\,\zeta^2}\right) \tag{3.58}$$

where ζ is the scale parameter and λ is the shape parameter of the Lognormal distribution, which are related to the Normal distribution parameters via the following equations

$$\lambda = \ln(\mu) - \left(\frac{1}{2}\,\zeta^2\right) \text{ and } \zeta = \sqrt{\ln\left(1 + \frac{\sigma^2}{\mu^2}\right)} \tag{3.59}$$

Thus, a Lognormal random variable X can be related to the standard Normal random variable Z with the following equation

$$Z = \frac{\ln(X) - \lambda}{\zeta} \tag{3.60}$$

According to Eq. (3.60), the Gauss-Hermite point for X $\left(x_j\right)$ can be related to the Gauss-Hermite point for Z $\left(z_j\right)$ via the following transformation

$$x_j = \exp(\lambda + \zeta\, z_j) \tag{3.61}$$

where z_j are the Gauss points obtained from Table 3.2.

Using Eqs. (3.57) and (3.61) function evaluation points x_j can be determined for any random variable *X* with Normal and Lognormal PDFs, respectively. The resulting function output $h(x_j)$ from each evaluation point x_j is then multiplied by the corresponding Gauss-Hermite Weights w_j and the resultant set of the of values (after the multiplication) are summed to yield the approximation of the integral shown in Eq. (3.54).

Table 3.1. Gaussian integration formula for the one-dimensional fraction moment calculation.

Distribution	Support Domain	Gaussian Quadrature	Numerical integration Formula
Uniform	[a, b]	Gauss-Legendre	$\sum_{j=1}^{L} w_j \left[\frac{1}{2} h\left(\frac{b-a}{2} z_j + \frac{b+a}{2}\right)\right]^k$
Normal	(-∞, +∞)	Gauss-Hermite	$\sum_{j=1}^{L} w_j \left[h(\mu + \sigma\, z_j)\right]^k$
Lognormal	(0, +∞)	Gauss-Hermite	$\sum_{j=1}^{L} w_j \{\, h[exp(\mu + \sigma\, z_j)]\}^k$
Exponential	(0, +∞)	Gauss-Laguerre	$\sum_{j=1}^{L} w_j \left[h(z_j/\lambda)\right]^k$
Weibull	(0, +∞)	Gauss-Laguerre	$\sum_{j=1}^{L} w_j \left[h\left(\theta\, z_j^{(1/\delta)}\right)\right]^k$

Table 3.2. Weights and points of the five order Gaussian quadrature rules.

Gaussian rules	*L*	1	2	3	4	5
Gauss-Legendre	w_j	0.23693	0.47863	0.56889	0.47863	0.23693
	z_j	-0.90618	-0.53847	0	0.53847	0.90618
Gauss-Hermite	w_j	0.01126	0.22208	0.53333	0.22208	0.01126
	z_j	-2.85697	-1.35563	0	1.35563	2.85697
Gauss-Laguerre	w_j	0.52176	0.39867	0.07594	0.00361	0.00002
	z_j	0.26356	1.4134	3.5964	7.0858	12.641

Note: w_j= Gauss weight; z_j= Gauss point; $L = 5$ for the fifth order Gauss quadrature rule.

3.4 M-DRM Implementation

The flowchart in Fig. 3.1 is followed to demonstrate the M-DRM implementation in this section, where for simplicity the response Y is calculated analytically instead of using FEA.

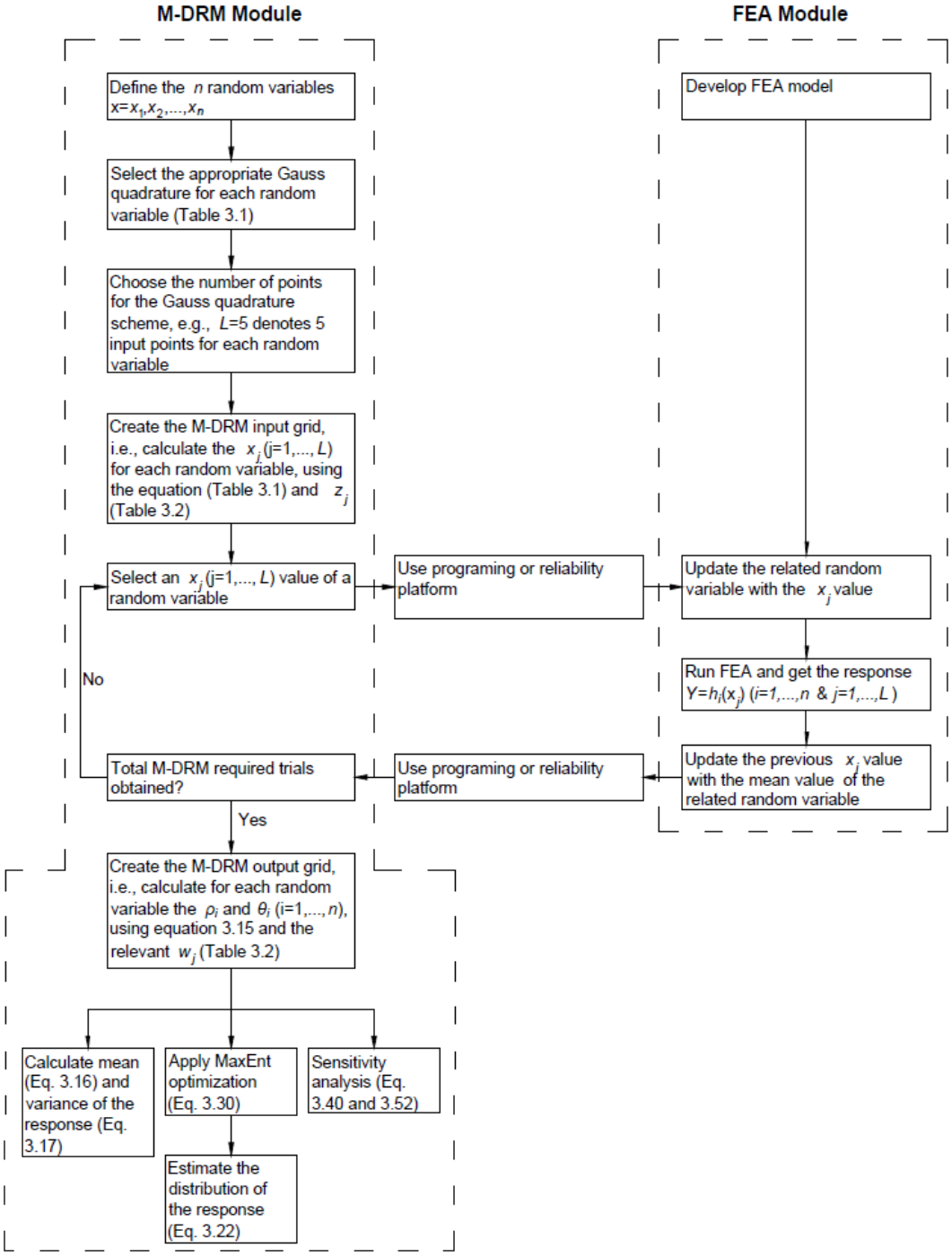

Fig. 3.1. Flowchart to connect M-DRM with finite element analysis.

3.4.1 Calculation of the Response

The implementation of M-DRM is demonstrated using the following analytical response function. According to the Canadian Standards (CSA A23.3-04), the punching shear resistance $(V_{R,CSA})$ of a slab-column connection without shear reinforcement is defined as

$$V_{R,CSA} = 0.38\,\lambda\,b_0\,d\,\sqrt{f_c'} \quad [f_c'\ in\ MPa] \tag{3.62}$$

where λ is a modification factor reflecting the reduced mechanical properties of lightweight concrete (for normalweight concrete $\lambda = 1$), b_0 is the control perimeter calculated as $b_0 = 4(d + c)$, d is the effective depth of the slab, f_c' is the compressive strength of the concrete and c is the dimension of the column at the face that we check the punching shear resistance. For this example we consider three input random variables $(n = 3)$, which follow the Normal probability distribution (Table 3.3).

Using the fifth-order $(L = 5)$ Gauss quadrature, an input grid is generated in order to evaluate the response. The Gauss Hermite formula is adopted, since all random variables follow the Normal distribution. In total we have 1+3×5 = 16 response evaluations (Table 3.4). For each evaluation point, i.e., M-DRM trial, the remaining random variables are hold fixed to their mean values. This forms 15 independent trials, with a 16th trial being reserved for the mean case, i.e., where all input random variables are set equal to their mean values.

Table 3.3. Statistics of random variables related to the shear strength of slabs.

Random Variable	Distribution	Nominal Value	Mean	Standard Deviation	Reference
f_c'	Normal	25 MPa	Nominal+6.0	3.57	Nowak et al. 2012
d	Normal	88.7 mm	Nominal-4.8	12.70	Mirza and MacGregor 1979b
c	Normal	150 mm	Nominal+3.0	20.66	Mirza 1996

Note: Above nominal values have been adopted from Adetifa and Polak (2005) for the slab SB1.

Table 3.4. Input Grid for the response evaluation.

Random Variable	Trial	z_j	f_c' (MPa) (Eq. (3.57))	d (mm) (Eq. (3.57))	c (mm) (Eq. (3.57))	$V_{R,CSA}$ (kN)
f_c'	1	-2.85697	**20.82**	83.90	153.00	137.8345
	2	-1.35563	**26.17**	83.90	153.00	154.5429
	3	0	**31.00**	83.90	153.00	168.2099
	4	1.35563	**35.83**	83.90	153.00	180.8469
	5	2.85697	**41.19**	83.90	153.00	193.8834
d	6	-2.85697	31.00	**47.62**	153.00	80.8441
	7	-1.35563	31.00	**66.68**	153.00	123.9769
	8	0	31.00	**83.90**	153.00	168.2099
	9	1.35563	31.00	**101.12**	153.00	217.4598
	10	2.85697	31.00	**120.18**	153.00	277.8586
c	11	-2.85697	31.00	83.90	**93.99**	126.3095
	12	-1.35563	31.00	83.90	**124.99**	148.3283
	13	0	31.00	83.90	**153.00**	168.2099
	14	1.35563	31.00	83.90	**181.00**	188.0915
	15	2.85697	31.00	83.90	**212.01**	210.1102
Fixed Mean Values	16	N/A	31.00	83.90	153.00	168.2099

Note: z_j denotes the Gauss Hermite points.

3.4.2 Calculation of the Response Statistical Moments

Once the response is calculated for the 16 trials, the mean (ρ_i) and the mean square (θ_i) of an i^{th} cut function is approximated as a weighted sum, using Eq. (3.18) (Table 3.5). Then, the M-DRM approximation is used, i.e. Eq. (3.12), in order to approximate the statistical moment of the response function (Table 3.6). For sake of comparison, Monte Carlo simulation (MCS) is also performed with 100,000 simulations. The results indicate the numerical accuracy of the proposed M-DRM, with much less trials compared to the MCS.

Table 3.5. Output Grid for each cut function evaluation.

Random Variable	Trial	w_j	$V_{R,CSA}$ (kN)	$w_j \times V_{R,CSA}$	ρ_i	$w_j \times V_{R,CSA}^2$	θ_i
	1	0.01126	137.8345	1.5517		213.87	
	2	0.22208	154.5429	34.3203		5303.95	
f_c'	3	0.53333	168.2099	89.7119	**167.9282**	15090.43	**28294.56**
	4	0.22208	180.8469	40.1617		7263.13	
	5	0.01126	193.8834	2.1826		423.18	
	6	0.01126	80.8441	0.9101		73.58	
	7	0.22208	123.9769	27.5322		3413.37	
d	8	0.53333	168.2099	89.7119	**169.5749**	15090.43	**29948.20**
	9	0.22208	217.4598	48.2926		10501.70	
	10	0.01126	277.8586	3.1279		869.13	
	11	0.01126	126.3095	1.42191		179.60	
	12	0.22208	148.3283	32.9401		4885.95	
c	13	0.53333	168.2099	89.7119	**168.2099**	15090.43	**28509.65**
	14	0.22208	188.0915	41.7706		7856.69	
	15	0.01126	210.1102	2.3653		496.97	
Fixed Mean Values	16	N/A	**168.2099**	N/A			

Note: w_j denotes the Gauss Hermite weights.

Table 3.6. Statistical moments of the response.

$V_{R,CSA}$	M-DRM (16 Trials)	MCS (10^6 Trials)	Relative Error (%)
First moment (kN)	169.29	169.19	0.06
Second moment (kN^2)	30175	30131	0.15
Stdev (kN)	38.94	38.81	0.35
COV	0.2300	0.2294	0.29

Note: M-DRM = Multiplicative Dimensional Reduction Method; MCS = Monte Carlo Simulation; Relative Error = $|MCS - MDRM|/MCS$; Stdev = Standard Deviation; COV = Coefficient of Variation.

3.4.3 Calculation of the Response Probability Distribution

The structural responses, obtained using M-DRM with 16 trials, are combined with the MaxEnt principle with fractional moment constraints, in order to estimate the response probability

distribution. Table 3.7 provides the Lagrange multipliers (λ_i) and the fractional exponents (α_i), which are used to estimate the probability distribution of the response. The use of three fractional moments $(m = 3)$ is sufficient, since entropy converges rapidly (Table 3.7). The estimated probability distribution of the punching shear resistance is compared to the MCS (Fig. 3.2). The results indicate the efficiency of the proposed M-DRM with only three fractional moments $(m = 3)$ and 16 trials. Then, the probability of failure (p_f) is estimated by plotting the probability of exceedance (POE). It is observed that M-DRM provides highly accurate approximation for almost the entire range of the output response distribution (Fig. 3.3). For instance, according to the associated POE and considering 300 kN as a safety limit, M-DRM with two and three fractional moments estimates 2.3×10^{-3} and 1.9×10^{-3} probability of exceedance the value of 300 kN, respectively. This is close to the estimated value of MCS (1.6×10^{-3}) indicating the accurate prediction of the proposed method.

Table 3.7. MaxEnt parameters for the punching shear resistance.

Fractional Moments	Entropy	i	0	1	2	3	4
	6.3472	λ_i	4.6714	0.0789			
m=1		α_i		0.5967			
		$M_X^{\alpha_i}$		21.238			
	5.0677	λ_i	93.134	-35.596	0.9076		
m=2		α_i		0.2609	0.7704		
		$M_X^{\alpha_i}$		3.7967	51.875		
	5.0674	λ_i	12.750	4.5071	-75.191	92.205	
m=3		α_i		0.6755	0.3758	0.2680	
		$M_X^{\alpha_i}$		31.842	6.8368	3.9355	
	5.0674	λ_i	54.434	2.1772	-2.7438	-8.5792	4.7664
m=4		α_i		0.7683	0.4432	0.5501	0.2847
		$M_X^{\alpha_i}$		51.310	9.6592	16.717	4.2872

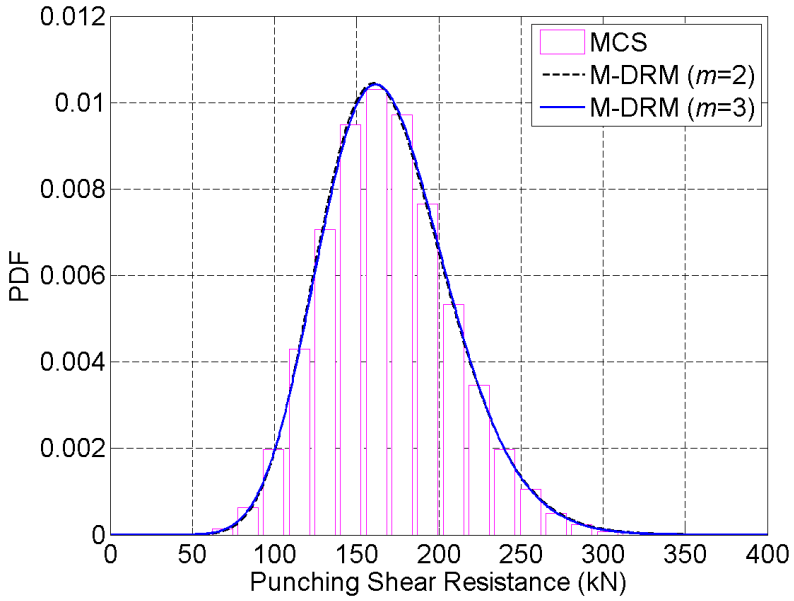

Fig. 3.2. Probability Distribution of the response.

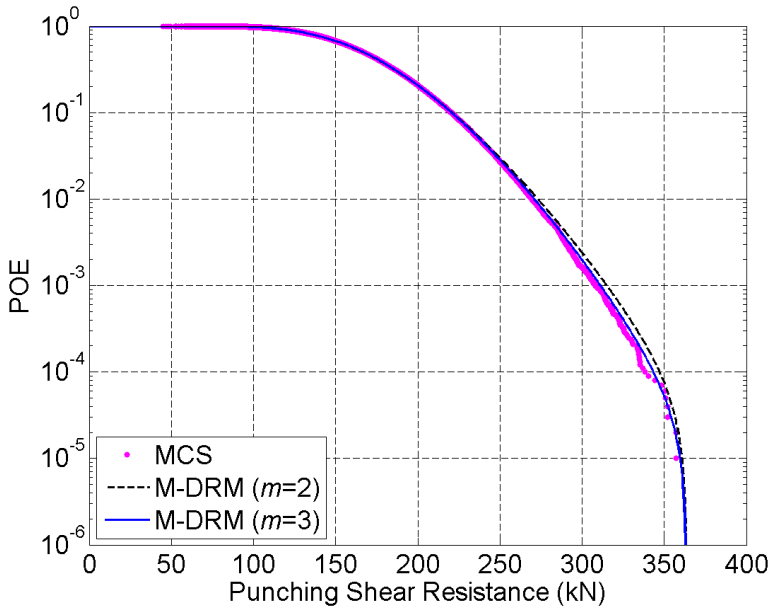

Fig. 3.3. Probability of Exceedance (POE) of the response.

3.4.4 Calculation of Sensitivity Coefficients

The primary and the total sensitivity coefficients are approximated using the already calculated mean (ρ_i) and the mean square (θ_i) of each cut function (Table 3.8). The ρ_i and θ_i have been

already calculated for the estimation of the response statistical moments. Therefore, the benefit of using M-DRM is that no other analytical effort is required for sensitivity analysis. It is observed that the variance of the static depth of the slab mostly contributes to the variance of the punching shear resistance. Thus, the response $V_{R,CSA}$ is most sensitive to the input random variable d, owing almost 80% of its variance to the variance of d. This high correlation is also confirmed from MCS with 100,000 trials (Fig. 3.4). The difference $S_{Ti} - S_i$ is really low, i.e., $S_{Ti} - S_i < 1\%$, indicating that none of the random variable i interacts with any other. The difference $1 - \sum_i S_i = 0.01$, also validates the negligible presence of interactions.

Table 3.8. Sensitivity coefficients.

Random Variable (i)	S_i	S_{Ti}	$S_{Ti} - S_i$
f_c'	0.0634	0.0665	0.31%
d	0.7837	0.7924	0.86%
c	0.1437	0.1501	0.65%
sum	0.99	1.01	N/A

Note: S_i denotes the primary sensitivity coefficient and S_{Ti} denotes the total sensitivity coefficient.

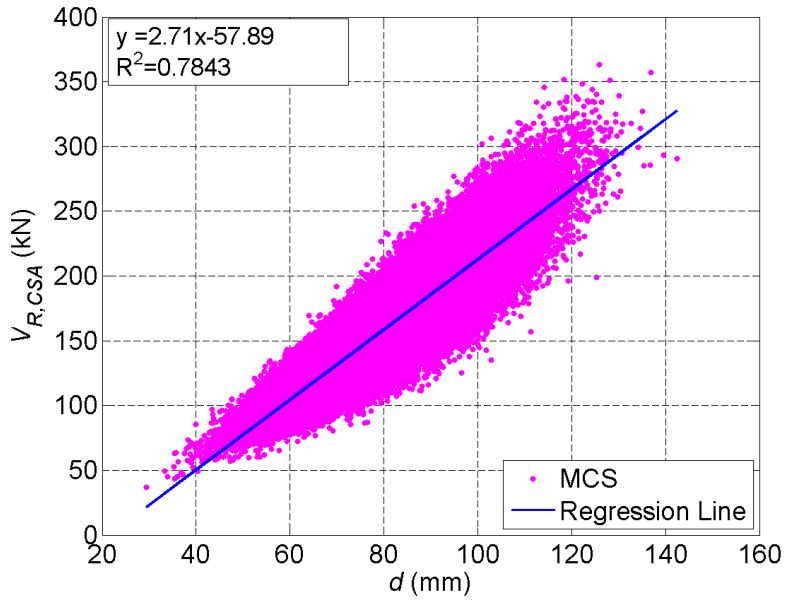

Fig. 3.4. Scatter plot of static depth versus punching shear resistance.

3.5 Conclusion

The chapter presents the multiplicative form of dimensional reduction method (M-DRM), for structural reliability and sensitivity analysis. This method is proposed for deriving the statistical moments and the probability distribution of the structural response. Then, the global sensitivity coefficients are derived as a by-product of the previous analysis, without any extra analytical effort. The efficiency and flexibility of M-DRM is its accuracy within a feasible computational time. M-DRM in conjunction with the rules of Gaussian quadrature creates an input grid of random variables, which is used to calculate the response. For each M-DRM trial, one random variable changes while the remaining ones are hold fixed to their mean value. At the end, one single trial is also performed, where all input random variables are set equal to their mean values. Then, based on the Gaussian quadrature, an output grid is created to calculate the mean and the mean square of each input random variable. It has been shown that M-DRM simplifies high dimensional moment integration to a product of low dimensional integrals. Thus, M-DRM is used to calculate the statistical moments (mean and variance) of the response.

The responses, obtained based on the above input grid, are combined with the maximum entropy principle. Fractional moments are used as constraints, which are obtained from the optimization procedure. The benefit here is that fractional moments do not have to be specified a priory. Instead, Lagrange multipliers and fractional exponents are computed based on this optimization, and then are used to estimate the probability distribution of the response. The demonstrated example shows that entropy converges rapidly after two fractional moments. Thus, only three fractional moments is sufficient to capture satisfactorily the response distribution. Probability of failure is also estimated based on the probability of exceedance (POE). No extra effort is required as POE uses the already calculated Lagrange multipliers and fractional exponents. Thus,

the analyst can estimate the probability of failure for several critical limits, based on one distribution only.

Monte Carlo simulation (MCS) is also carried out for the same example, in order to assess the accuracy of the proposed M-DRM. It is observed that the M-DRM statistical moments have a very small relative error (<1%) compared to the MCS. The estimated probability distribution of the response, obtained using M-DRM with three fractional moments, captures very well the response distribution, obtained using MCS, for almost the entire range. The calculated probabilities of failure are of the same order, which enhances the accuracy of the method.

Regarding the computational cost of the proposed method, the use of M-DRM with an L point Gauss scheme and n random variables, reduces the number of functional evaluation to the magnitude of $1 + nL$, leading to a small computational cost. Especially, for finite element analysis (FEA) of large scale or complex structures, each FEA trial may take an enormous amount of time. Thus, the proposed method is proved efficient and may be the only suitable compared to the MCS.

Global sensitivity analysis is also conducted, based on the already calculated mean and mean square of each input random variable. Global sensitivity means the contribution of variability (or variance) of one particular random variable to the overall (or global) variance of the output response. The results indicate that the punching shear resistance is mostly sensitive to the static depth of the slab, which is also confirmed by MCS. M-DRM with only 16 trials provides accurate estimates of the statistical moments, probability distribution and sensitivity coefficients of the structural response. In general, M-DRM needs a small amount of computational time to provide sufficiently several outcomes of interest, while a limitation of M-DRM is that it considers independent input random variables.

Chapter 4

Finite Element Reliability Analysis of Frames

4.1 Introduction

4.1.1 Pushover and Dynamic Analysis

Under severe earthquakes most buildings may deform beyond a structural limit. Thus, the earthquake response of a building, which will deform beyond its inelastic range, is of mainly importance in earthquake engineering (Chopra, 2012). Two main methods are primarily used to investigate the structural response due to ground seismic excitations. Pushover analysis (also called nonlinear static analysis) and dynamic analysis (also called nonlinear time history analysis), are widely used to approximate the inelastic structural response of a building.

Pushover analysis was presented by Saiidi and Sozen (1981) and is based on the assumption that the structural response can be related to the response of an equivalent single degree of freedom system. In the pushover analysis the structure is subjected to lateral applied static loads. Thus, the structure is pushed to specified displacement levels (Gupta and Krawinkler, 1999). Then, the structure is deformed inelastically and the analyst obtains the response of the building, e.g., roof displacement. This method is further described and recommended by the National Earthquake Hazard Reduction Program (NEHRP), i.e., FEMA 273 and FEMA 274 guidelines (1997). The pushover analysis is implemented easily and requires a fairly small computational cost. It provides a wide range of relevant information, although it may not estimate accurately the structural response, especially in case that a structure is subjected to severe earthquakes (Krawinkler, 1998).

For the dynamic analysis, the building is subjected to time varying excitation (Chopra, 2012). This means that the building is subjected to a ground motion, which represents the acceleration of the ground during an earthquake (Paulay and Priestley, 1992). The seismic load, in terms of input acceleration, is applied to the building in time increments Δt. Then, the equations of motions are solved and the analyst gets the structural response for every time step Δt (Clough and Penzien, 1992). Thus, several ground motion records are selected (Kalkan and Kunnath, 2007), based on past earthquakes or artificial accelerograms, and the seismic performance of the building is evaluated. Dynamic analysis can be considered as an accurate method, as long as the structure and the seismic input to the structure are modelled to be representative of reality (Gupta and Krawinkler, 1999). Thus, the selection of representative accelerograms is of paramount importance, since the output response in sensitive to the characteristic of the input seismic acceleration (Mwafy and Elnashai, 2001). Dynamic analysis provides the most accurate results, although its time variant nature may requires an enormous computational time (Clough and Penzien, 1992).

In this chapter, the OpenSees FEA software (McKenna et al., 2000) is used in order to apply finite element reliability (FERA) of structures under seismic loads. OpenSess is the official platform of the Pacific Earthquake Engineering Research (PEER) center, which is mainly developed for earthquake engineering. Another benefit of OpenSees is its open source code nature, which in conjunction with the already built in commands for reliability analysis (Der Kiureghian et al., 2006), results OpenSees to be a robust tool for FERA. A possible limitation here is that the user is required to have some expertise in advanced programing languages, e.g., Tcl, since writing source code can be a tedious task, especially for large scale structures.

4.1.2 Objective

The objective of this chapter is to examine the applicability, efficiency and accuracy of the proposed M-DRM, regarding the nonlinear finite element reliability and sensitivity analysis of structures, subjected to pushover and dynamic analysis. Thus, two structures made of reinforced concrete and steel are examined. In addition, the accuracy of M-DRM is also investigated, with respect to a large number of input random variables. Taken into account that time history analysis is time demanding, M-DRM is implemented for the investigation of structures subjected to repeated ground motions under input uncertainties. The suitability of M-DRM is going be examined for such high computational demanding problems.

4.1.3 Organization

The organization of this chapter is as follows. Section 4.2 presents how the Monte Carlo simulation (MCS), the first order reliability method (FORM) and the proposed M-DRM are implemented within the OpenSees software. Section 4.3 applies these three methods on a reinforced concrete and steel frame which is subjected to lateral static loading, i.e., pushover analysis. Section 4.4 adopts the two previous frames which are now subjected to time history analysis, i.e., dynamic analysis. For the dynamic analysis are used the MCS and the proposed M-DRM. Section 4.5 applies the proposed M-DRM to a steel moment resisting frame, which is subjected to single and repeated ground motions. Finally, conclusions are summarized in Section 4.6.

4.2 Finite Element Reliability Analysis

4.2.1 Monte Carlo Simulation

The Monte Carlo simulation (MCS) method may require a considerable amount of computational time, even when advanced techniques are used such as the importance sampling (Li and Zhang, 2011). Also, it may be hard to find a random variable simulator within general purpose FEA software (Shang and Yun, 2013). OpenSees overcomes this second challenge because it supports reliability algorithms. First, the deterministic finite element model is created using the string-based scripting language Tcl. Then MCS is performed using the parameter updating functionality (Scott and Haukaas, 2008).

In this study, the available reliability algorithms are enabled using the *reliability* command, the distribution for each random variable is identified using the *randomVariable* command, the random variables of interest are identified using the *parameter* command and the MCS is performed by updating the parameters of interest in each trial using the *updateParameter* command. Thus, once the random variables of interest are updated, FEA is performed for as many trials as MCS requires. The total number of required trials N is calculated as (Ang and Tang, 2007)

$$N \approx 1/\left(\mathrm{COV}^2 \times p_f\right) \tag{4.1}$$

where COV is the desirable coefficient of variation of the output response and p_f is the probability of failure.

4.2.2 First Order Reliability Method

The first order reliability method (FORM) (Hasofer and Lind, 1974), is an approximate method for calculating the reliability index and the probability of failure, based on a given performance function $g(\mathbf{x})$ as (Madsen et al., 1986; Melchers, 1987; Nowak and Collins, 2000)

$$g(\mathbf{x}) = y_c - h(\mathbf{x}) \tag{4.2}$$

FORM is based on an iterative process of the $g(\mathbf{x})$, which can provide accurate results for many engineering problems. In order to define the full probability distribution of the response, the critical limit y_c has to change and then to perform iterations for several $g(\mathbf{x})$. Thus, in this study the summation of these iterations for each $g(\mathbf{x})$, is reported as the total required trials for FORM. In FERA the performance function may not be available (it may be defined in an implicit form) and the use of a reliability platform is required to connect FORM with a general purpose FEA software (Pellissetti and Schuëller, 2006). In addition, the nonlinearity of the performance function may cause numerical difficulties and non-convergence of the numerical solution (Haukaas and Der Kiureghian, 2006). OpenSees supports FORM using the *runFORMAnalysis* command (Haukaas and Der Kiureghian, 2004) and it can be implemented using a modified step size for the iHLRH algorithm (Haukaas and Der Kiureghian, 2006).

4.2.3 Multiplicative Dimensional Reduction Method (M-DRM)

The major issue of FERA is to minimize the repetition of each FEA trial, because it can be a fairly time consuming task. Especially, in dynamic analysis problems each trial may take a considerable amount of time due to the applied time history. Also, this computational time can be further increased, since it also depends on the complexity of the structural model.

In this chapter, the proposed M-DRM is applied to reinforced concrete and steel frames, which are subjected to pushover and dynamic analysis. The proposed approach is fully automated, since it is implemented in OpenSees using Tcl programing and the parameter updating functionality, where each random variable is updated based on the Gauss scheme. Therefore, the available reliability algorithms are enabled using the *reliability* command, the random variables of interest are identified using the *parameter* command and the M-DRM is performed by updating each parameter of interest per trial using the *updateParameter* command. M-DRM requires the change of one input random variable per trial, while the remaining ones are held fixed to their mean values. Thus, the *array* command together with the *foreach* loop is also used.

4.3 Examples of Pushover Analysis

Two structural examples are used to examine the practical application and accuracy of the proposed M-DRM for FERA of structures subjected to pushover analysis. A two bay-two story reinforced concrete frame and a three bay-three story steel frame are subjected to lateral loads and pushover analysis is performed using OpenSees. The statistical moments of the roof lateral displacement are obtained using M-DRM and MCS. The probability distribution of the roof lateral displacement is obtained using M-DRM, MCS, FORM and lognormal distribution. Lognormal distribution is estimated using the mean and the standard deviation as calculated from M-DRM.

4.3.1 Example 1-Reinforced Concrete Frame

4.3.1.1 Reinforced Concrete Frame Description

A two-bay, two-story reinforced concrete frame (Fig. 4.1) is selected from literature (Haukaas and Der Kiureghian, 2006). The frame is subjected to lateral loads and static pushover analysis is performed. In addition to the lateral loads, the following gravity loads are applied; $G_3 = G_9 = 430$ kN, $G_2 = G_6 = G_8 = 850$ kN, $G_5 = 1700$ kN. Note that subscripts denote the number of the node at which the gravity load is applied (Fig. 4.1). The section reinforcement and structural dimensions are also shown in Fig. 4.1.

Each frame member is discretized in 4 displacement-based finite elements. Each member cross-section: (1) is discretized in 14 fibers in the in-plane direction; (2) has a concrete cover thickness equal to 75 mm; (3) is modeled by a uniaxial material model as shown in Fig. 4.2. The uniaxial nonlinear material models for steel and concrete (unconfined and confined) are shown in Fig. 4.2. A bilinear model is used in order to present the stress-strain response of the reinforcing steel, as shown in Fig. 4.2(a). A modified Kent–Park backbone curve with zero stress in tension and linear unloading/reloading is used in order to present: (1) the unconfined concrete material fibers of the concrete in columns' cover and of the concrete in girders, as shown in Fig. 4.2(b); (2) the confined concrete material fibers of the concrete in columns' core, as shown in Fig. 4.2(c).

Note that f_y is the yield strength of steel, E is the modulus of elasticity of steel, i.e., initial elastic tangent, b is the strain-hardening ratio, i.e., ratio between post-yield tangent and initial elastic tangent, f_c' is the concrete compressive strength at 28 days, f_{cu}' is the concrete crushing strength, ε_c is the concrete strain at maximum strength, ε_{cu} is the concrete strain at crushing strength (Mazzoni et al., 2007).

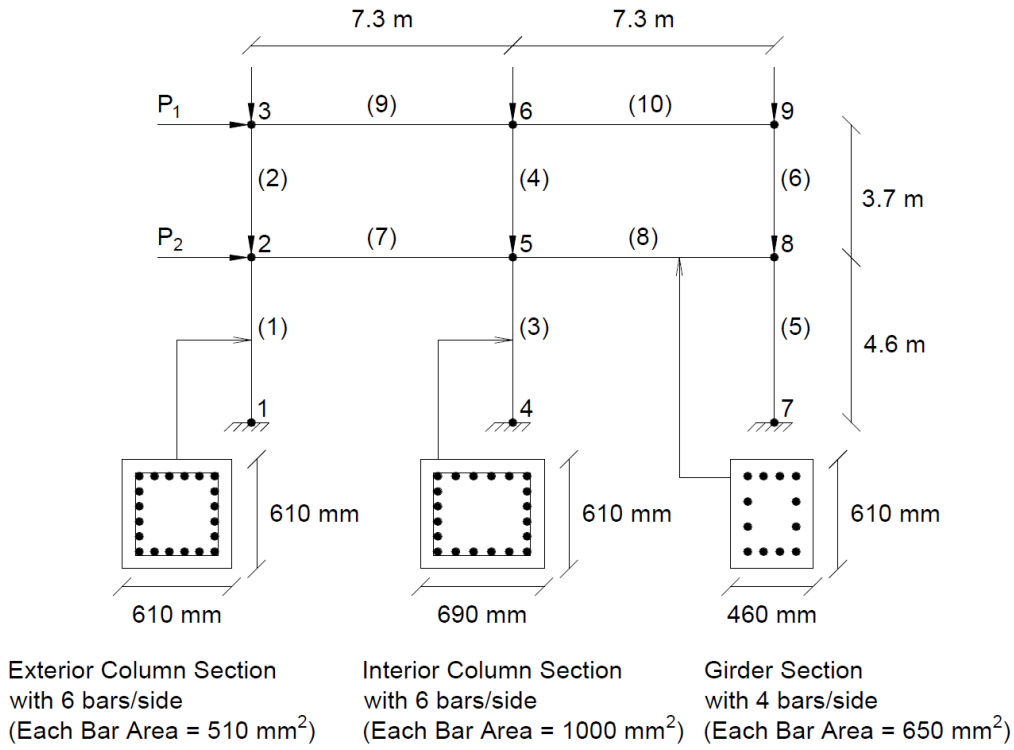

Fig. 4.1. Example 1–Reinforced concrete frame showing fiber sections, node numbers and element numbers (in parenthesis).

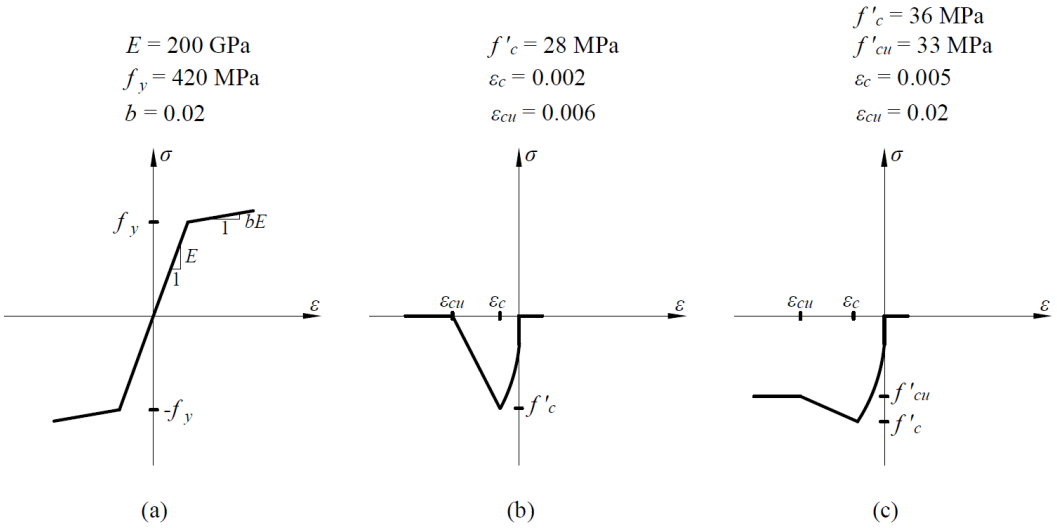

Fig. 4.2. Example 1–Reinforced concrete frame material models: (a) steel; (b) unconfined concrete in column cover regions and girders; (c) confined concrete in column core regions.

Each frame member is assigned one random variable for each material property. For the reliability analysis as uncertain are considered the material properties, the lateral loads and the nodal coordinates, with statistical properties listed in Table 4.1. Thus, in total we have 104 independent input random variables for the FERA of the reinforced concrete frame example.

Table 4.1. Statistical properties of random variables: Example 1–Reinforced concrete frame.

Parameter	Distribution	Mean	COV
f_y of reinforcing steel (10 RVs)	Lognormal	420 N/mm^2	5.0%
E of reinforcing steel (10 RVs)	Lognormal	200 kN/mm^2	5.0%
b of reinforcing steel (10 RVs)	Lognormal	0.02	10.0%
f_c' of core concrete in columns (6 RVs)	Lognormal	36 N/mm^2	15.0%
f_{cu}' of core concrete in columns (6 RVs)	Lognormal	33 N/mm^2	15.0%
ε_c of core concrete in columns (6 RVs)	Lognormal	0.005	15.0%
ε_{cu} of core concrete in columns (6 RVs)	Lognormal	0.02	15.0%
f_c' of cover concrete in columns and concrete in girders (10 RVs)	Lognormal	28 N/mm^2	15.0%
ε_c of cover concrete in columns and concrete in girders (10 RVs)	Lognormal	0.002	15.0%
ε_{cu} of cover concrete in columns and concrete in girders (10 RVs)	Lognormal	0.006	15.0%
lateral load at node 3 (P_1) and 2 (P_2) (2 RVs)	Lognormal	700 kN	20.0%
nodal coordinates (X and Y) (18 RVs)	Normal	As is	σ = 20mm

Note: RVs = random variables; σ = standard deviation; COV = coefficient of variation; X = horizontal coordinate; Y = vertical coordinate.

4.3.1.2 Input Grid for M-DRM

The examined problem involves 104 input random variables $(n = 104)$. Thus, the structural response is a product of 104 cut functions. Using a fifth-order $(L = 5)$ Gauss Hermite integration scheme, 521 trials are performed. The input data grid to perform FERA is given in Table 4.2. For example, consider a specific case of a cut function which corresponds to the compressive strength of concrete, f_c'. The five quadrature points for f_c' are given in Table 4.2 and the rest of 103 random variables are set equal to their mean values. OpenSees software performs FEA for

each of these 5 input data sets and the lateral displacement of the frame is recorded in the last column of Table 4.2. In this manner, computations are repeated for each cut function. Then, the probabilistic analysis is performed on the basis of these results in the next section.

Table 4.2. Input grid: Example 1–Reinforced concrete frame.

Random Variable	Trial	z_j	f_c' (MPa)	…	Y coordinate at node 9 (mm)	u_3 (mm) [OpenSees]
f_c' (MPa)	1	–2.85697	23.24	…	8300.0	60.7667
	2	–1.35563	29.08	…	8300.0	60.7656
	3	0	35.60	…	8300.0	60.7643
	4	1.35563	43.58	…	8300.0	60.7628
	5	2.85697	54.51	…	8300.0	60.7608
…	…	…	…	…	…	…
Y coordinate at node 9 (mm)	516	–2.85697	36.00	…	8242.8	60.6140
	517	–1.35563	36.00	…	8272.8	60.6929
	518	0	36.00	…	8300.0	60.7642
	519	1.35563	36.00	…	8327.1	60.8356
	520	2.85697	36.00	…	8357.1	60.9148
Fixed Mean Values	521	N/A	36.00	…	8300.0	60.7642

Note: z_j = Gauss Hermite points.

4.3.1.3 Statistical Moments of the Response

First the mean of each cut function is calculated as $\rho_i = \sum_{j=1}^{L} w_j u_{3ij}$, $i = 1,2,\dots,n$, where u_{3ij} is the lateral displacement of third node when i^{th} cut function is set at j^{th} quadrature point. Similarly, the mean square of each cut functions is calculated as $\theta_i = \sum_{j=1}^{L} w_j \left(u_{3ij}\right)^2$, $i = 1,2,\dots,n$. The overall response mean and variance are then approximated based on M-DRM, as show in previous chapter. This calculation procedure is illustrated in Table 4.3. The numerical results obtained from M-DRM and MCS are compared in Table 4.4. M-DRM estimates of mean and standard deviation of the response are almost identical to those obtained by MCS.

Table 4.3. Output grid: Example 1–Reinforced concrete frame.

Random Variable	Trial	w_j	$w_j \times u_3$ (mm)	ρ_i (mm)	$w_j \times (u_3)^2$ (mm^2)	θ_i (mm^2)
f_c' (MPa)	1	0.011257	0.681	56.3503	41.5675	3692.308
	2	0.22208	13.4948		820.0211	
	3	0.53333	32.4074		1969.2144	
	4	0.22208	13.4942		819.9455	
	5	0.011257	0.6840		41.5594	
…	…	…	…	…	…	…
Y coordinate at node 9 (mm)	516	0.011257	0.6823	56.3497	41.3589	3692.309
	517	0.22208	13.4787		818.0601	
	518	0.53333	32.4074		1969.2080	
	519	0.22208	13.5104		821.9115	
	520	0.011257	0.6857		41.7704	
Fixed Mean Values	521	N/A	N/A	N/A	N/A	N/A

Note: w_j = Gauss Hermite weights.

Table 4.4. Comparison of response statistics: Example 1–Reinforced concrete frame.

Response statistics	Max lateral displacement at node 3 (u_3)		
	M-DRM (521 Trials)	MCS (10^5 Trials)	Relative Error (%)
Mean (mm)	62.09	62.11	0.03
Standard deviation (mm)	14.50	14.51	0.10
Coefficient of variation	0.2335	0.2337	0.07

Note: M-DRM = multiplicative dimensional reduction method; MCS = Monte Carlo simulation; relative error = $|MCS - MDRM|/MCS$.

4.3.1.4 Probability Distribution of the Response

The maximum entropy principle is applied to estimate the probability distribution of the frame's lateral displacement, u_3. The Lagrange multipliers (λ_i) and the fractional exponents (α_i) are determined during the optimization procedure, which are then used to define the estimated probability distribution. Typically, three fractional moments ($m = 3$) are sufficient for the analysis, since entropy converges rapidly (Table 4.5).

Fig. 4.3 compares the probability density function (PDF) of the lateral displacement at node 3, which is obtained from MCS, M-DRM and lognormal distribution. PDFs of MCS and M-DRM are in fairly close agreement, while the lognormal distribution slightly fails to capture the peak of the PDF. The probability of exceedance (POE) curve shows that the MaxEnt distribution with three fractional moments can accurately model the distribution tail (Fig. 4.4). Note that FORM analysis is implemented using the modified step size for the iHLRF algorithm with $b_0 = 0.4$, as described in Haukaas and Der Kiureghian (2006). Then, FORM is executed for a range of 20 mm till 200 mm with an increment of 10 mm, leading to 95 trials in total. FORM may not be efficient in predicting accurately the distribution tail, although it needs much less trials than M-DRM. M-DRM with 521 structural analyses can provide almost the same result as that obtained from 100,000 simulations. Suppose the maximum allowable lateral displacement of node 3 is 166 mm (2% of the frame height). The probability of u_3 exceeding this limit is estimated by M-DRM as 7.12×10^{-4}, by FORM as 2.86×10^{-4} and by lognormal as 5.85×10^{-6}. M-DRM estimation is close to MCS result of 7.89×10^{-4}. Lognormal distribution highly overestimates the probability of exceedance, which may lead to unsafe predictions (Fig. 4.4).

Table 4.5. MaxEnt distribution parameters: Example 1–Reinforced concrete frame.

Fractional moments	Entropy	i	0	1	2	3
	5.252	λ_i	3.905	0.0629		
m=1		α_i		0.7427		
		$M_Y^{\alpha_i}$		21.376		
	3.8862	λ_i	38.211	2.3E+07	-109.239	
m=2		α_i		-4.0013	-0.2672	
		$M_Y^{\alpha_i}$		9.6E-08	0.3343	
	3.8859	λ_i	52.156	-252562	-87.79	2168441
m=3		α_i		-2.4545	-0.1463	-2.9925
		$M_Y^{\alpha_i}$		4.7E-05	0.5486	5.41E-06

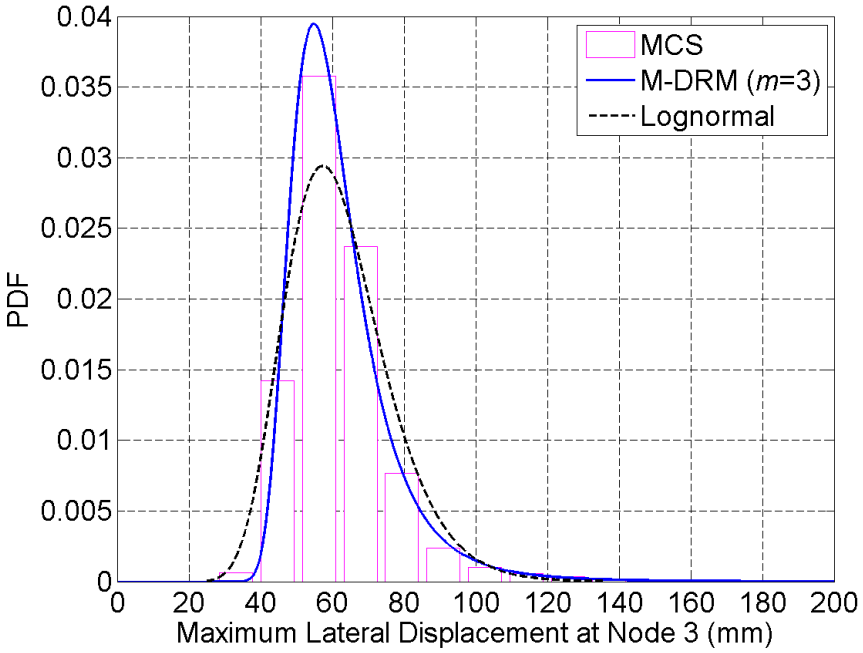

Fig. 4.3. Probability Distribution of the maximum lateral displacement at Node 3: Example 1– Reinforced concrete frame.

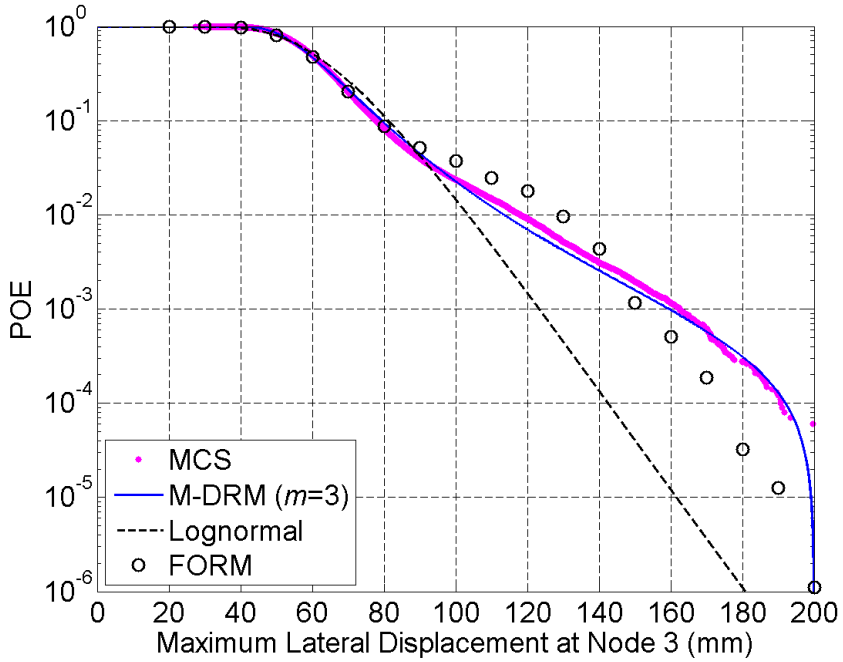

Fig. 4.4. Probability of Exceedance of the maximum lateral displacement at Node 3: Example 1– Reinforced concrete frame.

4.3.1.5 Global Sensitivity Indices using M-DRM

The benefit of M-DRM is that no extra computational effort is required in order to calculate the sensitivity indices. Thus, the global sensitivity index of each of 104 input random variable to the nodal displacement u_3, is evaluated according to the M-DRM. The 10 most important random variables are listed in Table 4.6. The lateral load at node 3 (P_1) has the highest contribution, 84.3%, followed by the lateral load P_2 with 14.6% contribution. Effectively, the two lateral loads basically contribute to about 99% to the variability of u_3, and the rest of the random variables have a very little influence over the response variability.

Table 4.6. Global Sensitivity Indices using M-DRM: Example 1–Reinforced Concrete Frame.

Rank	Object	Parameter	RV	S_i
1	Node 3	Load	P_1	0.8434
2	Node 2	Load	P_2	0.1462
3	Node 5	Coordinate	X	5.37E-04
4	Node 8	Coordinate	X	4.26E-04
5	Node 4	Coordinate	Y	2.97E-04
6	Member 5	Unconfined Concrete	f_c'	2.22E-04
7	Node 4	Coordinate	X	1.86E-04
8	Member 5	Steel	E	1.63E-04
9	Member 7	Unconfined Concrete	f_c'	1.54E-04
10	Node 7	Coordinate	X	1.30E-04

Note: RV= Random Variable; S_i = primary sensitivity coefficient.

4.3.1.6 Computational Time

The large saving in computational time is the main advantage of M-DRM. For the pushover analysis of the reinforced concrete frame, simulation of 100,000 FEM analyses takes 4.73 hours on a personal computer with Intel i7-3770 3rd Generation Processor and 16GB of RAM. M-DRM approximation based on 521 finite element analyses takes 1.47 minutes and MaxEnt method requires 2.5 minutes. Thus, total time taken by M-DRM is 3.97 minutes, which is merely

1.4% of the time taken by the simulation method. FORM with 95 trials takes 2.85 minutes which is close to that of M-DRM.

4.3.2 Example 2-Steel Frame

4.3.2.1 Steel Frame Description

A three-bay, three-story steel frame (Fig. 4.5) is selected from Haukaas and Scott (2006). The frame is subjected to lateral loads and static pushover analysis is performed. Note that the lateral load varies with the frame height, i.e., maximum value at the roof and zero value at the base of the frame. In addition to the lateral loads, gravity loads of 50 kN and 100 kN are applied to the external and internal connections, respectively (Fig. 4.5(a)). The steel cross section of each frame member is shown in Fig. 4.5(b). Similar to the previous example, a bilinear model is used in order to present the stress-strain response of the reinforcing steel, as shown in Fig. 4.5(c), where f_y is the yield strength of the steel, E is the modulus of elasticity of steel and b is the strain-hardening ratio (Mazzoni et al., 2007).

Each frame member is discretized in 8 displacement-based finite elements and has a set of random variables that model variability in material properties, cross-section dimensions and nodal coordinates. These random variables are independent and identically distributed across the frame members (Table 4.7). Thus, in total there are 179 independent input random variables for the FERA of the steel frame example.

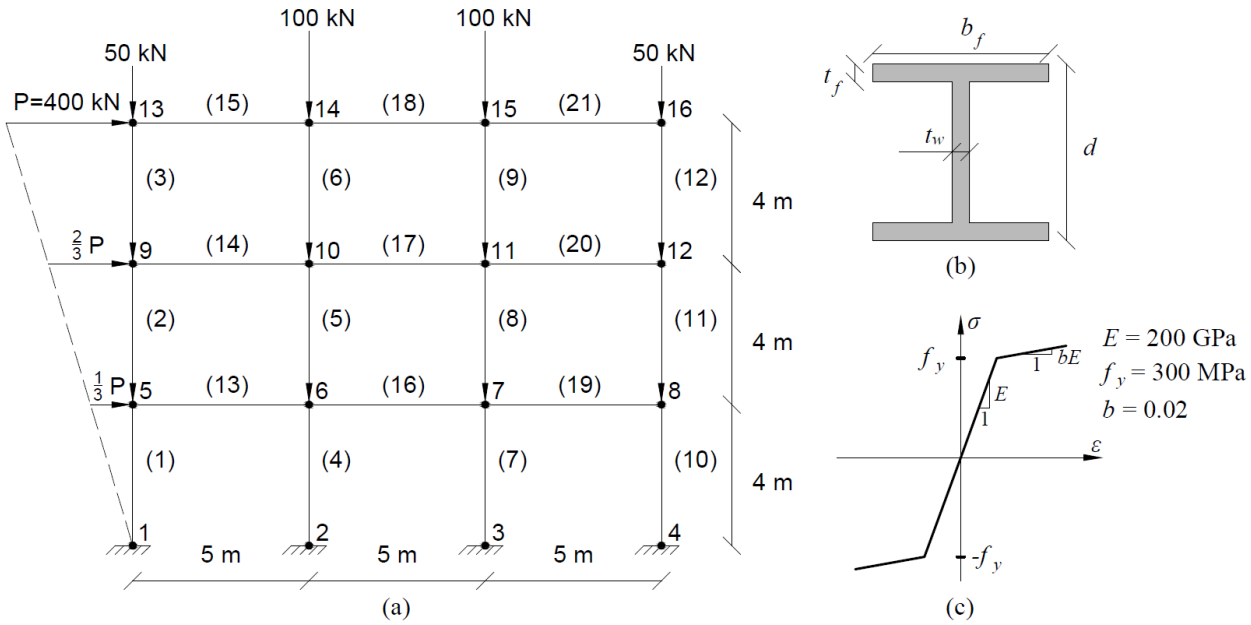

Fig. 4.5. Example 2–Steel frame showing: (a) node numbers and element numbers (in parenthesis); (b) steel cross-section; (c) material model for steel.

Table 4.7. Statistical properties of random variables: Example 2–Steel frame.

Parameter	Distribution	Mean	COV
E of steel (21 RVs)	Lognormal	200,000 N/mm^2	5.0%
f_y of steel (21 RVs)	Lognormal	300 N/mm^2	10.0%
b of steel (21 RVs)	Lognormal	0.02	10.0%
d of steel section (21 RVs)	Normal	250 mm	2.0%
t_w of steel section (21 RVs)	Normal	20 mm	2.0%
b_f of steel section (21 RVs)	Normal	250 mm	2.0%
t_f of steel section (21 RVs)	Normal	20 mm	2.0%
Y Nodal Coordinates (16 RVs)	Normal	As is	σ = 10mm
X Nodal Coordinates of Base (4 RVs)	Normal	As is	σ = 10mm
X Nodal Coordinates of 1st Floor (4 RVs)	Normal	As is	σ = 15mm
X Nodal Coordinates of 2nd Floor (4 RVs)	Normal	As is	σ = 20mm
X Nodal Coordinates of Roof (4 RVs)	Normal	As is	σ = 25mm

Note: RVs = random variables; σ = standard deviation; COV = coefficient of variation; X = horizontal coordinate; Y = vertical coordinate.

4.3.2.2 Statistical Moments of the Response

This example consists of 179 input random variables. Adapting the fifth-order Gauss Hermite integration scheme, M-DRM method requires 179 × 5+1 = 896 FEA trials. After obtaining the FEA results for each M-DRM trial, the mean and mean square of each random variable is calculated. MCS is also performed based on 10^5 trials. M-DRM estimates of the mean and standard deviation of the structural response have a small error, compared to the MCS results (Table 4.8). Thus, results indicate the accuracy and efficiency of the proposed method.

Table 4.8. Comparison of response statistics: Example 2–Steel frame.

Response statistics	Max lateral displacement at node 13 (u_{13})		
	M-DRM (896 Trials)	MCS (10^5 Trials)	Relative Error (%)
Mean (mm)	240.11	238.43	0.71
Standard deviation (mm)	23.83	24.72	3.60
Coefficient of variation	0.0992	0.1037	4.28

Note: M-DRM = multiplicative dimensional reduction method; MCS = Monte Carlo simulation; relative error = $|MCS - MDRM|/MCS$.

4.3.2.3 Probability Distribution of the Response

The maximum entropy principle is applied to estimate the probability distribution of the frame's lateral displacement, u_{13}. The MaxEnt distribution parameters are reported in Table 4.9, where again entropy converges rapidly for three fractional moments ($m = 3$).

The PDF and POE curves obtained from MCS, M-DRM with three fractional moments and lognormal distribution, are compared in Fig. 4.6 and Fig. 4.7, respectively. Fig. 4.7 also includes the FORM, which is implemented as described in previous example with $b_0 = 0.4$. For the POE curve, 125 trials in total are needed for FORM, since it is executed for a range of 160 mm till 400 mm with an increment of 10 mm. Once again, M-DRM and MCS results are in close agreement,

while FORM also captures satisfactorily the distribution response and lognormal distribution fails to capture the tail (Fig. 4.7). Considering the maximum allowable lateral displacement of node 13 as 360 mm (3% of the frame height), the probability of exceeding this limit (or probability of failure) is estimated by MCS as 3.30×10^{-4}, by M-DRM as 3.66×10^{-4}, by lognormal as 1.73×10^{-5} and by FORM as 1.19×10^{-4}. These results again confirm the accuracy of M-DRM achieved by a relatively small number of structural analyses.

Table 4.9. MaxEnt distribution parameters: Example 2–Steel frame.

Fractional moments	Entropy	i	0	1	2	3
	-0.174	λ_i	-1.959	3.9748		
m=1		α_i		0.5599		
		$M_Y^{\alpha_i}$		0.4493		
	-2.3353	λ_i	138.839	1.1481	-101.197	
m=2		α_i		-2.1825	-0.3532	
		$M_Y^{\alpha_i}$		23.266	1.6589	
	-2.3325	λ_i	148.479	0.0451	-54.084	-64.908
m=3		α_i		-3.6338	-0.1846	-0.2209
		$M_Y^{\alpha_i}$		193.291	1.3027	1.3724

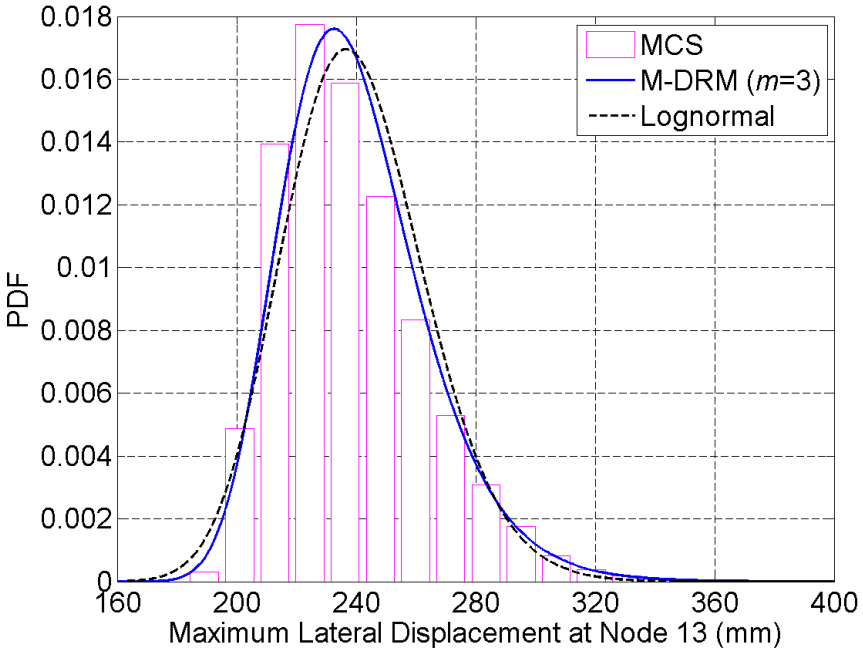

Fig. 4.6. Probability Distribution of the max lateral displacement at node 13: Example 2–Steel frame.

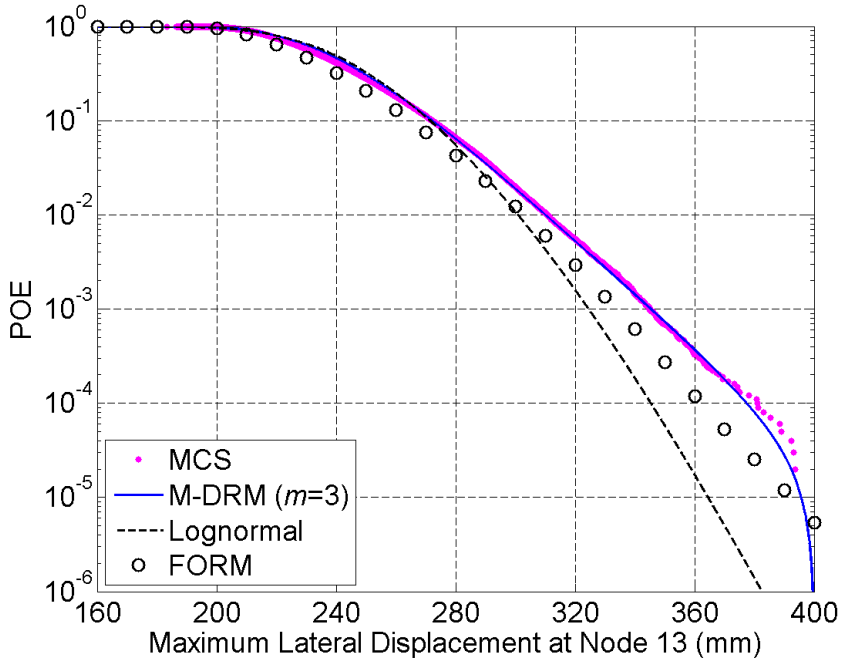

Fig. 4.7. Probability of Exceedance of the max lateral displacement at node 13: Example 2–Steel frame.

4.3.2.4 Global Sensitivity Indices using M-DRM

The global sensitivity index is calculated according to the M-DRM, for each of the 179 input random variables. The global sensitivity indices of the 15 most important variables are listed in Table 4.10. We observe that the yield strength of the steel members have the most influence to the structural response, since its variance contributes 82.23% to the response variance. Especially, for the yield strength of the internal base columns, this contribution equals to 47.06%, making them the most important variables for the seismic evaluation of the frame. In this example the applied loads are considered as deterministic. Thus, they do not appear in the sensitivity analysis.

Table 4.10. Global sensitivity indices using M-DRM: Example 2–Steel frame.

Rank	Object	RV	S_i
1	Member 4	f_y	0.1661
2	Member 7	f_y	0.1627
3	Member 19	f_y	0.1162
4	Member 13	f_y	0.1128
5	Member 10	f_y	0.0699
6	Member 1	f_y	0.0680
7	Member 8	f_y	0.0412
8	Member 5	f_y	0.0407
9	Member 16	f_y	0.0377
10	Member 4	d	0.0181
11	Member 7	d	0.0179
12	Member 19	d	0.0131
13	Member 13	d	0.0127
14	Member 10	d	0.0078
15	Member 1	d	0.0078

Note: RV= random variable; S_i = primary sensitivity coefficient.

4.3.2.5 Computational Time

M-DRM again provides an enormous saving in computational efforts, as simulation of 100,000 FEM analyses takes 17.71 hours on a personal computer with Intel i7-3770 3rd Generation

Processor and 16GB of RAM. M-DRM approximation based on 896 finite element analyses takes 9.52 minutes and MaxEnt method requires 1.33 minutes. Thus, total time taken by M-DRM is 10.85 minutes which is merely 1.02% of the time taken by the simulation method. Note that a relative reduction in computational efforts becomes more significant as the complexity of the problem increases. FORM with 125 trials takes 7.57 minutes which is again very close to the computational cost of M-DRM. Note that although M-DRM needs more trials comparing to FORM, the computational cost of the two methods is almost the same.

4.4 Examples of Dynamic Analysis

M-DRM is applied for FERA of structures subjected to dynamic analysis, using the previous two frame structures, where the lateral loads are removed and the frames are now subjected to time history analysis. For the dynamic analysis, the 1979 Imperial Valley earthquake ground motion is used, taken from the PEER Strong Motion Database (http://peer.berkeley.edu/smcat/). The Magnitude of the earthquake was 6.53, with a PGA equals to 0.143g at 10.84 sec (Fig. 4.8), as it was recorded from the Station USGS 931 EL Centro Array #12 (1979/10/15, 23:16).

The material properties are considered as uncertain, while the statistical moments of the roof lateral displacement are obtained using M-DRM and MCS. The probability distribution of the roof lateral displacement is obtained using M-DRM, MCS and lognormal distribution, where Lognormal distribution is approximated using the mean and the standard deviation as calculated from the M-DRM.

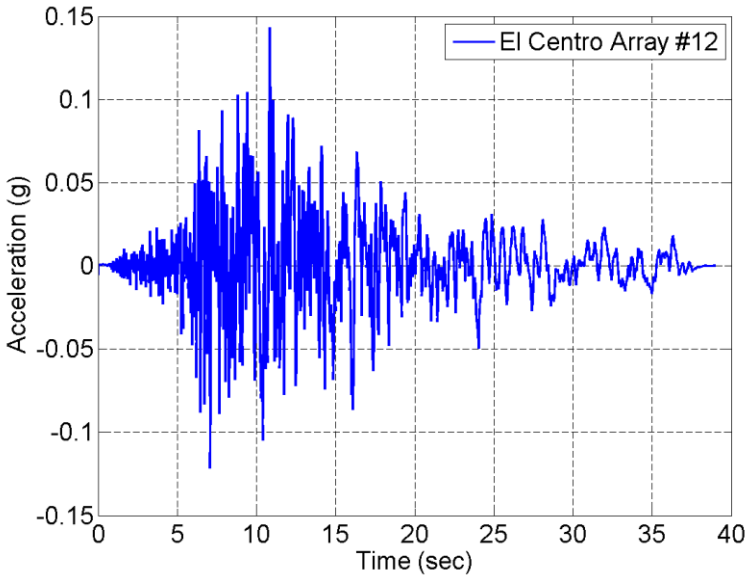

Fig. 4.8. Ground motion record for the earthquake 1979 Imperial Valley: EL Centro Array #12.

4.4.1 Example 3-Reinforced Concrete Frame

4.4.1.1 Reinforced Concrete Frame Description

Two-bay, two-story reinforced concrete frame is selected (Fig. 4.1). The lateral loads are removed and the frame is subjected to ground acceleration (Fig. 4.8). Pushover analysis gives a total reaction force at the supports equals to 1400 kN. Thus, the accelerogram of the earthquake is scaled so as to produce the same reaction force at the time of the PGA. For the reliability analysis, only the material properties are considered as uncertain (Table 4.1). Thus, for the FERA, we have 84 uncorrelated input random variables in total.

4.4.1.2 Statistical Moments of the Response

In this example, M-DRM requires 84 × 5+1 = 421 FEA trials. MCS is also performed based on 10^4 trials. M-DRM results of the mean and standard deviation of the structural response are in a

good agreement with the MCS results (Table 4.11). Thus, M-DRM provides sufficient estimates of the statistical moments.

Table 4.11. Comparison of response statistics: Example 3–Reinforced concrete frame.

Response statistics	Max lateral displacement at node 3 (u_3)		
	M-DRM (421 Trials)	MCS (10^4 Trials)	Relative Error (%)
Mean (mm)	63.23	60.94	3.77
Standard deviation (mm)	6.68	6.52	2.51
Coefficient of variation	0.1056	0.1069	1.21

Note: M-DRM = multiplicative dimensional reduction method; MCS = Monte Carlo simulation; relative error = $|MCS - MDRM|/MCS$.

4.4.1.3 Probability Distribution of the Response

The MaxEnt distribution parameters are reported in Table 4.12, where entropy converges for three fractional moments.

Table 4.12. MaxEnt distribution parameters: Example 3–Reinforced concrete frame.

Fractional moments	Entropy	i	0	1	2	3
m=1	5.7922	λ_i	1.649	1.5242		
		α_i		0.2414		
		$M_Y^{\alpha_i}$		2.7180		
m=2	3.3128	λ_i	144.286	5.9294	-29.7177	
		α_i		0.9571	0.6581	
		$M_Y^{\alpha_i}$		52.9051	15.2996	
m=3	3.3124	λ_i	182.355	-88.9150	48.2103	5.9159
		α_i		0.4534	0.2878	0.8975
		$M_Y^{\alpha_i}$		6.5493	3.2948	41.3194

The POE curves obtained from MCS, M-DRM with three fractional moments and lognormal distribution, are shown in Fig. 4.9. M-DRM and lognormal results are in a good agreement with the MCS results. Consider that 83 mm (1% of the frame height) is the maximum allowable

lateral displacement of node 3. The probability of u_3 exceeding this threshold is estimated by M-DRM as 2.69×10^{-3}, by lognormal as 4.21×10^{-3} and by MCS as 1.10×10^{-3}. Although M-DRM does not capture exactly the POE, it still gives safe predictions as it slightly underestimates the probability of failure.

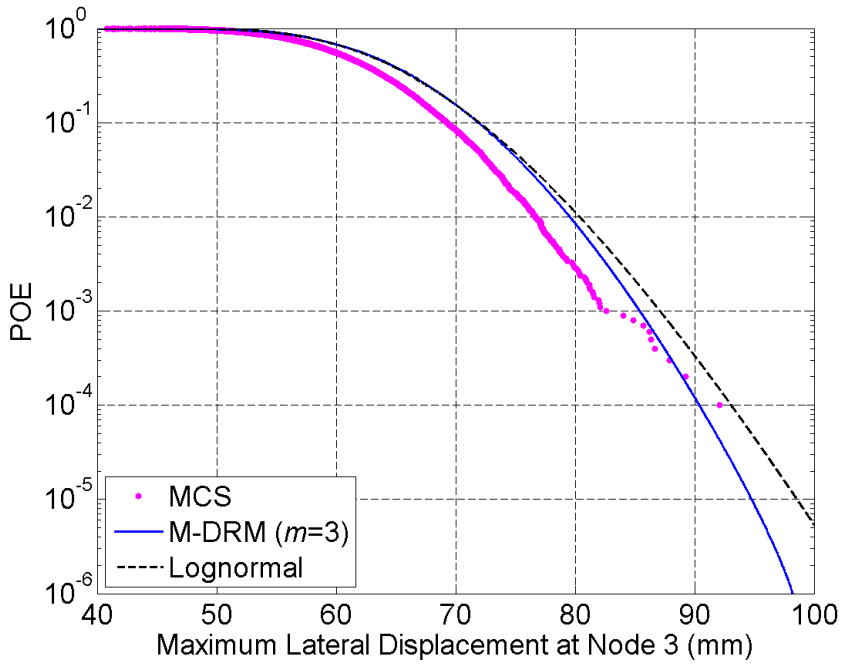

Fig. 4.9. Probability of Exceedance of the maximum lateral displacement at Node 3: Example 3–Reinforced concrete frame.

4.4.1.4 Global Sensitivity Indices using M-DRM

For each of the 84 input random variables, M-DRM is used to calculate the global sensitivity index. The primary sensitivity index is reported in Table 4.13, for the 10 most important variables to the nodal displacement u_3. For the two base columns (internal and left external), the variance of the concrete strength and concrete strain at that strength contribute 80.61% to the variance of the nodal displacement u_3. From this percentage, 55.29% is related to the unconfined

concrete. For all the base columns, unconfined concrete properties play a major role as they contribute 59.27% to the response variance.

Table 4.13. Global Sensitivity Indices using M-DRM: Example 3–Reinforced Concrete Frame.

Rank	Object	Parameter	RV	S_i
1	Member 3	Unconfined Concrete	f_c'	0.1424
2	Member 1	Unconfined Concrete	f_c'	0.1406
3	Member 1	Unconfined Concrete	ε_c	0.1360
4	Member 3	Unconfined Concrete	ε_c	0.1338
5	Member 3	Confined Concrete	f_c'	0.0683
6	Member 3	Confined Concrete	ε_c	0.0682
7	Member 1	Confined Concrete	ε_c	0.0588
8	Member 1	Confined Concrete	f_c'	0.0579
9	Member 5	Unconfined Concrete	f_c'	0.0205
10	Member 5	Unconfined Concrete	ε_c	0.0194

Note: RV= Random Variable; S_i = primary sensitivity coefficient.

4.4.1.5 Computational Time

Dynamic analysis is more time consuming, compared to the pushover analysis. For the examined problem, MCS with 10,000 FEA trials needs 11.74 hours. M-DRM approximation based on 421 FEA trials takes 32.44 minutes and MaxEnt method requires 1.30 minutes. Thus, total time taken by M-DRM is 33.74 minutes which is 4.79% of the time taken by the MCS. Note that MCS with 100,000 trials would require an extraordinary amount of time. Thus, MCS may not always be practical for the dynamic analysis of structures, while M-DRM can be considered an efficient alternative for that kind of problems.

4.4.2 Example 4-Steel Frame

4.4.2.1 Steel Frame Description

The previous analyzed three-bay, three-story steel frame is selected (Fig. 4.5). The lateral loads are removed and the frame is subjected to ground acceleration (Fig. 4.8). Pushover analysis gives a total reaction force at the supports equals to 800 kN. Thus, the accelerogram of the earthquake is scaled so as to produce the same reaction force at the time of the PGA. For the reliability analysis, only the material properties are considered as uncertain (Table 4.7). Thus, for the FERA, we have 63 uncorrelated input random variables in total.

4.4.2.2 Statistical Moments of the Response

M-DRM method requires 63 × 5+1 = 316 FEA trials, as we have 63 input random variables and is used the fifth-order Gauss Hermite integration scheme. MCS is also performed based on 10^4 trials. The M-DRM estimation of the response's mean value has a small error compared to the MCS result (Table 4.14). The M-DRM estimation of the response's standard deviation has a larger error, but still is in good agreement compared to the MCS result in terms of absolute values.

Table 4.14. Comparison of response statistics: Example 4–Steel frame.

Response statistics	Max lateral displacement at node 13 (u_{13})		
	M-DRM (316 Trials)	MCS (10^4 Trials)	Relative Error (%)
Mean (mm)	146.21	149.06	1.92
Standard deviation (mm)	13.19	10.05	31.21
Coefficient of variation	0.0902	0.0674	33.77

Note: M-DRM = multiplicative dimensional reduction method; MCS = Monte Carlo simulation; relative error = $|MCS - MDRM|/MCS$.

4.4.2.3 Probability Distribution of the Response

The probability distribution of the frame's lateral displacement u_{13} is estimated, based on the M-DRM together with the MaxEnt principle. The MaxEnt distribution parameters are reported in Table 4.15, where entropy converges for three fractional moments. The POE curves obtained from MCS, M-DRM with three fractional moments and lognormal distribution, are compared in Fig. 4.10. M-DRM is able to capture effectively the whole distribution of the response, while lognormal slightly fails to capture the tail.

Considering the maximum allowable lateral displacement of node 13 as 180 mm (1.5% of the frame height), the probability of exceeding this limit is estimated by MCS as 5.09×10^{-3}, by M-DRM as 6.65×10^{-3} and by lognormal as 9.25×10^{-3}. Once again, the results confirm the accuracy of M-DRM, using a relatively small number of FEA trials.

Table 4.15. MaxEnt distribution parameters: Example 4–Steel frame.

Fractional moments	Entropy	i	0	1	2	3
	-0.012	λ_i	-7.168	9.3665		
m=1		α_i		0.1397		
		$M_Y^{\alpha_i}$		0.7640		
	-2.915	λ_i	264.075	1227.9	-614.54	
m=2		α_i		1.4803	0.3097	
		$M_Y^{\alpha_i}$		0.0582	0.5508	
	-2.915	λ_i	365.573	-4E-05	1125.4	-694.79
m=3		α_i		2.5279	1.4179	0.2345
		$M_Y^{\alpha_i}$		0.0079	0.0656	0.6367

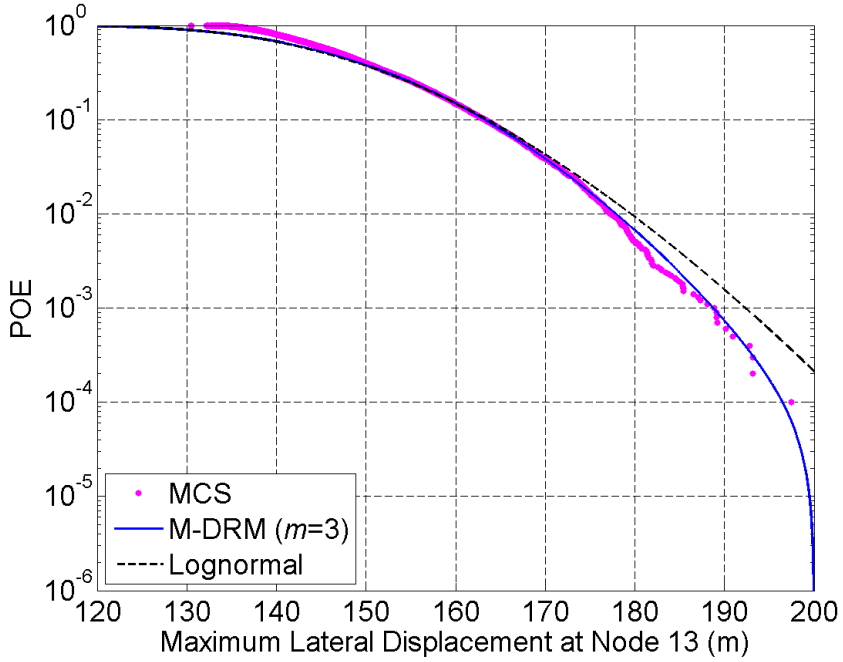

Fig. 4.10. Probability of Exceedance of the max lateral displacement at node 13: Example 4–Steel frame.

4.4.2.4 Global Sensitivity Indices using M-DRM

The global sensitivity indices of the 15 most important variables are listed in Table 4.10, as they are calculated based on M-DRM. For the dynamic analysis, the modulus of elasticity of steel has the most influence to the structural response, as its variance contributes 98.53% to the response variance. The modulus of elasticity of the external base columns contributes up to 52.71%, making them important for the seismic evaluation of the frame. It is observed that at the end of the time history analysis, the steel frame does not experience any permanent displacement. Thus, the M-DRM sensitivity analysis indicates that the modulus of elasticity of the steel is the most influential variable, since none of the frame's members experience yielding of the steel.

Table 4.16. Global sensitivity indices using M-DRM: Example 4–Steel frame.

Rank	Object	RV	S_i
1	Member 1	E	0.3246
2	Member 10	E	0.2025
3	Member 14	E	0.0860
4	Member 2	E	0.0814
5	Member 11	E	0.0642
6	Member 20	E	0.0488
7	Member 7	E	0.0377
8	Member 13	E	0.0359
9	Member 3	E	0.0200
10	Member 15	E	0.0192
11	Member 12	E	0.0160
12	Member 21	E	0.0152
13	Member 6	E	0.0143
14	Member 4	E	0.0118
15	Member 9	E	0.0077

Note: RV= random variable; S_i = primary sensitivity coefficient.

4.4.2.5 Computational Time

In this problem, MCS with 10,000 FEA trials needs 14.02 hours while M-DRM approximation based on 316 FEA trials takes 32.56 minutes and MaxEnt method requires 1.03 minutes. Thus, total time taken by M-DRM is 3.99% of the time taken by the MCS. Similar to Example 3, MCS may not always be suitable for dynamic analysis of structures, while M-DRM can provide accurate results within a feasible computational time.

4.5 Steel moment resisting frames

A steel moment resisting frame (MRF) consists of rigidly connected beams to columns, where this rigid frame system provides primarily resistance to the lateral load (Gupta and Krawinkler, 1999). This resistance is due to the rigid beam-to-column connection, which does not allow the frame to displace laterally without the beams and columns having bend (Bruneau et al., 1998).

Although, the MRFs are popular in high seismicity areas for several reasons, such as their high ductility and architectural versatility (Bruneau et al., 1998), the 1994 Northridge earthquake resulted to more than 100 failures of steel beam-column connections (Christopoulos et al., 2002), while the 1995 Kobe earthquake highlighted the severity of the problem (Gupta and Krawinkler, 1999). Apart the seismic load uncertainty, the material variability and structural modeling errors can also contribute to the capacity uncertainty (Wen, 2001). Thus, the proposed M-DRM will be implemented, in order to investigate the response variation of steel MRF subjected to different earthquakes considering several input uncertainties.

4.5.1 Steel MRF description

A three-story structure is selected from literature (Xue, 2012; Gong et al., 2012), which represents a hypothetical office building located in Vancouver, BC, Canada. The hypothetical three-story building has a symmetric structural layout and consists of four steel MRFs located at its perimeter (Fig. 4.11). Therefore, a pair of four-bay MRFs is able to withstand the seismic lateral loads in each principle direction. All four bays and three stories are each 9.14 m wide (center-to-center) and 3.96 m high, respectively. Only the East-West direction of the MRF is considered in this study, resulting to the 2D analysis of a four-bay three-story steel MRF (Fig. 4.12). The columns of the steel MRF are fixed to the ground level, while it is assumed to have rigid beam-to-column connections. The steel MRF is connected with a fictitious leaning column through rigid links at each story level, in order to take into account the effect of the interior gravity frames for the FEA. The seismic weight distribution is given in Fig. 4.12 (Xue, 2012; Gong et al., 2012), from which the seismic weight is equal to 4567 kN (29.1×4×9.14+3503) for the floor 2 and 3 and equal to 4850 kN (29.1×4×9.14+3881) for the roof.

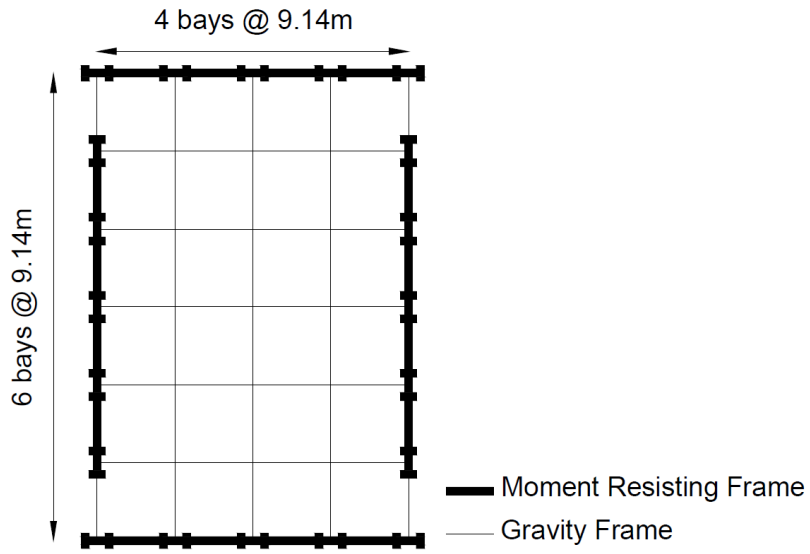

Fig. 4.11. Plane view of the three-story building showing the moment resisting frames and the gravity frames.

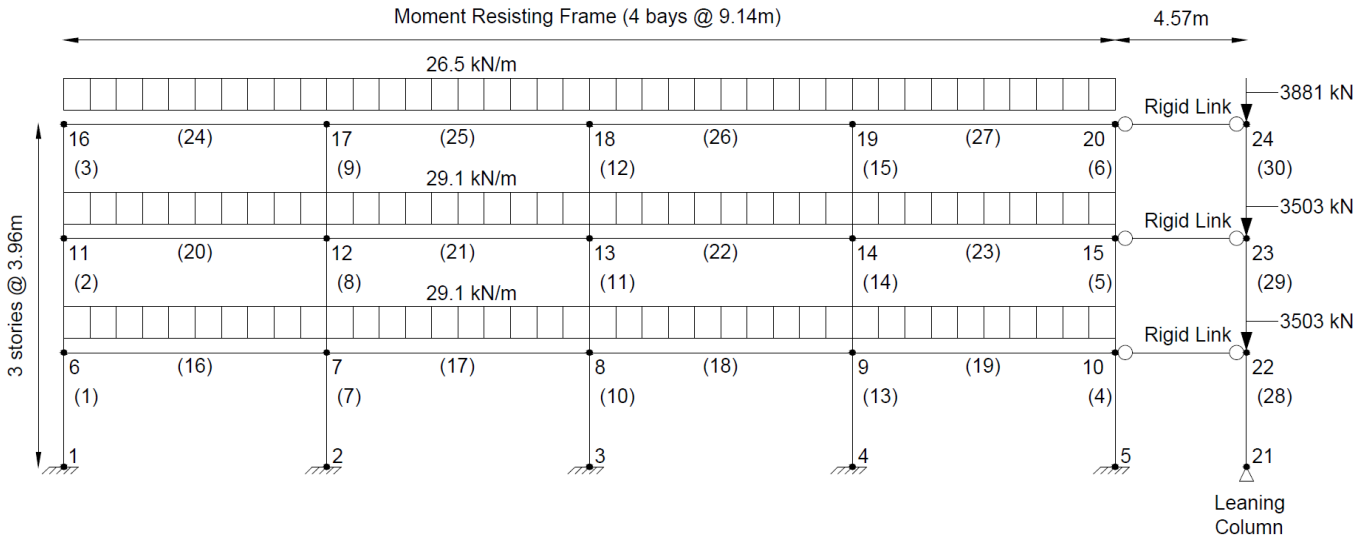

Fig. 4.12. Side view of East-West direction of the steel moment resisting frame showing geometry, seismic weight distribution, node numbers and element numbers (in parenthesis).

For a time history analysis the selected earthquakes have to be scaled, such that their response spectra should be equal or bigger than the design response spectrum throughout the period of interest. For the time history analysis are selected the same ground motions with the original

study (Xue, 2012; Gong et al., 2012), where they were scaled based on the design response spectrum for Vancouver, as specified by the National Building Code of Canada (NRCC 2010). The adopted ground motion time histories and the corresponding scale factors are show in Table 4.17. Similar to the previous dynamic analysis examples, these ground motions were taken from the PEER Strong Motion Database (http://peer.berkeley.edu/smcat/). The accelerogram for the 1979 Imperial Valley (EL Centro Array #12), 1989 Loma Prieta (Belmont Envirotech), 1994 Northridge (Old Ridge RT 090) and 1989 Loma Prieta (Presidio) is plotted in Fig. 4.8, Fig. 4.13, Fig. 4.14 and Fig. 4.15, respectively.

Table 4.17. Selected earthquakes records for the steel moment resisting frame.

Earthquake	Station	Magnitude	PGA (g)	Time of the PGA (sec)	Record duration (sec)	Scale Factor
1979 Imperial Valley	El Centro Array #12	6.5	0.143	10.845	39.01	2.1
1989 Loma Prieta	Belmont Envirotech	6.9	0.108	5.43	39.99	4.5
1994 Northridge	Old Ridge RT 090	6.7	0.568	8.24	39.98	0.8
1989 Loma Prieta	Presidio	6.9	0.2	12.05	39.985	1.5

Note: PGA= peak ground acceleration; g = gravity acceleration.

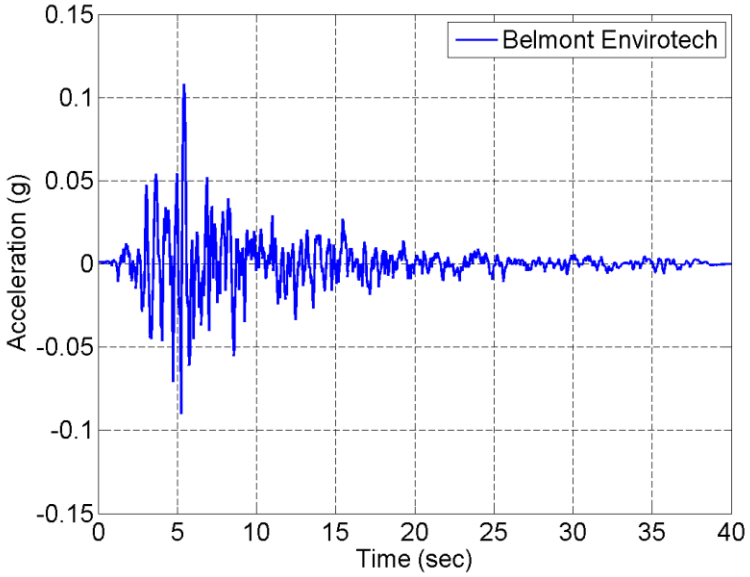

Fig. 4.13. Ground motion record for the earthquake 1989 Loma Prieta: Belmont Envirotech.

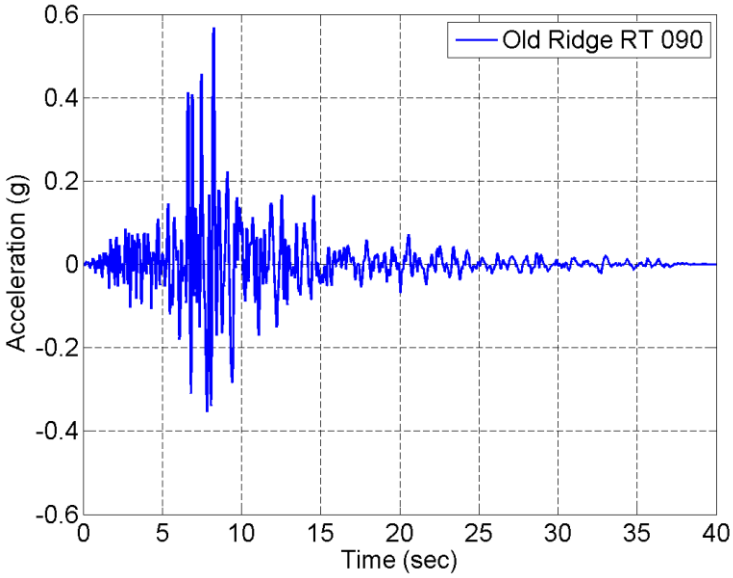

Fig. 4.14. Ground motion record for the earthquake 1994 Northridge: Old Ridge RT 090.

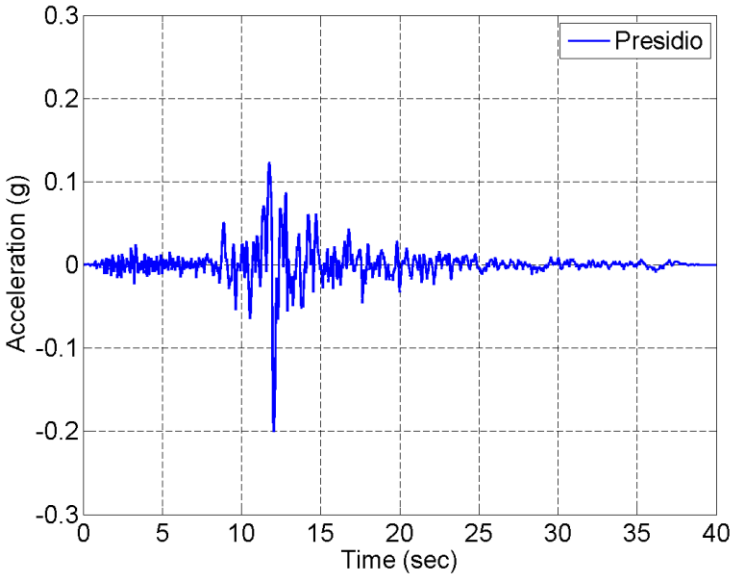

Fig. 4.15. Ground motion record for the earthquake 1989 Loma Prieta: Presidio.

The steel MRF consists of 27 structural members, while beams and columns are steel wide-flange sections, with 345 MPa grade steel and 248 MPa grade steel for the columns and beams, respectively. This difference in the grade steel is based on ductility consideration (Xue, 2012). In

this study is selected the optimal design #17 for the steel moment resisting frame, which was recommended by Xue (2012). Thus, are used exterior columns with W310x158 steel cross section, interior columns with W360x179 steel cross section, floor 2 beams with W610x82 steel cross section, floor 3 beams with W530x66 steel cross section and roof beams with W460x82 steel cross section. The basic dimensions of each selected cross section are presented in Table 4.18, while more information can be found in the Handbook of Steel Construction (CISC, 2010).

Table 4.18. Selected cross sections for the steel moment resisting frame.

Variable	Elements (Fig. 4.12)	Steel section	Depth d (mm)	Flange Width b_f (mm)	Flange Thickness t_f (mm)	Web Thickness t_w (mm)
Exterior columns	(1) to (6)	W310x158	327	310	25.1	15.5
Interior columns	(7) to (15)	W360x179	368	373	23.9	15.0
Floor 2 beams	(16) to (19)	W610x82	599	178	12.8	10.0
Floor 3 beams	(20) to (23)	W530x66	525	165	11.4	8.9
Roof beams	(24) to (27)	W460x82	460	191	16.0	8.9

The gravity columns were considered as hollow structural sections HSS254x254x13 (CISC, 2010), while the leaning column has a cross sectional area equal to 89,000 mm^2 and a moment of inertia equal to 845×10^6 mm^4, which correspond to the sum of the corresponding gravity column values. Similar to the previous examples, the frame is modeled and analyzed using the OpenSees FEA software, as described to the related literature (Xue, 2012; Gong et al., 2012).

4.5.2 Steel MRF subjected to single earthquakes under material uncertainty

First are considered as uncertain the material properties only, where each member of the steel MRF is assigned one random variable for each material property. These random variables are independent and identically distributed across the steel MRF members (Table 4.19). Thus, in total there are 81 (17×3) independent input random variables. M-DRM is implemented only, due to the high demanding computational cost. The fifth-order Gauss Hermite integration scheme is adopted, resulting to the M-DRM method with 81 × 5+1 = 406 FEA trials. The frame is subjected to each of the four previous earthquakes, considering the same input material uncertainties. The response of the steel frame, in terms of node displacement and inter-story drift, is recorded. The M-DRM approximation is used for the calculation of the lateral displacement statistics (Table 4.20) and the inter-story drift statistics (Table 4.21). The results indicate that the material uncertainty does not play a significant role to the response uncertainty, since it has been estimated a coefficient of variation less than 2%.

Table 4.19. Statistical properties of material random variables: Steel MRF.

Parameter	Distribution	Mean	COV
E of steel columns and beams (27 RVs)	Lognormal	200,000 N/mm^2	5.0%
f_y of steel columns (15 RVs)	Lognormal	345 N/mm^2	10.0%
f_y of steel beams (12 RVs)	Lognormal	248 N/mm^2	10.0%
b of steel columns and beams (27 RVs)	Lognormal	0.05	10.0%

Note: RVs = random variables; COV = coefficient of variation.

Table 4.20. Lateral displacement statistics: Steel MRF subjected to single earthquakes under material uncertainty.

Response	Location	El Centro Array #12		Belmont Envirotech		Old Ridge RT 090		Presidio	
		Mean (mm)	COV (%)	Mean (mm)	COV (%)	Mean (mm)	COV (%)	Mean (mm)	COV (%)
Lateral Displacement	Node 16	231.29	0.48	167.79	1.02	222.89	0.29	197.20	0.21
	Node 11	149.36	0.63	95.73	0.65	134.51	0.40	124.81	0.41
	Node 6	55.29	1.25	42.78	1.00	44.87	0.74	49.79	0.89

Table 4.21. Inter-story drift statistics: Steel MRF subjected to single earthquakes under material uncertainty.

Response	Location	El Centro Array #12		Belmont Envirotech		Old Ridge RT 090		Presidio	
		Mean (%)	COV (%)	Mean (%)	COV (%)	Mean (%)	COV (%)	Mean (%)	COV (%)
Inter-story drift	Story 1	1.40	1.25	1.08	1.00	1.13	0.74	1.26	0.89
	Story 2	2.39	0.51	1.67	1.16	2.32	0.35	2.02	0.26
	Story 3	2.08	0.95	2.43	0.74	2.33	0.73	2.01	0.57

4.5.3 Steel MRF subjected to single earthquakes under node mass uncertainty

The mass at each node of the steel MRF is considered as uncertain only. Each node takes the half mass of each element, which is framing to that node, and this value is considered as the mass mean value for each node. Then, the mass at each node is assumed to have a lognormal distribution with a 10% coefficient of variation, resulting to 18 (18×1) independent input random variables in total, since they are not correlated. The M-DRM method requires $18 \times 5+1 = 91$ FEA trials, since the fifth-order Gauss Hermite integration scheme is adopted. The lateral displacement statistics (Table 4.22) and the inter-story drift statistics (Table 4.23), show an increased coefficient of variation compared to the material uncertainty results. Especially for the earthquake 1989 Loma Prieta: Belmont Envirotech, the coefficient of variation of the roof lateral displacement is 14.40%. Thus, the mass uncertainty plays an important role to the response uncertainty, compared to the material uncertainty. In addition, the results indicate the importance of the ground motion selection in these types of analyses.

Table 4.22. Lateral displacement statistics: Steel MRF subjected to single earthquakes under node mass uncertainty.

Response	Location	El Centro Array #12		Belmont Envirotech		Old Ridge RT 090		Presidio	
		Mean (mm)	COV (%)	Mean (mm)	COV (%)	Mean (mm)	COV (%)	Mean (mm)	COV (%)
Lateral Displacement	Node 16	229.01	5.33	168.09	14.40	220.06	3.49	197.75	1.79
	Node 11	149.23	4.91	98.74	4.62	133.35	2.86	125.31	1.22
	Node 6	55.78	5.92	44.11	4.60	44.99	4.23	49.70	1.80

Table 4.23. Inter-story drift statistics: Steel MRF subjected to single earthquakes under node mass uncertainty.

Response	Location	El Centro Array #12		Belmont Envirotech		Old Ridge RT 090		Presidio	
		Mean (%)	COV (%)	Mean (%)	COV (%)	Mean (%)	COV (%)	Mean (%)	COV (%)
Inter-story drift	Story 1	1.41	5.92	1.11	4.60	1.14	4.23	1.26	1.80
	Story 2	2.37	5.12	1.68	13.70	2.29	3.56	2.03	2.05
	Story 3	2.05	7.96	2.41	7.85	2.32	5.50	2.01	2.75

4.5.4 Steel MRF subjected to repeated earthquakes under material uncertainty

It has been observed that structures can be subjected to repeated earthquakes, which may occur at brief time intervals (Amadio et al., 2003). Thus, each of the aforementioned ground motion records is applied twice to the steel MRF. For example, the hypothetical sequence for applying twice the 1979 Imperial Valley earthquake (EL Centro Array #12) is shown in Fig. 4.16. A time gap, i.e., zero ground acceleration, is applied between the two hypothetical seismic events, in order to cease the moving of the structure due to damping (Hatzigeorgiou and Beskos, 2009). This time gap is assumed to be equal to the duration of the single seismic event (Table 4.17), since it is almost equal to 40 seconds for each aforementioned earthquake (Fragiacomo et al.,

2004). For instance, the duration of the single 1979 Imperial Valley earthquake (EL Centro Array #12) is equal to 39.01 sec., resulting to a time gap $t_{ElCentro} = 39.01$ sec.

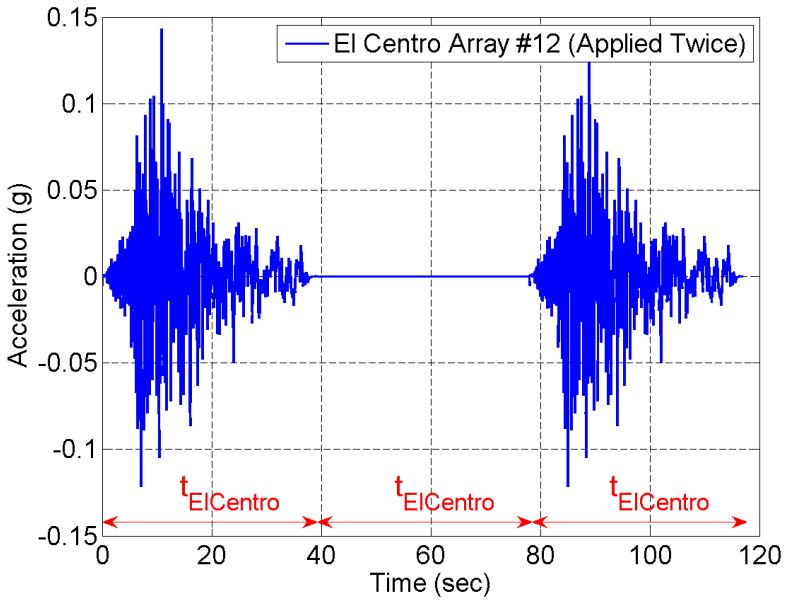

Fig. 4.16. Seismic sequence of using twice the ground motion record for the earthquake 1979 Imperial Valley: EL Centro Array #12.

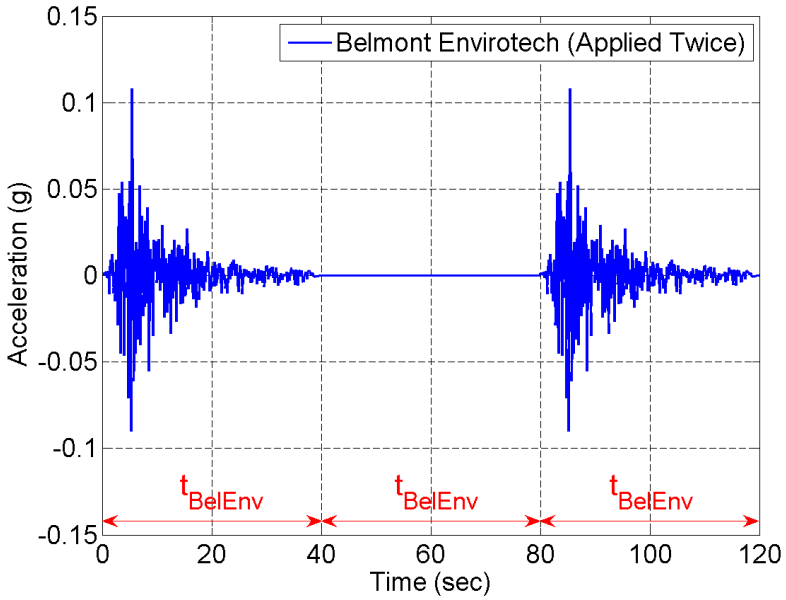

Fig. 4.17. Seismic sequence of using twice the ground motion record for the earthquake 1989 Loma Prieta: Belmont Envirotech.

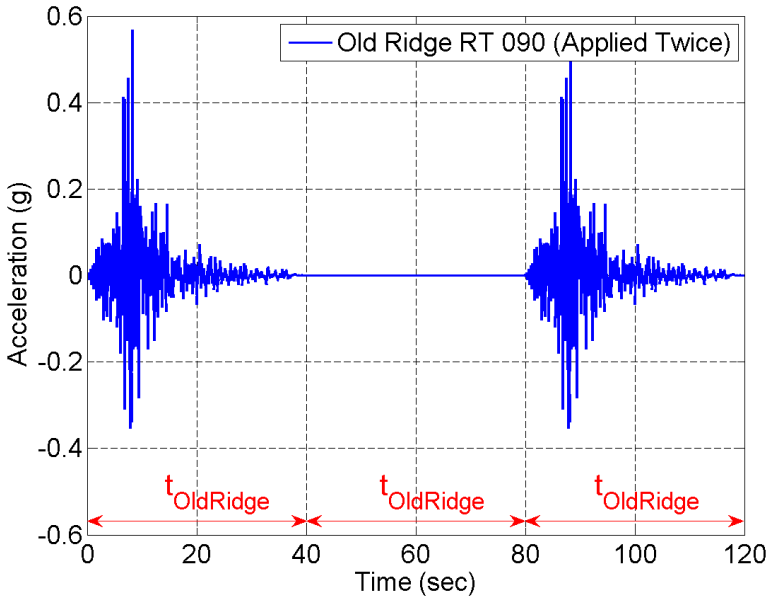

Fig. 4.18. Seismic sequence of using twice the ground motion record for the earthquake 1994 Northridge: Old Ridge RT 090.

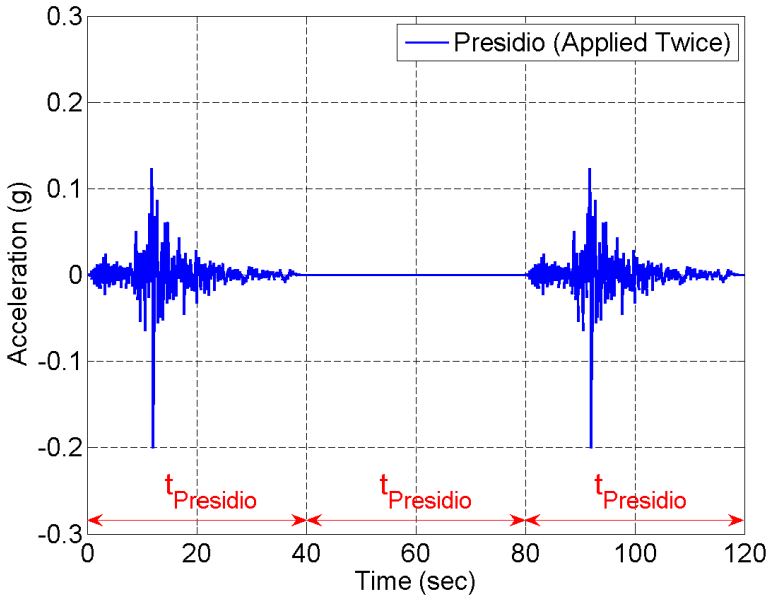

Fig. 4.19. Seismic sequence of using twice the ground motion record for the earthquake 1989 Loma Prieta: Presidio.

The steel MRF is subjected to these repeated earthquakes considering as random variables the same material properties (Table 4.19) with the previous analyzed single event (Section 4.5.2). M-DRM is implemented with 406 trials for each seismic sequence. Although, there is a slightly increase in the coefficient of variation of the lateral displacement (Table 4.24) and the inter-story drift (Table 4.25), comparing to the single event results under material uncertainty, still the total response uncertainty is not primarily affected by the material uncertainty.

Table 4.24. Lateral displacement statistics: Steel MRF subjected to repeated earthquakes under material uncertainty.

Response	Location	Earthquake applied twice (in sequence)							
		El Centro Array #12		Belmont Envirotech		Old Ridge RT 090		Presidio	
		Mean (mm)	COV (%)	Mean (mm)	COV (%)	Mean (mm)	COV (%)	Mean (mm)	COV (%)
Lateral Displacement	Node 16	249.52	0.69	183.14	1.29	240.48	0.48	214.83	0.49
	Node 11	160.58	0.80	98.41	1.21	144.21	0.53	136.22	0.67
	Node 6	59.77	1.62	46.11	1.07	47.84	0.88	54.72	1.44

Table 4.25. Inter-story drift statistics: Steel MRF subjected to repeated earthquakes under material uncertainty.

Response	Location	Earthquake applied twice (in sequence)							
		El Centro Array #12		Belmont Envirotech		Old Ridge RT 090		Presidio	
		Mean (%)	COV (%)	Mean (%)	COV (%)	Mean (%)	COV (%)	Mean (%)	COV (%)
Inter-story drift	Story 1	1.51	1.62	1.16	1.07	1.20	0.88	1.38	1.44
	Story 2	2.55	0.56	1.81	1.43	2.48	0.46	2.19	0.41
	Story 3	2.25	1.08	2.59	0.72	2.51	0.88	2.17	0.76

4.5.5 Steel MRF subjected to repeated earthquakes under node mass uncertainty

The steel MRF is subjected to the previous four hypothetical scenarios of repeated earthquakes, considering only the node masses as random variables, similar to the previous analyzed single

event (Section 4.5.3). The lateral displacement statistics (Table 4.26) and the inter-story drift statistics (Table 4.27), show an increased coefficient of variation compared to the material uncertainty results, under repeated earthquakes. Again, the earthquake 1989 Loma Prieta: Belmont Envirotech predicts a 16.33% coefficient of variation for the roof lateral displacement, indicating the importance of the selected earthquake and the major role of the mass uncertainty to the outcome response.

Table 4.26. Lateral displacement statistics: Steel MRF subjected to repeated earthquakes under node mass uncertainty.

		Earthquake applied twice (in sequence)							
		El Centro Array #12		Belmont Envirotech		Old Ridge RT 090		Presidio	
Response	Location	Mean (mm)	COV (%)	Mean (mm)	COV (%)	Mean (mm)	COV (%)	Mean (mm)	COV (%)
Lateral Displacement	Node 16	245.33	6.01	184.82	16.33	239.43	5.36	215.37	1.59
	Node 11	159.19	5.58	108.82	10.33	144.01	4.49	136.68	1.29
	Node 6	59.60	6.31	46.79	9.29	48.14	5.32	54.77	1.99

Table 4.27. Inter-story drift statistics: Steel MRF subjected to repeated earthquakes under node mass uncertainty.

		Earthquake applied twice (in sequence)							
		El Centro Array #12		Belmont Envirotech		Old Ridge RT 090		Presidio	
Response	Location	Mean (%)	COV (%)	Mean (%)	COV (%)	Mean (%)	COV (%)	Mean (%)	COV (%)
Inter-story drift	Story 1	1.50	6.31	1.18	9.29	1.21	5.32	1.38	1.99
	Story 2	2.52	5.76	1.84	15.72	2.48	5.35	2.20	1.84
	Story 3	2.20	8.27	2.57	9.63	2.50	8.12	2.17	2.74

4.5.6 Computational Time

The dynamic analysis of repeated earthquakes can be a highly demanding computational task, since the single time history analysis of structures may requires an enormous computational cost (Table 4.28). M-DRM seems to overcome this challenge, since the required trials can be

performed within a feasible computational time. For instance, M-DRM with 406 trials requires approximately 12.5 hours for applying twice the 1979 Imperial Valley earthquake (EL Centro Array #12), i.e., in sequence with a total duration of 120 seconds approximately. Furthermore, M-DRM can be considered as an efficient tool for these types of problems, since 91 trials require less than 4.5 hours, approximately, for each hypothetical scenario of repeated ground motions.

Table 4.28. Computational time using M-DRM: Single and repeated earthquakes.

Earthquake	Computational time (minutes)			
	Earthquake applied once		Earthquake applied twice (in sequence)	
	Material uncertainty (406 Trials)	Mass uncertainty (91 Trials)	Material uncertainty (406 Trials)	Mass uncertainty (91 Trials)
El Centro Array #12	104	25	394	190
Belmont Envirotech	150	37	782	248
Old Ridge RT 090	145	38	767	240
Presidio	98	35	759	237

4.6 Conclusion

The chapter presents the efficiency and robustness of the proposed multiplicative dimensional reduction method (M-DRM) for the finite element reliability analysis (FERA) of structures under lateral loads. First, four nonlinear FEA examples are considered in order to approximate the probability of failure. The Monte Carlo simulation (MCS) and the M-DRM method are both implemented using the OpenSees FEA software and the parameter updating functionality. Pushover and dynamic analysis is performed on a reinforced concrete and steel frame, under several input uncertainties. These examples were chosen due to the nonlinear limit state functions, where M-DRM is able to approximate the probability of failure with sufficient accuracy and computational cost.

For the frames subjected to lateral static loads, i.e., pushover analysis, the probability distribution of the structural response can also be approximated using the first order reliability method (FORM). However, it is well known that the accuracy of FORM depends on the degree of nonlinearity of the response. This is confirmed in the reinforced concrete frame example, where FORM does not converge in a stable manner to the correct solution. Although, FORM requires the less total trials for the presented examples, its total computational time is almost the same with the M-DRM. For the frames subjected to ground motion records, i.e., dynamic analysis, FORM may not be implemented due to the highly required computational cost. For example, for each limit state function, FORM has to be executed at the end of each time step of the time history, but not in a sequence, due to material state changes. In other words, for each n^{th} time step, the structure is analyzed till that n^{th} step and then FORM has to be performed.

The other advantage of the proposed approach is the significant reduction in computational efforts, while preserving accuracy that is fairly comparable to the MCS, as illustrated by the numerical examples presented in this study. Nonlinear pushover analysis of the steel frame with 179 input random variables highlights this point quite well. M-DRM with 896 FEA trials provides the same estimation accuracy as 100,000 simulations, while the computational time of M-DRM (10.85 minutes) is merely a fraction (1.02%) of that of the Monte Carlo simulations (17.71 hours).

The global sensitivity of the input variables to the response variance is a by-product of the analysis. Thus, it is not required any additional analytical effort for calculating the sensitivity coefficients, which provide the influence of each input variable to the output response. Thus, M-DRM method combined with the MaxEnt principle provides a viable approach for the complete probabilistic analysis of practical problems that are modelled using FEA.

MCS may not always be suitable for the single dynamic analysis of structures, due to the time variant nature of this type of analysis. Moreover, FERA may not be easily performed for structures subjected to several repeated earthquakes. Thus, several dynamic analyses of a steel moment resisting frame (MRF) are performed with the solely use of the M-DRM. The results indicate that the total response uncertainty (coefficient of variation), is not primarily affected by the material uncertainty of the steel MRF subjected to different earthquakes. However, the mass uncertainty indicates the importance of the selected earthquake to the variance of the output response. Thus, M-DRM can be considered as an easy to implement and accurate tool for these types of demanding analyses.

Chapter 5

Probabilistic Finite Element Analysis of Flat Slabs

5.1 Introduction

5.1.1 Flat Slabs

Flat plate or flat slab is the type of connection where the slab is directly supported to the column without the use of beams (Park and Robert, 1980). The first American flat slab was built by C. A. P. Turner in 1906 in Minneapolis (Sozen and Siess, 1963). Actually, it is a slab of uniform thickness supported either directly on columns, as shown in Fig. 5.1(a), or with the use of capital and drop panels, as shown in Fig. 5.1(b). They are constructed in various ways (in-situ or precast), they vary in structural forms (e.g., solid, waffle, etc.) and they can be either reinforced or prestressed (Cope and Clark, 1984). They are used widely in apartments and similar buildings, as they experience relatively light loads, and they are most economical for spans from 4.5 m to 6 m (MacGregor and Wight, 2005). They use a very simple formwork and less complex arrangement of reinforcement, which makes them much cheaper (Park and Robert, 1980). The absence of beams gives freedom at the organization of the interior space, i.e., a more flexible layout, because they provide various plans for succeeding storeys and a wide range of column spacing (Ajdukiewicz and Starosolski, 1990). Thus, this type of construction offers many advantages such as reduction in cost and time, simplicity and architectural features.

The main vulnerability of flat slabs is the punching shear failure around the column, which happens when the shear capacity of the slab-column joint is lost (MacGregor and Bartlett, 2000). When a heavy vertical load is applied on the slab-column connection, cracks first occur inside

the slab and near the area of the column. Then, cracks propagate through the thickness of the slab forming an angle between 20 degrees and 45 degrees to the bottom of the slab. This crack propagation can lead to punching shear failure which eventually happens along the cracks (MacGregor and Wight, 2005). The main issue here is that this failure happens in a brittle way with no warning, as even close to the failure these cracks may not be visible (Megally and Ghali, 1999). Therefore, punching shear is a critical design case for reinforced concrete flat slabs, while the provisions for punching shear design and detailing of the shear reinforcement differ considerably among the various European and American design codes (Albrecht, 2002).

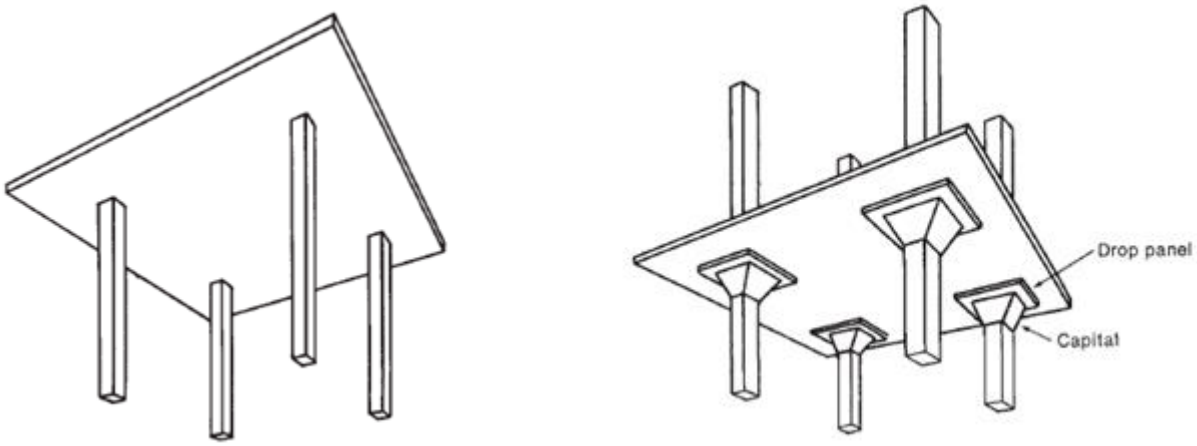

(a) **(b)**

Fig. 5.1. Flat slab (plate) supported on columns (scanned from MacGregor and Wight, 2005): (a) Flat plate (slab) floor; (b) Flat slab with capital and drop panels.

The design codes have been derived from many tests which take into account the common reinforcement practices in the respective countries (Albrecht, 2002). For instance, according to Ranking and Long (1987) in the UK and in the USA the development of design approaches has followed different routes. The British codes (BSI 1972 and BSI 1985) are based primarily on the work of Regan (1974) and the American code (ACI 318) is based primarily on the work of Moe

(1961). According to Gardner (2011), CEB-FIP Model Code of 1990 (CEB-FIP MC90) was fundamental in the development of Eurocode (EC2 2004). EC2 punching shear provisions is similar to CEB-FIP MC90 but: (1) it further provides limits on the size effect and reinforcement that will be used in the relevant equation; (2) it provides a provision for in-plane stresses that will be used in the relevant equation; (3) introduces a minimum shear strength expression. Although, the punching shear capacity increases as the amount of the flexural steel increases, the behaviour of the connection becomes more brittle (Gardner, 2011). Thus, EC2 adopts a maximum limit of two percent ($\rho \leq 0.02$) for the flexural reinforcement ratio that will be used in the relevant design equation.

Some more inconsistencies exist between the design codes. For example, the maximum permissible shear stress is taken on different critical perimeters around the column (Ranking and Long, 1987). Thus, critical perimeter is usually located between 0.5d to 2d from the face of the column (Albrecht, 2002). For the EC2, the shear stress depends on the level of the flexural reinforcement, on the size effect and on the concrete strength, while for the ACI the shear stress depends only on the concrete strength (Sacramento et al., 2012). This usually results in very different predictions of the punching strength for the same specimen (Ranking and Long, 1987).

All the design codes, in order to assure safety, adopt load increase factors and strength reduction factors, since the applied loads and the strength of reinforced concrete members are both random variables (Lu and Lin, 2004). Although the punching shear strength of a flat slab is calculated by the designer as a nominal value, the actual punching shear strength is affected by many parameters. Concrete strength, slab thickness, column size, shear reinforcement and flexural reinforcement can be considered as parameters that have an important contribution to the punching shear strength of flat slabs (Theodorakopoulos and Swamy, 2002). Therefore,

probabilistic analysis shall be employed in the punching shear failure study of reinforced concrete flat slabs.

5.1.2 Objective

The first objective is to present how nonlinear FEA can be implemented effectively, in order to predict the structural behavior as realistically as possible. For that reason two 3D isolated interior reinforced concrete flat slabs with and without shear reinforcement are analysed with the FEA software ABAQUS. The concrete damaged plasticity model, offered by ABAQUS, is adopted for the modeling of the concrete.

Then FEA is extended to probabilistic analysis by applying the Monte Carlo simulation (MCS) and the proposed multiplicative dimensional reduction method (M-DRM). Thus, this chapter also presents limitations, which can be a barrier for probabilistic FEA to be applied on large scale 3D structures, and how M-DRM can overcome these easily and efficiently making it an easy to use technique. M-DRM is also implemented for sensitivity analysis, in order to examine how uncertainty, associated with the model's input parameters, impacts the structural response of the analyzed interior flat slabs (with and without shear reinforcement).

Comparison between the shear unreinforced and the shear reinforced specimens is performed based on the calculated structural response of the slabs. Probabilistic analysis using current design codes (ACI 318 2011; EC2 2004) and a punching shear model, i.e., critical shear crack theory, are critically compared to the probabilistic FEA results, so as to determine the degree of conservatism associated with current design practices (ACI, EC2) and the predictive capability of the punching shear model (CSCT).

5.1.3 Organization

The organization of this chapter is as follows. Section 5.2 presents the punching shear experiment of an interior flat slab with and without shear reinforcement. Section 5.3 presents the FE analysis, the model that is used for the concrete and the FE results compared to test results. In Section 5.4, MCS and the proposed M-DRM are both implemented for the probabilistic FE analysis, where MCS is used as a benchmark in order to check the accuracy of the M-DRM results. Sensitivity analysis using M-DRM is also presented in Section 5.4, which also estimates which input random variables affect more the behavior of flat slabs. Section 5.5 demonstrates how punching shear strength is calculated based on the selected design codes (ACI, EC2) and punching shear model (CSCT), and shows the critical assessment between the design codes and the critical shear crack theory (CSCT) compared to the probabilistic FEA results. Finally, conclusions are summarized in Section 5.6.

5.2 Punching Shear Experiments

Two isolated interior slab-column specimens have been taken from a prototype structure with spans between columns of 3.75 m in both directions (Adetifa and Polak, 2005). SB1 is the slab without shear reinforcement and SB4 denotes the specimen with shear reinforcement (Fig. 5.2). Both slabs had the same dimensions and flexural reinforcement. The dimensions of the specimens were 1800x1800x120 mm and during the test simple supports were applied at distances of 1500x1500 mm. For the compression flexural reinforcement 10M@200 mm bars were used, while for the tension flexural reinforcement 10M@100 mm and 10M@90 mm for bottom and top layers, respectively. The yield strength of the flexural reinforcement was 455 MPa. The columns had a square cross-section of 150x150 mm with height 150 mm beyond the

top and bottom faces of the slab. The columns were reinforced with four 20M bars and four 8M stirrups. The compressive stress and tensile stress of concrete for the specimen SB1 was 44 MPa and 2.2 MPa, respectively. Slab SB4 had a compressive stress of concrete equal to 41 MPa and a tensile stress equal to 2.1 MPa. During the tests, the loading was applied through the column stub under displacement control. Specimen SB1 failed in punching shear at a load of 253 kN and displacement 11.9 mm, while specimen SB4 failed in flexure at a load of 360 kN and displacement 29.8 mm. The specimen SB4 has retrofitted with four rows of shear bolts (eight bolts in each row). The diameter of the shear bolts was 9.5 mm and the yield strength 381 MPa. The first row of the shear bolts was placed at distance 50 mm from the column's face and the next rows were placed at distance 80 mm between them. The schematic drawing and side section of specimens SB1 and SB4 are illustrated in Fig. 5.2 and Fig. 5.3, respectively.

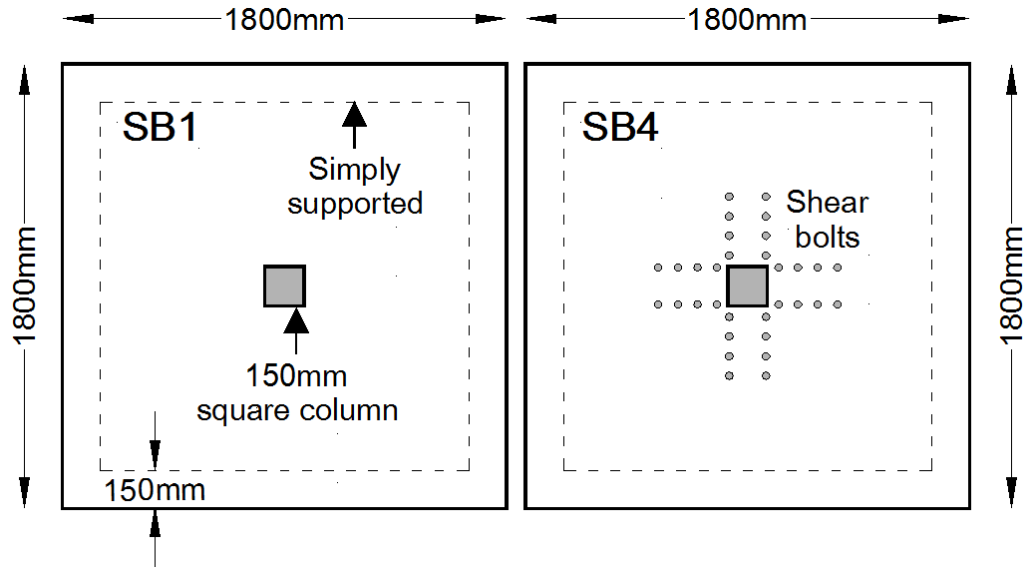

Fig. 5.2. Schematic drawing: Specimen without shear bolts (SB1) and with shear bolts (SB4).

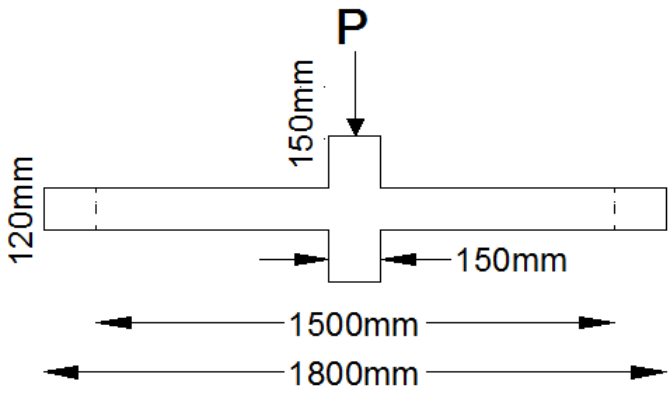

Fig. 5.3. Side section: Specimen SB1 and SB4.

5.3 Finite Element Analysis

Deterministic FEA is applied to the reinforced concrete slab-column connections using the commercial FEA software ABAQUS. Symmetry in both geometry and loading allows using only one quarter of each slab-column connection for the simulation in ABAQUS (Fig. 5.4). The concrete is modeled using 8-noded hexahedral elements with reduced integration (C3D8R) in order to avoid the shear locking problem. The reinforcement is modeled using 2-noded 3D linear truss elements (T3D2). Perfect bond is assumed between concrete and reinforcement through the embedded method. The reinforcement layout for the specimen SB4 is shown in Fig. 5.5. SB1 has the same reinforcement layout with the SB4, except for the shear bolts.

Through the thickness of the slab (120 mm) 6 brick elements were used with 20 mm mesh size in the adopted mesh. The slab SB1 was simulated with 9211 mesh elements and 11194 nodes, while the specimen SB4 was simulated with 9539 mesh elements and 11534 nodes. The shear bolts increased the concrete strength of the column in the tested specimen SB4. For that reason the concrete in column was modeled as elastic in the FEA. Simple supports were introduced

around the bottom edges of the specimens in the loading direction, where the summation of the reactions at these supports gives the ultimate load.

The load is applied with velocity through the column stub by performing quasi-static analysis in ABAQUS/Explicit. Even if the explicit method demands a large number of increments, the equations are not solved in each increment, leading to a smaller cost per increment compared to an implicit method. The small increments which are required in explicit dynamic methods make the ABAQUS/Explicit solver well suited for all the nonlinear problems. For accuracy in quasi-static analyses a smooth amplitude curve should be adopted simulating the increasing velocity. Mass scaling is introduced in ABAQUS/Explicit in order to be reduced the computational time for the following probabilistic analyses. The density of the concrete and the reinforcement was increased by a factor of 100, resulting in an increase in the time increment for the analysis by a factor of 10. The energy balance equation was evaluated at the end of each analysis in order to estimate whether or not each simulation has produced a proper quasi-static response. Among the constitutive models for simulating the behavior of concrete, the concrete damaged plasticity model that ABAQUS offers was chosen and a short description of this model is presented in the next section.

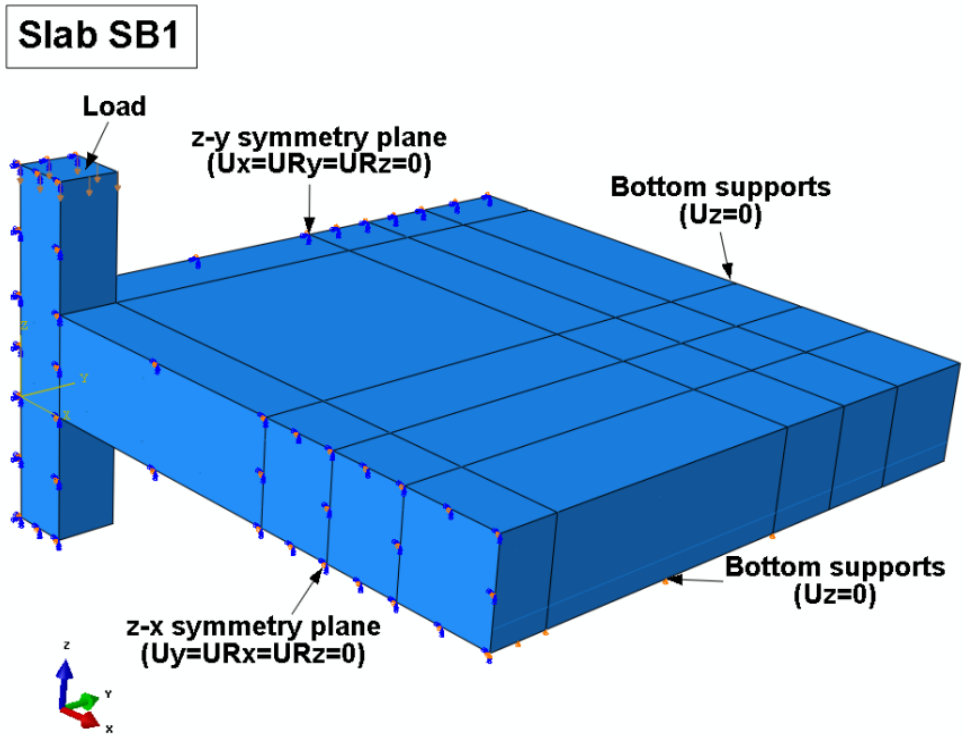

Fig. 5.4. Geometry and boundary conditions for the specimen SB1 (Note: Consider the same for the specimen SB4).

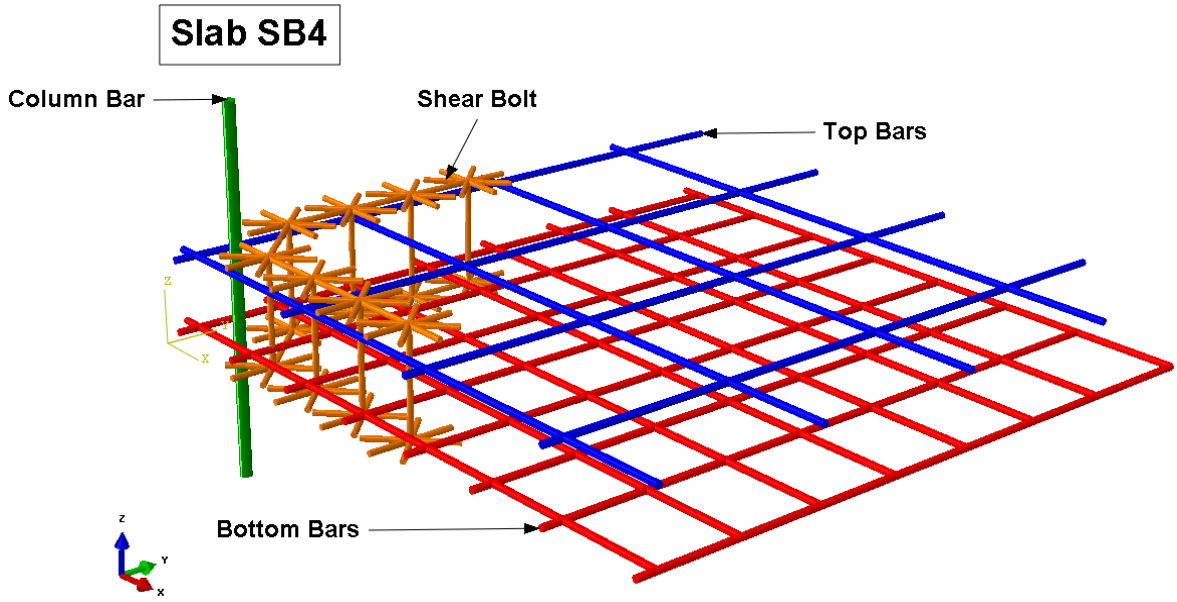

Fig. 5.5. Reinforcement layout for the specimen SB4 (Note: Consider the same for the specimen SB1 except the shear bolts).

5.3.1 Constitutive Modeling of Reinforced Concrete

Here is presented a short description of the adopted constitutive modeling of concrete. The concrete damaged plasticity model in ABAQUS is a continuum and plasticity-based damage model, in which the two main failure mechanisms are: (1) the tensile cracking; (2) the compressive crushing. The model uses a yield function that has been proposed by Lubliner (1989) and then modified by Lee and Fenves (1998). Non-associated flow rule is adopted using the Drucker-Prager hyperbolic function as the flow potential function.

In this work, in tension the concrete is described with a bilinear stress-crack displacement response according to Hillerborg (1985) (see Fig. 5.6), depending on the fracture energy (G_f) of concrete that represents the area under the stress-crack width curve. In order to be minimized the localization of the fracture the stress-strain response is defined as it is presented in Fig. 5.7. The critical length (l_c) in the current simulation is 20 mm, defined as the cubic root of the element volume. The fracture energy (G_f) is obtained from the CEB-FIP Model Code 90 (1993), which depends on the maximum aggregate size and the compressive strength of concrete. Thus, the fracture energy for the slab SB1 is defined equal to 0.082 N/mm, while for the slab SB4 is defined equal to 0.077 N/mm. Concrete in compression is modeled with the Hognestad parabola (Fig. 5.8). Reinforcement is defined with an elastic behavior through the modulus of the elasticity (E_s) and the Poisson's ratio (v) of which typical values are 200 GPa and 0.3, respectively. Bilinear strain hardening response is adopted according to the test results (Fig. 5.9). All model and material properties that are used in these analyses are adopted from literature (Genikomsou and Polak, 2015).

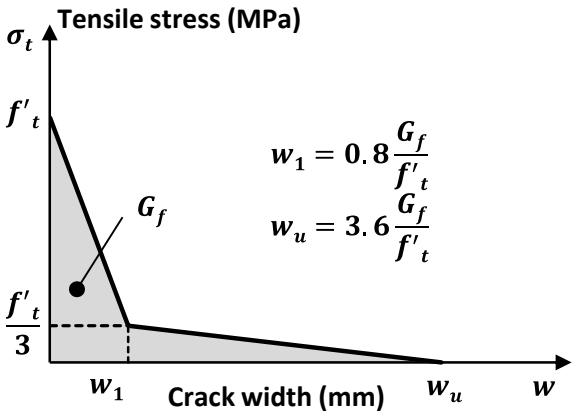

Fig. 5.6. Uniaxial tensile stress-crack width relationship for concrete.

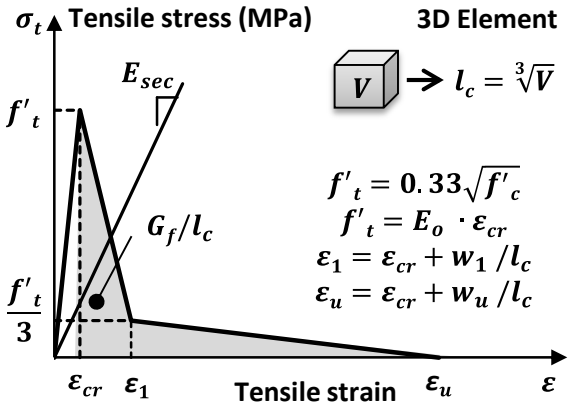

Fig. 5.7. Uniaxial tensile stress-strain relationship for concrete.

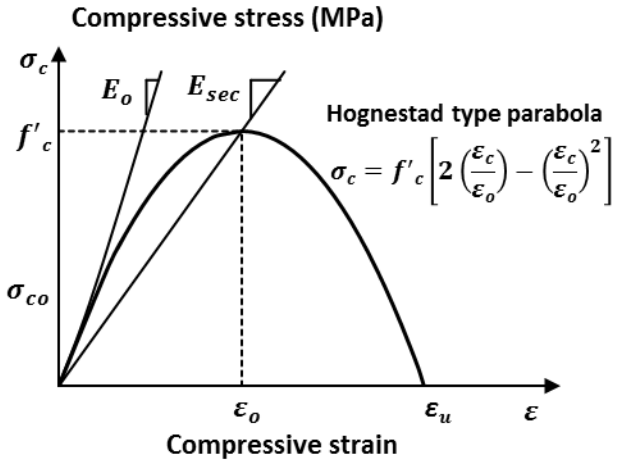

Fig. 5.8. Uniaxial compressive stress-strain relationship for concrete.

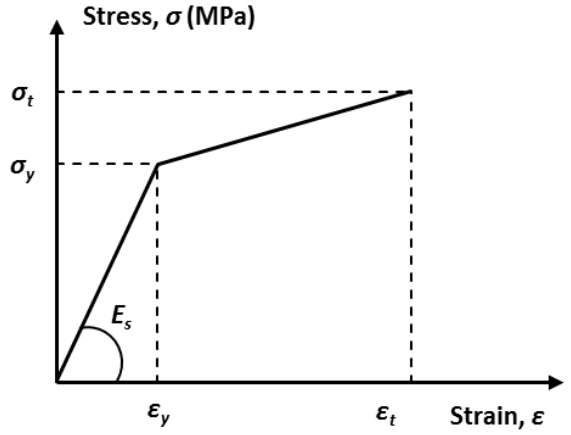

Fig. 5.9. Stress-strain relationship for steel.

5.3.2 Load-deflection response and crack pattern of the slabs

The FEA results of the slab-column connections are in good agreement with the tested responses in terms of ultimate load-displacement curves and cracking pattern. The response obtained from the simulation of the slab SB1, predicts a brittle punching shear failure which is in agreement with the experiment (Fig. 5.10). The ultimate load and displacement in the quasi-static analysis

are in units of 227 kN and 10.4 mm, respectively, compared to the test results that were 253 kN and 11.9 mm. The cracking pattern at failure of the simulated specimen SB1 is presented at the bottom of the slab (Fig. 5.12). Firstly, the cracking occurs tangentially at the area of the maximum bending moment near the column and then the cracking spreads radially towards the slab edges as the load increases. At the ultimate load, the shear crack opens suddenly and more shear cracks are developed outside the punching shear cone. The smeared crack approach in the concrete damaged plasticity model in ABAQUS considers the crack directions by assuming that the direction of the cracking is parallel to the direction of the maximum principal plastic strain.

Fig. 5.11 compares the experimental and numerical results, in terms of load-deflection response for the specimen SB4. Tested and numerical results are in good agreement. Slab SB4 failed in flexure, which is obvious from the relevant graph (Fig. 5.11), since the shear bolts increased both the ultimate load and ductility of the specimen. According to the test results, specimen SB4 failed at a load of 360 kN and displacement 29.8 mm, compared to the FEA results that showed failure at the load of 341 kN and displacement 25.2 mm. Slab SB4 experienced bending cracks near the column at the tension side of the slab. The shear cracks were developed outside the shear reinforced area, causing the flexural failure. Fig. 5.13 shows the cracks on the tension side of the slab SB4 at failure.

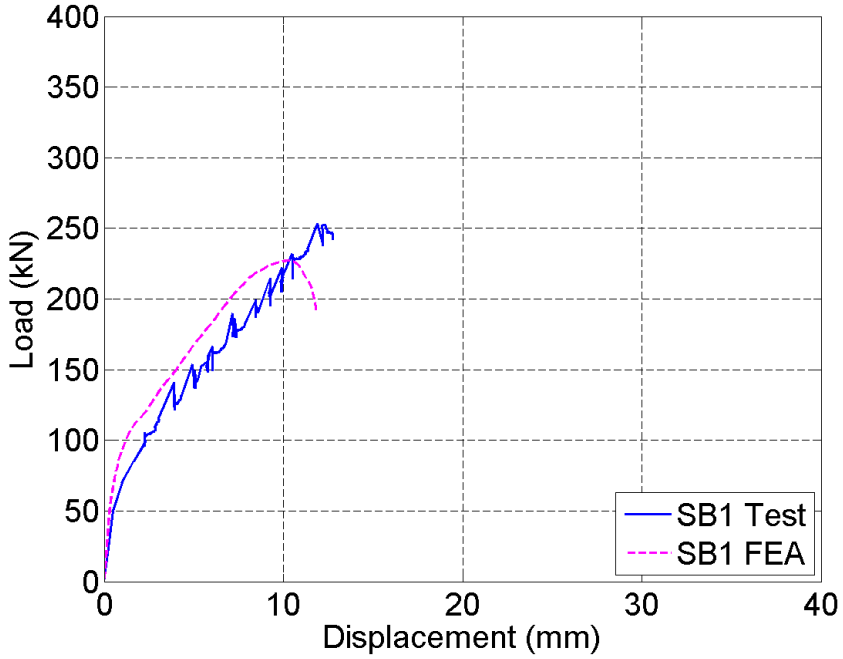

Fig. 5.10. Curves of Load-Displacement: Slab SB1.

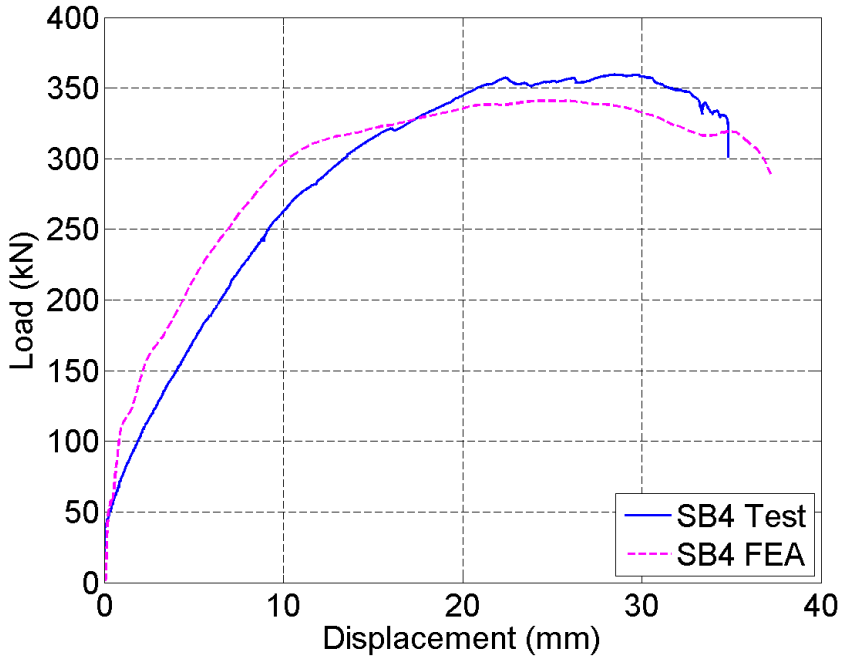

Fig. 5.11. Curves of Load-Displacement: Slab SB4.

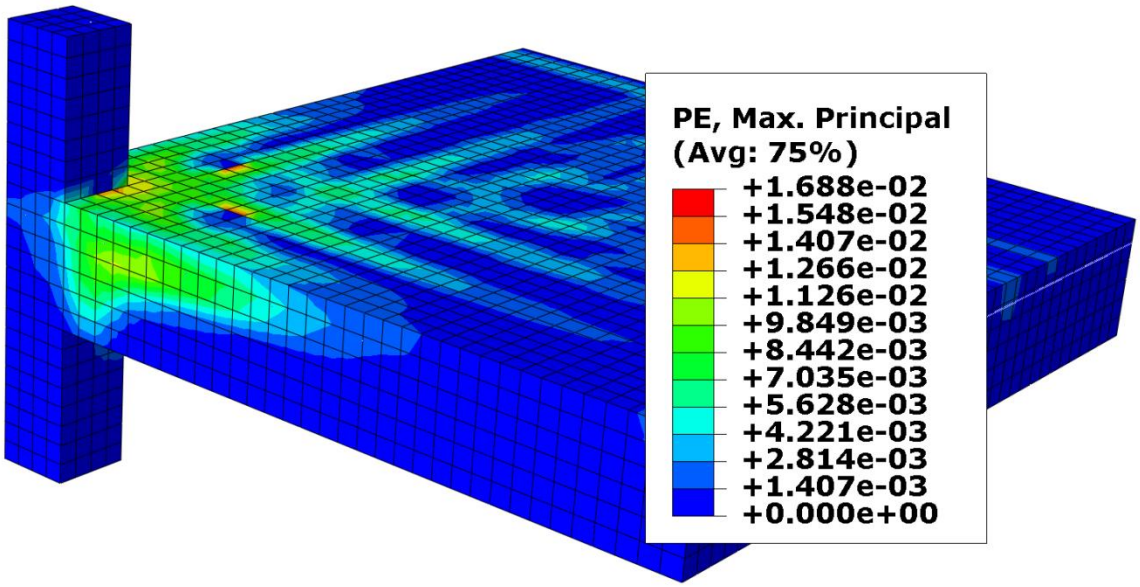

Fig. 5.12. Ultimate load cracking pattern at the bottom of the slab SB1: Quasi-static analysis in ABAQUS/Explicit.

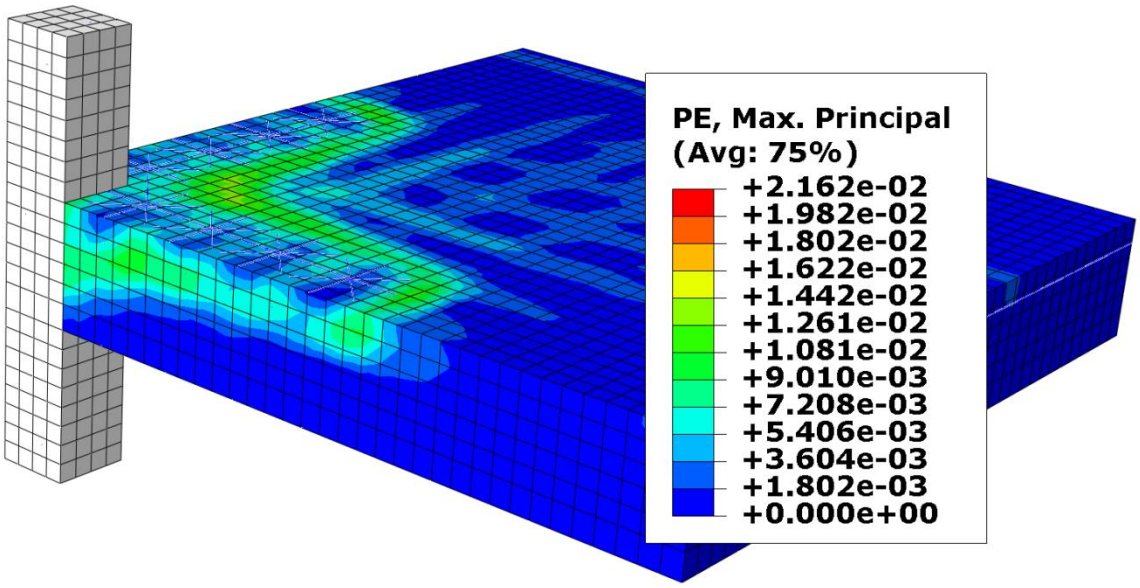

Fig. 5.13. Ultimate load cracking pattern at the bottom of the slab SB4: Quasi-static analysis in ABAQUS/Explicit.

Fig. 5.14. Ultimate load cracking pattern at the bottom of the slab SB1: Test results (scanned from Adetifa and Polak 2005).

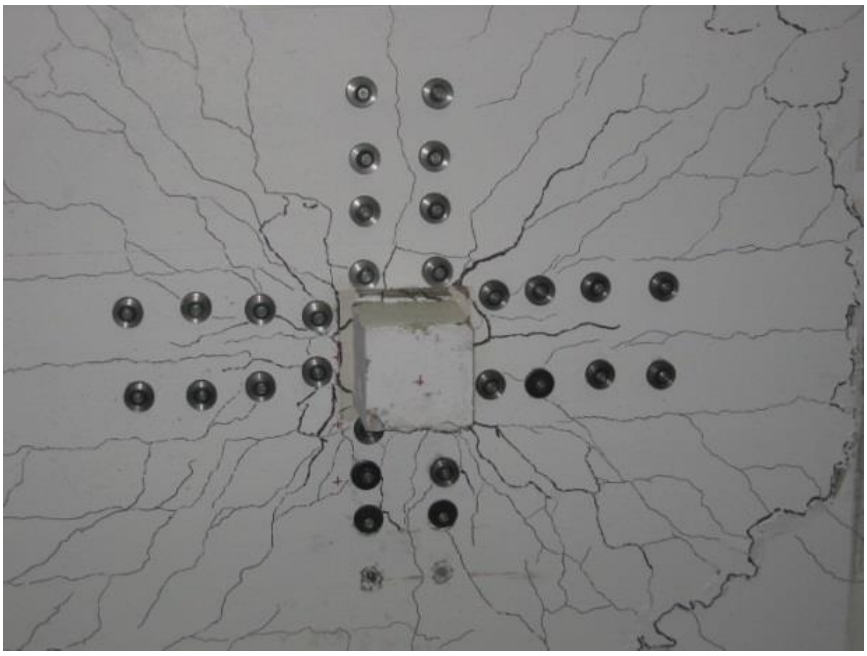

Fig. 5.15. Ultimate load cracking pattern at the bottom of the slab SB4: Test results (scanned from Adetifa and Polak 2005).

5.4 Probabilistic Finite Element Analysis

5.4.1 General

In order to apply probabilistic FEA is required to link a general purpose FEA program, i.e., ABAQUS, with an existing reliability platform, i.e., NESSUS or ISIGHT, or we can take advantage of the free, general-purpose and high-level Python programing language, since Python Development Environment (PDE) is supported from the ABAQUS GUI. PDE can be used for developing the deterministic FE model and then coupling it with the reliability problem, due to uncertain input parameters.

5.4.2 Monte Carlo Simulation

In order to apply MCS, we have to update the random variables of interest for each FEA trial. Python programing is used in order to develop the deterministic FE model and then the input random variables of interest are being updated based on the idea of parameter updating functionality, which has been used to the previous chapter to update OpenSees (McKenna et al., 2000) parameters with the use of the Tcl programing (Scott and Haukaas, 2008). Once the input random variables of interest are being updated, deterministic FEA in ABAQUS is performed and the result is stored in an output file which has an output database format (.odb). This procedure is repeated as many times as MCS requires, producing the same number of .odb files as the number of trials. Then, another Python script is being developed in order to extract the values of interest from the .odb files (Fig. 5.16). Although, quasi-static type of analysis is faster than static analysis, for the SB1 and SB4 problem quasi-static analysis needs 505 and 614 seconds to run, respectively, for each trial on a personal computer with Intel i7-3770 3rd Generation Processor and 16GB of RAM. Therefore, MCS is being performed considering only 10^3 trials, for both SB1

and SB4. For comparison purposes, MCS results are presented in the next section together with the M-DRM results.

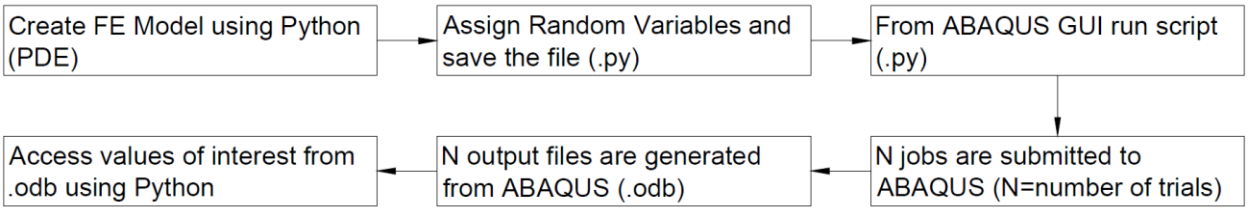

Fig. 5.16. Flowchart for linking ABAQUS with Python for probabilistic FEA.

5.4.3 Multiplicative Dimensional Reduction Method

Here M-DRM is applied on slab-column connections with and without shear reinforcement, i.e., SB4 and SB1, so as to be evaluated its accuracy and efficiency for both probabilistic and sensitivity analysis of nonlinear large scale reinforced concrete structures. Although, in these examples Python code has been developed in order to link ABAQUS with M-DRM, M-DRM can also be implemented without the need of programing (or a linking platform), since it requires a small number of trials. Thus, based on the M-DRM input grid, the analyst can insert manually the value of the random variable of interest, i.e., without having to automate the M-DRM trials, making M-DRM an applicable and easy to use method.

5.4.3.1 Flat Slab without Shear Reinforcement (SB1)

Probabilistic FEA is applied to the previous analysed reinforced concrete slab-column connection without shear reinforcement (SB1), due to uncertain input material properties (Table 5.1). Each member of the flat slab is assigned one random variable for each material property, leading to a total of 18 random variables.

Table 5.1. Statistical properties of random variables for the slab SB1.

Material	Random Variable	Distribution	Nominal Value	Mean	COV	Reference
Concrete (Slab & Column)	f_c' (MPa) (2RVs)	Normal	44	1.14×Nominal	0.145	Nowak et al., 2012
	f_t' (MPa) (2RVs)	Normal	2.2	Nominal	$\mathrm{COV}_{f_c'}$	Ellingwood et al., 1980
	γ_c (kN/m^3) (2RVs)	Normal	24	Nominal	0.03	Ellingwood et al., 1980
Steel (Slab & Column)	E_s (GPa) (3RVs)	Normal	200	Nominal	0.033	Mirza and Skrabek, 1991
	γ_s (kN/m^3) (3RVs)	Normal	78	Nominal	0.03	Assumed
Steel in Slab (10M Bars)	f_y (MPa) (2RVs)	Normal	455	1.2×Nominal	0.04	Nowak and Szerszen, 2003a
	A_s (mm^2) (2RVs)	Normal	100	Nominal	0.015	Rakoczy and Nowak, 2013
Steel in Column (20M Bars)	f_y (MPa) (1RV)	Normal	455	1.15×Nominal	0.05	Nowak and Szerszen, 2003a
	A_s (mm^2) (1RV)	Normal	300	Nominal	0.015	Rakoczy and Nowak, 2013

Note: RVs = Random Variables; f_c' = compressive strength of concrete; f_t' = tensile strength of concrete; γ_c = density of concrete; E_s = modulus of elasticity of reinforcement; γ_s = density of reinforcement; f_y = yield strength of reinforcement; A_s = cross-section area of reinforcement.

5.4.3.1.1 Calculation of Response Moments

Using the M-DRM method, by considering the previous 18 input random variables and the fifth-order $(L = 5)$ Gauss-Hermite points for the standard normal random variable, function evaluation points $h(x_j)$ can be found for each random variable and an input grid can be generated leading to a Total Number of Function Evaluations = 1+18×5 = 91. Each trial corresponds only to one input random variable, while the remaining random variables are hold

fixed at their mean values forming 90 independent trials, with a 91th trial being reserved for the mean case, i.e., where all input random variables are set equal to their mean values (Table 5.2).

Table 5.2. Input Grid for the ultimate load for the slab SB1.

Input Random Variable	Trial	Gauss-Hermite Points (z_j)	f_c' (MPa)]	…	γ_s (kN/m^3)	P_{ij} (kN)
f_c' (MPa)	1	–2.85697	**29.38**	…	78.00	201.9612
	2	–1.35563	**40.30**	…	78.00	221.7581
	3	0	**50.16**	…	78.00	235.9828
	4	1.35563	**60.02**	…	78.00	247.2946
	5	2.85697	**70.94**	…	78.00	257.5682
…	…	…	…	…	…	…
γ_s (kN/m^3)	86	–2.85697	50.16	…	**71.31**	235.9832
	87	–1.35563	50.16	…	**74.83**	235.9822
	88	0	50.16	…	**78.00**	235.9828
	89	1.35563	50.16	…	**81.17**	235.9810
	90	2.85697	50.16	…	**84.69**	235.9818
Fixed Mean Values	91	N/A	50.16	…	78.00	235.9828

Note: P_{ij} is the structural response according to probabilistic FEA, i.e., ultimate load or ultimate displacement.

First the mean of each cut function is calculated as $\rho_i = \sum_{j=1}^{L} w_j P_{ij}$, $i = 1,2,\dots,n$, where P_{ij} is the structural response, i.e., ultimate load or ultimate displacement obtained from ABAQUS, when the i^{th} cut function is set at the j^{th} quadrature point. Similarly, the mean square of cut functions was calculated as $\theta_i = \sum_{j=1}^{L} w_j \left(P_{ij}\right)^2$, $i = 1,2,\dots,n$. This calculation procedure is illustrated in Table 5.3. In fact any fractional moment of order α can be approximated in a similar manner as $M_Y^{\alpha} \approx \sum_{j=1}^{L} w_j \left(P_{ij}\right)^{\alpha}$. From here, the proposed M-DRM is applied in order to compute the output distribution statistics, i.e., the first product moment and the second product moment. Then, the standard deviation (σ_Y) of the response function is calculated as the square

root of the variance (V_Y). The numerical results obtained from M-DRM are compared to the results obtained from MCS. As observed M-DRM estimations have small relative error comparing to MCS, resulting to a good numerical accuracy of the method (Table 5.4).

Table 5.3. Output Grid for the ultimate load for the slab SB1.

Input Random Variable	Trial	Gauss-Hermite Weights (w_j)	$w_j \times P_{ij}$ (kN)	ρ_k (kN)	$w_j \times (P_{ij})^2$	θ_k (kN^2)
f_c' (MPa)	1	0.011257	2.2735	**235.1959**	459.171	**55408.15**
	2	0.22208	49.247		10920.9	
	3	0.53333	125.85		29700.2	
	4	0.22208	54.918		13580.9	
	5	0.011257	2.8995		746.832	
…	…	…	…	…	…	…
γ_s (kN/m^3)	86	0.011257	2.6565	**235.9823**	626.903	**55687.65**
	87	0.22208	52.405		12366.8	
	88	0.53333	125.85		29700.2	
	89	0.22208	52.405		12366.7	
	90	0.011257	2.6565		626.896	
Fixed Mean Values	91	N/A	N/A	N/A	N/A	N/A

Note: P_{ij} is the structural response according to probabilistic FEA, i.e., ultimate load or ultimate displacement.

Table 5.4. Output Distribution statistics of the structural response for the slab SB1.

SB1	Ultimate Disp. (mm)		Ultimate Load (kN)		Relative Error (%)	
	M-DRM (91 Trials)	MCS (10^3 Trials)	M-DRM (91 Trials)	MCS (10^3 Trials)	Ultimate Disp.	Ultimate Load
Mean	9.1613	9.1599	234.7299	235.3731	0.01	0.27
Stdev	0.5183	0.5628	15.5032	15.3923	7.90	0.72
COV	0.0566	0.0614	0.0661	0.06539	7.92	0.99

Note: M-DRM = Multiplicative Dimensional Reduction Method; MCS = Monte Carlo Simulation; Relative Error = $|MCS - MDRM|/MCS$; Stdev = Standard Deviation; COV = Coefficient of Variation.

5.4.3.1.2 Estimation of Response Distribution

Structural responses obtained using M-DRM method, are used in conjunction with the Maximum Entropy (MaxEnt) principle with fractional moment constraints. Thus, estimated PDF $\left(\hat{f}_X(x)\right)$ of the structural response is estimated based on Lagrange multipliers (λ_i) and fractional exponents (α_i) $(i = 1,2,\dots,m)$, which are reported on Table 5.5 and Table 5.6 for the ultimate load and ultimate displacement of SB1, respectively. Entropy is practically constant for $m \geq 2$ as shown on Table 5.5 and Table 5.6, so it is sufficient to use only three fractional moments $(m = 3)$.

The estimated MaxEnt PDF of the output response is then compared to the MCS results. It is observed that the estimated PDF of the ultimate load obtained from the M-DRM with three fractional moments $(m = 3)$ and only 91 trials, is in close agreement with the ultimate load obtained from the MCS with 10^3 trials (Fig. 5.17). Same applies for the ultimate displacement (Fig. 5.19).

In general, the probability of failure (p_f) can be estimated by plotting the probability of exceedance (POE) obtained from M-DRM. In this example, probabilistic FEA provides the resistance of the slab-column connection, thus, probability of failure cannot be calculated here. However, it is observed that M-DRM provides highly accurate approximation for almost the entire range of the output response distribution (Fig. 5.18 and Fig. 5.20). For example, according to the associated POE and considering the tested ultimate load of 253 kN, M-DRM with three fractional moments $(m = 3)$ estimates 1.19×10^{-1} probability of exceedance the value of 253 kN, which is close to the estimated value of MCS (1.31×10^{-1}), indicating the accurate prediction of the proposed method (Fig. 5.18).

Table 5.5. MaxEnt parameters for the ultimate load for the slab SB1.

Fractional Moments	Entropy	i	0	1	2	3	4
	7.448	λ_i	–0.9275	4.3659			
m=1		α_i		0.1194			
		$M_X^{\alpha_i}$		1.9184			
	4.1633	λ_i	326.394	301.87	–320.52		
m=2		α_i		0.8419	0.8329		
		$M_X^{\alpha_i}$		99.020	94.266		
	4.1633	λ_i	349.347	13.216	3.532	-41.288	
m=3		α_i		0.5945	0.9783	0.6483	
		$M_X^{\alpha_i}$		25.645	208.51	34.406	
	4.1632	λ_i	402.423	34.808	-113.57	-60.171	84.311
m=4		α_i		0.9852	0.5595	0.9336	0.7203
		$M_X^{\alpha_i}$		216.55	21.186	163.34	50.984

Table 5.6. MaxEnt parameters for the ultimate displacement for the slab SB1.

Fractional Moments	Entropy	i	0	1	2	3	4
	3.5238	λ_i	1.512	0.6692			
m=1		α_i		0.4971			
		$M_X^{\alpha_i}$		3.0061			
	0.7806	λ_i	655.832	6543.8	-4955.4		
m=2		α_i		-0.8884	-0.5189		
		$M_X^{\alpha_i}$		0.1402	0.3173		
	0.7806	λ_i	566.305	-5034.8	5875.7	838.24	
m=3		α_i		-0.4508	-0.9046	-0.2361	
		$M_X^{\alpha_i}$		0.3689	0.1352	0.5930	
	0.7805	λ_i	678.573	-8254.4	3078.6	4932.9	1786.0
m=4		α_i		-0.5437	-0.9848	-0.7157	-0.6334
		$M_X^{\alpha_i}$		0.3003	0.1133	0.2053	0.2463

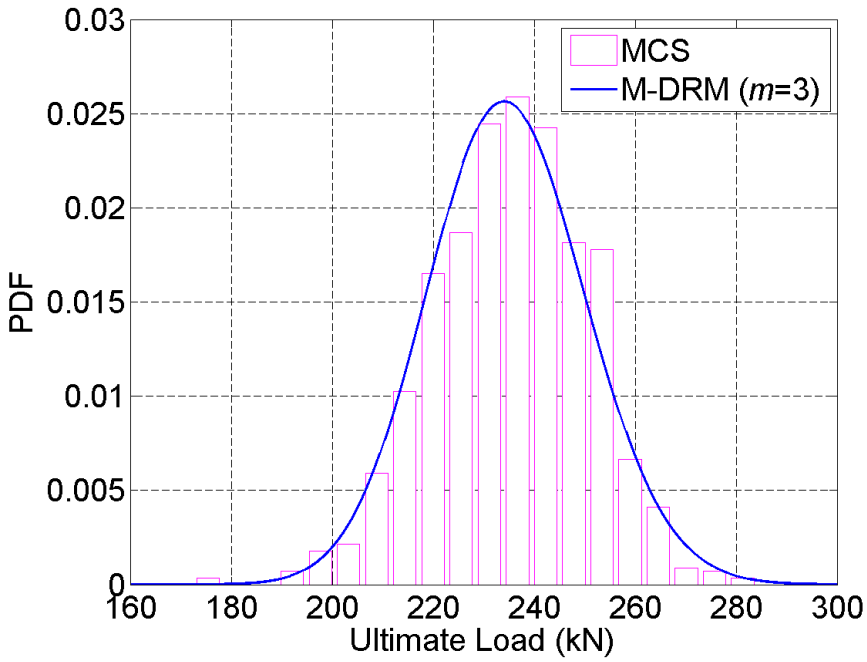

Fig. 5.17. Probability Distribution of the ultimate load for the slab SB1.

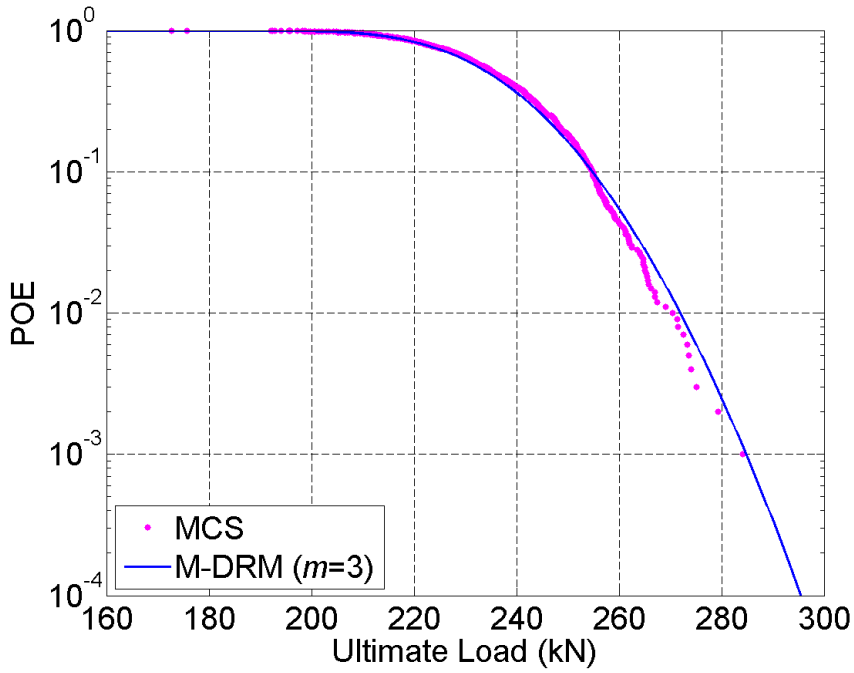

Fig. 5.18. Probability of Exceedance (POE) of the ultimate load for the slab SB1.

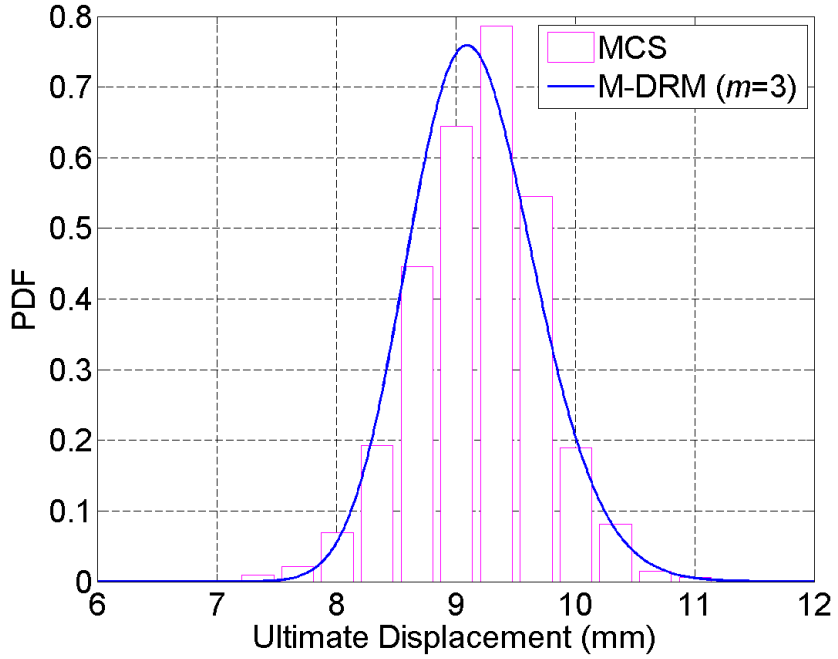

Fig. 5.19. Probability Distribution of the ultimate displacement for the slab SB1.

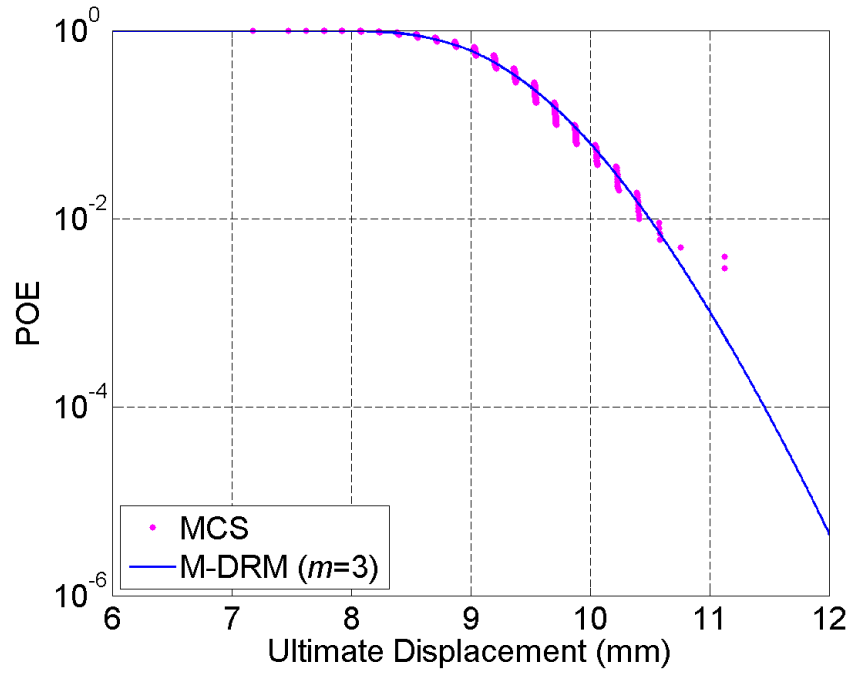

Fig. 5.20. Probability of Exceedance (POE) of the ultimate displacement for the slab SB1.

5.4.3.1.3 Global Sensitivity Analysis

The 18 input random variables are listed according to the primary sensitivity coefficient S_i, in order to examine which affects more and which less the calculated output response, i.e., ultimate load (Table 5.7) and ultimate displacement (Table 5.8).

Table 5.7. Sensitivity indices for the ultimate load for the slab SB1.

Rank	Material	Random Variable	S_i (%)
1	Concrete in Slab	f_t'	60.85
2	Concrete in Slab	f_c'	37.81
3	Bottom Steel in Slab	E_s	1.16
4	Bottom Steel in Slab	A_s	0. 23
5	Concrete in Column	f_t'	2.78E-02
6	Concrete in Column	f_c'	5.09E-03
7	Concrete in Slab	γ_c	3.66E-03
8	Top Steel in Slab	E_s	5.19E-04
9	Top Steel in Slab	A_s	1.02E-04
10	Concrete in Column	γ_c	1.03E-05
11	Bottom Steel in Slab	γ_s	4.75E-06
12	Steel in Column	E_s	3.23E-06
13	Steel in Column	A_s	2.32E-06
14	Top Steel in Slab	γ_s	6.19E-07
15	Steel in Column	γ_s	2.24E-07
16	Bottom Steel in Slab	f_y	1.58E-8
17	Top Steel in Slab	f_y	1.58E-8
18	Steel in Column	f_y	3.07E-11

For the ultimate load case, the sensitivity coefficient for the tensile strength of concrete in slab is equal to 60.85%. This is essentially the ratio of the variance of the ultimate load, when all the input random variables except the tensile strength of concrete in slab are hold fixed to their mean values, to the overall variance of the ultimate load. This shows that the ultimate load is most sensitive to the input random variable f_t', owing 60.85% of its variance to the variance of the input random variable f_t'. The uncertainty in material model predicts the critical role of the

tensile parameter in punching shear failure, followed by the compressive strength of concrete in slab.

For the ultimate displacement case, except the major contribution of the tensile (51.75%) and the compressive strength (35.98%) of concrete in slab, the contribution of bottom reinforcement in slab has been increased indicating that the modulus of elasticity (7.49%) and the cross-section area of steel (4.77%) also contribute to the ultimate displacement of the slab.

Table 5.8. Sensitivity indices for the ultimate displacement for the slab SB1.

Rank	Material	Random Variable	S_i (%)
1	Concrete in Slab	f_t'	51.75
2	Concrete in Slab	f_c'	35.98
3	Bottom Steel in Slab	E_s	7.49
4	Bottom Steel in Slab	A_s	4.77
5	Concrete in Column	f_c'	9.99E-02
6	Concrete in Column	f_t'	4.15E-04
7	Concrete in Column	γ_c	2.73E-04
8	Concrete in Slab	γ_c	2.09E-04
9	Steel in Column	E_s	4.68E-06
10	Steel in Column	A_s	8.29E-07
11	Bottom Steel in Slab	E_s	7.23E-07
12	Bottom Steel in Slab	A_s	6.62E-07
13	Top Steel in Slab	f_y	3.13E-11
13	Bottom Steel in Slab	f_y	3.13E-11
13	Steel in Column	f_y	3.13E-11
13	Top Steel in Slab	γ_s	3.13E-11
13	Bottom Steel in Slab	γ_s	3.13E-11
13	Steel in Column	γ_s	3.13E-11

5.4.3.1.4 Computational Time

M-DRM provides an enormous saving of computational time. For instance, each deterministic FEA takes 505 seconds to run on a personal computer with Intel i7-3770 3rd Generation Processor and 16GB of RAM. Therefore, MCS with 1,000 simulations requires 140.28 hours while M-DRM with 91 simulations requires 12.77 hours. M-DRM also includes the MaxEnt

method which requires 160 seconds, thus M-DRM total computational time equals to 12.81 hours, which is merely 9.13% of the time taken by the Monte Carlo simulation.

5.4.3.2 Flat Slab with Shear Reinforcement (SB4)

Probabilistic FEA is applied to the previous analysed reinforced concrete slab-column connection with shear reinforcement (SB4), where based on the results of the sensitivity analysis of SB1, the number of input random variables has been decreased, leading to a total of 8 random variables (Table 5.9).

Table 5.9. Statistical properties of random variables for the slab SB4.

Material	Random Variable	Distribution	Nominal Value	Mean	COV	Reference
Concrete (Slab)	f_c' (MPa) (1RV)	Normal	41	1.15×Nominal	0.15	Nowak et al., 2012
	f_t' (MPa) (1RV)	Normal	2.1	Nominal	$\mathrm{COV}_{f_c'}$	Ellingwood et., al. 1980
Slab Bottom Reinforcement (10M Bars)	E_s (GPa) (1RV)	Normal	200	Nominal	0.033	Mirza and Skrabek, 1991
	A_s (mm^2) (1RV)	Normal	100	Nominal	0.015	Rakoczy and Nowak, 2013
Shear Bolts (9.5 mm Diameter)	E_s (GPa) (1RV)	Normal	200	Nominal	0.033	Mirza and Skrabek, 1991
	γ_s (kN/m^3) (1RV)	Normal	78	Nominal	0.03	Assumed
	f_y (MPa) (1RV)	Normal	381	Nominal	0.04	Assumed
	A_s (mm^2) (1RV)	Normal	70.88	Nominal	0.015	Rakoczy and Nowak, 2013

Note: RV = Random Variable; f_c' = compressive strength of concrete; f_t' = tensile strength of concrete; E_s = modulus of elasticity of reinforcement; γ_s = density of reinforcement; f_y = yield strength of reinforcement; A_s = cross-section area of reinforcement.

5.4.3.2.1 Calculation of Response Moments

Mean and standard deviation of the structural response are estimated, based on the M-DRM method which requires 8 × 5+1 = 41 FEA trials and on the MCS with 10^3 FEA trials. M-DRM mean and standard deviation estimations have a small error compared to MCS results (Table 5.10).

Table 5.10. Output Distribution statistics of the structural response for the slab SB4.

SB4	Ultimate Disp. (mm)		Ultimate Load (kN)		Relative Error (%)	
	M-DRM (41 Trials)	MCS (10^3 Trials)	M-DRM (41 Trials)	MCS (10^3 Trials)	Ultimate Disp.	Ultimate Load
Mean	24.9873	25.3042	342.2826	343.1181	1.25	0.24
Stdev	4.9458	4.8038	15.7136	15.2349	2.96	3.14
COV	0.1979	0.1898	0.0459	0.0444	4.26	3.39

Note: M-DRM = Multiplicative Dimensional Reduction Method; MCS = Monte Carlo Simulation; Relative Error = $|MCS - MDRM|/MCS$; Stdev = Standard Deviation; COV = Coefficient of Variation.

5.4.3.2.2 Estimation of Response Distribution

Using M-DRM, the MaxEnt distribution parameters are reported on Table 5.11 and Table 5.12, for the ultimate load and ultimate displacement, respectively, of the slab SB4. These parameters are then used to estimate the PDF (Fig. 5.21) and POE (Fig. 5.22) of the ultimate load and the PDF (Fig. 5.23) and POE (Fig. 5.24) of the ultimate displacement. M-DRM provides PDF and POE curves which are in very close agreement comparing to MCS curves. Based on the rapid convergence of entropy (Table 5.11 and Table 5.12), three fractional moments ($m = 3$) are sufficient in the analysis.

Table 5.11. MaxEnt parameters for the ultimate load for the slab SB4.

Fractional Moments	Entropy	i	0	1	2	3	4
	7.8262	λ_i	–0.5493	4.1731			
m=1		α_i		0.1194			
		$M_X^{\alpha_i}$		2.0069			
	4.1748	λ_i	676.505	457.52	-487.44		
m=2		α_i		0.8419	0.8329		
		$M_X^{\alpha_i}$		136.05	129.08		
	4.1744	λ_i	344.533	20.765	59.618	-37.523	
m=3		α_i		0.9933	0.3463	0.9106	
		$M_X^{\alpha_i}$		329.12	7.5429	203.19	
	4.1743	λ_i	302.462	-99.973	72.234	202.02	-135.84
m=4		α_i		0.9027	0.9448	0.4909	0.4893
		$M_X^{\alpha_i}$		193.99	247.99	17.536	17.372

Table 5.12. MaxEnt parameters for the ultimate displacement for the slab SB4.

Fractional Moments	Entropy	i	0	1	2	3	4
	4.3781	λ_i	2.9135	0.1634			
m=1		α_i		0.6828			
		$M_X^{\alpha_i}$		8.9644			
	2.9853	λ_i	609.825	-546.90	32.904		
m=2		α_i		0.0905	0.4686		
		$M_X^{\alpha_i}$		1.3362	4.4969		
	2.9851	λ_i	706.197	-245.94	69.289	-447.85	
m=3		α_i		0.0442	0.3896	0.1218	
		$M_X^{\alpha_i}$		1.1521	3.4875	1.4771	
	2.9851	λ_i	440.583	1866.4	-63.521	-210.14	-1954.0
m=4		α_i		0.2713	0.03197	0.2695	0.2477
		$M_X^{\alpha_i}$		2.3851	1.1073	2.3713	2.2110

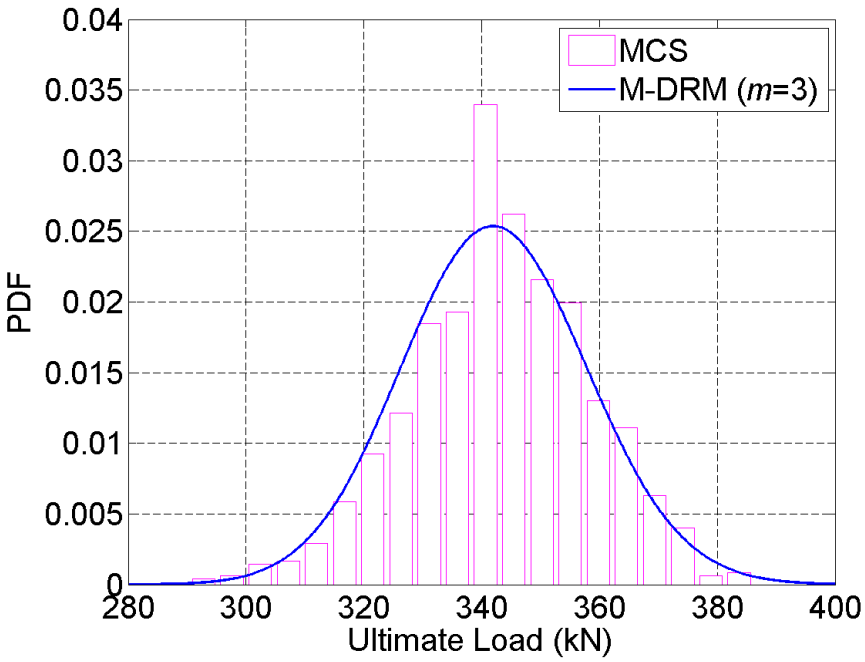

Fig. 5.21. Probability Distribution of the ultimate load for the slab SB4.

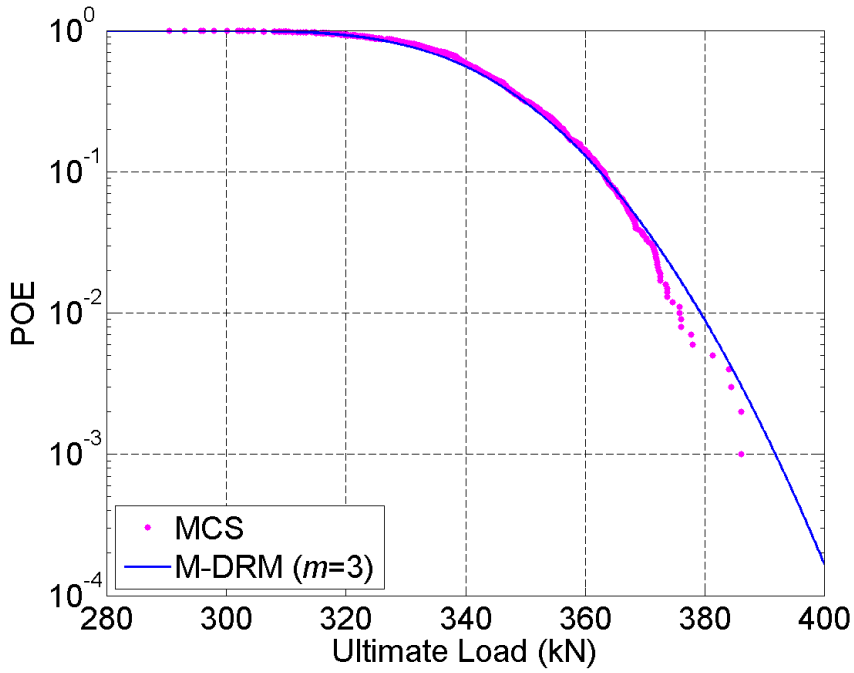

Fig. 5.22. Probability of Exceedance (POE) of the ultimate load for the slab SB4.

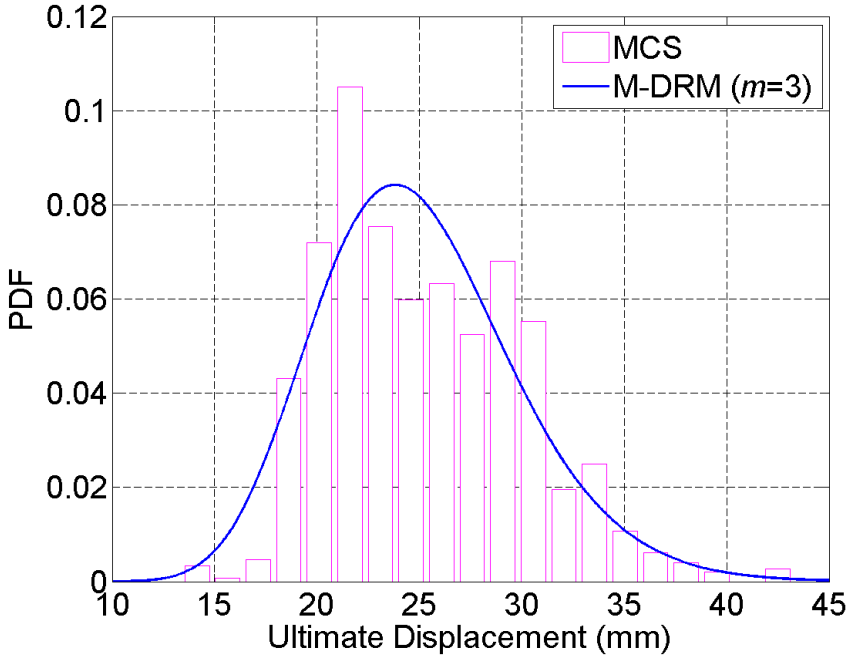

Fig. 5.23. Probability Distribution of the ultimate displacement for the slab SB4.

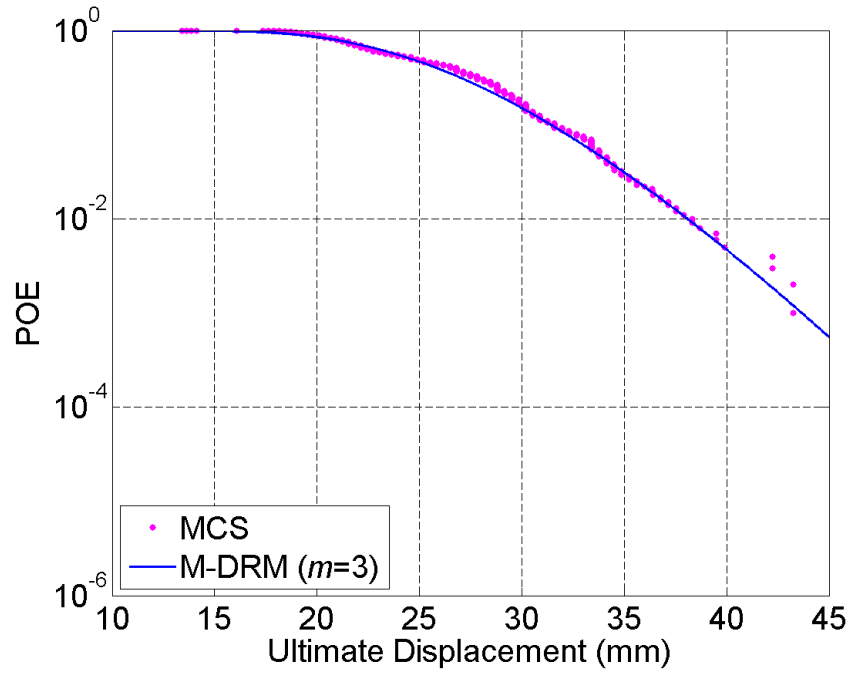

Fig. 5.24. Probability of Exceedance (POE) of the ultimate displacement for the slab SB4.

5.4.3.2.3 Global Sensitivity Analysis

For the slab SB4, the primary sensitivity coefficient S_i of the 8 input random variables are listed for the ultimate load (Table 5.13) and ultimate displacement (Table 5.14), where the dominant parameter is the compressive strength of concrete, contrary to SB1 where the dominant parameter is the tensile strength of concrete. This can be justified as failure in flexure is more sensitive to the compressive strength of concrete, while punching shear failure is more sensitive to the tensile strength of concrete.

Table 5.13. Sensitivity indices for the ultimate load for the slab SB4.

Rank	Material	Random Variable	S_i (%)
1	Concrete in Slab	f_c'	91.11
2	Concrete in Slab	f_t'	3.28
3	Bottom Steel in Slab	E_s	2.41
4	Bottom Steel in Slab	A_s	1.73
5	Shear Bolts	f_y	1.17
6	Shear Bolts	A_s	0.30
7	Shear Bolts	γ_s	0.02
8	Shear Bolts	E_s	0.003

Table 5.14. Sensitivity indices for the ultimate displacement for the slab SB4.

Rank	Material	Random Variable	S_i (%)
1	Concrete in Slab	f_c'	80.84
2	Bottom Steel in Slab	A_s	8.89
3	Bottom Steel in Slab	E_s	6.09
4	Concrete in Slab	f_t'	2.99
5	Shear Bolts	f_y	0.91
6	Shear Bolts	A_s	0.64
7	Shear Bolts	γ_s	0.22
8	Shear Bolts	E_s	0.09

Similar to SB1, the contribution of SB4 slab bottom reinforcement is increased from 4.14% (ultimate load) to 14.98% (ultimate displacement). Contrary to SB1 that failed in punching shear, SB4 failed in flexure meaning that the slab is more ductile, since the shear bolts provide higher

ductility. Thus, the variation of bottom flexural reinforcement leads to the high increase of ultimate displacement COV, from 5.66% (SB1) to 19.79% (SB4).

5.4.3.2.4 Computational Time

M-DRM provides accurate results with a significant saving of computational time. For the SB4 example, each deterministic FEA takes 614 seconds to run on a personal computer with Intel i7-3770 3rd Generation Processor and 16GB of RAM. Therefore, MCS with 1,000 simulations requires 170.55 hours while M-DRM with 41 simulations requires 6.99 hours. M-DRM also includes the MaxEnt method which requires 110 seconds, thus M-DRM total computational time equals to 7.02 hours, which is merely 4.12% of the time taken by the Monte Carlo simulation.

5.5 Probabilistic Analysis based on Design Codes and Model

5.5.1 General

Current punching shear design codes and models vary based on the different approaches and theories that they have been developed (Albrecht, 2002). European code (EC2) adopts the critical perimeter at a distance 2d from the column's face in order to calculate the punching shear resistance of the slab. However, the ACI code and the critical shear crack theory (CSCT) (Muttoni, 2008; Ruiz and Muttoni, 2009) adopt the critical section at distance 0.5d from the column's face.

Contrary to EC2 and CSCT, ACI code does not account for the flexural reinforcement ratio and size effect. CSCT calculates the punching shear capacity based on the rotation of the slab. Especially, for the shear reinforced slabs CSCT examines the failure not only inside and outside the shear reinforced area, as the design codes do, but also due to the crushing of the concrete

struts. Regarding the calculated punching shear capacity flat slabs with shear reinforcement, EC2 considers the critical perimeter at distance 1.5d from the outer shear reinforcement, while ACI and CSCT consider this distance as 0.5d.

In this work, the American design code (ACI 318 2011), the European design code (EC2 2004) and the critical shear crack theory (CSCT) are critically discussed and compared to the results obtained from the probabilistic FEA on specimens SB1 and SB4. Also, below are illustrated the punching shear design equations according to current design practices (ACI, EC2) and punching shear model (CSCT), for flat slabs with and without shear reinforcement.

5.5.2 ACI 318-11 (2011)

5.5.2.1 Flat Slabs without Shear Reinforcement

According to ACI 318-11 (2011), the punching shear strength of a slab-column connection without shear reinforcement is defined as

$$V_{R,ACI} = min \begin{Bmatrix} 0.17 \left(1 + \frac{2}{\beta}\right) \lambda \, b_0 \, d \sqrt{f_c'} \\ 0.083 \left(\frac{\alpha_s \, d}{b_0} + 2\right) \lambda \, b_0 \, d \sqrt{f_c'} \\ 0.33 \, \lambda \, b_0 \, d \sqrt{f_c'} \end{Bmatrix} [f_c' \; in \; MPa] \quad (5.1)$$

where β is the ratio of long side to short side of the column, λ is a modification factor reflecting the reduced mechanical properties of lightweight concrete (for normalweight concrete $\lambda = 1$), b_0 is the control perimeter (defined at a distance $d/2$ from the column face), d is the effective depth of the slab, f_c' is the compressive strength of concrete, $\alpha_s = 40$ for interior columns, $\alpha_s = 30$ for edge columns and $\alpha_s = 20$ for corner columns.

5.5.2.2 Flat Slabs with Shear Reinforcement

The punching shear strength inside the shear reinforcement zone is defined as

$$V_{R,in,ACI} = V_{C,ACI} + V_{S,ACI} \leq \begin{Bmatrix} 0.5\, b_0\, d\, \sqrt{f_c'}\ (for\ stirrups) \\ 0.66\, b_0\, d\, \sqrt{f_c'}\ (for\ studs) \end{Bmatrix} [f_c'\ in\ MPa] \tag{5.2}$$

where $V_{C,ACI}$ is the contribution of concrete and $V_{S,ACI}$ is the contribution of shear reinforcement. Using shear stirrups as shear reinforcement, $V_{C,ACI}$ can be calculated as

$$V_{C,ACI} = min \begin{Bmatrix} 0.09\, \left(1 + \frac{2}{\beta}\right)\, \lambda\, b_0\, d\, \sqrt{f_c'} \\ 0.042\, \left(\frac{\alpha_s\, d}{b_0} + 2\right)\, \lambda\, b_0\, d\, \sqrt{f_c'} \\ 0.17\, \lambda\, b_0\, d\, \sqrt{f_c'} \end{Bmatrix} [f_c'\ in\ MPa] \tag{5.3}$$

where the contribution of concrete is reduced 50%, e.g., from $1/3 = 0.33$ in Eq. (5.1) to $1/6 = 0.17$ in Eq. (5.3). Using shear studs as shear reinforcement, $V_{C,ACI}$ can be calculated as

$$V_{C,ACI} = min \begin{Bmatrix} 0.13\, \left(1 + \frac{2}{\beta}\right)\, \lambda\, b_0\, d\, \sqrt{f_c'} \\ 0.062\, \left(\frac{\alpha_s\, d}{b_0} + 2\right)\, \lambda\, b_0\, d\, \sqrt{f_c'} \\ 0.25\, \lambda\, b_0\, d\, \sqrt{f_c'} \end{Bmatrix} [f_c'\ in\ MPa] \tag{5.4}$$

where the contribution of concrete is reduced 25%, e.g., from $1/3 = 0.33$ in Eq. (5.1) to $1/4 = 0.25$ in Eq. (5.4). The contribution of shear reinforcement is defined as.

$$V_{S,ACI} = \left(A_V\, f_{yt}\, d\right)/s\ [f_c'\ in\ MPa] \tag{5.5}$$

where A_V is area of shear reinforcement, f_{yt} is the specified yield strength of shear reinforcement and s is the spacing of shear reinforcement. The punching shear strength outside the shear reinforcement zone is defined as

$$V_{R,out,ACI} = 0.165\, b_{0,out}\, d\, \sqrt{f_c'}\ [f_c'\ in\ MPa] \tag{5.6}$$

where $b_{0,out}$ is the critical section outside the shear reinforcement (defined at a distance $d/2$ from the last shear stirrup). According to ACI 318-11 (2011), the punching shear strength of a slab-column connection with shear reinforcement is defined as

$$V_{R,ACI} = min\left(V_{R,in,ACI}\,;\, V_{R,out,ACI}\right) \tag{5.7}$$

5.5.3 EC2 (2004)

5.5.3.1 Flat Slabs without Shear Reinforcement

Unlike ACI, EC2 takes into account both the flexural reinforcement and the size effect. According to EC2 (2004) the punching shear strength of a slab-column connection without shear reinforcement is defined as

$$V_{R,EC2} = 0.18\, b_0\, d\, k\, (100\, \rho\, f_{ck})^{1/3} \geq (v_{min}\, b_0\, d)\ [f_{ck}\ in\ MPa] \tag{5.8}$$

where b_0 is the control perimeter (set at a distance $2d$ from the column face), d is the effective depth of the slab, f_{ck} is the characteristic compressive cylinder strength of concrete, ρ is the flexural reinforcement ratio $(\rho \leq 0.02)$, $k = 1 + \sqrt{(200/d)} \leq 2\ (d\ in\ mm)$ is a factor accounting for the size effect and the minimum punching shear stress is defined as $v_{min} = 0.035\, k^{3/2}\, {f_{ck}}^{1/2}$. Note that although an increase in the flexural reinforcement increases the punching shear capacity, the behaviour of the connection becomes more brittle (Gardner, 2011), thus EC2 adopts $\rho \leq 0.02$.

Based on the fact that f_c' represents the 9% percentile and f_{ck} represents the 5% percentile of the average compressive strength of concrete, the following relationship has been adopted from literature to transform f_c' to f_{ck} (Reineck et al., 2003)

$$f_{ck} = f_c' - 1.6\ [MPa] \tag{5.9}$$

5.5.3.2 Flat Slabs with Shear Reinforcement

The punching shear strength inside the shear reinforcement zone is defined as

$$V_{R,in,EC2} = 0.75\, V_{C,EC2} + V_{S,EC2} \tag{5.10}$$

where $V_{C,EC2}$ is the contribution of concrete as defined in Eq. (5.8) which is reduced 25%, and $V_{S,EC2}$ is the contribution of shear reinforcement defined as

$$V_{S,EC2} = 1.5\,(d/s_r)\, A_{sw}\, f_{ywd,ef} \tag{5.11}$$

where s_r is the radial spacing of shear reinforcement, A_{sw} is the area of one perimeter of shear reinforcement around the column and $f_{ywd,ef}$ is the effective design strength of the punching shear reinforcement and is defined as

$$f_{ywd,ef} = 250[MPa] + 0.25\, d \leq f_{ywd}[MPa] \tag{5.12}$$

where f_{ywd} is the design yield strength of shear reinforcement. The punching shear strength outside the shear reinforcement zone is defined as

$$V_{R,out,EC2} = 0.18\, b_{0,out}\, d\, k\, (100\, \rho\, f_{ck})^{1/3}\, [f_{ck}\ in\ MPa] \tag{5.13}$$

where $b_{0,out}$ is the critical section outside the shear reinforcement (defined at a distance $1.5d$ from the last placed shear reinforcement, where 1.5 is the recommended value). According to EC2 (2004), the punching shear strength of a slab-column connection with shear reinforcement is defined as

$$V_{R,EC2} = min\left(V_{R,in,EC2}\,;\, V_{R,out,EC2}\right) \tag{5.14}$$

5.5.4 Critical Shear Crack Theory (CSCT 2008, 2009)

5.5.4.1 Flat Slabs without Shear Reinforcement

Contrary to the empirical design equations that ACI and EC2 adopt, the critical shear crack theory (Muttoni, 2008; Ruiz and Muttoni, 2009) is based on a mechanical model, where punching shear strength of a slab-column connection without shear reinforcement is defined as (Muttoni, 2008)

$$V_{R,CSCT} = \frac{3}{4} \frac{b_0\, d\, \sqrt{f_c}}{1 + \left(15 \frac{\psi\, d}{d_{g0} + d_g}\right)} \; [f_c \; in \; MPa] \tag{5.15}$$

where b_0 is the control perimeter (set at a distance of $0.5d$ from the support region with circular corners), d is the effective depth of the slab, ψ is the slab rotation, d_{g0} is a reference aggregate size equal to $16\, mm$, d_g is the maximum aggregate size, f_c is the average compressive strength of concrete. In order to transform f_c' to f_c the following relationship has been used (Reineck et al., 2003):

$$f_c = f_c' + 2.4 \; [MPa] \tag{5.16}$$

The rotation of the slab is expressed as

$$\psi = 1.5 \frac{r_s}{d} \frac{f_y}{E_s} \left(\frac{V}{V_{flex}}\right)^{3/2} \tag{5.17}$$

where r_s is the radius of the slab, f_y is the yield stress of the flexural reinforcement, $E_s$is the modulus of elasticity of the flexural reinforcement, V is the applied force and V_{flex} is the flexural strength of the slab specimen which is reached when the radius of the yield zone (r_y) equals the radius of the slab r_s, and can be expressed as

$$V_{flex} = 2\pi\, m_R \frac{r_s}{r_q - r_c} \tag{5.18}$$

where r_q is the radius of the load introduction at the perimeter, r_c is the radius of circular column and m_R is the nominal moment capacity per unit width calculated as

$$m_R = \rho\, f_y\, d^2 \left(1 - \frac{\rho\, f_y}{2\, f_c}\right) \tag{5.19}$$

where ρ is the flexural reinforcement ratio.

The failure criterion, i.e., Eq. (5.15), expresses the punching shear strength reduction of the slab-column connection as the rotation of the slab increases. The Load-Rotation curve of the slab, i.e., Eq. (5.17), expresses the increase of the rotation of the slab-column connection as the applied force on the slab increases. The point where these two curves are intersected expresses the punching shear strength of the flat slab (Fig. 5.25). This point is obtained by solving Eq. (5.17) in terms of V and then iterations are performed to find the optimum rotation value (ψ) for which the difference between V_{RCSCT} and V is minimum, i.e., $\left|V_{R,CSCT} - V\right| \approx 0$. In this study, these iterations were conducted using the simplex search method (Lagarias et al. 1998) in MATLAB and the punching shear strength and rotation of SB1 are estimated as 220 kN and 0.0162, respectively (Fig. 5.25).

5.5.4.2 Flat Slabs with Shear Reinforcement

A reinforced concrete slab-column connection with shear reinforcement may fail due to three different punching failure modes: (1) punching inside the shear reinforcement zone, (2) punching outside the shear reinforcement zone, (3) crushing of the concrete near the column. In most codes, the crushing strength check is usually performed by limiting the maximum shear strength (ACI) or by reducing the strength of concrete (EC2) (Ruiz and Muttoni, 2009).

The punching shear strength inside the shear reinforcement zone is defined as

$$V_{R,in,CSCT} = V_{C,CSCT} + V_{S,CSCT} \tag{5.20}$$

where $V_{C,CSCT}$ is the contribution of concrete as defined in Eq. (5.15) and $V_{S,CSCT}$ is the contribution of shear reinforcement defined as

$$V_{S,CSCT} = \frac{E_s\,\psi}{6}\,A_{sw} \leq f_{ywd}\,A_{sw} \tag{5.21}$$

where E_s is the modulus of elasticity, A_{sw} is the amount of shear reinforcement within the perimeter at d from the edge of the support region and f_{ywd} is the design yield strength of shear reinforcement. The punching shear strength outside the shear reinforcement zone is defined as

$$V_{R,out,CSCT} = \frac{3}{4}\,\frac{b_{0,out}\,d_v\,\sqrt{f_c}}{1+\left(15\frac{\psi\,d}{d_{g0}+d_g}\right)}\;[f_c\;in\;MPa] \tag{5.22}$$

where $b_{0,out}$ is the control perimeter (set at a distance of $0.5d$ from the last placed shear reinforcement) and d_v is the reduced effective depth in order to account the pull out of shear reinforcement. The crushing shear strength is defined as

$$V_{R,crush,CSCT} = \lambda\left(\frac{3}{4}\,\frac{b_0\,d\,\sqrt{f_c}}{1+\left(15\frac{\psi\,d}{d_{g0}+d_g}\right)}\right)[f_c\;in\;MPa] \tag{5.23}$$

where λ is set equal to 3.0 for well anchored shear reinforcement, otherwise λ is set equal to 2.0. According to CSCT (Ruiz and Muttoni 2009), the punching shear strength of a slab-column connection with shear reinforcement is defined as

$$V_{R,CSCT} = min\left(V_{R,in,CSCT}\,;\,V_{R,out,CSCT}\,;\;V_{R,crush,CSCT}\right) \tag{5.24}$$

For a slab-column connection with shear reinforcement, the failure criterion is expressed by Eqs. (5.20), (5.22) and (5.23), depending on the punching failure mode that a flat slab will fail. Following the same procedure as already described in previous section, the punching shear strength and rotation of SB4 are estimated as 317 kN and 0.0284, respectively. It is obvious from

Fig. 5.26 that the specimen SB4 will fail outside the shear reinforced area, which is in agreement with the experimental results.

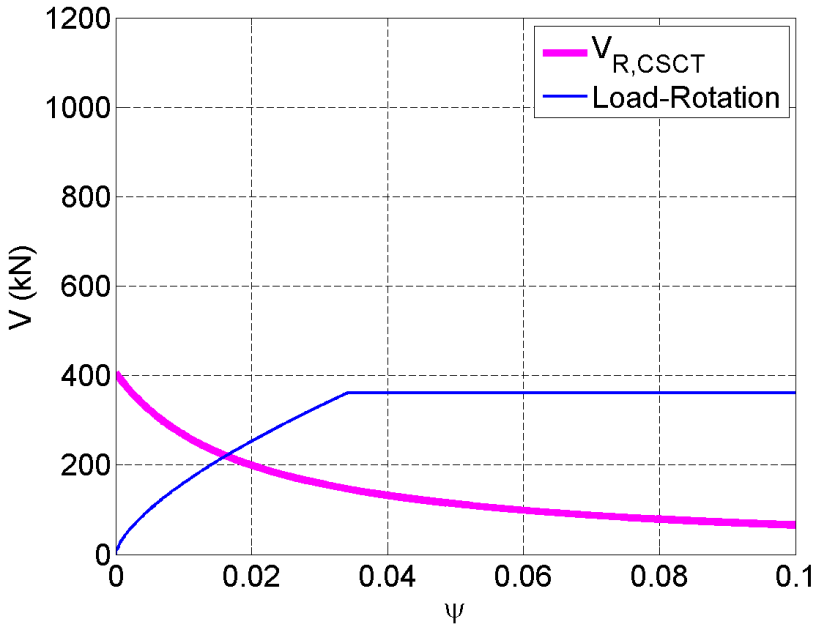

Fig. 5.25. Deterministic Punching Shear Strength of SB1 according to CSCT (Muttoni 2008).

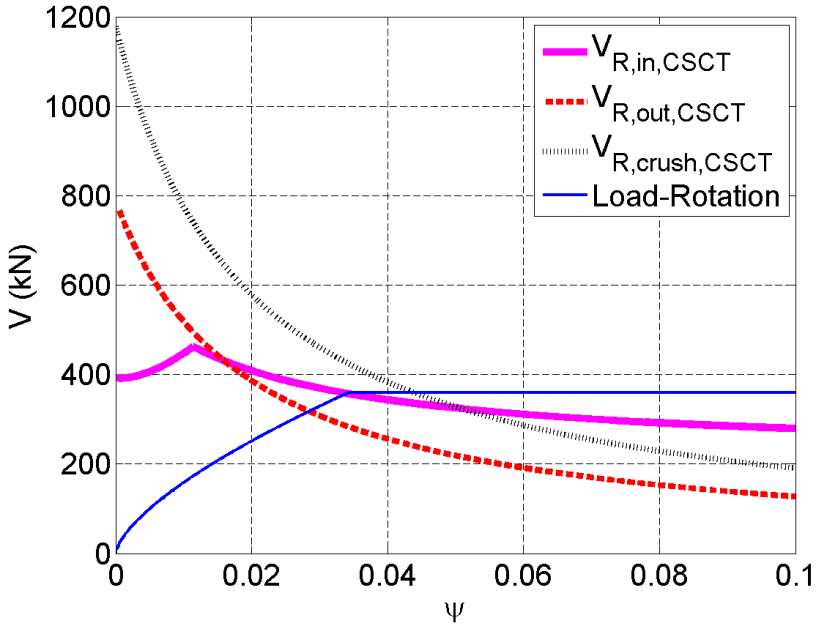

Fig. 5.26. Deterministic Punching Shear Strength of SB4 according to CSCT (Ruiz and Muttoni 2009).

5.5.5 Results

Deterministic analysis shows that SB1 slab will fail at a load of 189 kN and 202 kN according to ACI and EC2, respectively. Slab SB4 will fail at a load of 237 kN and 251 kN according to ACI and EC2, respectively. Based on these results, it can be concluded that ACI predicts the most conservative failure loads which mainly happens due to the fact that ACI does not consider the size effect and the flexural reinforcement ratio.

Probabilistic analysis based on the current design codes (ACI and EC2) and the punching shear model (CSCT) has been performed. MCS was performed with only one random variable, i.e., compressive strength of concrete, since it is the dominant parameter that affects the punching shear strength of flat slabs. Design practices and models use the square root (ACI, CSCT) and cubic root (EC2) of concrete compressive strength, which actually represents the tensile strength of concrete. Statistical moments are reported for both SB1 (Table 5.15) and SB4 (Table 5.16). Both design codes and CSCT give safe predictions for slabs, as the ratio of punching shear resistance mean value is less than 1. PDFs for SB1 (Fig. 5.27) and SB4 (Fig. 5.28) indicate this point quite well.

ACI code calculates the most conservative punching shear resistance values for both slabs. Quite interesting are the results obtained from the probabilistic analysis of the specimen SB4 (with shear reinforcement). The mean values as calculated from the M-DRM and CSCT were increased around 100 kN compared to the mean values of the specimen SB1 (slab without shear reinforcement). However, comparing the mean values of the design codes, we can note that both were increased around 50 kN for the slab SB4 compared to the slab SB1. Therefore, it can be concluded that CSCT is able to take into consideration the effect of the shear reinforcement in a better way compared to the design codes, predicting really well the increase in the strength

because of the shear bolts, since the results correspond very well to the results obtained from the M-DRM. EC2 and CSCT have slightly smaller coefficients of variation than the ACI, as they take into consideration the flexural reinforcement ratio and size effect.

The provisions which include reinforcement ratio and size effect terms have smaller coefficients of variation than those provisions that do not include them (Gardner, 2011). According to the probabilistic analysis results, the same was observed since the CSCT and the EC2 have smaller coefficients of variation compared to the ACI. However, this seems to be the case for the flat slab with shear reinforcement (SB4) only, since for the flat slab without shear bolts (SB1) the ACI coefficient of variation is closer to the M-DRM result.

Table 5.15. Output Distribution statistics of punching shear resistance for the slab SB1.

SB1	Punching Shear Resistance, V_u(kN)				Ratio, $V_{u(CSCT,ACI,EC2)}/V_{u(M-DRM)}$		
	M-DRM (91 Trials)	CSCT (10^5 Trials)	ACI (10^5 Trials)	EC2 (10^5 Trials)	CSCT	ACI	EC2
Mean	234.73	228.57	201.39	210.67	0.97	0.86	0.90
Stdev	15.50	10.15	14.81	10.73	0.65	0.96	0.69
COV	0.0661	0.0444	0.0735	0.0509	0.67	1.11	0.77

Table 5.16. Output Distribution statistics of punching shear resistance for the slab SB4.

SB4	Punching Shear Resistance, V_u(kN)				Ratio, $V_{u(CSCT,ACI,EC2)}/V_{u(M-DRM)}$		
	M-DRM (41 Trials)	CSCT (10^5 Trials)	ACI (10^5 Trials)	EC2 (10^5 Trials)	CSCT	ACI	EC2
Mean	342.28	329.13	253.69	262.54	0.96	0.74	0.77
Stdev	15.71	14.03	19.29	13.87	0.89	1.22	0.88
COV	0.0459	0.0426	0.0761	0.0528	0.93	1.65	1.15

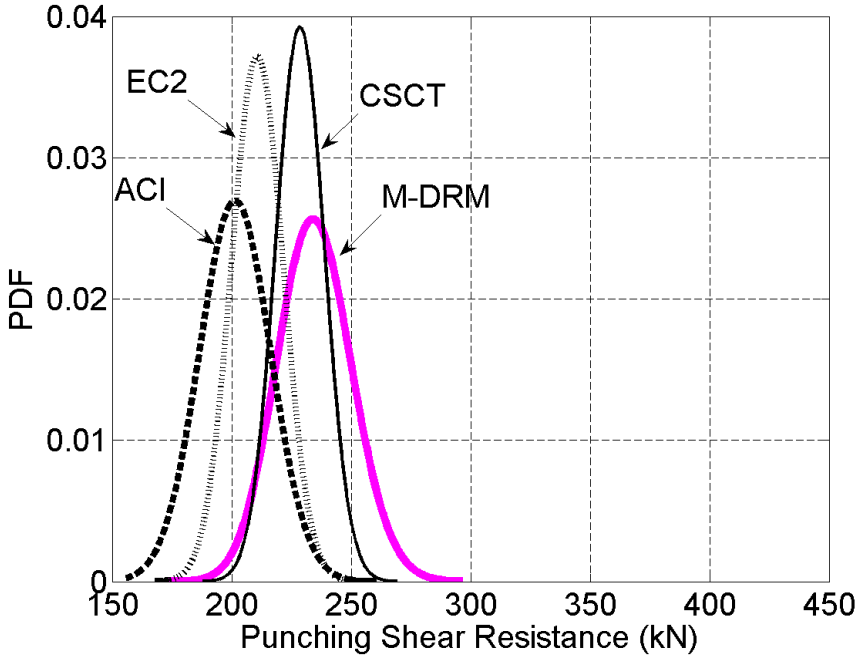

Fig. 5.27. Probability Distribution of the punching shear resistance for the slab SB1.

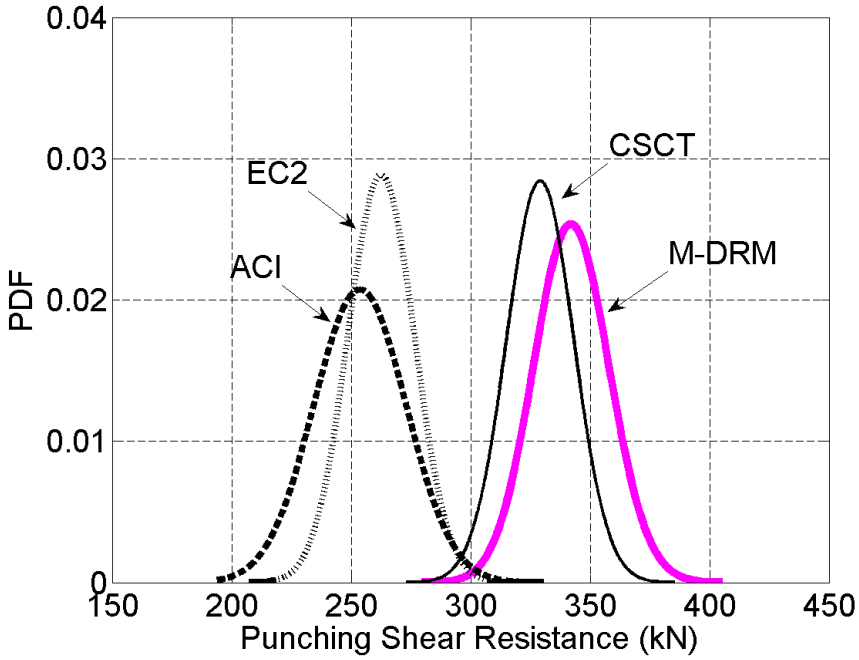

Fig. 5.28. Probability Distribution of the punching shear resistance for the slab SB4.

5.6 Conclusion

This chapter presents how uncertainty can be implemented in conjunction with finite element analysis (FEA). Two 3D reinforced concrete flat slabs are developed using commercial FEA software (ABAQUS). The behavior of the concrete is modeled using the concrete-damaged plasticity model. The model accurately predicts the behavior of the flat slab, in terms of ultimate load-displacement and cracking pattern. The quasi-static analysis in ABAQUS/Explicit is considered as the FE solution procedure, since it takes less time compared to the static analysis.

The probabilistic analysis uses both the Monte Carlo simulation (MCS) and the multiplicative dimensional reduction method (M-DRM). ABAQUS does not include both FEA and uncertainty in its interface. Therefore, in order to update the random variables of interest in each trial, Python programing code is developed for both MCS and M-DRM. Python code is selected since the Python Development Environment (PDE) is supported from the ABAQUS GUI. Here, the link between ABAQUS and Python programing language for probabilistic FEA is performed using the idea of parameter updating.

The results obtained from M-DRM are in a good agreement with the results obtained from MCS, making M-DRM a quick, robust and easy to implement tool. As it has already been shown, MCS may be prohibited due to extreme computational cost, when each FEA trial takes a long time, and due to the advanced required knowledge in programing languages and/or in computational platforms. M-DRM requires much less trials than MCS making it more flexible and easy to use, as M-DRM can also be implemented without the need of a linking platform or a programing language and requires much less total computational cost comparing to MCS. Nonlinear analysis of 3D flat slab demonstrates this point quite well, as for SB1 the computational time of M-DRM is merely a fraction (9.13%) of that of the MCS with 1,000 trials. Furthermore, for SB4 the

computational time of M-DRM is merely a fraction (4.12%) of that of the MCS with 1,000 trials showing a relative reduction in computational cost as the complexity of the problem increases.

M-DRM is also used for sensitivity analyses where the output structural response, i.e., ultimate load and ultimate displacement, owns most of its variance to the variance of the concrete strength that will be used in the slab. Punching failure (SB1) is more sensitive to the tensile strength of concrete, while flexural failure (SB4) is more sensitive to the compressive strength of concrete. For the ultimate load case, tensile and compressive strength of concrete are the dominant parameters for the slab-column behaviour, having a sensitivity coefficient equal to 60.85% (SB1) and 91.11% (SB4), respectively. The ultimate displacement of a flat slab is also affected by the flexural reinforcement that will be placed inside the slab, since the contribution of the flexural reinforcement is increased from 1.39% to 12.26% (SB1) and from 4.14% to 14.98% (SB4). However, the flexural reinforcement contribution primarily affects flat slabs with shear reinforcement, because they are more ductile. This is clearly shown from the coefficient of variation of the ultimate displacement, which is increased from 5.66% (SB1) to 19.79% (SB4), since the shear bolts provide ductility to SB4.

Current design practises (ACI and EC2) and the punching shear model (CSCT), predict quite well the slab-column behavior, due to input uncertain parameters. ACI, EC2 and CSCT do not overestimate the punching shear capacity of both slabs, leading to safe predictions. However, CSCT considers in a better way the effect of the shear reinforcement, compared to the design codes, since it predicts really well the punching shear resistance increase because of the shear bolts.

Chapter 6

Probabilistic Finite Element Assessment of Prestressing Loss of NPPs

6.1 Introduction

6.1.1 Background

Nuclear power plants (NPP) play a major role for the global energy supplies, while in the province of Ontario (Canada) 50% of the electricity is generated by the NPP (Mirhosseini et al., 2014). The CANDU (CANada Deuterium Uranium) nuclear reactors are housed in a containment structure which consists of a concrete base, a cylindrical perimeter wall, a ring beam and a dome (Simmonds et al., 1979), with dimensions as shown in Fig. 6.1 (Murray and Epstein, 1976a; Murray et al., 1978). The main function of the containment is to prevent any radioactive leakage to the environment, if a serious failure occurs to the process system (Pandey, 1997). Thus, the containment is designed to withstand the loss of coolant accident (LOCA), where both temperature and pressure are increased inside the containment due to steam release, leading to increased tensile stresses in the concrete walls (Lundqvist and Nilsson, 2011). Therefore, the containment is made of pretsressed concrete, either using bonded or unbonded tendons (Anderson et al., 2008), in order to ensure integrity and leak tightness in case of an accident (Anderson, 2005). However, the containment integrity is vulnerable to prestressing losses due to actual material deformations, i.e., creep and shrinkage of concrete and relaxation of tendons, and due to corrosion of the tendons (Pandey, 1997).

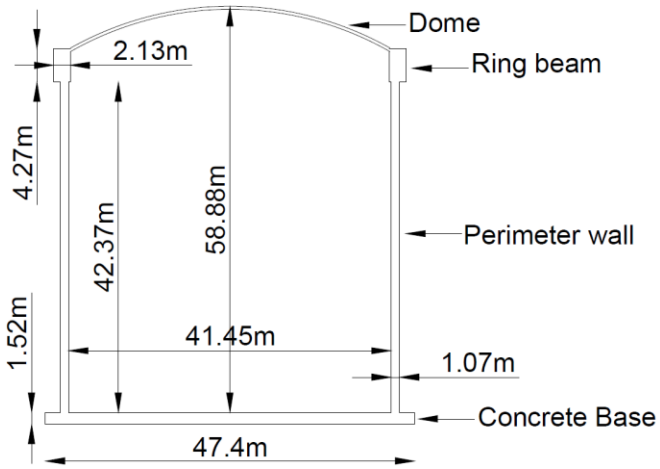

Fig. 6.1. Sketch of the containment structure (dimensions adopted from Murray and Epstein, 1976a; Murray et al., 1978).

For the evaluation of the bonded prestressing system, Appendix A of the CSA N287.7 (2008) provides three types of tests on both bonded and unbonded test beams, namely flexural tests, lift-off tests and a destructive test, while a more detailed review on the above inspection procedures can be found in literature (Pandey, 1996a). In general, flexural tests involve testing of at least 12 bonded beams to evaluate the concrete cracking, but do not quantify the pretsress losses. Lift-off tests require the testing of at least 4 unbonded beams to measure the prestressing loss at the end of the tendon, but cannot detect corrosion, since the tendons are permanently greased, and cannot evaluate the prestressing loss of bonded systems. Destructive test uses a sample from the previous flexural test bonded beam to detect corrosion through visual examination of the tendon. Thus, based on the previous, the direct assessment of the prestressing loss of the bonded tendons is not possible.

Regarding containments with unbonded tendons, the lift-off technique is general used during regular in-service inspections, in order to assess the prestressing loss at the end of the tendons (Anderson et al., 2008). However, the average prestreesed loss along the tendon can be

significantly larger compared to the measured prestressing loss in the end of the tendon (Anderson et al., 2005).

On the other hand, Clause 6 and 7 of the CSA N287.6 (2011) provide the proof test and the leakage rate test requirements, respectively. These are non-destructive techniques, which involve the pressurizing of an existing containment structure. This predefined pressure is equal to 1.15 times the design pressure for the proof test and equal to the design pressure for the leakage rate test (CSA N287.6-11). Under this load the stress-strain is measured in order to be assessed the strength and design criteria of the containment (proof test) and the leak tightness of the containment boundary (leakage rate test), where a more detailed review can be found in literature (Pandey, 1996b). Thus, this paper examines if the proof test and/or the leakage rate test can provide us with indirect information, i.e., measured strains during pressure tests, from which the prestressing loss can be assessed for bonded prestressing systems. Probabilistic finite element analysis is applied, since the strain changes during a pressure test will have a distribution due to uncertainties, but this distribution is expected to change as a result of the prestressing losses. Therefore, there is a need to investigate this change in the distribution of the concrete strain with respect to the prestressing loss in tendons.

6.1.2 Objective

The main objective of this chapter is to estimate the distribution of the concrete strain (hoop and axial), during the leakage rate test or the proof test, which can be related to prestressing loss in tendons. For example, mean of the losses can be related to the mean of the strain distribution.

To investigate this problem, four pretressed wall specimens, each corresponding to a 1/4 scale wall portion of a prototype nuclear containment structure, are selected from the literature and

analysed using ABAQUS. The distribution of concrete strain in early and late life of the structure is analyzed. This chapter also demonstrates the applicability of the probabilistic FEA to nuclear containment structures.

The prestressing force is modeled using two ways, i.e., by applying either initial stress or initial thermal strain to the tendons. This chapter also discusses the implementation and accuracy of the two prestressing modeling techniques, when the finite element method is used.

6.1.3 Organization

The organization of this chapter is as follows. Section 6.2 presents a detailed description of the four tested wall segments, together with some basic calculations of the developed prestressing force under internal pressure based on the thin-wall analysis. Section 6.3 presents the FE analysis of the selected specimens, the two ways of modeling the prestressing in tendons and the comparison between the FEA results and the test results. In Section 6.4, MCS is performed nine times for each specimen, i.e., for two base cases and for seven hypothetical cases, where only the material properties and the prestressing loss are considered as random variables. Section 6.4 also demonstrates the probabilistic framework which is used for the assessment of the average concrete strains with the average prestressing loss and for evaluating the correlation between these two. Finally, conclusions are summarized in Section 6.5.

6.2 Wall specimens

6.2.1 Test Description

The selected wall specimens (Fig. 6.3) are part of a research program at the University of Alberta, which was sponsored by the Atomic Energy Control Board of Canada. The main objective of the research program was to investigate the overpressure effect on the Gentilly-2 type secondary containment structures (Elwi and Murray, 1980). The first report of the series is divided in two volumes (Murray and Epstein, 1976a; Murray and Epstein, 1976b) and provides the description of the prototype containment structure and the main objectives of the research.

A series of test were conducted on reinforced concrete wall segments (specimens 4 and 7) and on prestressed concrete wall segments (specimens 1 to 3, 5 to 6 and 8 to 14), leading to 14 tested specimens in total. All tested specimens except specimen 7, correspond to a 1/4 scale of the prototype containment. Thus, each specimen has a width of 266.7 mm, i.e., almost one-fourth of the wall thickness, and a tendon duct size almost one-fourth the size of ducts used in the prototype. Specimen 7 was considered in order to be evaluated the scale effects. Thus, the thickness of specimen 7 was increased 1.5 times, i.e., 400.05 mm, which corresponds to a 1/3 scale of the prototype containment, while its reinforcement size, reinforcement spacing and concrete cover was also increased proportionally. The lateral dimensions were chosen as three times the wall thickness, i.e., $3 \times 266.7 = 800.1$ mm, due to laboratory restrictions regarding the total lateral applied force, and due to crack observations regarding allowing the formation of more than one through the wall crack. The technical report No. 81 (Simmonds et al., 1979) provides a detailed description and the test results of the specimens 1 to 9 and 11 to 13, while the technical report No. 80 (Rizkalla et al., 1979) provides a detailed description and the test results of the two additional specimens involving air leakage, i.e., specimens 10 and 14.

In his study, the specimens 1, 2, 3 and 8 are selected, which are square panels of 800.1 mm with a width of 266.7 mm (Fig. 6.2). Specimens 1 and 2 represent the prestressing conditions and loading of the cylindrical wall of the containment structure (Fig. 6.1). Specimen 3 represents the prestressing conditions and loading of the dome of the containment structure. Specimen 8 is identical to the specimen 1 and 2 except that here the concrete cover is increased to 31.75 mm, compared to 12.70 mm, in order to be evaluated the effects of the concrete cover on cracking (Simmonds et al., 1979).

The selected specimens are prestressed in both directions. The hoop (or circumferential) direction consists of 4 tendons with 7 smooth wires in each tendon. The axial (or meridional) direction consists of 3 tendons with 6 smooth wires in each tendon. Each smooth wire has a diameter of 7.01 mm, yield strength of 1627 MPa, ultimate strength of 1820 MPa and modulus of elasticity of 200 GPa. Apart from the tendons, all the selected specimens are reinforced with two grids, where each grid consists of 10 #10 (metric units) non-prestressed bars in each direction (Fig. 6.2). Each bar of the non-prestressed reinforcement has yield strength of 401 MPa, ultimate strength of 603 MPa and modulus of elasticity of 200 GPa. During the test the load was applied in both directions with a different loading ratio for specimens 1, 2 and 8 and with the same loading ratio for specimen 3. A detailed overview of the variables that were considered in the selected wall segments is given in Table 6.1.

In the prototype containment structure, the 4 tendon direction represents the horizontal direction, while the three tendon direction represents the vertical direction (Fig. 6.3(a)). The capacity of the testing machine was bigger in the vertical direction (Simmonds et al., 1979). Thus the testing segment was rotated 90 degrees compared to the corresponding orientation in the prototype

structure (Fig. 6.3(b)). The detailed location of the 3 tendon (Axial) and 4 tendon (Hoop) direction are shown in Fig. 6.4 and Fig. 6.5, respectively.

Table 6.1. Overview of variables considered in the wall segment tests (Simmonds et al., 1979).

	Non-prestressed reinforcement		Concrete		Loading ratio	Prestressing force in tendons (effective after losses)	
Specimen	Per layer	Min. cover (mm)	Compressive strength (MPa)	Modulus of elasticity (MPa)	Axial/Hoop	f_{PH} (MPa)	f_{PA} (MPa)
1	10 #10 @ 76.2mm	12.70	35	25924	1:2	931.5	850.1
2	10 #10 @ 76.2mm	12.70	31	27027	1:2	919.8	855.6
3	10 #10 @ 76.2mm	12.70	39	22201	1:1	930.1	857.1
8	10 #10 @ 76.2mm	31.75	34	38335	1:2	934.9	887.4

Note: Non-prestressed reinforcement layer is reported here in metric units, while in the relevant reference is reported in the imperial units, i.e., 10 #3 @ 3 inches; Axial refers to the 3 tendon direction; Hoop refers to the 4 tendon direction; f_{PH} = prestressing force in hoop direction; f_{PA} = prestressing force in axial direction

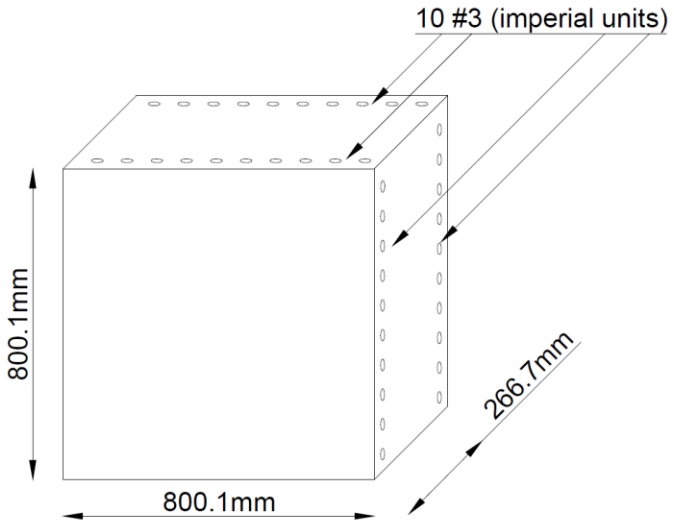

Fig. 6.2. Sketch of the wall specimen with the non-prestressed reinforcement.

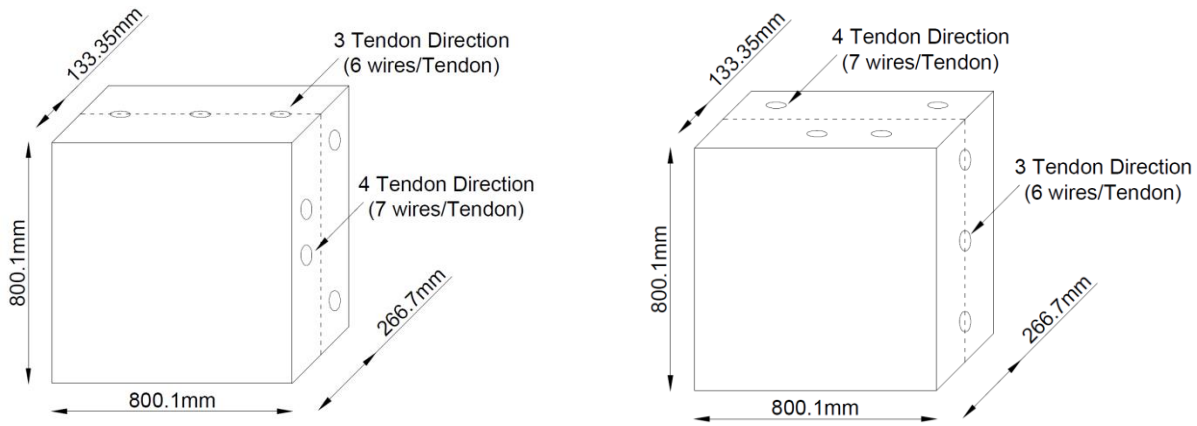

Fig. 6.3. Sketch of the wall specimen with the prestressed reinforcement: (a) tendon orientation in the containment structure; (b) tendon orientation in the wall segment specimen.

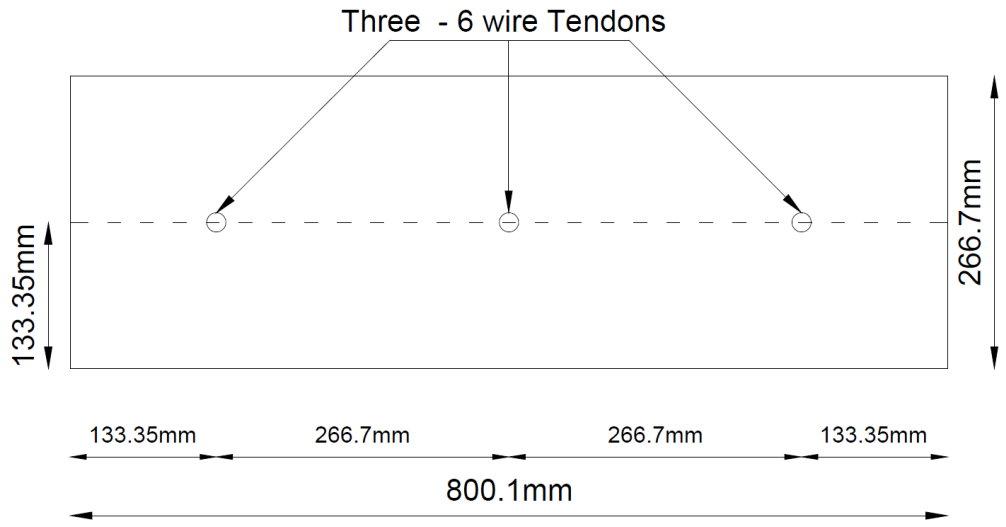

Fig. 6.4. Sketch of the 3 tendon location (axial or meridional direction).

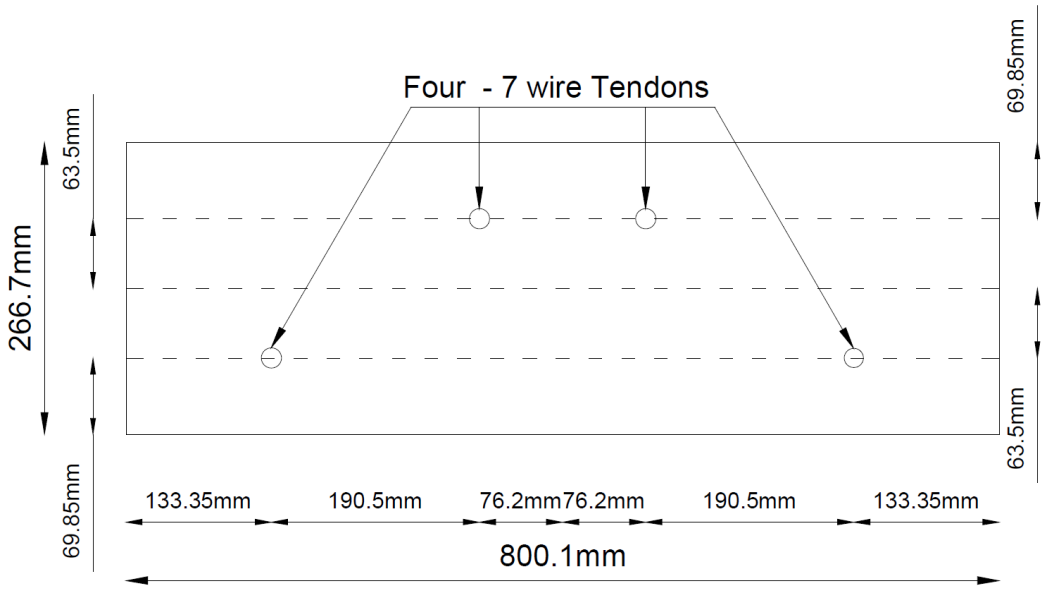

Fig. 6.5. Sketch of the 4 tendon location (hoop or circumferential direction).

6.2.2 Developed prestressing force under internal pressure

The prototype containment structure has been designed for an internal pressure equal to 124 kPa (Murray and Epstein, 1976a), while the internal dimeter is equal to 41,452.8 mm ≈ 41.45 m and the wall thickness is equal to 1,066.8 mm ≈ 1.07 m (Fig. 6.1). The containment has an inner-radius to wall-thickness ratio bigger than 10, i.e., $r/t = 20{,}726.4/1{,}066.8 = 19.43 > 10$. Thus, the containment can be analyzed using the thin-wall analysis (Hibbeler, 2011), in order to calculate the developed stresses under any internal pressure inside the containment. For a thin-wall cylindrical pressure vessel the developed stresses are calculated as (Beer et al., 2006)

$$\sigma_H = p\, r/t \tag{6.1}$$

$$\sigma_A = p\, r/2t \tag{6.2}$$

where σ_H is the hoop stress (also called circumferential), σ_A is the axial stress (also called meridional), p is the internal pressure, r is the internal radius and t is the wall thickness. In general, when $r/t = 10$ the thin-wall analysis predicts stresses which are approximately 4% less

than the actual maximum stress, while as the r/t ratio is increased the relative error is decreased (Hibbeler, 2011). Therefore, the developed stresses under the design pressure $p = 0.124$ MPa are calculated as $\sigma_H = 2.41$ MPa and $\sigma_A = 1.205$ MPa, considering a thin-wall analysis for the containment. The wall segments represent part of the containment, e.g., specimens 1, 2 and 8 represent part of the containment's cylindrical wall. Thus, under internal pressure the developed stresses result in developed forces in hoop and axial direction which are calculated as

$$F_H = \sigma_H A \tag{6.3}$$

$$F_A = \sigma_A A \tag{6.4}$$

where F_H is the hoop force, F_A is the axial force and A is the cross section area in each direction. Each specimen is a square panel (800.1 mm) with a width of 266.7 mm, resulting to a cross section area $A = 213{,}387$ mm^2 for both directions. Therefore, under the design pressure $p = 0.124$ MPa, the developed force in the hoop direction is calculated as $F_H = 514.26$ kN and in the axial direction is calculated as $F_A = 257.13$ kN. For the proof test the applied pressure is equal to 1.15 times the design pressure and for the leakage rate test the applied pressure is equal to the design pressure (CSA N287.6-11). Thus, the required hoop prestressing force after losses is $F_{H,proof} = 591.40$ kN for the proof test and $F_{H,leak} = 514.26$ kN for the leakage rate test, while the required axial prestressing force after losses is $F_{A,proof} = 295.70$ kN for the proof test and $F_{A,leak} = 257.13$ kN for the leakage rate test.

6.3 Finite Element Analysis

Deterministic FEA is applied to the selected wall specimens (1, 2, 3 and 8) using ABAQUS. Simple supports are introduced around the bottom edge and the one lateral edge of the specimens, while the load is applied with a small velocity through the top and the other lateral

edge of the specimens (Fig. 6.6). The summation of the reactions at these supports gives the total measured load in each direction. Quasi-static analysis in ABAQUS/Explicit is performed using small velocity, leading to a smaller computational cost per increment compared to the implicit method (Genikomsou and Polak, 2015). The concrete is modeled using 8-noded hexahedral elements with reduced integration (C3D8R), while the reinforcement is modeled using 2-noded 3D linear truss elements (T3D2). The embedded option is adopted which assumes perfect bond between the concrete and the reinforcement, while the reinforcement layout for the specimens is shown in Fig. 6.7. A mesh sensitivity study was performed in advance, indicating that the results are almost non mesh sensitive. Thus, the concrete part of the specimens is meshed using only one brick element, in order to decrease the total computational time for each FE analysis.

The behavior of the concrete is simulated using the concrete damaged plasticity model, which is described in the previous chapter. In this study the Poisson's ratio is set equal to $v = 0.2$, the dilation angle is set equal to $\psi = 36^o$, the shape factor is set equal to $K_c = 0.667$, and the stress ratio is set equal to $\sigma_{b0}/\sigma_{c0} = 1.16$. The fracture energy ($G_f$) is obtained from the CEB-FIP Model Code 90 (1993), depending on the maximum aggregate size and the compressive strength of concrete. Thus, the fracture energy for the specimen 1, 2, 3 and 8 is defined equal to 0.0703 N/mm, 0.0655 N/mm, 0.0749 N/mm and 0.0691 N/mm, respectively. The elastic behavior of both non-prestressed reinforcement and tendons is defined through the modulus of elasticity (E_s) and the Poisson's ratio (v) with values equal to 200 GPa and 0.3, respectively. The plastic behavior of both non-prestressed reinforcement and tendons is defined based on an input stress-strain relationship, which is shown in Table 6.2 (Elwi and Murray, 1980).

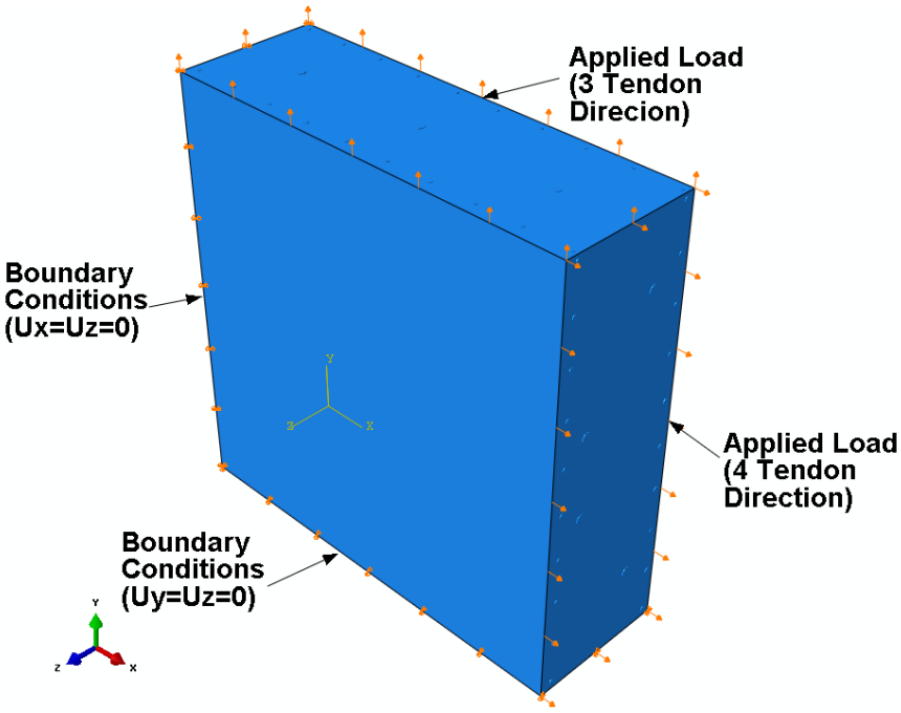

Fig. 6.6. Geometry, load and boundary conditions of the specimens.

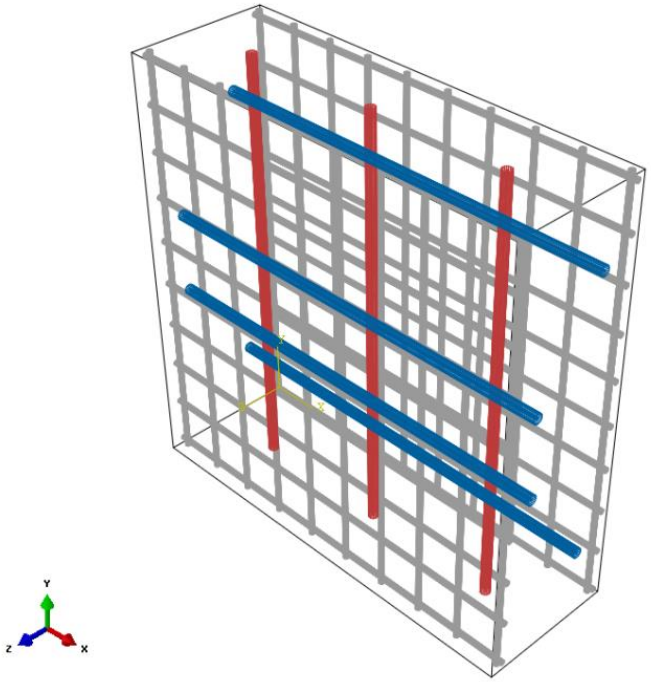

Fig. 6.7. Reinforcement layout of the specimens.

Table 6.2. Steel stress-strain relationship (Elwi and Murray, 1980).

Non-prestressed bars		Prestressed tendons	
σ (Mpa)	ε (10^{-3})	σ (Mpa)	ε (10^{-3})
0	0	0	0
401	2.04	1413	6.97
480	40.00	1572	8.40
-	-	1634	10.00
-	-	1655	12.00
-	-	1724	20.00
-	-	1732	41.00

6.3.1 Modeling of the prestressing force

The prestressing in tendons can be modelled by applying either initial stress or initial temperature to the tendons. Using the first approach (initial stress), the prestressing to the tendons is introduced in the initial step. In the following step, the end of the tendons are fully restrained (Ux=Uy=Uz=0), while these boundary conditions are deactivated in the subsequent step and simple supports are introduced to the bottom and to the one lateral edge of the specimen (Fig. 6.6). In that way, the prestressing action is taking place. In the final step, the load is applied to the top and to the other lateral edge of the specimen (Fig. 6.6). Using the second approach (initial temperature), the temperature of the environment, i.e., 20^{o} C, is introduced to the tendons in the initial step, together with the simple supports to the bottom and to the one lateral edge of the specimen. In the following step, the prestressing action is taking place by applying a new temperature value to the tendons calculated as $\Delta T = \sigma_{pe}/(a\ E_s)$, where σ_{pe} is the prestressing in tendon, a is the thermal coefficient of linear expansion of the tendon and E_s is the modulus of elasticity of the tendon. The coefficient of linear expansion of the steel is considered as 10^{-5} (1/ ^{o}C). The final step is the same as the final step of the first approach. The initial stress approach requires 4 steps in total with a computational cost equal to 114 seconds per FE analysis. The initial temperature approach requires 3 steps in total with a computational cost equal to 78

seconds per FE analysis. Each FE analysis is executed on a personal computer with Intel i7-3770 3rd Generation Processor and 16GB of RAM.

6.3.2 FEA results

The FEA results of the selected specimens are in good agreement compared to the test results, in terms of load-strain curves. For the hoop direction specimen 3 requires half applied load compared to the specimens 1, 2 and 8 (Table 6.1). Thus, for specimen 3 the maximum strain obtained from the FEA reaches the value of 0.012 (Fig. 6.12), while for specimens 1, 2 and 8 reaches the value of 0.024. Due to the initial prestressed to the tendons, the FE analysis records negative strains indicating that the concrete is in compression. Therefore, FEA results start from negative strains, contrary to the test results which start from zero strain. In the following load-strain curves, temperature refers to the initial temperature approach and stress refers to the initial stress approach for modeling the prestressing in tendons.

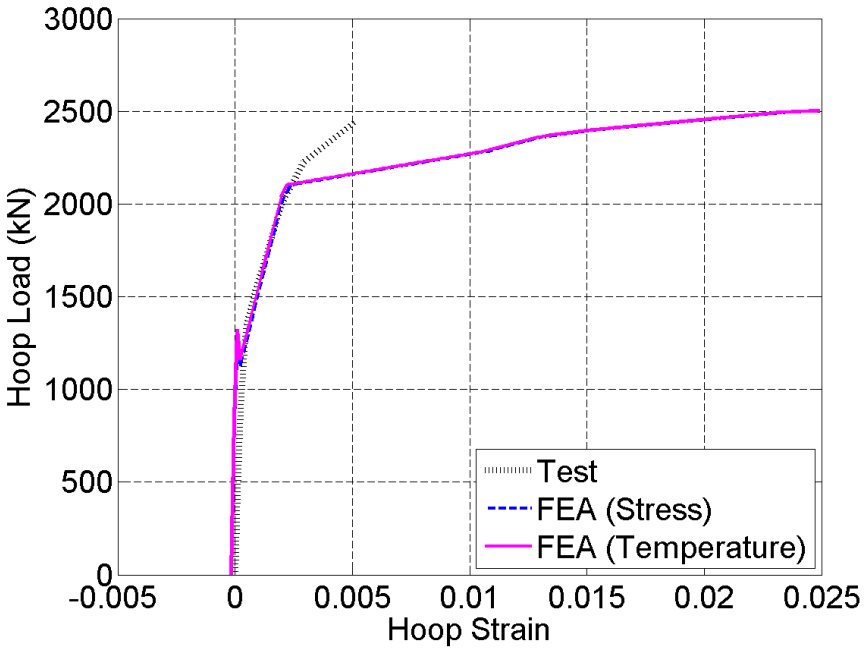

Fig. 6.8. Curves of load-strain: Hoop direction of specimen 1.

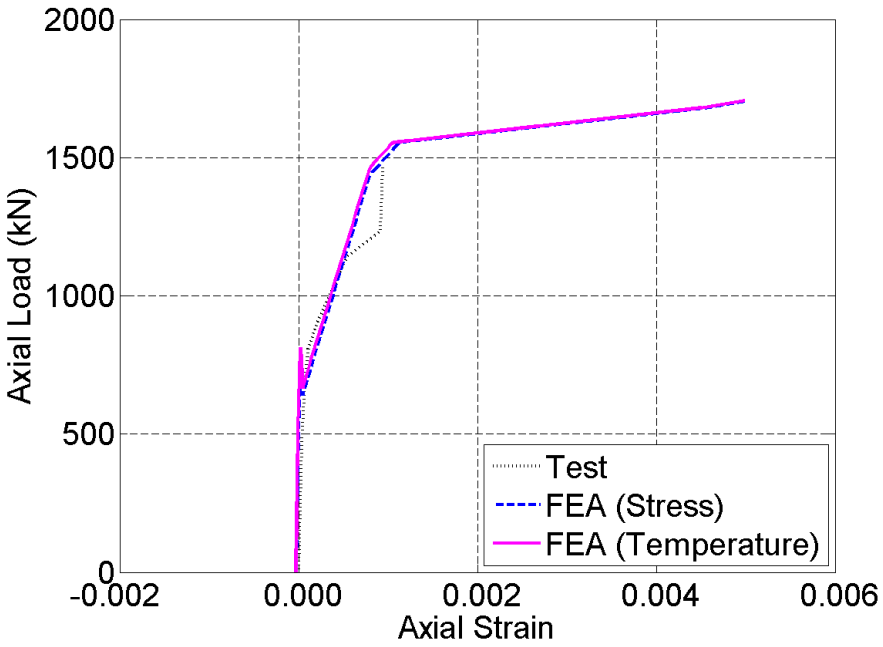

Fig. 6.9. Curves of load-strain: Axial direction of specimen 1.

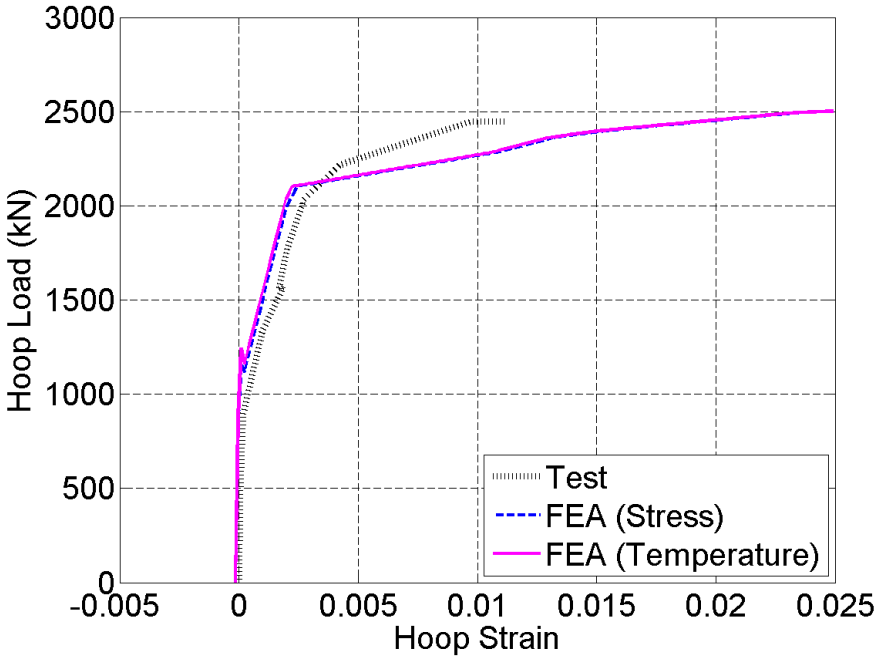

Fig. 6.10. Curves of load-strain: Hoop direction of specimen 2.

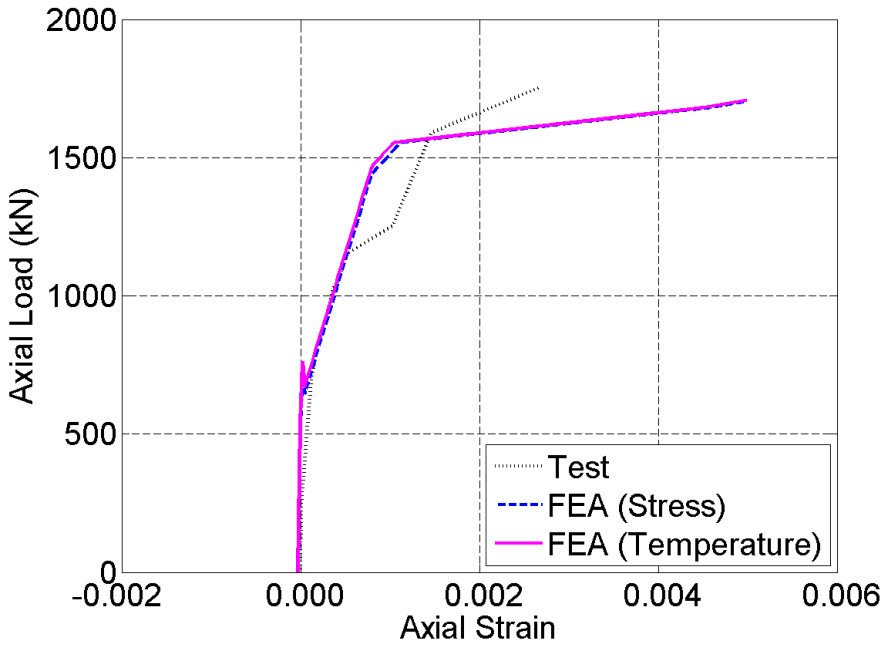

Fig. 6.11. Curves of load-strain: Axial direction of specimen 2.

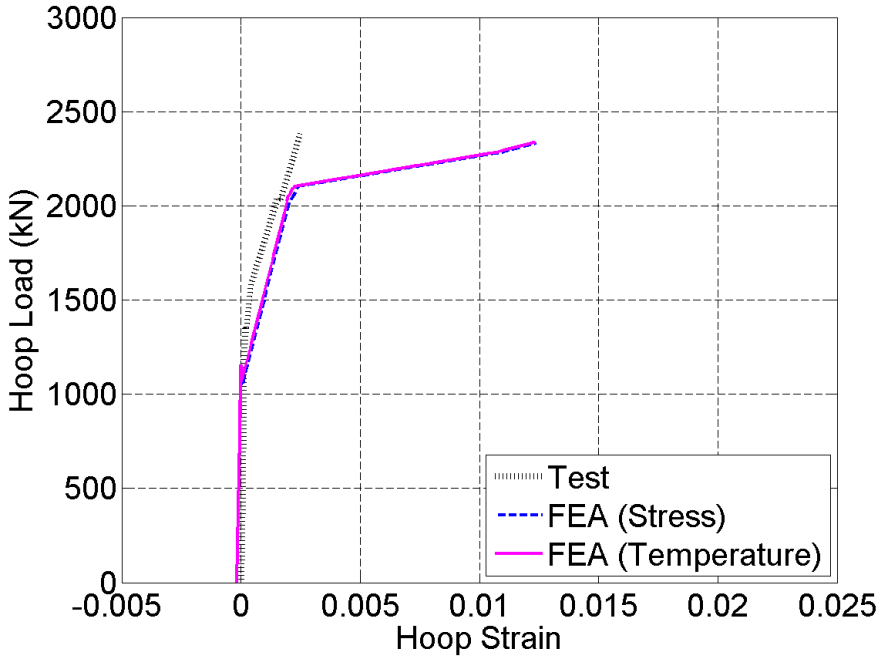

Fig. 6.12. Curves of load-strain: Hoop direction of specimen 3.

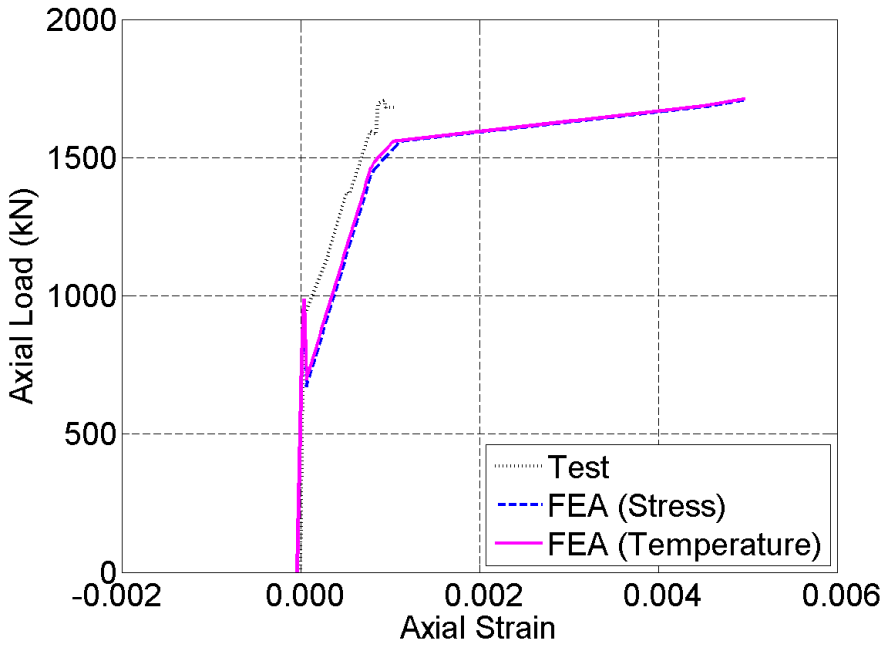

Fig. 6.13. Curves of load-strain: Axial direction of specimen 3.

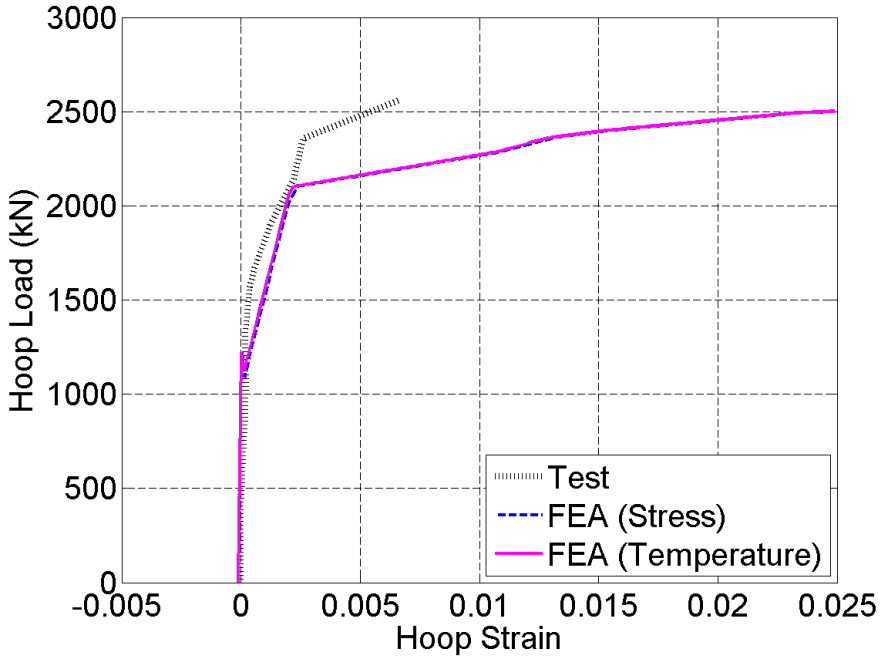

Fig. 6.14. Curves of load-strain: Hoop direction of specimen 8.

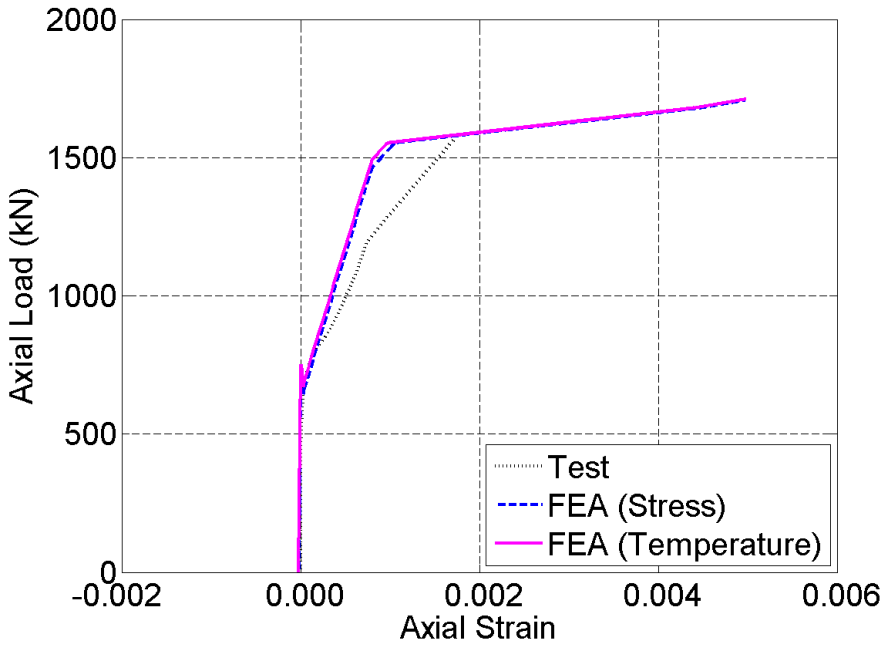

Fig. 6.15. Curves of load-strain: Axial direction of specimen 8.

For the leakage rate test, it is found that the required hoop prestressing force is $F_{H,leak} = 514.26$ kN and the required axial prestressing force is $F_{A,leak} = 257.13$ kN. Considering that the load-strain curves for all specimens are linear in that range, linear interpolation is applied for the previous mentioned forces. In this way, we are able to estimate the hoop and the axial concrete strains based on the leakage rate test (Table 6.3). In a similar manner, the hoop and the axial concrete strains are estimated based on the proof test, i.e., strains which correspond to $F_{H,proof} = 591.40$ kN and $F_{A,proof} = 295.70$ kN, respectively (Table 6.4). Both ways of modeling the prestressing force provide similar strain results, but the initial stress approach requires more computational time. Thus, the initial temperature approach for modeling the prestressing is chosen for the subsequent analysis.

Table 6.3. Calculated concrete strains based on the loading used for the leakage rate test.

Specimen	Hoop Strain (μ)		Axial strain (μ)	
	FEA		FEA	
	Temperature	Stress	Temperature	Stress
1	-79.81	-74.06	-43.29	-39.85
2	-75.93	-69.11	-42.33	-39.23
3	-96.03	-90.89	-45.99	-41.97
8	-55.76	-51.34	-32.76	-30.33

Note: Negative sign denotes compression in the FEA results; Temperature refers to the initial temperature approach for modeling the prestressing; Stress refers to the initial stress approach for modeling the prestressing; μ is the micro symbol for denoting a factor of 10^{-6}

Table 6.4. Calculated concrete strains based on the loading used for the proof test.

Specimen	Hoop Strain (μ)		Axial strain (μ)	
	FEA		FEA	
	Temperature	Stress	Temperature	Stress
1	-68.39	-62.64	-38.62	-35.17
2	-64.93	-58.11	-37.83	-34.73
3	-83.86	-78.63	-39.77	-35.76
8	-47.85	-43.44	-29.54	-27.12

Note: Negative sign denotes compression in the FEA results; Temperature refers to the initial temperature approach for modeling the prestressing; Stress refers to the initial stress approach for modeling the prestressing; μ is the micro symbol for denoting a factor of 10^{-6}

6.4 Probabilistic Finite Element Analysis

6.4.1 General

Probabilistic FEA is applied using the Monte Carlo simulation (MCS). As uncertain are considered the material properties, i.e., 13 random variables (Table 6.5, Table 6.6, Table 6.7), and the prestressing loss in hoop and axial direction, i.e., 2 random variables (Table 6.8), leading to 15 random variables in total for each specimen. Similar to the previous chapter, ABAQUS Python Development Environment (PDE) is used for developing the deterministic FE model and

then for updating the uncertain input parameters for each FE simulation, while all the computations are performed using a personal computer with Intel i7-3770 3rd Generation Processor and 16GB of RAM. The coefficient of variation (COV) of the prestressing force is considered as 4% for a new structure (age < 5 years) and as 12% for an old structure (age > 30 years) (Ellingwood, 1984). This increase of the COV with time is reflecting the variability of the long-time losses mechanisms, i.e., creep and shrinkage of concrete (Pandey 1997; Anderson et al. 2008). Thus, for the hypothetical cases of excessive degradation, i.e., 20% to 50% prestressing loss, the COV is slightly increased to 15% (Table 6.8).

Table 6.5. Statistics of concrete in each specimen.

Specimen	Random Variable	Distribution	Mean	COV	Reference
1	f_c' (MPa)	Normal	35	0.135	Nowak et al., 2012
	f_t' (MPa)	Normal	1.95	$\mathrm{COV}_{f_c'}$	Ellingwood et al., 1980
	E_c (MPa)	Normal	25924	0.08	Rajashekhar and Ellingwood, 1995
2	f_c' (MPa)	Normal	31	0.14	Nowak et al., 2012
	f_t' (MPa)	Normal	1.85	$\mathrm{COV}_{f_c'}$	Ellingwood et al., 1980
	E_c (MPa)	Normal	27027	0.08	Rajashekhar and Ellingwood, 1995
3	f_c' (MPa)	Normal	39	0.13	Nowak et al., 2012
	f_t' (MPa)	Normal	2.06	$\mathrm{COV}_{f_c'}$	Ellingwood et al., 1980
	E_c (MPa)	Normal	22201	0.08	Rajashekhar and Ellingwood, 1995
8	f_c' (MPa)	Normal	34	0.135	Nowak et al., 2012
	f_t' (MPa)	Normal	1.95	$\mathrm{COV}_{f_c'}$	Ellingwood et al., 1980
	E_c (MPa)	Normal	38335	0.08	Rajashekhar and Ellingwood, 1995
1, 2, 3, 8	γ_c (kN/m^3)	Normal	24	0.03	Ellingwood et al., 1980

Note: f_c' = compressive strength of concrete; $f_t' = 0.33\sqrt{f_c'}$ = tensile strength of concrete; E_c = modulus of elasticity of concrete; γ_c = density of concrete

Table 6.6. Statistics of non-prestressed reinforcement in each specimen.

Specimen	Random Variable	Distribution	Mean	COV	Reference
1, 2, 3, 8	f_y (MPa)	Normal	401	0.04	Nowak and Szerszen, 2003a
	E_s (GPa)	Normal	200	0.033	Mirza and Skrabek, 1991
	A_s (mm^2)	Normal	71.2	0.015	Rakoczy and Nowak, 2013
	γ_s (kN/m^3)	Normal	78	0.03	Assumed

Note: f_y = yield strength of steel; E_s = modulus of elasticity of steel; A_s = cross-section area of steel (#10 Bars in metric units); γ_s = density of steel

Table 6.7. Statistics of Prestressed reinforcement in each specimen.

Specimen	Random Variable	Distribution	Mean	COV	Reference
1, 2, 3, 8	f_y (MPa)	Normal	1627	0.025	Nowak and Szerszen, 2003a
	E_s (GPa)	Normal	200	0.033	Mirza and Skrabek, 1991
	A_s (mm^2) per wire	Normal	38.6	0.015	Rakoczy and Nowak, 2013
	γ_s (kN/m^3)	Normal	78	0.03	Assumed

Note: f_y = yield strength of steel; E_s = modulus of elasticity of steel; A_s = cross-section area of steel (hoop direction consists of 7 wires per tendon; axial direction consists of 6 wires per tendon); γ_s = density of steel

Table 6.8. Statistics of prestressing losses in each specimen.

Specimen	Prestressing Loss Scenario	Random Variable	Distribution	Mean	COV	Reference
1, 2, 3, 8	3%	f_{PH} (MPa)	Normal	$0.97f_{PH}$	0.04	Ellingwood, 1984
		f_{PA} (MPa)	Normal	$0.97f_{PA}$	0.04	Ellingwood, 1984
	15%	f_{PH} (MPa)	Normal	$0.85f_{PH}$	0.12	Ellingwood, 1984
		f_{PA} (MPa)	Normal	$0.85f_{PA}$	0.12	Ellingwood, 1984
	20%	f_{PH} (MPa)	Normal	$0.80f_{PH}$	0.15	Assumed
		f_{PA} (MPa)	Normal	$0.80f_{PA}$	0.15	Assumed
	25%	f_{PH} (MPa)	Normal	$0.75f_{PH}$	0.15	Assumed
		f_{PA} (MPa)	Normal	$0.75f_{PA}$	0.15	Assumed
	30%	f_{PH} (MPa)	Normal	$0.70f_{PH}$	0.15	Assumed
		f_{PA} (MPa)	Normal	$0.70f_{PA}$	0.15	Assumed
	35%	f_{PH} (MPa)	Normal	$0.65f_{PH}$	0.15	Assumed
		f_{PA} (MPa)	Normal	$0.65f_{PA}$	0.15	Assumed
	40%	f_{PH} (MPa)	Normal	$0.60f_{PH}$	0.15	Assumed
		f_{PA} (MPa)	Normal	$0.60f_{PA}$	0.15	Assumed
	45%	f_{PH} (MPa)	Normal	$0.55f_{PH}$	0.15	Assumed
		f_{PA} (MPa)	Normal	$0.55f_{PA}$	0.15	Assumed
	50%	f_{PH} (MPa)	Normal	$0.50f_{PH}$	0.15	Assumed
		f_{PA} (MPa)	Normal	$0.50f_{PA}$	0.15	Assumed

Note: 3% prestressing loss refers to a new structure (age < 5 years); 15% prestressing loss refers to an old structure (age > 30 years); 20% to 50 % prestressing loss refers to an old structure (hypothetical scenarios of excessive degradation); f_{PH} = prestressing force in hoop direction (Table 6.1); f_{PA} = prestressing force in axial direction (Table 6.1)

6.4.2 Probability distribution of concrete strains

MCS is applied with 10^3 trials for each specimen and prestressing loss scenario$(4\ specimen \times 9\ scenarios/specimen = 36\ scenarios)$ and the ABAQUS results are stored in terms of load-strain values. Similar to the previous section, for each MCS the concrete strain can be calculated using linear interpolation, for either proof or leakage rate test. In this study, for the probabilistic

analysis we consider only the leakage rate test. Thus, linear interpolation is performed for each trial and the strains are calculated, i.e., the hoop strain is calculated for $F_{H,leak} = 514.26$ kN and the axial strain is calculated for $F_{A,leak} = 257.13$ kN. This results to a vector of 10^3 values of the hoop strain for each scenario and to the same amount of values for the axial strain. The calculated hoop and axial strains are considered to follow a Normal distribution based on their histograms. Indicatively, this is clearly shown for the hoop strain (Fig. 6.16) and the axial strain (Fig. 6.17) of the specimen 2 for the 3% prestressing loss scenario.

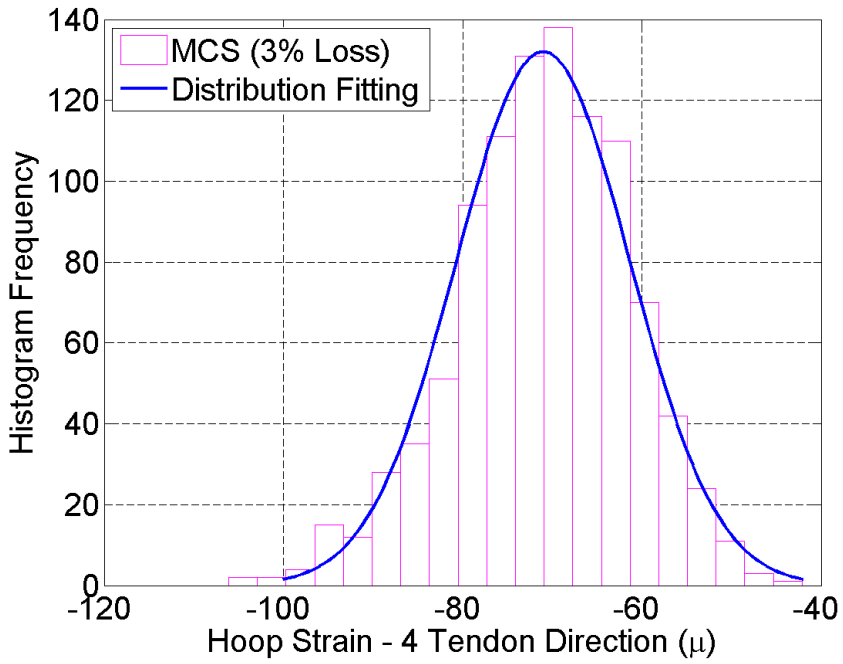

Fig. 6.16. Histogram and distribution fitting of the hoop strain: Leakage rate test for specimen 2 with 3% loss of prestressing.

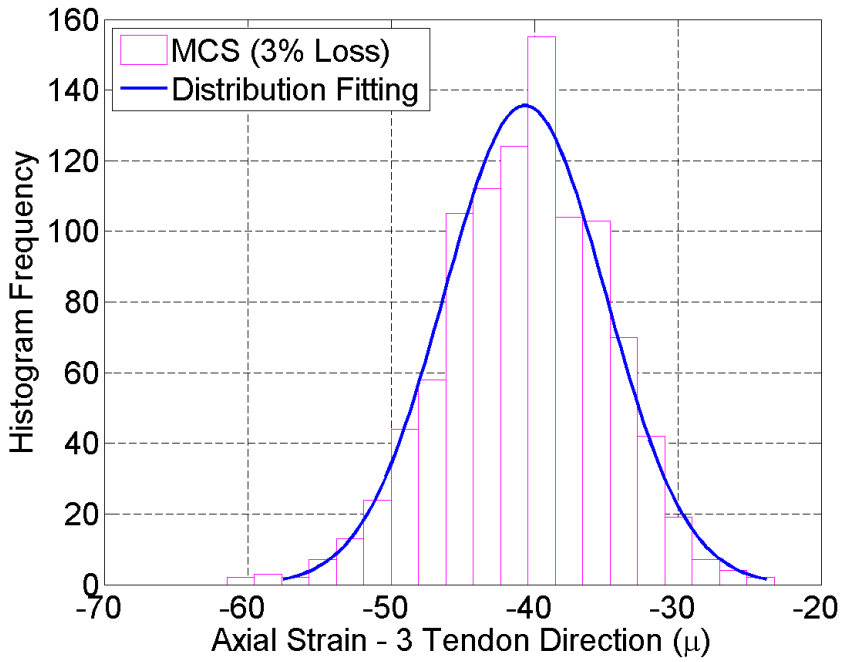

Fig. 6.17. Histogram and distribution fitting of the axial strain: Leakage rate test for specimen 2 with 3% loss of prestressing.

In addition to histograms, the probability papers can also be used in order to determine whether the observed data follow a particular distribution (Nowak and Collins, 2000), since probability papers are graphs where the observed data are plotted together with their probabilities (Ang and Tang, 2007). Therefore, the normal portability paper is plotted for the calculated hoop and axial strains. Indicatively, the linearity of the normal probability paper plot, for the hoop strain (Fig. 6.18) and the axial strain (Fig. 6.19) of the specimen 2 for the 15% prestressing loss scenario, indicates that the calculated strains are represented very well by the Normal distribution. Both histograms and normal probability paper plots indicate that the probability distribution of the calculated hoop and axial strain is following the Normal distribution, with mean and standard deviation as reported in the following tables (Table 6.9, Table 6.10, Table 6.11, Table 6.12).

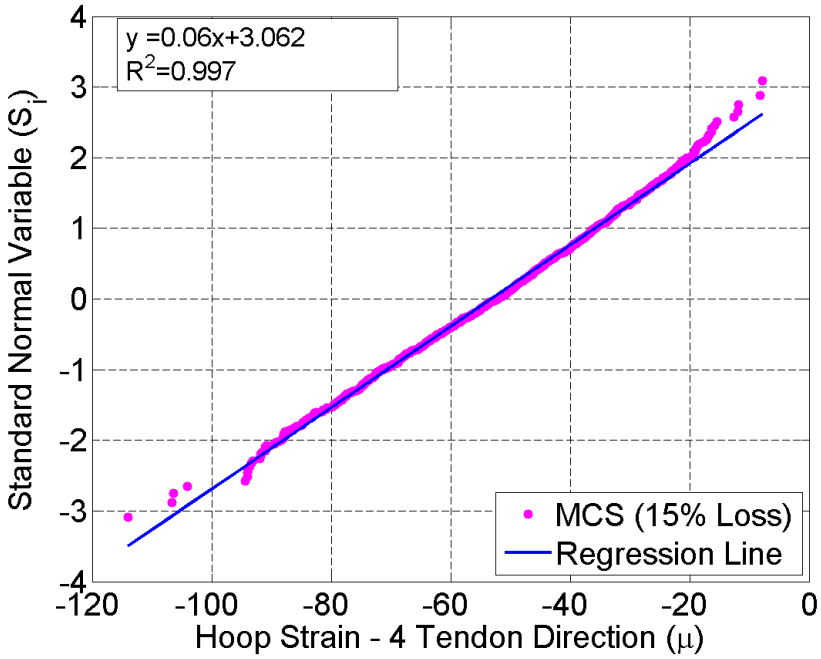

Fig. 6.18. Normal probability paper plot of the hoop strain: Leakage rate test for specimen 2 with 15% loss of prestressing.

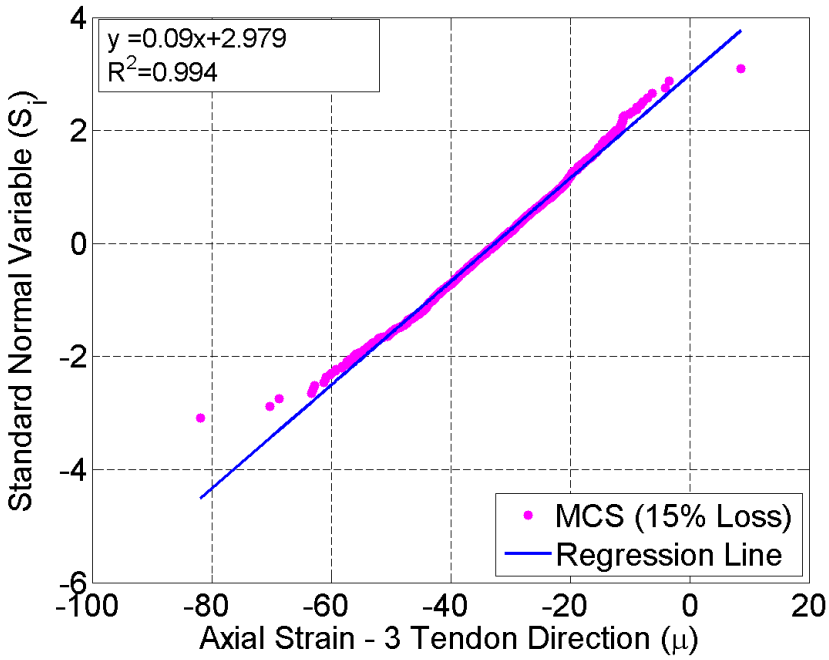

Fig. 6.19. Normal probability paper plot of the axial strain: Leakage rate test for specimen 2 with 15% loss of prestressing.

Table 6.9. Statistics of concrete strains: Leakage rate test for specimen 1.

Scenario	Average prestressing loss	Hoop strain (leakage rate test – Specimen 1)			Axial strain (leakage rate test – Specimen 1)		
		Mean (μ)	Stdev (μ)	COV	Mean (μ)	Stdev (μ)	COV
Base case (structure starting life)	3%	-81.40	11.63	0.1429	-40.43	5.91	0.1461
Base case (structure near end of life)	15%	-58.67	18.56	0.3164	-32.38	11.39	0.3518
Cases of excessive degradation	20%	-51.08	21.06	0.4124	-28.75	13.07	0.4547
	25%	-42.10	20.42	0.4849	-26.02	11.85	0.4554
	30%	-36.23	18.74	0.5172	-21.83	10.76	0.4932
	35%	-28.24	17.41	0.6164	-18.36	10.38	0.5654
	40%	-20.85	15.75	0.7555	-14.91	9.98	0.6693
	45%	-12.13	15.07	1.2425	-11.27	8.83	0.7840
	50%	-5.15	13.76	2.6726	-7.85	8.38	1.0684

Note: Stdev = Standard Deviation; COV = Coefficient of Variation; μ is the micro symbol for denoting a factor of 10^{-6}

Table 6.10. Statistics of concrete strains: Leakage rate test for specimen 2.

Scenario	Average prestressing loss	Hoop strain (leakage rate test – Specimen 2)			Axial strain (leakage rate test – Specimen 2)		
		Mean (μ)	Stdev (μ)	COV	Mean (μ)	Stdev (μ)	COV
Base case (structure starting life)	3%	-71.02	9.67	0.1361	-40.66	5.61	0.1380
Base case (structure near end of life)	15%	-53.21	17.26	0.3243	-32.57	10.84	0.3327
Cases of excessive degradation	20%	-47.41	20.15	0.4249	-29.41	13.02	0.4429
	25%	-40.33	18.57	0.4606	-25.25	11.94	0.4729
	30%	-31.83	17.71	0.5565	-22.30	10.92	0.4896
	35%	-25.24	16.30	0.6460	-18.09	9.68	0.5351
	40%	-17.36	15.40	0.8874	-14.85	9.34	0.6288
	45%	-10.35	15.30	1.4787	-10.88	8.66	0.7952
	50%	-2.06	14.64	7.0894	-7.29	7.72	1.0580

Note: Stdev = Standard Deviation; COV = Coefficient of Variation; μ is the micro symbol for denoting a factor of 10^{-6}

Table 6.11. Statistics of concrete strains: Leakage rate test for specimen 3.

Scenario	Average prestressing loss	Hoop strain (leakage rate test – Specimen 3)			Axial strain (leakage rate test – Specimen 3)		
		Mean (μ)	Stdev (μ)	COV	Mean (μ)	Stdev (μ)	COV
Base case (structure starting life)	3%	-93.44	12.45	0.1333	-43.44	6.35	0.1462
Base case (structure near end of life)	15%	-73.36	20.93	0.2853	-33.58	12.63	0.3762
Cases of excessive degradation	20%	-64.01	24.43	0.3817	-29.43	14.02	0.4764
	25%	-55.30	22.24	0.4023	-25.40	14.02	0.5521
	30%	-45.80	21.14	0.4616	-21.25	13.07	0.6152
	35%	-38.57	20.07	0.5204	-16.80	12.14	0.7226
	40%	-29.27	18.45	0.6303	-13.07	10.71	0.8195
	45%	-19.00	17.07	0.8986	-8.43	10.35	1.2275
	50%	-11.84	15.49	1.3084	-4.26	9.39	2.2059

Note: Stdev = Standard Deviation; COV = Coefficient of Variation; μ is the micro symbol for denoting a factor of 10^{-6}

Table 6.12. Statistics of concrete strains: Leakage rate test for specimen 8.

Scenario	Average prestressing loss	Hoop strain (leakage rate test – Specimen 8)			Axial strain (leakage rate test – Specimen 8)		
		Mean (μ)	Stdev (μ)	COV	Mean (μ)	Stdev (μ)	COV
Base case (structure starting life)	3%	-52.73	7.49	0.1421	-31.18	4.54	0.1456
Base case (structure near end of life)	15%	-38.48	14.66	0.3810	-24.58	8.28	0.3369
Cases of excessive degradation	20%	-32.72	17.80	0.5439	-21.94	9.67	0.4408
	25%	-27.27	18.87	0.6919	-18.85	9.05	0.4799
	30%	-20.47	18.48	0.9029	-15.91	8.79	0.5522
	35%	-12.02	20.58	1.7118	-11.87	8.33	0.7012
	40%	-2.53	20.09	7.9332	-8.84	8.22	0.9294
	45%	6.74	21.53	3.1928	-4.06	7.94	1.9546
	50%	16.96	20.45	1.2061	0.27	8.12	30.4079

Note: Stdev = Standard Deviation; COV = Coefficient of Variation; μ is the micro symbol for denoting a factor of 10^{-6}

The probability distribution of the hoop strain and the axial strain is plotted for each specimen, which follows the Normal distribution with mean and standard deviation as reported in the previous tables (Table 6.9, Table 6.10, Table 6.11, Table 6.12). For sake of clarity, the probability distribution of the concrete strain in each direction (hoop and axial) for each specimen is plotted for the two base cases, i.e., 3% and 15 % prestressing loss, together with the two hypothetical cases of excessive degradation, i.e., 25% and 50% prestressing loss. It is observed that the mean value of the strain is increased with the increase of the prestressing loss, resulting to the strain distribution shifting to the right. The next section examines how we can quantify this shifting with respect to the prestressing loss.

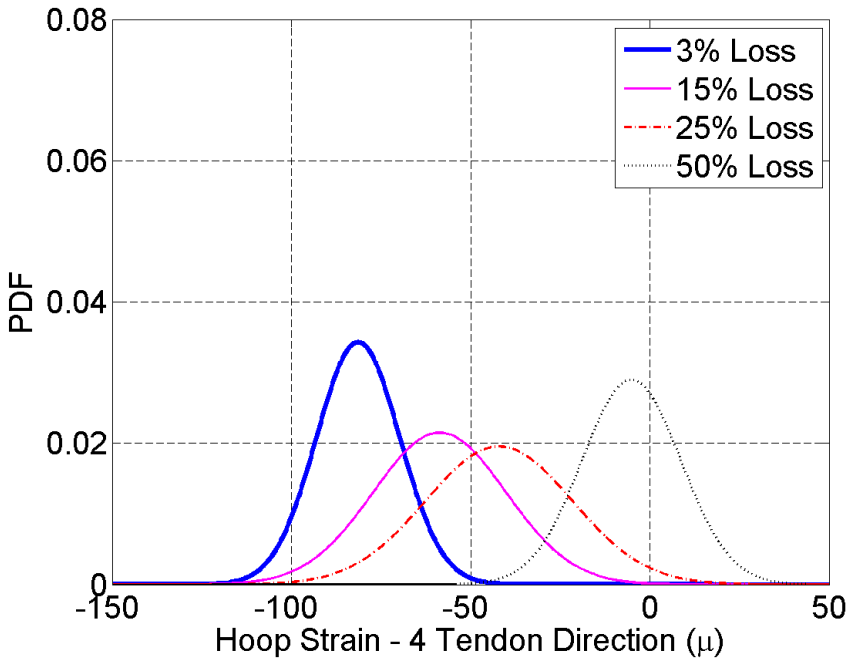

Fig. 6.20. Probability distribution of the hoop strain: Leakage rate test for specimen 1.

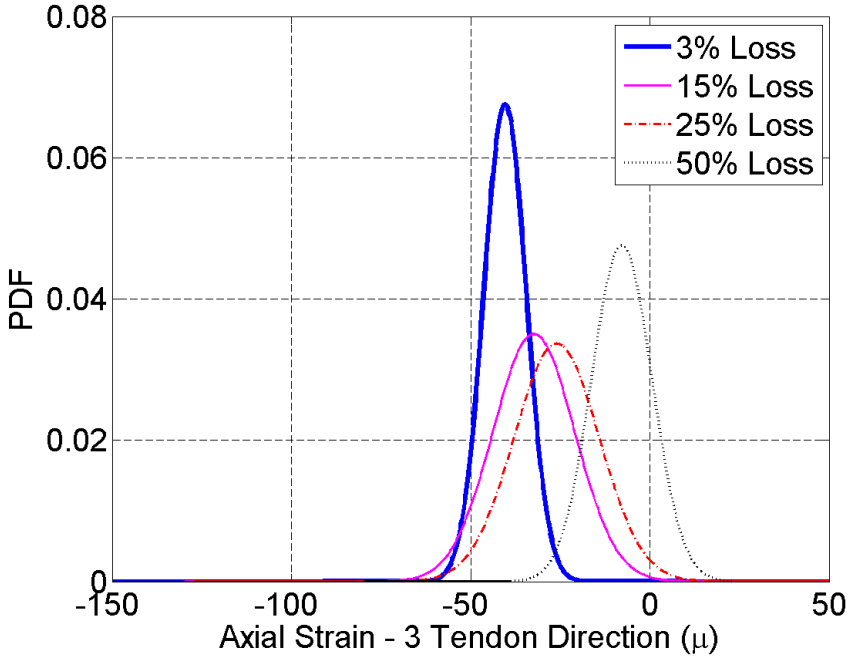

Fig. 6.21. Probability distribution of the axial strain: Leakage rate test for specimen 1.

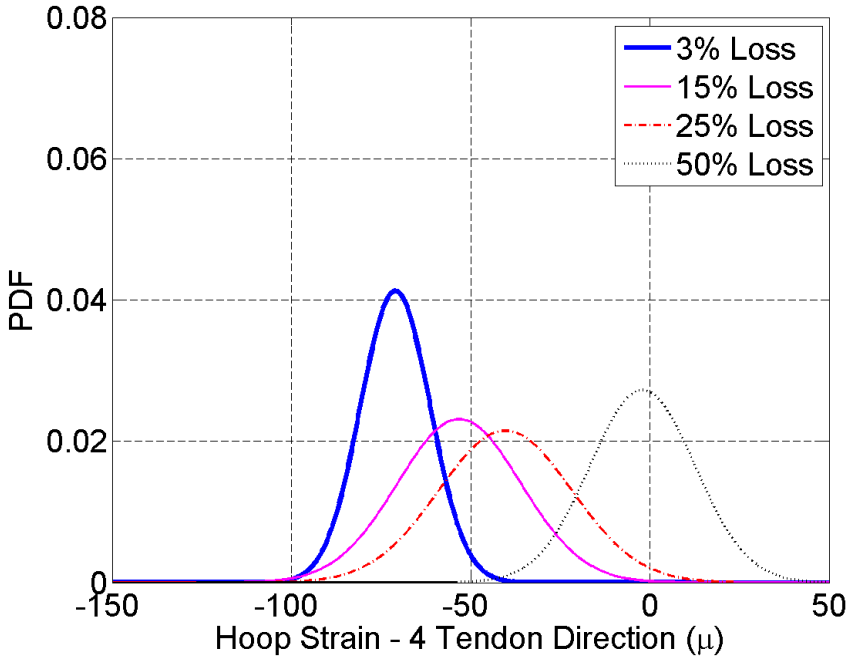

Fig. 6.22. Probability distribution of the hoop strain: Leakage rate test for specimen 2.

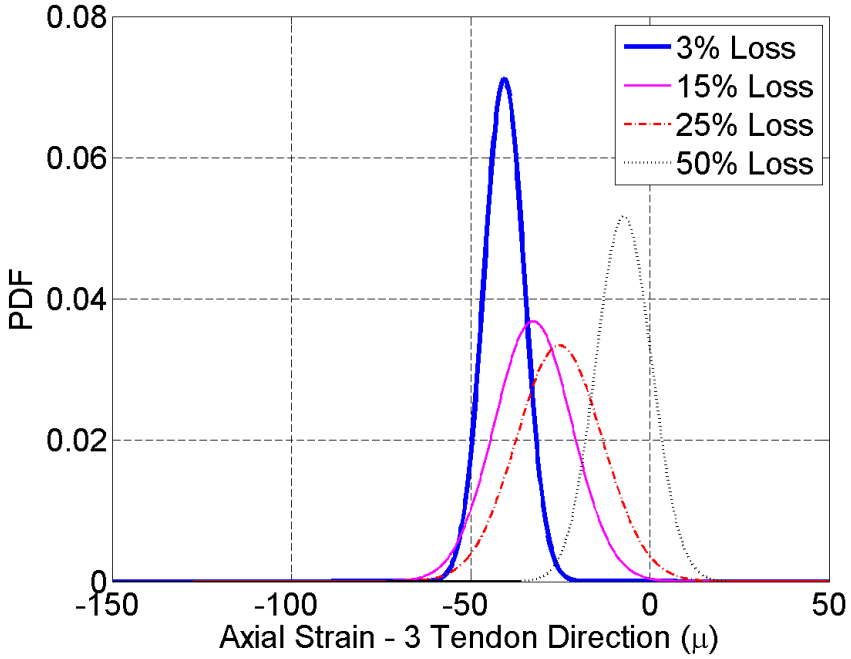

Fig. 6.23. Probability distribution of the axial strain: Leakage rate test for specimen 2.

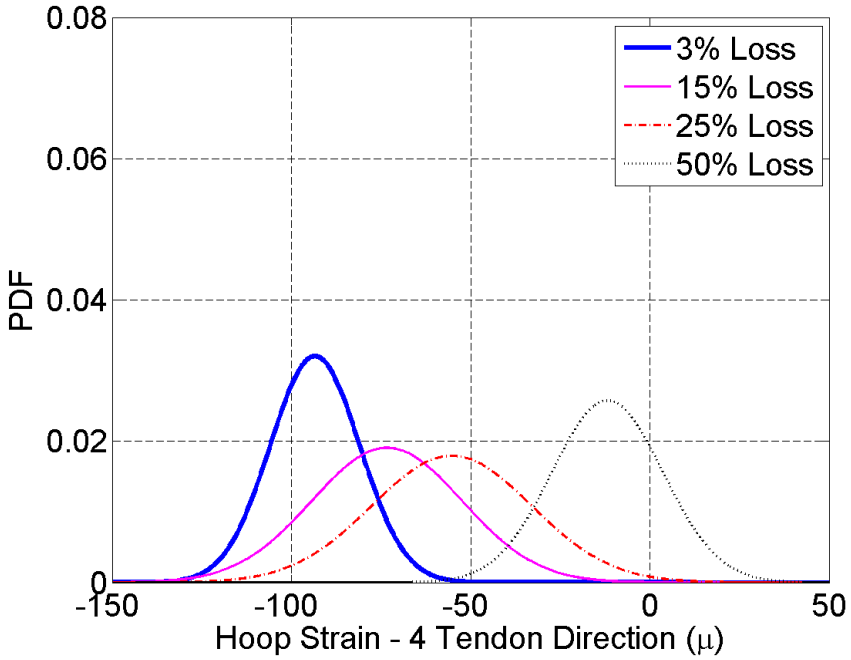

Fig. 6.24. Probability distribution of the hoop strain: Leakage rate test for specimen 3.

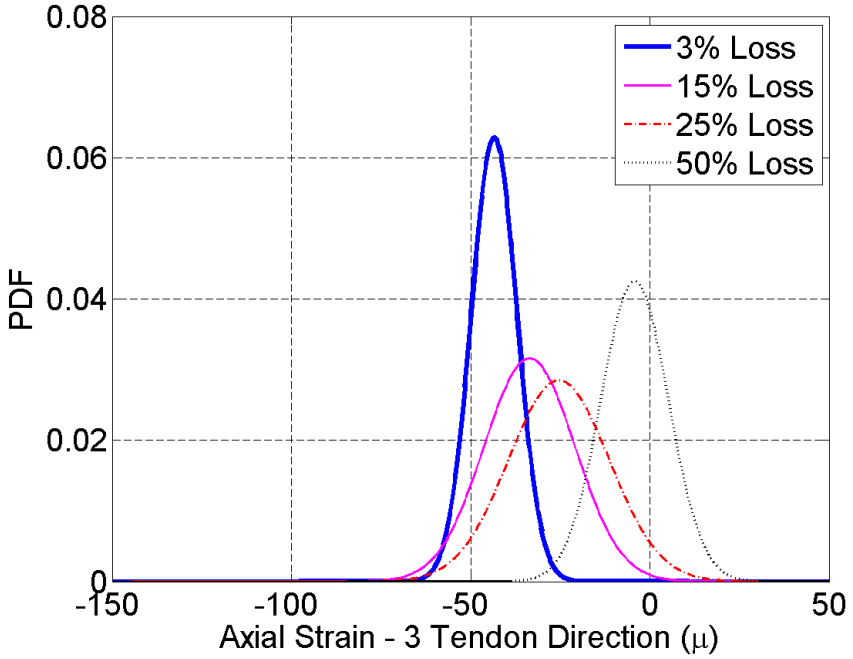

Fig. 6.25. Probability distribution of the axial strain: Leakage rate test for specimen 3.

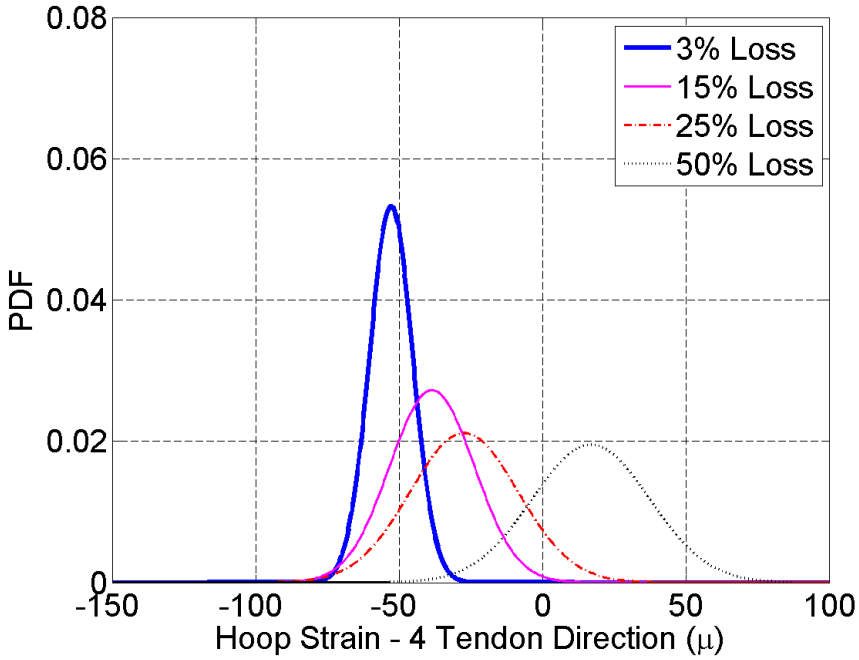

Fig. 6.26. Probability distribution of the hoop strain: Leakage rate test for specimen 8.

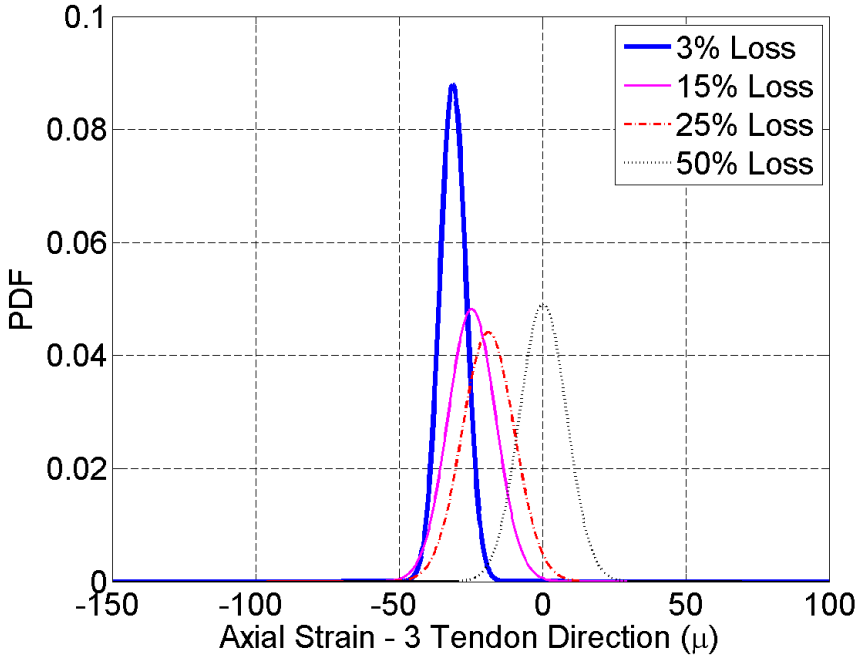

Fig. 6.27. Probability distribution of the axial strain: Leakage rate test for specimen 8.

6.4.3 Probability of increased concrete strains due to increased prestressing loss

Since the concrete strain is an effect of the prestressing loss, the magnitude of this effect can be quantified using a parameter β, which is similar to the reliability index (Madsen et al., 1986; Nowak and Collins, 2000)

$$\beta = \frac{\mu_X - \mu_Y}{\sqrt{(\sigma_X)^2 + (\sigma_Y)^2 - (2\,\rho_{XY}\,\sigma_X\,\sigma_Y)}} \tag{6.5}$$

where X is the strain distribution for the base case (X = 3% or 15% loss) and Y is the strain distribution in case of a degraded component (Y = 20% to 50%), μ_X is the mean value of the concrete strain for the selected base case, μ_Y is the mean value of the concrete strain for each excessive degradation case, σ_X is the standard deviation of the concrete strain for the selected base case, σ_Y is the standard deviation of the concrete strain for each excessive degradation case

and $\rho_{XY} = 0$ since they are considered uncorrelated. The probability is then calculated as (Nowak and Collins, 2000; Ang and Tang, 2007)

$$p = [X \leq Y] = p[X - Y \leq 0] = \Phi(-\beta) \tag{6.6}$$

where p is the probability of the concrete strain for each excessive degradation case exceeding the concrete strain of the selected base case and Φ is the standard Normal distribution function with mean equal to zero and standard deviation equal to one.

In the following tables (Table 6.13, Table 6.14, Table 6.15, Table 6.16) is reported for each specimen the probability of having increased concrete strains, due to increased prestressing loss, with respect to the concrete strain of the 15% base case. The results indicate that the probability of having a concrete strain bigger than the base case is increased with the increase of the prestressing loss. For the hoop strain, this probability ranges from 0.59 to 0.61 for the case of 20% prestressing loss and from 0.85 to 0.89 for the 35% case. Thus, measuring the concrete strain, e.g., during the leakage rate test, and comparing it with the measured concrete strain of a selected base case, can provide us information with respect to the prestressing loss. For instance, a probability of the hoop concrete strain ranging from 0.78 to 0.82 indicates a 30% prestressing loss. Fig. 6.28 and Fig. 6.29 demonstrate this point quite well for the hoop and the axial direction, respectively, while a correlation of the prestressing loss with the concrete strain is examined in the next section.

Table 6.13. Probability of the concrete strain during a test exceeding the concrete strain in the 15% base case: Leakage rate test for specimen 1.

Scenario	Average prestressing loss	Hoop strain (leakage rate test – Specimen 1)		Axial strain (leakage rate test – Specimen 1)	
		β	$p = \Phi(-\beta)$	β	$p = \Phi(-\beta)$
Base case (structure near end of life)	15%	N/A	N/A	N/A	N/A
Cases of excessive degradation	20%	-0.2703	6.07E-01	-0.2095	5.83E-01
	25%	-0.6004	7.26E-01	-0.3870	6.51E-01
	30%	-0.8507	8.03E-01	-0.6733	7.50E-01
	35%	-1.1955	8.84E-01	-0.9092	8.18E-01
	40%	-1.5534	9.40E-01	-1.1531	8.76E-01
	45%	-1.9462	9.74E-01	-1.4646	9.28E-01
	50%	-2.3161	9.90E-01	-1.7342	9.59E-01

Note: p = probability of the concrete strain (due to prestressing loss) exceeding the concrete strain of the 15% base case.

Table 6.14. Probability of the concrete strain during a test exceeding the concrete strain in the 15% base case: Leakage rate test for specimen 2.

Scenario	Average prestressing loss	Hoop strain (leakage rate test – Specimen 1)		Axial strain (leakage rate test – Specimen 1)	
		β	$p = \Phi(-\beta)$	β	$p = \Phi(-\beta)$
Base case (structure near end of life)	15%	N/A	N/A	N/A	N/A
Cases of excessive degradation	20%	-0.2187	5.87E-01	-0.1866	5.74E-01
	25%	-0.5082	6.94E-01	-0.4539	6.75E-01
	30%	-0.8646	8.06E-01	-0.6678	7.48E-01
	35%	-1.1784	8.81E-01	-0.9963	8.40E-01
	40%	-1.5501	9.39E-01	-1.2383	8.92E-01
	45%	-1.8587	9.68E-01	-1.5634	9.41E-01
	50%	-2.2604	9.88E-01	-1.8997	9.71E-01

Note: p = probability of the concrete strain (due to prestressing loss) exceeding the concrete strain of the 15% base case.

Table 6.15. Probability of the concrete strain during a test exceeding the concrete strain in the 15% base case: Leakage rate test for specimen 3.

Scenario	Average prestressing loss	Hoop strain (leakage rate test – Specimen 1)		Axial strain (leakage rate test – Specimen 1)	
		β	$p = \Phi(-\beta)$	β	$p = \Phi(-\beta)$
Base case (structure near end of life)	15%	N/A	N/A	N/A	N/A
Cases of excessive degradation	20%	-0.2906	6.14E-01	-0.2198	5.87E-01
	25%	-0.5913	7.23E-01	-0.4337	6.68E-01
	30%	-0.9264	8.23E-01	-0.6788	7.51E-01
	35%	-1.1996	8.85E-01	-0.9580	8.31E-01
	40%	-1.5802	9.43E-01	-1.2384	8.92E-01
	45%	-2.0126	9.78E-01	-1.5400	9.38E-01
	50%	-2.3625	9.91E-01	-1.8632	9.69E-01

Note: p = probability of the concrete strain (due to prestressing loss) exceeding the concrete strain of the 15% base case.

Table 6.16. Probability of the concrete strain during a test exceeding the concrete strain in the 15% base case: Leakage rate test for specimen 8.

Scenario	Average prestressing loss	Hoop strain (leakage rate test – Specimen 1)		Axial strain (leakage rate test – Specimen 1)	
		β	$p = \Phi(-\beta)$	β	$p = \Phi(-\beta)$
Base case (structure near end of life)	15%	N/A	N/A	N/A	N/A
Cases of excessive degradation	20%	-0.2501	5.99E-01	-0.2069	5.82E-01
	25%	-0.4690	6.80E-01	-0.4668	6.80E-01
	30%	-0.7636	7.77E-01	-0.7178	7.64E-01
	35%	-1.0473	8.53E-01	-1.0819	8.60E-01
	40%	-1.4452	9.26E-01	-1.3493	9.11E-01
	45%	-1.7364	9.59E-01	-1.7880	9.63E-01
	50%	-2.2031	9.86E-01	-2.1424	9.84E-01

Note: p = probability of the concrete strain (due to prestressing loss) exceeding the concrete strain of the 15% base case.

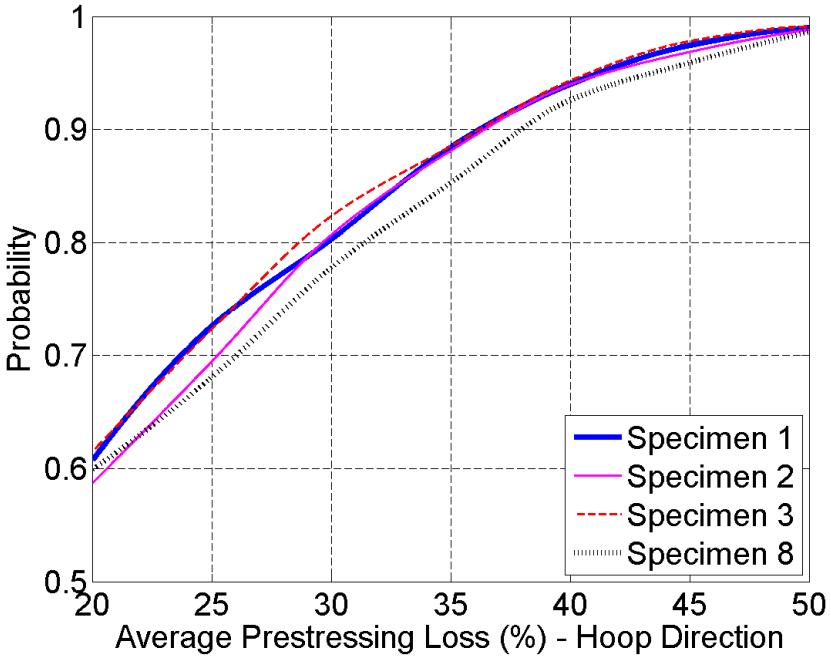

Fig. 6.28. Probability of the concrete strain during a test exceeding the concrete strain in the 15% base case: Leakage rate test and hoop direction.

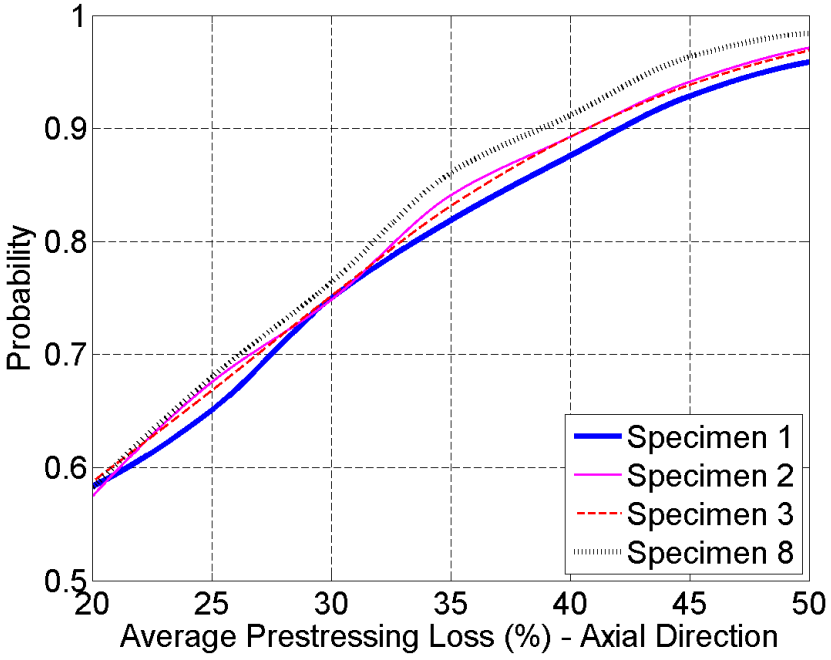

Fig. 6.29. Probability of the concrete strain during a test exceeding the concrete strain in the 15% base case: Leakage rate test and axial direction.

6.4.4 Correlation of the prestressing loss with the concrete strains

Correlation analysis, also called regression analysis, is a statistical technique in order to estimate the relationship between two variables (Montgomery and Runger, 2003; Ross, 2004; Ang and Tang, 2007). Based on the calculated high probability that an increase of the average prestressing loss would result to an increased average concrete strain, correlation analysis is performed to check the relationship between these two. The following figures indicate a high linear correlation between the average concrete strain and the average prestressing loss in tendons, since the coefficient of determination of the straight regression line is almost one ($R^2 \approx 1$) for all the examined specimens and for both directions (hoop and axial).

This high correlation indicates that a causal relationship exists between the prestressing loss and the concrete strain, which is actually what we expected, since the leakage rate test and the proof test pressurize the containment within its elastic range in order to avoid cracking of the containment. Thus, the results validate that the measures of the elastic concrete strains during periodic inspection procedures (pressure testing), can be used for providing information regarding the prestressing loss in tendons, e.g., to quantify the prestressing loss.

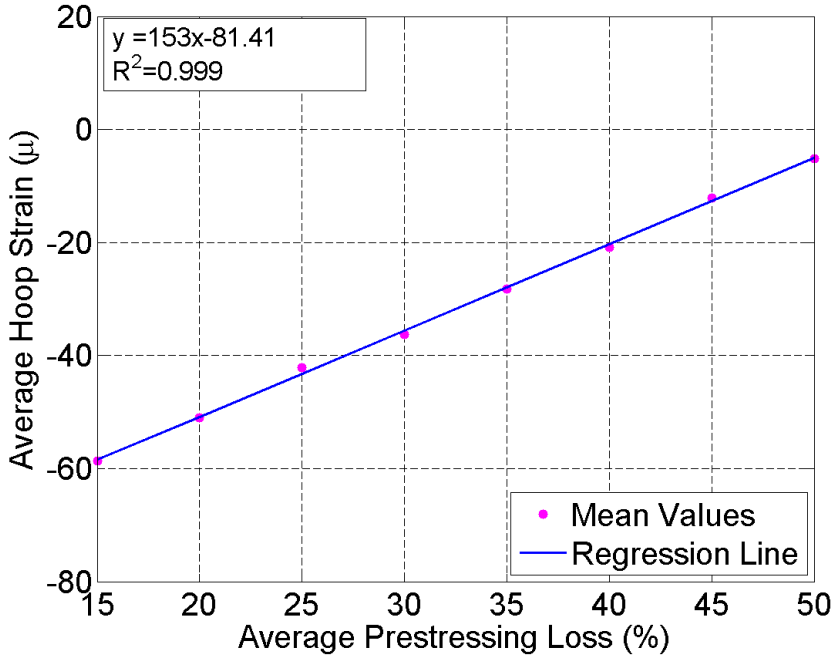

Fig. 6.30. Correlation between prestressing loss and hoop strain: Leakage rate test for specimen 1.

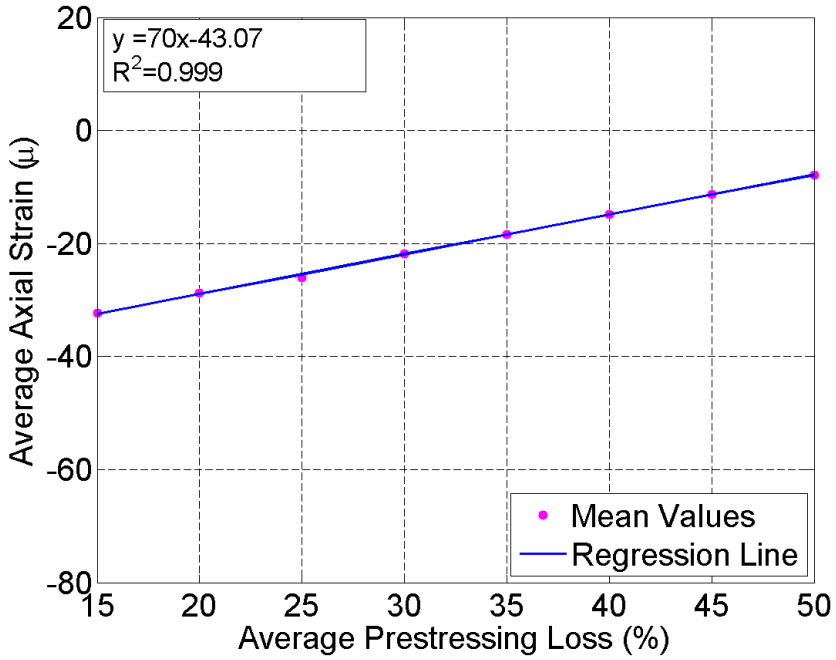

Fig. 6.31. Correlation between prestressing loss and axial strain: Leakage rate test for specimen 1.

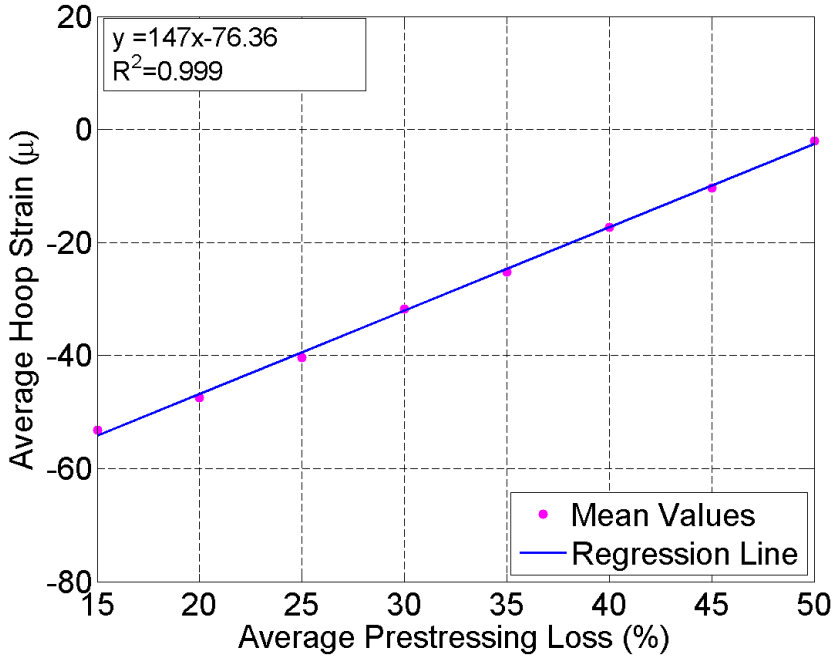

Fig. 6.32. Correlation between prestressing loss and hoop strain: Leakage rate test for specimen 2.

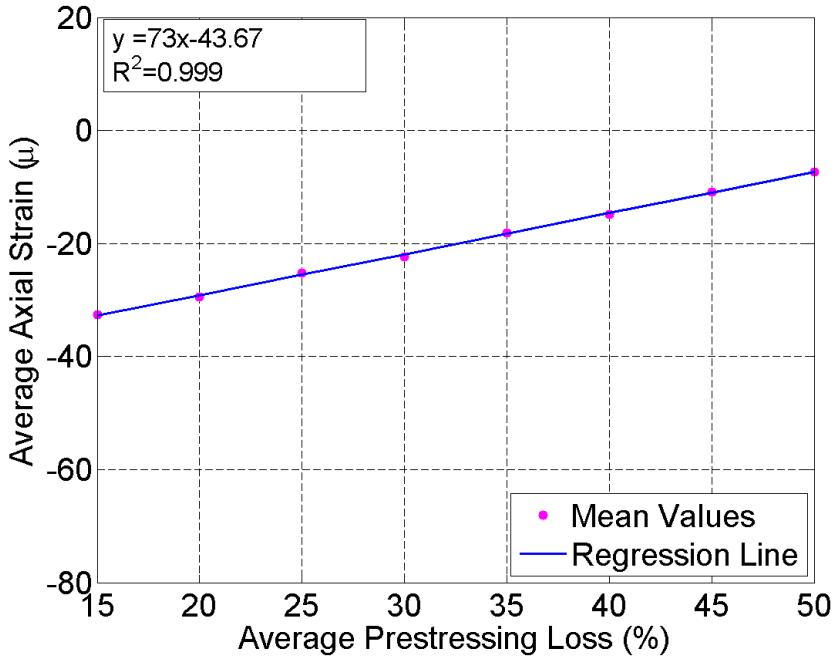

Fig. 6.33. Correlation between prestressing loss and axial strain: Leakage rate test for specimen 2.

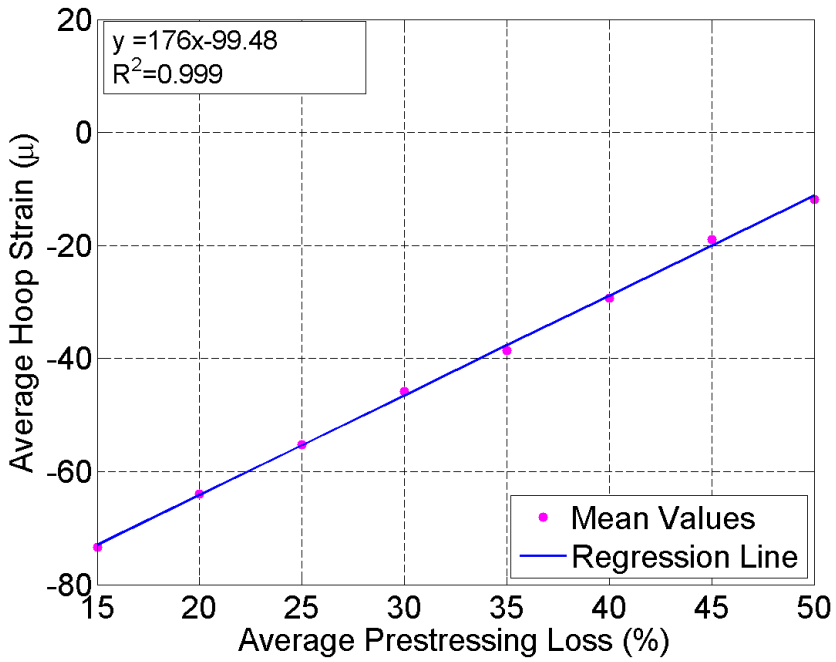

Fig. 6.34. Correlation between prestressing loss and hoop strain: Leakage rate test for specimen 3.

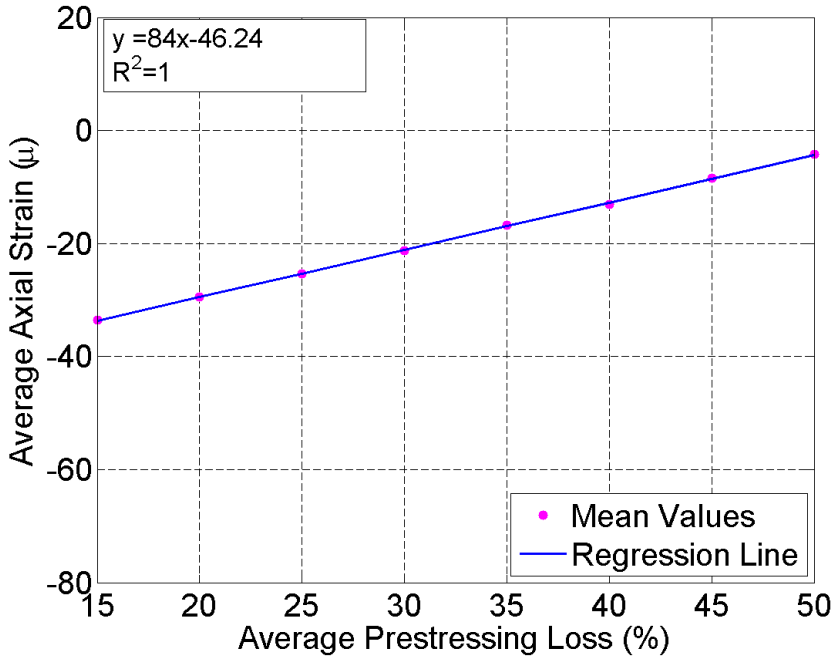

Fig. 6.35. Correlation between prestressing loss and axial strain: Leakage rate test for specimen 3.

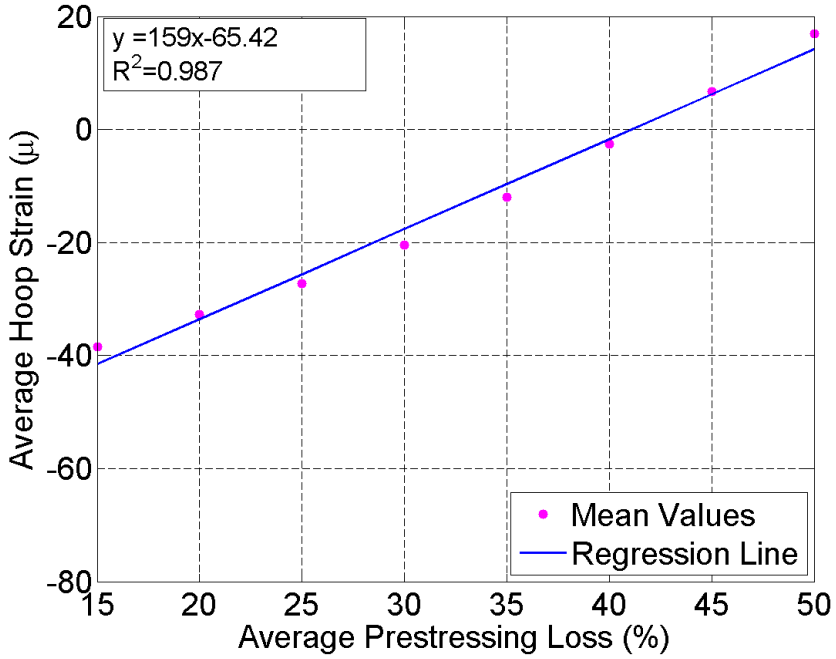

Fig. 6.36. Correlation between prestressing loss and hoop strain: Leakage rate test for specimen 8.

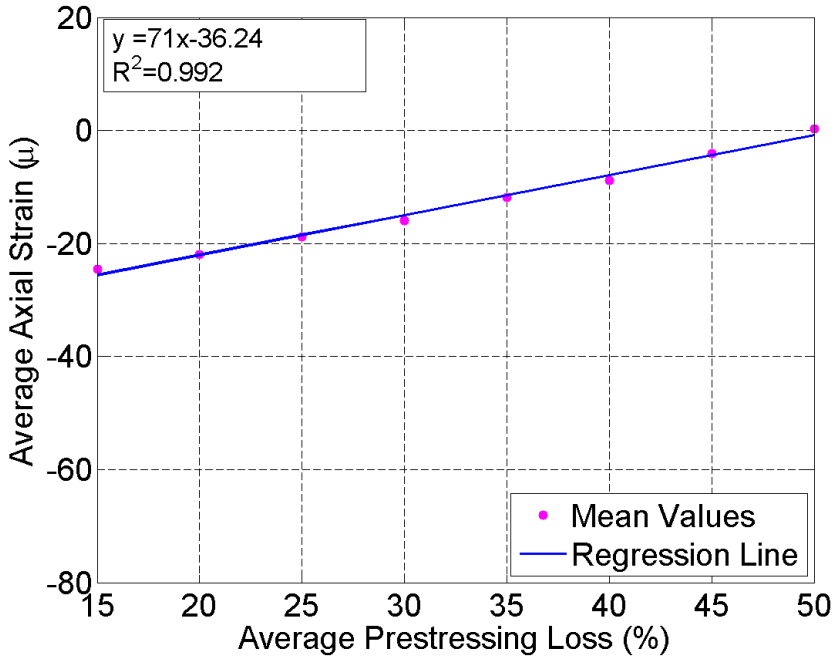

Fig. 6.37. Correlation between prestressing loss and axial strain: Leakage rate test for specimen 8.

6.5 Conclusion

This chapter presents a probabilistic analysis of the effect of presstressing losses on the distribution of concrete strain. Four 3D wall segments, already tested at the University of Alberta, are modeled and analyzed using ABAQUS. The prestressing force of the tendons is modeled using two different approaches, i.e., by introducing either initial stress or initial temperature variation to the tendons. Deterministic FEA results indicate the accuracy of the two modeling techniques, in terms of load-strain curves. However, the initial strain technique requires slightly more computational time, since one extra step has to be introduced. Thus, the adopted initial temperature approach can be considered as a computational economic technique for modeling the prestressing force.

The Monte Carlo simulation (MCS) is chosen for the probabilistic analysis, since the analyzed specimens do not require an enormous amount of computational time. However, the previously proposed multiplicative dimensional reduction method (M-DRM) can be used for future finite element studies on real concrete containment structures. MCS is implemented in ABAQUS with the use of the Python programing, as it was introduced in the previous chapter. The results indicate a high probability of increase in the concrete strain with the increase of the prestressing loss, while this probability can be used for quantifying the prestressing loss. The regression analysis results indicate a highly linear relationship between the average concrete strain and the average prestressing loss, validating that the measured elastic concrete strains during periodic inspections can be used for quantifying the prestressing loss in tendons. This probabilistic framework can be further applied for real scale concrete containment structures.

Chapter 7

Conclusions and Recommendations

7.1 Summary

Chapter 3 demonstrated the logic and developed the mathematical equations of the multiplicative dimensional reduction method (M-DRM). The method can be used for estimating the statistical moments and the probability distribution of the structural response and the sensitivity coefficients with respect to the structural response. A simple example was implemented, in order to demonstrate clearly the steps of the M-DRM.

Chapter 4 presented the applicability of the M-DRM to the nonlinear finite element analysis (FEA) of 2D structures subjected to pushover and dynamic analysis. Relevant Tcl programing code was developed, in order to link the OpenSees FEA software with the uncertainty problem. In total, five large scale problems were modeled and analyzed. First, two structural frames were subjected to pushover analysis, using the Monte Carlo simulation (MCS), the first order reliability method (FORM) and the M-DRM. Next, these frames were subjected to dynamic analysis, using the MCS and the M-DRM. Finally, a steel moment resisting frame (MRF) was subjected to several single and repeated ground motion records, where only the proposed M-DRM was performed, mainly due to the high computational cost.

Chapter 5 applies the M-DRM for nonlinear probabilistic FEA of 3D structures. Relevant Python programing code was developed, in order to: (1) link the ABAQUS with the applied reliability methods; (2) extract the values of interest after each FEA trial. The MCS was also performed apart the M-DRM. In total, two large scale problems were modeled and analyzed. At the end of

the chapter, probabilistic analysis was also performed based on the American and the European design code for punching shear of reinforced concrete flat slabs, together with the critical shear crack theory.

Chapter 6 examined the relationship between the average prestressing loss in tendons and the average concrete strains for a nuclear containment structure. Four 3D prestressed concrete wall segments were modeled and analyzed, which correspond to a 1/4 scale of a prototype nuclear containment structure, while two basic techniques were examined for modelling the prestressed concrete using FEA. Seven hypothetical scenario of prestressing loss were investigated, together with two scenarios corresponding to a new structure (age < 5 years) and an old structure (age > 30 years). For the uncertainty part, only the MCS was performed, since the computational cost was affordable.

7.2 Conclusions

This research has implemented a general computational framework for reliability and sensitivity analysis of structures, which are modeled and analyzed using the finite element method (FEM). Conclusions based on the findings of this research are grouped in two main categories as follows:

1) Findings regarding the M-DRM use for practical problems:

- The M-DRM can be considered as a viable approach for the probabilistic finite element analysis of large scale structures, since it is efficient, easily applicable and computationally economic approach.

- M-DRM can be used for a complete probabilistic analysis, since it provides the statistical moments, the probability distribution and the sensitivity coefficients, which are related to the structural response of interest.
- Sensitivity analysis can be performed without requiring any extra analytical effort.
- M-DRM together with the maximum entropy principle provides the probability distribution of the structural response. The probability of failure can be calculated based on this distribution, which is hard to be estimated in FEA, since the limit state function is usually defined in an implicit form.
- For dynamic analysis problems, M-DRM can be considered as a viable alternative for probabilistic FEA, since by nature the dynamic analysis is computational demanding.
- For 3D nonlinear FEA, M-DRM can also be considered as a viable alternative method for probabilistic FEA, since deterministic nonlinear FEA of real structures usually requires an enormous amount of computational time.
- M-DRM is flexible and easy to be implemented, since for a small number of input random variables, M-DRM trials can be performed using any deterministic FEA software, without the use of programing code and/or reliability platform.

2) Findings with respect to the investigated structural examples:

- When pushover analysis is used, the variance of the lateral applied load plays a significant role to the variance of the structural response, compared to the material and geometry uncertainties.

- When ground motions records are used, either alone or in a sequence, the uncertainty in the mass of a structure may plays a significant role to the variance of the structural response, compared to the material uncertainties of the structure.
- For a reinforced concrete slab-column connection, the punching shear failure and the flexural failure are most sensitive to the tensile strength and the compressive strength, respectively, of the concrete that will be used in the slab.
- For a reinforced concrete slab-column connection with shear reinforcement, the coefficient of variation of the ultimate displacement indicates that the flexural reinforcement of the flat slab significantly affects the maximum deformation of the slab, since the system is more ductile due to the placed shear reinforcement.
- For a reinforced concrete slab-column connection without shear reinforcement, the coefficient of variation of the ultimate displacement indicates that the flexural reinforcement of the flat slab does not significantly affect the maximum deformation of the slab, since the system will fail in a brittle way due to the absence of the shear reinforcement.
- The American and the European design code, together with the investigated punching shear model, indicate their accuracy of predicting well the reinforced concrete flat slab behavior. However, the punching shear model seems to predict more accurately the punching shear resistance of the flat slab with shear reinforcement, indicating a better predictive capability of the critical shear crack theory for flat slabs with shear reinforcement, compared to the investigated design codes.
- Concrete strain measurements during the leakage rate tests can be used as an indirect approach for the estimation of the average prestressing loss of bonded tendons.

- The probability of having an increased concrete stain is increasing with the increase of the prestressing loss in tendons, while this probability can be used for quantifying the prestressing loss.
- The regression analyses indicate that the average concrete strains increase linearly with the increase of the average prestressing loss in tendons, validating the use of measured elastic concrete strains for quantifying the prestressing loss.

7.3 Recommendations for Future Research

Future research can extend the capability of the proposed framework for practical recommendations of several problems, whiles some scientific aspects were out of the scope of this study. For example:

- The proposed method considers uncorrelated input random variables, which may not be always the case. Thus, the method should be further investigated, for taking into account correlated input random variables.
- The probability distribution of each input random variable may highly affect the output response. Although, in this study most of the input distributions were chosen from literature, still some distributions were assumed. Thus, further analyses should be performed considering input variables with different and more representative probability distributions.
- The analysis of the frames subjected to ground motion records, has been performed using a 2D nonlinear analysis. In order to take into account potential torsional effects, e.g., due to buildings' irregularities, the probabilistic framework should be extended to a 3D nonlinear probabilistic FEA of structures subjected to dynamic analysis.

- The necessity of analyzing structures subjected to several repeated earthquakes has occurred due to relevant true events. Thus, probabilistic FEA for structures subjected to more than two repeated earthquakes (and/or different scenarios of two repeated earthquakes) should be performed, in order to investigate the structural reliability due to a sequence of earthquakes.
- The previous investigation, i.e., repeated earthquakes, should be extended to the impact of fire following an earthquake, since historical events show that this is a typical occurrence.
- There are cases where openings have to be created in existing reinforced concrete flat slabs, usually for the installation of mechanical equipment. Thus, the current probabilistic framework can be used for the assessment of these slabs, considering as uncertain the size and the location of these potential openings, apart the material properties.
- Regarding nuclear power plants, the proposed framework can be further applied to real scale containment structures, which can be analyzed using the finite element method, for assessing the prestressing loss uncertainties. Also, the proof test can be examined for predicting the tendon's prestressing loss, since only the leakage rate test was examined in this study.
- For the current research, programing code was developed in either Tcl or Python, for connecting M-DRM with the determinstc FEA, while the M-DRM optimization was perfomed using MATLAB programing. The developed code could be further expanded including also the M-DRM optimization routine, for optimizing the fractional moments, within the relevant Tcl and Python codes.

References

ABAQUS. Abaqus Analysis User's Manual. Version 6.12, Dassault Syst. Simulia Corp., Providence, RI, USA.

ABAQUS. Abaqus Scripting User's Manual. Version 6.12, Dassault Syst. Simulia Corp., Providence, RI, USA.

ACI 318 (2011). Building code requirements for structural concrete (ACI 318-11). ACI Committee 318, Farmington Hills, MI, USA.

Adetifa, B., and Polak, M. A. (2005). Retrofit of slab column interior connections using shear bolts. ACI Structural Journal, 102(2), 268-274.

Ajdukiewicz, A., and Starosolski, W. (1990). Reinforced concrete slab-column structures. Developments in Civil Engineering, Elsevier Science, Amsterdam, Netherlands.

Akula, V. (2014). Multiscale reliability analysis of a composite stiffened panel. Composite Structures, 116, 432-440.

Albrecht, U. (2002). Design of flat slabs for punching – European and North American practices. Cement & Concrete Composites, 24(6), 531-538.

Anderson, P., Berglund, L-E, and Gustavsson, J. (2005). Average force along unbonded tendons: a field study at nuclear reactor containments in Sweden. Nuclear Engineering and Design, 235(1), 91-100.

Anderson, P. (2005). Thirty years of measured prestress at Swedish nuclear reactor containments. Nuclear Engineering and Design, 235(21), 2323-2336.

Anderson, P., Hansson, M., and Thelanderson, S. (2008). Reliability-based evaluation of the prestress level in concrete containments with undonded tendons. Structural Safety, 30(1), 78-89.

Ang, H-S A., and Tang, H. W. (2007). Probability concepts in engineering: emphasis on applications in civil & environmental engineering. John Wiley and Sons Inc, Hoboken, NJ, USA.

Amadio, C., Fragiacomo, M., and Rajgelj, S. (2003). The effects of repeated earthquake ground motions on the non-linear response of SDOF systems. Earthquake Engineering and Structural Dynamics, 32(2), 291-308.

Balomenos, G. P., Polak, M. A., and Pandey, M. D. (2014). Reliability analysis of a reinforced concrete slab-column connection without shear reinforcement. ASCE-SEI Structures Congress 2014, April 3-5, Boston, MA, USA.

Balomenos, G. P., Pandey, M. D., and Polak, M. A. (2014). Reliability analysis of reinforced concrete flat slab system with shear reinforcement against punching shear failure. 8th International Conference of Analytical Models and New Concepts in Concrete and Masonry Buildings, AMCM2014, June 16-18, Wroclaw, Poland.

Balomenos, G. P., and Pandey, M. D. (2015). Finite element reliability analysis of structures using the dimensional reduction method. 12th International Conference on Applications of Statistics and Probability in Civil Engineering, ICASP12, July 12-15, Vancouver, Canada.

Balomenos, G. P., Genikomsou, A. S., Polak, M. A., and Pandey, M. D. (2015). Efficient method for probabilistic finite element analysis with application to reinforced concrete slabs. Engineering Structures, 103(8), 85-101.

Balomenos, G. P., and Pandey, M. D. (2015). Finite element reliability and sensitivity analysis of structures using the multiplicative dimensional reduction method. Structure and Infrastructure Engineering (accepted).

Bathe, K-J (1982). Finite element procedures in engineering analysis. 1st Ed., Prentice Hall, Inc., Englewood Cliffs, NJ, USA.

Beer, F. P., Johnston, R. E., and DeWolf, J. T. (2006). Mechanics of materials. 4th Ed., McGraw-Hill, Boston, MA, USA.

Benjamin, J. R., and Cornell, A. C. (1970). Probability, Statistics and Decision for Civil Engineers. McGraw-Hill, Boston, MA, USA.

Beyer, W. H. (1987). CRC standard mathematical tables. CRC Press, Taylor & Francis Group, Boca Raton, FL, USA.

Blatman, G., and Sudret, B. (2010). Efficient computation of global sensitivity indices using sparse polynomial chaos expansion. Reliability Engineering & System Safety, 95(11), 1216-1229.

Bruneau, M., Uang, C-M., and Whittaker, A. (1998). Ductile design of steel structures. 1st Ed., McGraw-Hill, New York, USA.

BSI (1972). Code of practice for the structural use of concrete. British Standards Institution (BSI), CP 110, Part 1, London, UK.

BSI (1985). Code of practice for design and construction. British Standards Institution (BSI), BS 110, Part 4, London, UK.

Canadian Standard Association (CSA), A23.3-04 (2004). Design of Concrete Structures. Mississauga, ON, Canada.

Canadian Standard Association (CSA), N287.6 (2011). Pre-operational proof and leakage rate testing requirements for concrete containments structures for nuclear power plants. Mississauga, ON, Canada.

Canadian Standard Association (CSA), N287.7 (2008). In-service examination and testing requirements for concrete containment structures for CANDU nuclear power plants. Mississauga, ON, Canada.

Castillo, E., Mínguez, R., and Castillo, C. (2008). Sensitivity analysis in optimization and reliability problems. Reliability Engineering & System Safety, 93(12), 1788-1800.

CEB-FIP MC 90 (1993). Design of concrete structures. CEB-FIP Model Code 1990, Thomas Telford Services Ltd., London, UK.

Christopoulos, C., Filiatrault, A., Uang C-M., and Folz, B. (2002). Posttensioned energy dissipating connections for moment-resisting steel frames. ASCE Journal of Structural Engineering, 128(9), 1111-1120.

Choi, K. K., and Kim, N-H (2005). Structural sensitivity analysis and optimization 1: linear systems, Springer, NY, USA.

Choi, S-K, Grandhi, R. V., and Canfield, R. A. (2007). Reliability-based structural design. Springer, London, UK.

Chopra, A. (2012). Dynamics of structures: theory and applications to earthquake engineering. 4th Ed., Prentice Hall, Upper Saddle River, New Jersey, USA.

Chowdhury, R., Rao B. N., and Prasad, A. M. (2009a). High-dimensional model representation for structural reliability analysis. Communications in Numerical Methods in Engineering, 25(4), 301-337.

Chowdhury, R., and Rao B. N. (2009b). Assessment of high dimensional model representation techniques for reliability analysis. Probabilistic Engineering Mechanics, 24(1), 100-115.

CISC (2010). Handbook of steel construction. 10th Ed., Canadian Institute of Steel Construction, Willowdale, ON, Canada.

Clough, R. W. (1960). The finite element method in plane stress analysis. Proceeding of the second ASCE Conference on Electronic Computation, Pittsburgh, PA, USA.

Clough, R. W., and Penzien, J. (1992). Dynamics of structures. 2nd Ed., McGraw-Hill, New York, USA.

Collins, M. P., Bentz, E. C., Sherwood, E. G., and Xie, L. (2008). An adequate theory for the shear strength of reinforced concrete structures. Magazine of Concrete Research, Institution of Civil Engineers (ICE), 60(9), 635-650.

Cope, R. J., and Clark, L. A. (1984). Concrete slabs: analysis and design. Elsevier Applied Science, London, UK.

Davis, P. J., and Rabinowitz, P. (1984). Methods of numerical integration. Academic Press Inc., London, UK.

Der Kiureghian, A., and Ke, J-B. (1988). The stochastic finite element method in structural reliability. Probabilistic Engineering Mechanics, 3(2), 83-91.

Der Kiureghian, A., Haukaas, T., and Fijimura, K. (2006). Structural reliability software at the University of California, Berkeley. Structural Safety, 28(1-2), 44-67.

Der Kiureghian, A. (2008). Analysis of structural reliability under parameter uncertainties. Probabilistic Engineering Mechanics, 23(4), 351-358.

Der Kiureghian, A., and Ditlevsen, O. (2009). Aleatory or Epistemic? Does it matter? Structural Safety, 31(2), 105-112.

Ditlevsen, O., and Madsen, H. (1996). Structural reliability methods. John Wiley and Sons, Chichester, West Sussex, UK.

EC2 (2004). Eurocode 2: Design of concrete structures-Part 1: general rules and rules for buildings. European Standard (EN) EN 1992-1-1:2004, Brussels, Belgium.

Ellingwood, B. R., Galambos, T. V., MacGregor, J. G., and Cornell, C. A. (1980). Development of probabilities based load criterion for American national standard A58. NBS Special Publication No. 577, National Bureau of Standards, Washington, D.C., USA.

Ellingwood, B. R. (1984). Probability based safety checking of nuclear plant structures. NUREG/CR-3628, Brookhaven National Laboratory, Upton, NY, USA.

Ellingwood, B. R. (2006). Structural safety special issue: General-purpose software for structural reliability analysis. Structural Safety, 28(1-2), 1-2.

El-Reedy, M. A. (2013). Reinforced Concrete Structural Reliability. CRC Press, Taylor & Francis Group, Boca Raton, FL, USA.

Elwi, A.E., and Murray, D.W. (1980). Nonlinear analysis of axisymmetric reinforced concrete structures. Structural Engineering Report No. 87. Department of Civil Engineering, University of Alberta, Edmonton, Alberta, Canada.

FEMA 273 (1997). NEHRP Guidelines for the seismic rehabilitation of buildings. Federal Emergency Management Agency (FEMA), Washington, D.C., USA.

FEMA 274 (1997). NEHRP commentary on the guidelines for the seismic rehabilitation of buildings. Federal Emergency Management Agency (FEMA), Washington, D.C., USA.

Fish, J., and Belytschko, T., (2007). A first course in finite elements. John Wiley and Sons Ltd, West Sussex, England, UK.

Fragiacomo, M., Amadio, C., and Macorini, L. (2004). Seismic response of steel frames under repeated earthquakes. Engineering Structures, 26(13), 2021-2035.

Gacuci, D. G. (2003). Sensitivity and uncertainty analysis: theory (Volume I). Chapman & Hall/CRC, Boca Raton, FL, USA.

Genikomsou, A. S., and Polak, M. A. (2015). Finite element analysis of punching shear of concrete slabs using damaged plasticity model in ABAQUS. Engineering Structures, 98(4), 38-48.

Ghanem, R. G., and Spanos, P. D. (1991). Stochastic finite elements: a spectral approach. 1st Ed., Springer-Verlag, New York, USA.

Gong, Y., Xue, Y., and Grierson D. E. (2012). Energy-based design optimization of steel building frameworks using nonlinear response history analysis. Constructional Steel Research, 68(1), 43-50.

Grierson, D. E. (1983). The intelligent use of structural analysis. Perspectives in Computing, 3(4), 32-39.

Gupta, A., and Krawinkler, H. (1999). Seismic demands for performance evaluation of steel moment resisting frames. Technical Report No 132, John A. Blume Earthquake Engineering Center, Stanford University, CA, USA.

Haldar, A., and Mahadevan, S. (2000). Reliability assessment using stochastic finite element analysis. John Wiley and Sons Inc, NY, USA.

Hasofer, A. M., and Lind, N. C. (1974). Exact and invariant second-moment code format. ASCE Journal of the Engineering Mechanics Division, 100(1), 111-121.

Hatzigeorgiou, G. D., and Beskos, D. E. (2009). Inelastic displacement ratios for SDOF structures subjected to repeated earthquakes. Engineering Structures, 31(11), 2744-2755.

Haukaas, T., and Der Kiureghian, A. (2004). Finite element reliability and sensitivity methods for performance-based engineering. Report No. PEER 2003/14, Pacific Earthquake Engineering Research Center, Univ. of California, Berkeley, CA, USA.

Haukaas, T., and Der Kiureghian, A. (2006). Strategies for finding the design point in non-linear finite element reliability analysis. Probabilistic Engineering Mechanics, 21(2), 133-147.

Haukaas, T., and Scott, M. H. (2006). Shape sensitivities in the reliability analysis of nonlinear frame structures. Computers & Structures, 84(15-16), 964-977.

Haukaas, T., and Der Kiureghian, A. (2007). Methods and object-oriented software for FE reliability and sensitivity analysis with application to a bridge structure. ASCE Journal of Computing in Civil Engineering, 21(3), 151-163.

Hibbeler, R. C. (2011). Statics and mechanics of materials. 3rd Ed., Pearson Prentice Hall Inc., Upper Saddle River, NJ, USA.

Homma, T., and Saltelli, A. (1996). Importance measures in global sensitivity analysis of nonlinear models. Reliability Engineering & System Safety, 52(1), 1-17.

Hurtado, J. E., and Barbat, A. H. (1998). Monte Carlo techniques in computational stochastic mechanics. Archives of Computational Methods in Engineering, 5(1), 3-30.

Hutton, D. V. (2004). Fundamentals of finite element analysis. International Edition, McGraw-Hill, Boston, MA, USA.

Inverardi, P., and Tagliani, A., (2003). Maximum entropy density estimation from fractional moments. Communication in Statistics−Theory and Methods, 32(2), 327-0345.

ISIGHT (2010). Getting started guide. Dassault Syst. Simulia Corp., Providence, RI, USA.

Jaynes, E. (1957). Information theory and statistical mechanics. Physical Review, 106(4), 620-630.

Kalkan, E., and Kunnath, S. K. (2007). Assessment of current nonlinear static procedures for seismic evaluation of buildings. Engineering Structures, 29(3), 305-316.

Krawinkler, H. (1998). Pros and cons of pushover analysis of seismic performance evaluation. Engineering Structures, 20(4-6), 452-464.

Koduru, S. D., and Haukaas, T. (2010). Feasibility of FORM in finite element reliability analysis. Structural Safety, 32(2),145-153.

Kroese, D. P., Taimre, T., and Botev, Z. I. (2011). Handbook of Monte Carlo methods. John Wiley and Sons Inc, Hoboken, NJ, USA.

Kythe, P. K., and Schäferkotterr, M. R. (2004). Handbook of computational methods for integration. CRC Press, Chapman and Hall, Boca Raton, FL, USA.

Lagarias, J., Reeds, J., Wright, M., and Wright, P. (1998). Convergence properties of the Nelder-Mead simplex method in low dimensions. SIAM J. Optimization, 9(1), 112-147.

Lee, J., and Fenves, G. L. (1998). A plastic-damage concrete model for earthquake analysis of dams. Earthquake Engineering and Structural Dynamics, 27, 937-956.

Lee, J-O, Yang Y-S, and Ruy, W-S (2002). A comparative study on reliability-index and target-performance-based probabilistic structural design optimization. Computers & Structures, 80(3-4), 257-269.

Li, Genyuan, Rosenthal, C., and Rabitz, H. (2001). High dimensional model representations. The Journal of Physical Chemistry, American Chemical Society, 105(33), 7765-7777.

Li, Gang, and Zhang, K. (2011). A combined reliability analysis approach with dimension reduction method and maximum entropy method. Structural and Multidisciplinary Optimization, 43(1), 121-134.

Liu, G. R., and Quek, S. S. (2003). The finite element method: a practical approach. Butterworth-Heinemann, Oxford, UK; Boston, MA, USA.

Liu, P-L, and Der Kiureghian, A. (1991). Optimization algorithms for structural reliability. Steructural Safety, 9(3), 161-177.

Logan, D.L. (2007). A first course in the finite element method. 4th Ed., Nelson/Thomson Publishing, Toronto, ON, Canada.

Lopez, R. H., Torii, A. J., Miguel L. F. F., and Souza Cursi, J. E. (2015). Overcoming the drawbacks of the FORM using a full characterization method. Structural Safety, 54, 57-63.

Low, B. K., and Tang, H. W. (1997). Efficient reliability evaluation using spreadsheet. ASCE Journal of Engineering Mechanics, 123(7), 749-752.

Lu, W. Y., and Lin, I. J. (2004). A study on the safety of shear design of reinforced concrete beams. Cambridge Journal of Mechanics, 20(4), 303-309.

Lubliner, J., Oliver, J., Oller, S., and Onate, E. (1989). A plastic-damage model for concrete. International Journal of Solids and Structures, 25(3), 299-326.

Lundqvist, P., and Nilsson, L-O (2011). Evaluation of prestress losses in nuclear reactor containments. Nuclear Engineering and Design, 241(1), 168-176.

MacGregor, J. G., and Bartlett, M. F. (2000). Reinforced concrete: mechanics and design. 1st Canadian Ed., Pearson Prentice Hall Inc., Scarborough, ON, Canada.

MacGregor, J. G., and Wight, J. K. (2005). Reinforced concrete: mechanics and design. 4th Ed., Pearson Prentice Hall Inc., Upper Saddle River, NJ, USA.

Madsen, H. O., Krenk, S., and Lind, N. C. (1986). Methods of structural safety. Prentice Hall, Inc., Englewood Cliffs, NJ, USA.

Mazzoni, S., McKenna, F., Scott, M. H., Fenves, G. L., et al. (2007). OpenSees command language manual–version 2. Univ. of California–Berkeley, CA, USA.

McKenna, F., Fenves, G. L., and Scott, M. H. (2000). Open System for Earthquake Engineering Simulation. Univ. of California–Berkeley, CA, USA. (http://opensees.berkeley.edu).

Megally, S., and Ghali, A. (1999). Design for punching shear in concrete. ACI Special Publication, SP183-3, 37-66.

Melchers, R.E. (1987). Structural reliability: analysis and prediction. Ellis Horwood series in Civil Engineering, Ellis Horwood Limited, Chichester, West Sussex, UK.

Metropolis, N., and Ulam, S. (1949). The Monte Carlo method. Journal of the American Statistical Association, 44(247), 335-341.

Mirhosseini, S., Polak, M. A., and Pandey, M. D. (2014). Nuclear radiation effect on the behavior of reinforced concrete elements. Nuclear Engineering and Design, 269(Special Issue), 57-65.

Mirza, S. A., and MacGregor, J. G. (1979a). Statistical study of shear strength of reinforced concrete slender beams. ACI Journal Proceedings, JL76-47, 76(11), 1159-1177.

Mirza, S. A., and MacGregor, J. G. (1979b). Variations in dimensions of reinforced concrete members. ASCE Journal of the Structural Division, 105(4), 751-766.

Mirza, S. A., and Skrabek, B. W. (1991). Reliability of short composite bean-column strength interaction. ASCE Journal of Structural Engineering, 117(8), 2320-2339.

Moe, J. (1961). Shearing strength of reinforced concrete slabs and footings under concentrated loads. Development Department Bulletin D47, Portland Cement Association, Skokie, Illinois. USA.

Montgomery, D. C., and Runger, G. C. (2003). Applied Statistics and Probability for Engineers, 3rd Ed., John Wiley and Sons Inc, NY, USA.

Morrison, S. J. (2009). Statistics for engineers: an introduction. John Wiley and Sons Ltd, Chichester, West Sussex, UK.

Murray, D.W., and Epstein, M. (1976a). An elastic stress analysis of a Gentilly type containment structure Volume 1. Structural Engineering Report No. 55. Department of Civil Engineering, University of Alberta, Edmonton, Alberta, Canada.

Murray, D.W., and Epstein, M. (1976b). An elastic stress analysis of a Gentilly type containment structure Volume 2 (Appendices B to F). Structural Engineering Report No. 56. Department of Civil Engineering, University of Alberta, Edmonton, Alberta, Canada.

Murray, D.W., Rohardt, A. M., and Simmonds, S. H. (1977). A classical flexibility analysis for gentilly type containment structures. Structural Engineering Report No. 63. Department of Civil Engineering, University of Alberta, Edmonton, Alberta, Canada.

Murray, D.W., Chitnuyanondh, L., Wong, C., and Rijub-Agha, K. Y. (1978). Inelastic analysis of prestressed concrete secondary containments. Structural Engineering Report No. 67. Department of Civil Engineering, University of Alberta, Edmonton, Alberta, Canada.

Muttoni, A. (2008). Punching shear strength of reinforced concrete slabs without transverse reinforcement. ACI Structural Journal, 105(4), 440-450.

Mwafy, A. M., and Elnashai, A. S. (2001). Static pushover versus dynamic collapse analysis of RC buildings. Engineering Structures, 23(5), 407-424.

NESUSS. Southwest Research Institute (SRI), San Antonio, TX, USA.

Nowak, A. S., and Collins, K. R. (2000). Reliability of structures. McGraw-Hill, New York, USA.

Nowak, A. S., and Szerszen, M. M. (2003a). Calibration of design code for buildings (ACI 318): part 1 - statistical models for resistance. ACI Structural Journal, 100(3), 377-382.

Nowak, A. S., and Szerszen, M. M. (2003b). Calibration of design code for buildings (ACI 318): part 2 - reliability analysis and resistance factors. ACI Structural Journal, 100(3), 383-391.

Nowak, A. S., Rakoczy, A. M., and Szeliga, E. K. (2012). Revised statistical resistance models for R/C structural components. ACI Special Publication, SP284-6, 1-16.

NRCC (2010). National Building Code of Canada. National Research Council of Canada, Ottawa, ON, Canada.

Olver, F., Lozier, D., Boisvert, R., and Clark, Ch. (2010). NIST handbook of mathematical functions. National Institute of Standards and Technology (NIST), Cambridge University Press, New York, USA.

Park, R., and Gamble, W. L. (1980). Reinforced concrete slabs. John Wiley and Sons Inc, NY, USA.

Pandey, M. D. (1996a). Reliability-based inspection of prestressed concrete containment structures. INFO-0639, Atomic Energy Control Board of Canada, Ottawa, ON, Canada.

Pandey, M. D. (1996b). Proof testing of CANDU concrete containment structures. INFO-0646, Atomic Energy Control Board of Canada, Ottawa, ON, Canada.

Pandey, M. D. (1997). Reliability-based assessment of integrity of bonded prestressed concrete containment structures. Nuclear Engineering and Design, 176(3), 247-260.

Pandey, M. D. (2000). Direct estimation of quantile functions using the maximum entropy principle. Structural Safety, 22(1), 61-79.

Pandey, M. D., and Zhang, X. (2012). System reliability analysis of the robotic manipulator with random joint clearances. Mechanism and Machine Theory, 58, 137-152.

Papadrakakis, M, and Kotsopoulos, A. (1999). Parallel solution methods for stochastic finite element analysis using Monte Carlo simulation. Computer Methods in Applied Mechanics and Engineering, 168(1-4), 305-320.

Patelli, E., Panayirci, M., Broggi, M., Goller, B., Beaurepaire, P., Pradlwater, H. J., and Schuëller, G. I. (2012). General purpose software for efficient uncertainty management of large scale finite element models. Finite Elements in Analysis and Design, 51, 31-48.

Paulay, T., and Priestley, M. J. N. (1992). Seismic design of reinforced concrete and masonry buildings. John Wiley and Sons Inc, NY, USA.

Pellissetti, F. M., and Schuëller, G. I. (2006). On general purpose software in structural seliability. An overview. Structural Safety, 28(1-2), 3-16.

Polak, M. A. (2005). Ductility of reinforced concrete flat slab-column connections. Computer-Aided Civil and Infrastructure Engineering, 20(3): 184-193.

Polak, M. A., and Bu, W. (2013). Design considerations for shear bolts in punching shear retrofit of reinforced concrete slabs. ACI Structural Journal, 110(1), 15-26.

Rabitz, H., and Aliş, Ö. (1999). General foundations of high-dimensional model representations. Journal of Mathematical Chemistry, 25(2-3), 197-233.

Rackwitz, R., and Fiessler, B (1978). Structural reliability under combined random load sequences. Computers & Structures, 9(5), 489-494.

Rahman, S., and Xu, H. (2004). A univariate dimension-reduction method for multi-dimensional integration in stochastic mechanics. Probabilistic Engineering Mechanics, 19(4), 393-408.

Rajashekhar, M. R., and Ellingwood, B. R. (1995). Reliability of reinforced-concrete cylindrical shells. ASCE Journal of Structural Engineering, 121(2), 336-347.

Rakoczy, A. M., and Nowak, A. S. (2013). Resistance model of lightweight concrete members. ACI Materials Journal, 110(1), 99-108.

Ramírez, P., and Carta, J.A. (2006). The use of wind probability distribution derived from the maximum entropy principle in the analysis of wind energy. A case study. Energy Conversion and Management, 47(15−16), 2564-2577.

Rankin, G. I. B., and Long, A. E. (1987). Predicting the punching strength of conventional slab-column specimens. Proceedings of the Institution of Civil Engineers, Part 1, 82(2), 327-346.

Rao, B. N., Chowdhury, R., Prasad, M. A., Singh, R. K., and Kushwaha H. S. (2009). Probabilistic characterization of AHWR inner containment using high-dimensional model representation. Nuclear Engineering and Design, 239(6), 1030-1041.

Rao, B. N., Chowdhury, R., Prasad, M. A., Singh, R. K., and Kushwaha H. S. (2010). Reliability analysis of 500MWe PHWR inner containment using high-dimensional model representation. International Journal of Pressure Vessels and Piping, 87(5), 230-238.

Regan, P. E. (1974). Design for punching shear. The Structural Engineer, Institution of Structural Engineers, 52(6), 197-207.

Reh, A., Beley, J-D., Mukherjee, S., and Khor, E. H. (2006). Probabilistic finite element analysis using ANSYS. Structural Safety, 28(1-2), 17-43.

Reineck, K-H., Kuchma, D., Kim, K-S., and Marx, S. (2003). Shear database of reinforced concrete members without shear reinforcement. ACI Structural Journal, 100 (2), 240-249.

Rizkalla, S. H., Simmonds, S. H., and MacGregor, J. G. (1979). Leakage tests of wall segments of reactor containments. Structural Engineering Report No. 80. Department of Civil Engineering, University of Alberta, Edmonton, Alberta, Canada.

Rombach, G. A. (2011). Finite element design of concrete structures: practical problems and their solution. 2nd Ed., ICE Publishing, London, UK.

Rosenblueth, E. (1975). Point estimates for probability moments. Proceedings of the National Academy of Sciences, 72(10), 3812-3814.

Rosenblueth, E. (1981). Two point estimates in probabilities. Applied Mathematical Modelling, 5(5), 329-335.

Ross, S. M. (2004). Introduction to probability and statistics for engineers and scientist. 3rd Ed., Elsevier/Academic Press, Boston, MA, USA.

Ruiz, M., F., and Muttoni, A. (2009). Applications of critical shear crack theory to punching of reinforced concrete slabs with transverse reinforcement. ACI Structural Journal, 106(4), 485-494.

Saiidi, M., and, Sozen, M. A. (1981). Simple nonlinear seismic analysis of R/C structures. ASCE Journal of the Structural Division, 107(ST5), 937-953.

Sacramento, P. V. P., Ferreira, M. P., Oliveira, D. R. C., Melo, G. S. S. A. (2012). Punching strength of reinforced concrete flat slabs without shear reinforcement. IBRACON Structures and Materials Journal, 5(5), 659-691.

Saltelli, A., and Sobol′, I. M. (1995). About the use of rank transformation in sensitivity analysis of model output. Reliability Engineering & System Safety, 50(3), 225-239.

Saltelli, A., Chan K. and Scott E. (2000). Sensitivity analysis. John Wiley and Sons Inc, NY, USA.

Saltelli, A., Tarantola, S., Campologno, F., and Ratto, M. (2004). Sensitivity analysis in practice: a guide to assessing scientific models. John Wiley and Sons Ltd, Chichester, West Sussex, UK.

Saltelli, A., Ratto, M., Andres, T., Campologno, F., Cariboni, J., Gatelli, D., Saisana, M., and Tarantola, S. (2008). Global sensitivity analysis: the primer. 1st Ed., John Wiley and Sons Ltd, Chichester, West Sussex, UK.

Santosh, T. V., Saraf, R. K., Ghosh, A. K., and Kushwaha, H. S. (2006). Optimum step length selection rule in modified HL-RF method for structural reliability. International Journal of Pressure Vessels and Piping, 83(10), 742-748.

Schuëller, G.I., and Pradlwarter, H.J. (2006). Computational stochastic structural Analysis (COSSAN). A software tool. Structural Safety, 28(1-2), 68-82.

Scott, M. H., and Haukaas, T. (2008). Software framework for parameter updating and finite-element response sensitivity analysis. ASCE Journal of Computing in Civil Engineering, 22(5), 281–291.

Shang, S., and Yun, G-J. (2013). Stochastic finite element with material uncertainties: implementation in a general purpose software. Finite Element in Analysis and Design, 64, 65-78.

Shanon, E. (1949). The mathematical theory of communication. Univ. of Illinois Press, Urbana, IL, USA.

Simmonds, S. H., Rizkalla, S. H., and MacGregor, J. G. (1979). Tests of wall segments from reactor containments Volume 1. Structural Engineering Report No. 81. Department of Civil Engineering, University of Alberta, Edmonton, Alberta, Canada.

Sobol′, I. M. (1994). A primer for the Monte Carlo method. CRC Press, Boca Raton, FL, USA.

Sobol′, I. M. (2001). Global sensitivity indices for nonlinear mathematical models and their Monte Carlo estimates. Mathematics and Computers Simulation, 55(1-3), 271-280.

Sozen, M. A., and Siess, C. P. (1963). Investigation of multiple-panel reinforced concrete floor slabs, design methods-their evolution and comparison, Journal of the American Concrete Institute, 60(8), 999-1028.

Stefanou, G. (2009). The stochastic finite element method: past, present and future. Computer Methods in Applied Mechanics and Engineering, 198(9-12), 1031-1051.

Sudret, B., and Der Kiureghian, A. (2000). Stochastic finite element methods and reliability: a state-of-the-art report. UCB/SEMM-2000/08, Dept. of Civil and Env. Engineering, Univ. of California–Berkeley, CA, USA.

Sudret, B., and Der Kiureghian, A. (2002). Comparison of finite element reliability methods. Probabilistic Engineering Mechanics, 17(4), 337-348.

Sudret, B. (2008). Global sensitivity analysis using polynomial chaos expansion. Reliability Engineering & System Safety, 93(7), 964-979.

Thaker, B., Riha, D., Fitch, S., Huyse, L., and Pleming, J. (2006). Probabilistic engineering analysis using NESSUS software. Structural Safety, 28(1-2), 83-107.

Theodorakopoulos, D. D., and Swamy, R. N. (2002). Ultimate punching shear strength analysis of slab-column connections. Cement and Concrete Composites, 24(6), 509-521.

Tunga, M.A., and Demiralp, M. (2004). A factorized high dimensional model representation on the partitioned random discrete data. Applied Numerical Analysis and Computational Mathematics, 1(1), 231-241.

Tunga, M.A., and Demiralp, M. (2005). A factorized high dimensional model representation on the nodes of a finite hyperprismatic regular grid. Applied Mathematics and Computation, 164(3), 865-883.

Turner, M.J., Clough, R.W., Martin, H.C., and Topp, L.J. (1956). Stiffness and deflection analysis of complex structures. Journal of the Aeronautical Sciences, 23(9), 805-823.

Wen, Y. K. (2001). Reliability and performance-based design. Structural Safety, 23(4), 407-428.

Xu, H., and Rahman, S. (2004). A generalized dimension-reduction method for multidimensional integration in stochastic mechanics. International Journal for Numerical Methods in Integration, 61(12), 1992-2019.

Xue, Y. (2012). Capacity design optimization of steel building frameworks using nonlinear time-history analysis. PhD Thesis, Department of Civil and Environmental Engineering, University of Waterloo, Waterloo, ON, Canada.

Zhang, X. (2013). Efficient computational methods for structural reliability and global sensitivity analyses. PhD Thesis, Department of Civil and Environmental Engineering, University of Waterloo, Waterloo, ON, Canada.

Zhang, X., and Pandey, M. D. (2013). Structural reliability analysis based on the concepts of entropy, fractional moment and dimensional reduction method. Structural Safety, 43(4), 28-40.

Zhang, X., and Pandey, M. D. (2014). An effective approximation for variance-based global sensitivity analysis. Reliability Engineering & System Safety, 121(17), 164-174.

Zhao, Y-G, and Ono, T. (1999). A general procedure for first/second-order reliability method (FORM/SORM). Structural Safety, 21(2), 95-112.

Zienkiewicz, O. C. (1995). Origins, milestones and directions of the finite element method – A personal view. Archives of Computational Methods in Engineering, 2(1), 1-48.

Zienkiewicz, O. C., and Taylor, R. L. (2000). The finite element method: Volume 1-the basis. 5th Ed., Butterworth-Heinemann, Oxford, UK; Boston, MA, USA.

Zwillinger, D. (2011). CRC standard mathematical tables and formulae. CRC Press, Taylor & Francis Group, Boca Raton, FL, USA.